

**Kinetic studies of propane oxidation on  
Mo and V based mixed oxide catalysts**

vorgelegt von  
M. Sc. Chemiker  
Lénárd-István Csepei  
aus Zalău/Zilah/Zillenmarkt (Rumänien)

Von der Fakultät II – Mathematik und Naturwissenschaften  
der Technischen Universität Berlin  
zur Erlangung des akademischen Grades  
Doktor der Naturwissenschaften  
- Dr. rer. nat. -

genehmigte Dissertation

Promotionsausschuss:

Vorsitzender:	Prof. Dr. A. Thomas
Berichter/Gutachter:	Prof. Dr. R. Schomäcker
Berichter/Gutachter:	Prof. Dr. R. Schlögl
Berichter/Gutachter:	Prof. Dr. M. Muhler

Tag der wissenschaftliche Aussprache: 19. August 2011

Berlin 2011  
D 83



## **Acknowledgements/Danksagung**

The work presented in this thesis was carried out in the time interval between February 2007 and June 2011 at the Inorganic Chemistry Department of the Fritz Haber Institute of the Max Planck Society in Berlin.

Foremost, I would like to thank to Prof. Dr. Robert Schlögl for giving me the opportunity to carry out the doctoral studies at this Institute. In the same time, I would like to express my gratitude for giving me this interesting topic and the constructive criticism during the discussions. I also would like to thank Dr. Annette Trunschke for introducing me in the topic of the present thesis, for the fruitful discussions and new ideas and for contributing to my professional development.

The substantial contributions of the department members to this work are also acknowledged. I thank Yury Kolen'ko, Almudena Celaya Sanfiz, ZiRong Tang and Olaf Timpe for catalyst synthesis; Gisela Lorenz for the nitrogen physisorption experiments; Gisela Weinberg and Wei Zhang for the SEM-EDX and the STEM measurements; Edith Kitzelmann for the XRD measurements; Sabine Wrabetz for the microcalorimetric experiments; Raoul Blume, Michael Hävecker and Detre Teschner for the XPS experiments and data analysis; Benjamin Frank, Kazu Amakawa, Péter Schnörch, Tom Cotter, Manfred Schuster, Anton Nagy and Sylvia Reiche for the helpful discussions. Special thanks are addressed to Siegfried Engelschalt and Raoul Naumann d'Alnoncourt for their help in setting up the reactor system and to Frank Girgsdies for the in-situ XRD experiment and data analysis on the effect of steam and the redox potential. Finally, the help of all the members of the department and the workshops is acknowledged.

Last but not least, I would like to express my gratitude to my parents and my former supervisor Dr. Csaba Bolla for encouraging me to undertake the doctoral studies abroad and for their continuous moral support along these years.

To my parents

## Eidesstattliche Versicherung

Hiermit erkläre ich, dass ich die Dissertation selbst angefertigt habe. Die Arbeit enthält – auch in Anteilen – keine Kopien anderer Arbeiten. Verwendete Hilfsmittel und Quellen sind vollständig angegeben. Die Namen aller Wissenschaftler, die mit mir zusammengearbeitet haben, sind in den Anlagen vollständig genannt.

## Abstract

The present work concentrates on the systematic kinetic study of the one-step propane oxidation to acrylic acid over a well defined, phase-pure M1 MoVTeNbO<sub>x</sub> catalyst. The bulk structural stability of the catalyst is a key issue for kinetic studies. The stability of the phase-pure M1 MoVTeNbO<sub>x</sub> catalyst under various conditions (steam-containing, steam-free, net reducing, stoichiometric and net oxidizing feed compositions) was evidenced by an in-situ XRD experiment which suggested that the bulk structure is homogeneous and constant under reaction conditions. Thereby, the heterogeneously catalyzed reactivity is exclusively determined by the surface properties, which in turn, are controlled by the chemical potential of the gas phase.

A kinetic study on the reaction variables (temperature, steam content and redox potential) was carried out. Stable catalytic performance was observed for all the conditions. Cycling experiments showed the reversibility of the conversion and selectivity decrease upon exposing the catalyst to dry and reducing feed, respectively. Further catalytic experiments revealed that the reactivity spans over 5 orders of magnitude in the order of acrolein oxidation >> propylene oxidation > propane oxidation >> carbon monoxide oxidation ~ water gas shift reaction. The negligible CO oxidation activity suggested that the CO and CO<sub>2</sub> are formed via two independent pathways in propane oxidation over M1. The stage-wise addition of oxygen lead to an improvement of the catalytic performance by 5% compared to the conventional single-tube reactor. Further experiments in the two-stage reactor revealed that the phase-pure M1 is not reoxidized by N<sub>2</sub>O. The addition of propylene in the two-stage reactor revealed a slight competitive adsorption on the active sites with propane, which observation was supported by the results of microcalorimetric experiments. On the other hand, the addition of CO and CO<sub>2</sub> in the two-stage reactor showed that these products do not adsorb competitively with the educt or intermediates.

In the literature much of the kinetic data was reported for ill-defined catalyst surfaces. In contrast to that, the present work reports the kinetic study of propane selective oxidation to acrylic acid on a well defined phase-pure and structurally stable M1 MoVTeNbO<sub>x</sub> catalyst. This study may contribute to the better kinetic and mechanistic understanding of the propane selective oxidation reaction.

## Zusammenfassung

Die vorliegende Arbeit enthält systematische kinetische Untersuchungen zur einstufigen, selektiven Oxidation von Propan zu Acrylsäure an wohl definierten, phasenreinen M1-MoVTaNbO<sub>x</sub>-Katalysatoren. Die Stabilität der phasenreinen M1-Katalysatoren unter verschiedenen Reaktionsbedingungen (in Wasserdampf, wasserdampffrei, netto-reduzierende, stöchiometrische und netto-oxidierende Feed-Zusammensetzung) konnte in In-situ-XRD-Experimenten bewiesen werden. Da die Festkörperstruktur homogen ist und beständig unter Reaktionsbedingungen, kann die unterschiedliche Reaktivität des heterogenen Katalysators allein durch seine Oberflächeneigenschaften bestimmt werden, welche wiederum stark vom chemischen Potential der Gasphase abhängen.

Es wurden kinetische Studien zu den Reaktionsparametern Temperatur, Wasserdampfanteil und Redoxpotential durchgeführt, wobei die Systeme unter allen Bedingungen stabile Katalysatorleistungen aufwiesen. Zyklische Experimente zeigten die Reversibilität des Umsatz- und Selektivitätsrückgangs, sowohl unter wasserfreiem als auch reduzierendem Feed. Zudem konnten in den Katalysatortests Unterschiede in den Reaktivitäten von bis zu 5 Größenordnungen ermittelt werden, mit Acrolein >> Propylen > Propan >> CO-Oxidation~Wassergas-Shift. Die bestimmte Oxidationsaktivität von CO war vernachlässigbar klein, was die Bildung von CO und CO<sub>2</sub> auf zwei voneinander unabhängigen Reaktionspfaden suggeriert. Über eine stufenweise Zufuhr von Sauerstoff konnte eine Steigerung der katalytischen Aktivität um 5% im Vergleich zum konventionellen, einstufigen Reaktor erreicht werden. Die Versuche im zweistufigen Reaktor zeigten auch, dass der phasenreine M1-Katalysator in N<sub>2</sub>O nicht reoxidiert. Weiterhin konnte unter Zugabe von Propylen im zweistufigen Reaktor eine teilweise kompetitive Adsorption zu Propan an die aktiven Zentren des Katalysators beobachtet werden. Im Gegensatz dazu, stand die Adsorption von CO und CO<sub>2</sub> nicht in Konkurrenz mit der Adsorption von Edukten oder Zwischenprodukten.

Die kinetischen Untersuchungen der, im Gegensatz zu den meisten Systemen in der Literatur, wohl definierten, strukturstabilen M1-MoVTaNbO<sub>x</sub>-Katalysatoren könnten einen entscheidenden Beitrag zum Verständnis von Kinetik und Reaktionsmechanismus der Propanoxidation leisten.

## Table of contents

<b>Acknowledgements/Danksagung</b> .....	i
<b>Eidesstattliche Versicherung</b> .....	iii
<b>Abstract</b> .....	iv
<b>Zusammenfassung</b> .....	v
<b>Table of contents</b> .....	vi
<b>Chapter 1 Introduction and motivation</b> .....	1
1.1 Introduction .....	1
1.2. Overview on the literature results .....	3
1.2.1. The selective oxidation of propylene .....	3
1.2.2. Oxidative dehydrogenation of propane .....	8
1.2.3. The direct oxidation of propane to acrylic acid .....	13
1.2.3.1. Generalities .....	13
1.2.3.2. Identification of propane selective oxidation pathways .....	14
1.2.3.3. Active sites on MoVTeNbO <sub>x</sub> catalysts .....	20
1.2.3.4. The effect of acid-base character of the catalyst .....	24
1.2.3.5. The effect of steam .....	25
1.2.3.6. The effect of redox potential of gas phase and oxygen species .....	27
1.2.4. Reactor designs, operation modes .....	31
1.2.4.1. Conventional laboratory scale reactors .....	31
1.2.4.2. Catalytic membrane- and multi-stage reactor designs .....	33
1.2.5. Reaction kinetics .....	37
1.3. Motivation .....	38
References Chapter 1 .....	40
<b>Chapter 2. Experimental methods</b> .....	44
2.1. Physico-chemical characterization of the catalysts .....	44
2.1.1. Nitrogen physisorption .....	44
2.1.2. X-Ray Diffraction .....	44
2.1.3. Scanning Electron Microscopy (SEM/EDX) and Scanning Transmission Electron Microscopy (STEM) .....	45
2.1.4. X-Ray Photoelectron Spectroscopy (XPS) .....	45
2.1.5. Microcalorimetry .....	45
2.2. The experimental setup for propane oxidation .....	46
2.2.1. The gas dosing system .....	46
2.2.2. Reactor tube characteristics .....	48
2.2.3. Estimation of the Weisz-number, the Thiele modulus and the effectiveness factor .....	51
2.2.4. The two stage reactor system .....	52
2.2.5. The analytical system .....	55
2.2.6. Calibration of the GC-MS .....	57
2.2.7. Data analysis .....	59
2.3. Catalyst synthesis and characterization .....	61

2.3.1. The synthesis of phase pure M1 MoVTeNbO <sub>x</sub> catalyst .....	61
References Chapter 2 .....	63

<b>Chapter 3. Structural stability of the M1 MoVTeNbO<sub>x</sub> catalyst under propane oxidation conditions .....</b>	<b>65</b>
3.1. Abstract .....	65
3.2. Introduction .....	65
3.3. In-situ XRD study on the effect of steam and oxygen.....	68
3.4. STEM analysis of the catalyst before and after the in-situ XRD experiment .....	72
3.5. Conclusions .....	75
References Chapter 3 .....	76

<b>4. Kinetic studies of propane oxidation to acrylic acid on a phase-pure MoVTeNbO<sub>x</sub> catalyst .....</b>	<b>77</b>
4.1. Abstract .....	77
4.2. Kinetic studies on phase-pure M1 MoVTeNbO <sub>x</sub> .....	77
4.2.1. Variation of the contact time and temperature .....	78
4.2.2. Variation of the steam content .....	81
4.2.3. Variation of the propane content .....	88
4.2.4. Variation of the oxygen content .....	90
4.2.5. Propylene oxidation .....	93
4.2.6. Acrolein oxidation .....	98
4.2.7. CO oxidation and water gas shift reaction .....	100
4.2.8. Comparison of the reactivity of propane, propylene, acrolein and carbon monoxide oxidation reactions .....	104
4.3. Two-stage reactor used as a distributor of oxidizing and reducing gases .....	106
4.3.1. Addition of O <sub>2</sub> and N <sub>2</sub> O .....	107
4.3.2. Addition of propylene.....	113
4.3.3. Addition of CO .....	116
4.3.4. Addition of CO <sub>2</sub> .....	117
4.4. Conclusions .....	119
References Chapter 4 .....	120

<b>Chapter 5. Post synthesis treatment of the phase-pure M1 MoVTeNbO<sub>x</sub> catalyst.</b>	<b>122</b>
5.1.1. Abstract .....	122
5.1.2. Introduction .....	122
5.2. Modifying agents and procedure .....	124
5.3. Characterization of the modified samples .....	127
5.3.1. N <sub>2</sub> physisorption .....	127
5.3.2. X-ray diffraction .....	127
5.3.3. SEM/EDX .....	128
5.3.4. XAS and XPS .....	131
5.3.5. Microcalorimetry .....	134
5.4. Catalytic experiments .....	141
5.4.1. Propane oxidation .....	141
5.4.2. Kinetic analysis of propane oxidation over the modified catalysts .....	144

5.4.3. Propylene oxidation .....	148
5.4.4. CO oxidation and water gas shift reaction .....	150
5.5. Conclusions .....	153
References Chapter 5 .....	155
<b>Chapter 6. Exploratory experiments .....</b>	<b>157</b>
6.1. Introduction .....	157
6.2. Propane oxidation reactivity on different Mo and V based catalysts .....	158
6.3. Propylene oxidation reactivity on different Mo and V based catalysts .....	166
6.4. Exploratory reaction pathway analysis of propane oxidation on phase-pure M1 catalyst .....	169
6.5. Exploratory kinetic modeling on propane oxidation on phase-pure MoVTenbO <sub>x</sub> catalyst .....	178
6.5.1. The effect of temperature .....	178
6.5.2. The effect of steam .....	180
References Chapter 6 .....	182
<b>General Conclusions and Outlook .....</b>	<b>184</b>
<b>Appendices .....</b>	<b>189</b>
Appendix 5.1. Reaction networks of propane oxidation over the modified catalysts...	189
Appendix 6.1. Modeling the delplots for a reaction pathway that contains multiple rank product .....	193
Appendix 6.2. Program for implementing Model 1 in Berkeley Madonna .....	198
Appendix 6.3. The physical properties of the gas mixtures with different steam contents .....	199
<b>Acknowledgements for permission to reprint published materials .....</b>	<b>201</b>
<b>List of abbreviations .....</b>	<b>202</b>
<b>List of figures .....</b>	<b>204</b>
<b>List of tables .....</b>	<b>207</b>

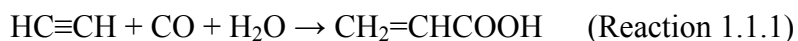
## Chapter 1. Introduction and motivation

### 1.1 Introduction

Based on economical and ecological considerations, many attempts have been undertaken during the last decades to replace petroleum by other feedstock for producing chemicals and polymers. The use of C2-C4 components of the natural gas for this purpose is one option [1-3].

Acrylic acid and acrylonitrile are very important monomers. The global crude acrylic acid market reached around 3.2 million tons by the end of 2005 and the demand increased steadily with ca. 4%/year. Esterification of crude acrylic acid yields acrylates, which are used to produce various homo- and copolymers by emulsion polymerization with manifold applications ranging from coatings (ca. 44% of the total market), adhesives (ca. 19% of the total market), and fibres to textiles (ca. 7% of the total market). Acrylic acid in its glacial form is used to produce polyacrylic acid and polyacrylates for superabsorbents (ca. 11% of the total market), inks, detergents and dispersants (ca. 8% of the total market).

Acrylic acid has been produced in commercial processes starting from acetylene, ethylene or propylene, respectively. In the last century, acrylic acid was mainly manufactured by means of an acetylene-based process (Reaction 1.1.1) developed by Reppe in the 1930's in Germany. The process was commercialized by the BASF in Ludwigshafen, Germany, in the 1950's.



This process was operated at 200°C and 80 bar applying a catalyst that contains a carbonyl forming metal, such as nickel. The plant in Ludwigshafen was closed in the 1990's with the start-up of a new propylene-based plant in Antwerp, Belgium.

The direct oxidation of propylene to acrylic acid was developed by Nippon Shokubai using catalysts like Mo-W-Te-Sn-Co-O or Nb-W-Co-Ni-Bi-Fe-Mn-Si-Zr-O at 325-350°C with 65 and 75% yield, respectively [2-4]. The reaction is very exothermic

( $\Delta H = -598 \text{ kJ/mol}$ ). The process requires maintaining the temperature between 325 and 350°C in order to attain an economically reasonable propylene conversion, but under these conditions, significant total oxidation occurs, which causes a decrease of selectivity. Moreover, the catalyst shows significant deactivation. For these reasons, the process turned out to be uneconomic.

Nowadays, a two stage oxidation process starting from propylene is exclusively used worldwide. In the first step propylene is oxidized to acrolein at 350±50°C over promoted molybdenum-bismuth systems (Reaction 1.1.2).



Promoted molybdenum-vanadium systems and temperatures around 210-250°C are used to oxidize acrolein to acrylic acid (Reaction 1.1.3).



Both of these steps are rather exothermic. In the first step a yield of 90% acrolein can be attained. During the second step a yield of 97% acrylic acid can be reached. The overall acrylic acid yield is around 87%.

Upcoming new process developments include

- biotransformation processes (e.g., using lactic acid as an intermediate)
- oxidation of propane via propylene (oxidative dehydrogenation) and acrolein (three stage process), or
- direct oxidation of propane to acrylic acid in one step.

The price of propylene is 1105 €/ton [5], while the price of acrylic acid is currently 1825€/ton [6]. On the other hand, the propane is much cheaper than propylene, it costs ca. 345 €/ton [6]. Because the feedstock cost accounts about 80% of the profited cost, the

realization of the direct (one step) oxidation of propane to acrylic acid would be economically very important [1, 2].

Due to the apparent attractiveness with respect to potential utilization of the low cost propane feedstock, considerable research activities were initiated in the last two decades for the selective oxidation of propane to acrylic acid. However, propane is less reactive than propylene, therefore, higher temperatures or more active catalysts are needed to activate it. The increase of temperature causes the increase of conversion, but usually also enhances the formation of side products (propionic and acetic acids) and/or total combustion products (CO and CO<sub>2</sub>), which results in the decrease of selectivity and yield of the process. Hence the development of an active and selective catalyst for the direct (one-step) transformation of propane to acrylic acid is still a challenging task [1-3]. Owing to the price difference between propane and propylene and the high performance of the two-stage propylene oxidation process, a yield of 50-60% would be needed for the one step propane oxidation process in order to replace the actual process.

## **1.2. Overview on the literature results**

The literature overview consists of five main parts. In the first part the propylene selective oxidation is presented, which is industrially applied. In the second part the main results concerning propane oxidative dehydrogenation are summarized. The third part concentrates on the one-step propane oxidation reaction. Here the current knowledge from literature about the reaction pathways, active sites and effects of the operating variables (acid-basic properties of the catalyst, feed composition) are presented. In the last two parts reactor design and reaction kinetic considerations are summarized. The motivations for the present study are outlined at the end of this chapter.

### **1.2.1. The selective oxidation of propylene**

The oxidation of propylene to acrolein has been studied on various catalysts, mainly on bismuth molybdates, Cu<sub>2</sub>O and multi-component metal oxides (i.e: SbSnO, CoMoTeO, NiMoTeO, VPTeO, etc.).

Based on structural considerations, kinetic studies, IR and Raman spectroscopic investigations, and reactivity studies using isotopically labeled feeds and intermediates, the organic reaction mechanism of propylene oxidation over bismuth molybdates has been proposed according to the scheme depicted in Figure 1.2.1 [7-9.]. The involvement of lattice oxygen atoms was postulated.

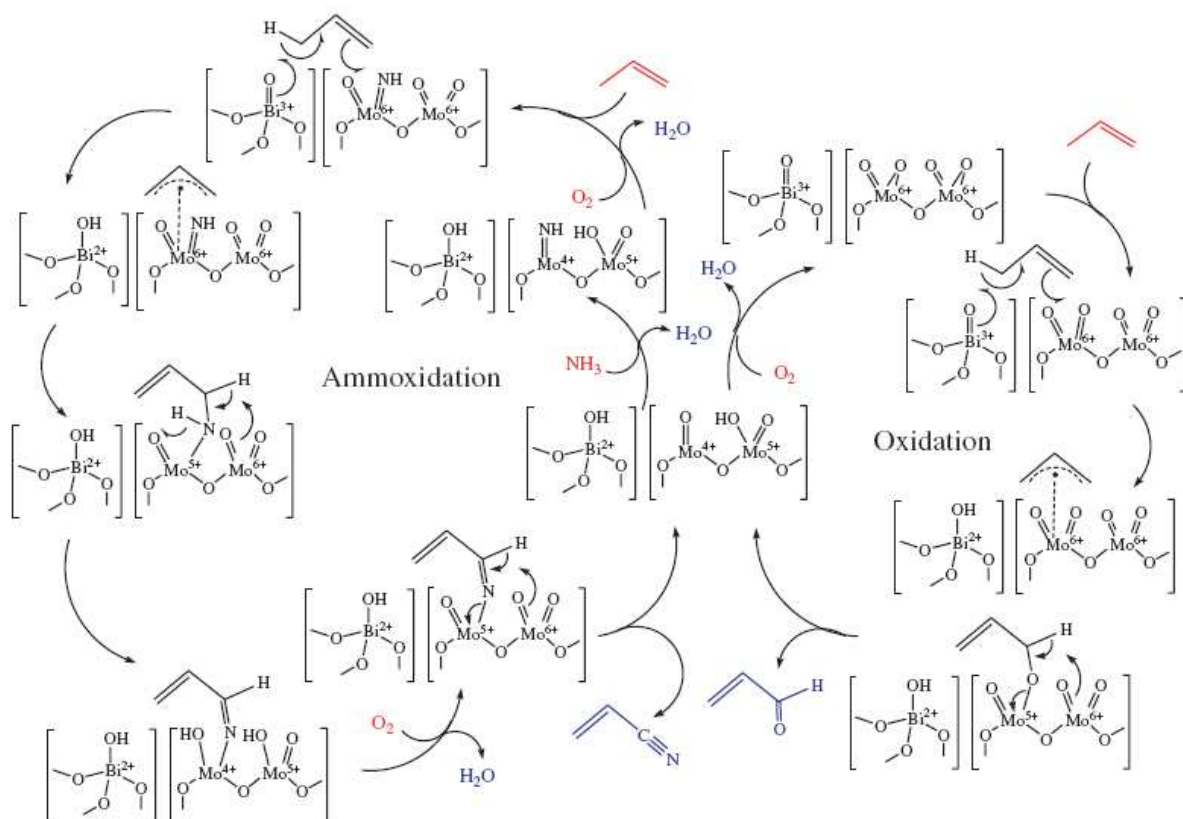


**Figure 1.2.1.** Propylene oxidation and ammoxidation mechanism over bismuth molybdate catalysts as proposed by Grasselli et al. [9].

According to the reaction mechanism depicted on Figure 1.2.1, propylene is chemisorbed on di-oxo molybdenum sites with molybdenum in the highest oxidation state. The C-H bonds in the methyl group of chemisorbed propylene are activated by withdrawing electron density towards the molybdenum atom. The rate determining step is the abstraction of an  $\alpha$ -methyl hydrogen atom as a  $\text{H}\cdot$  radical by an adjacent  $\text{Bi}^{3+}$  site forming an allyl radical adsorbed as a  $\pi$  complex on the Mo di-oxo species (homolytic C-H bond splitting). Oxygen insertion and abstraction of the second hydrogen atom occur on adjacent di-oxo Mo sites. The metal-oxo group attacks the allyl intermediate forming a  $\sigma$ -



According to Bettahar et al. [12], the reaction scheme demonstrated in Figure 1.2.2 may also be interpreted in terms of proton abstraction on basic Bi-O groups, leading to a symmetric  $\pi$ -allyl anionic intermediate coordinated to the molybdenum di-oxo species (heterolytic C-H bond splitting). The allyl-anion is subsequently oxidized to a  $\pi$ -allyl cation on a redox active site. Then the nucleophilic Mo-O group attacks the  $\pi$ -allyl cation and transforms it into  $\sigma$ -allylic alkoxide. This unsaturated oxygenated intermediate loses another H atom in a subsequent redox step and it is transformed into acrolein [12].

It was claimed that:

- The reaction steps are sequential ones, not simultaneous concerted steps. However, Bettahar et al. pointed out that the mechanism may also occur through a  $S_N2$  type mechanism by nucleophilic attack of the  $O^{2-}$  anion to the C=C bond concerted with hydride abstraction from the  $CH_3$  group [12].
- The reaction occurs on a specific ensemble Bi/Mo-site, there is no movement, desorption/re-adsorption of the intermediate species.
- The intermediates that appear after the rate determining step, are transformed instantly into other intermediates, or desorbed (the surface coverage of adspecies produced after the rate determining step is negligible).
- Gaseous  $O_2$  dissociates rapidly and re-oxidizes the vacancy, without forming adsorbed oxygen species [3].

The theoretical study on the propylene oxidation mechanism over Bi-Mo catalysts carried out by Jang et al. supported the experimental observations [13]. In order to determine the possible reaction routes, the thermodynamic quantities such as C-H bond dissociation enthalpies and free enthalpies were calculated using the density functional theory (DFT). The geometry of each considered structure was optimized. The vibrational frequencies were calculated from the Hessian matrices and used for calculation of zero-point energies and thermodynamic quantities (enthalpy and free enthalpy) of the reaction. The calculations of C-H bond dissociation enthalpies and free enthalpies revealed that the weakest bond in the propylene molecule is the methylene ( $C_\alpha-H_\alpha$ ) bond ( $\Delta G=+288.3$

kJ/mol). In order to determine the olefin activating site, the  $\alpha$ -hydrogen atom abstracting ability of both  $\text{Mo}_3\text{O}_9$  and  $\text{Bi}_4\text{O}_6$  clusters was investigated. All of the O-atoms in the  $\text{Bi}_4\text{O}_6$  structure are equivalent, however, in  $\text{Mo}_3\text{O}_9$  cluster there are two types of O atoms: bridging (Mo-O-Mo) and terminal ones (M=O). The free enthalpy of  $\text{C}_\alpha\text{-H}_\alpha$  activation on the two different Mo sites was calculated to be  $\Delta G=+179.1$  kJ/mol and  $\Delta G=+113.4$  kJ/mol, respectively, depending on whether the abstracted H-atom is linked to the terminal oxo-group (M=O) or to the bridging oxygen atom (Mo-O-Mo), respectively. Therefore, the bond activation by the terminal M=O group is thermodynamically favored. This is in accordance with the conclusions derived from the experimental observations. However, in both cases, the H-atom abstraction step is much too endothermic. The C-H bond cleavage on the  $\text{Bi}^{3+}$  site is even more endothermic, probably because the linking of hydrogen atom to the bridging O-atom leads to Bi-O cleavage, and the resulting structure is not favorable. In turn, the dissociative chemisorption of  $\text{O}_2$  oxidizes the  $\text{Bi}^{3+}$  site to  $\text{Bi}^{5+}$  (Reaction 1.2.1), on which the hydrogen atom abstraction is more favorable (Reaction 1.2.2).



The dissociative chemisorption of  $\text{O}_2$  was found to be enhanced by the presence of  $\text{Fe}^{2+}/\text{Fe}^{3+}$  redox couple. This is the explanation of the outstanding performance of Mo-Bi-Co-Fe-O catalyst, on which 90% conversion was attained, compared to only 20% conversion on binary bismuth-molybdates.

Furthermore, the calculations revealed that

- the allyl species is coordinated preferably to the Mo=O group,
- the oxygen insertion occurs at the Mo=O group to which the allyl species is coordinated,
- the second H-atom abstraction occurs at the adjacent Mo=O group, and subsequently the acrolein formed is desorbed,

- after the desorption of the water molecule, the reduced molybdenum site is re-oxidized by O<sub>2</sub> in an exothermic step.

In summary, the olefin activation was suggested to occur on the Bi-site, while the further chemical transformations occur on the Mo-sites.

### 1.2.2. Oxidative dehydrogenation of propane

Chen et al. carried out a kinetic analysis and isotopic tracer studies in order to identify the elementary steps in the ODH of propane [14, 15]. Three kinds of ZrO<sub>2</sub> supported MoO<sub>x</sub> catalysts were used, with different MoO<sub>3</sub> loadings and thermal pretreatment conditions (Table 1.2.1).

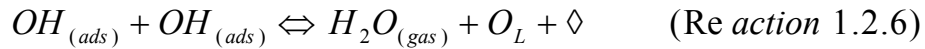
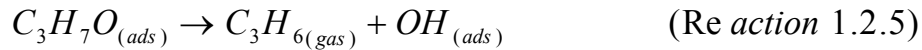
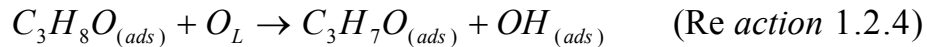
**Table 1.2.1.** The characteristics of catalysts studied in [14 ].

<b>catalyst</b>	<b>MoO<sub>3</sub> loading (wt %)</b>	<b>temperature of the thermal treatment (K)</b>	<b>structure of the Mo-species</b>
MoO <sub>x</sub> /ZrO <sub>2</sub>	11	773	MoO <sub>x</sub> oligomers
MoO <sub>3</sub> /ZrO <sub>2</sub>	37	673	bulk MoO <sub>3</sub>
ZrMo <sub>2</sub> O <sub>8</sub> /ZrO <sub>2</sub>	37	873	bulk ZrMo <sub>2</sub> O <sub>8</sub>

The catalytic tests were carried out in a quartz micro-reactor, using small amount of catalyst (0.020-0.100 g). Varying the flow rate, the conversions were held at low values, below 2% with respect to propane and 20% with respect to O<sub>2</sub>. The chemical and isotopic composition of products was analyzed using a GC-MS equipment. It was found that propylene is the most abundant product. The rate of propylene combustion was found to be 80 times higher than the rate of propane combustion. The rate law of propane oxidative dehydrogenation was found to be the same for all three catalysts. This fact suggested a similar mechanism. A first order kinetics with respect to propane and zeroth order with respect to oxygen was observed, when steam was not present in the initial gas mixture. The presence of steam inhibited the propylene production. Based on the

observations, the following mechanism for propane ODH over the ZrO<sub>2</sub> supported MoO<sub>x</sub> catalysts was proposed:

- The first step (Reaction 1.2.3.) is the rapid, non-dissociative adsorption of propane by interaction with lattice oxygen atoms (O<sub>L</sub>).
- The second step (Reaction 1.2.4.) is the C-H bond activation by H-atom abstraction from the adsorbed propane using a neighboring O<sub>L</sub>. A mixture of C<sub>3</sub>H<sub>8</sub> and C<sub>3</sub>D<sub>8</sub> underwent oxidative dehydrogenation without forming C<sub>3</sub>H<sub>8-x</sub>D<sub>x</sub> mixed isotopomers, suggesting that the steps involving C-H bond activation are irreversible.
- In the third step (Reaction 1.2.5) a hydrogen atom is removed from the methyl group, propylene and a surface hydroxyl group is formed.
- Two neighboring surface hydroxyl groups are recombining in the fourth step (Reaction 1.2.6), water is desorbed, and a vacancy is formed.
- The reoxidation of two neighboring vacancies by an oxygen molecule (Reaction 1.2.7) was suggested to close the catalytic cycle.



Reactions of <sup>18</sup>O<sub>2</sub>/C<sub>3</sub>H<sub>8</sub> on supported Mo<sup>16</sup>O<sub>x</sub> species lead to the preferential initial appearance of lattice <sup>16</sup>O atoms in H<sub>2</sub>O, CO, and CO<sub>2</sub> products, indicating that the lattice oxygen is required for C-H bond activation and for the ultimate oxidation of the adsorbed products. The kinetic isotopic effect of CH<sub>3</sub>CD<sub>2</sub>CH<sub>3</sub> with respect to CH<sub>3</sub>CH<sub>2</sub>CH<sub>3</sub> is 1.7, which is slightly smaller than the value of 2.3 obtained when using CD<sub>3</sub>CD<sub>2</sub>CD<sub>3</sub> and CH<sub>3</sub>CH<sub>2</sub>CH<sub>3</sub>. This finding was interpreted as both methyl and methylene groups can be involved in the rate determining step required for propane activation.

Based on the inhibitory effect of steam on propylene production, it was assumed that the recombination of the two OH-groups (reaction step 1.2.6) is reversible. The isotopic tracer study supported this assumption, as H-D exchange occurs readily between  $C_3H_6$  and  $D_2O$  or  $C_3D_6$  and  $H_2O$ , suggesting that OH recombination steps are reversible and quasi-equilibrated.

When a mixture of  $^{18}O$  and  $^{16}O$  was used as oxidant, the  $^{18}O^{16}O$  mixed isotopomer was not detected in the gas phase, suggesting an irreversible  $O_2$  dissociation step for the reoxidation of the reduced active site. However, it is notable that the reoxidation of the reduced site can not occur in a single step because it would require a four electron transfer from two reduced centers. Moreover, statistically it is not very probable that there are two reduced centers (vacancies) within the bond length of the oxygen molecule. Certainly, the electron transfer and breaking of the O-O bond should occur in consecutive steps.

Kinetic and isotopic studies of propane ODH over  $ZrO_2$  supported  $VO_x$  catalysts lead to the same observations described above [14-16]. First order kinetics with respect to  $C_3H_8$  was found on both the supported and bulk catalysts, when steam was not present in the initial gas mixture. The presence of water clearly inhibited the propane ODH and changed the reaction order with respect to propane and oxygen. Without  $H_2O$  in the initial gas mixture, zero order kinetics was observed with respect to  $O_2$ . In presence of steam, the rate of propylene formation was reduced considerably (by about 30%), and the partial reaction order of  $O_2$  was found to be greater than zero in this case. The elementary steps were considered to be identical with those for the ODH of propane over  $ZrO_2$  supported  $MoO_x$  catalyst. In this case, the lattice oxygen  $O_L$  was designated for  $V=O$  or  $V-O-V$  structures,  $OH_{(ads)}$  stands for  $V-O-H$  terminal hydroxyl group, while the vacancy ( $\diamond$ ) corresponding the reduced redox site ( $V^{4+}$  or  $V^{3+}$ ) [16]. Kinetic isotopic effect measurements demonstrated that the methylene C-H group is activated first.

Jibril studied the kinetics of ODH of propane on alumina supported metal-oxides, rare earth metal oxides and metal phosphates [17]. The temperature dependence of propane conversion was investigated; activation energies ( $E_A$ ) and logarithm of pre-exponential

factors ( $\ln A$ ) were evaluated. A compensation effect was noted, as significant linear correlation was found between the  $E_A$  and  $\ln A$  within the three groups of studied catalysts. The existence of the compensation effect in reactions catalyzed by similar catalysts suggests the same mechanism within the three groups of catalysts.

Fu et al. reported a detailed DFT study on the mechanism of propane activation over molybdenum oxide catalyst [18]. The  $\text{Mo}_3\text{O}_9$  cluster was chosen as a model for the catalyst. Two basis sets (6-31G\* and 6-31G\*\*) were tested for geometry optimization. No significant changes were found between the modeled geometries. 6 possible ways of C-H bond activation were considered:

- two kinds of 2+2 pathways, which involve the homolytic dissociation of the C-H bond at a Mo=O group, leading to carbide or hydride,
- 3+2 (homolytic dissociation on a O=Mo=O group) and 5+2 (homolytic dissociation on a O=Mo-O-Mo=O group) paths, both of them lead to hydroxyl- and alkoxy species directly,
- direct O atom insertion by a M=O group in the C-H bond, giving an alcohol,
- the 2+4 pathway involves linking of both the methyl and methylene C-H bonds simultaneously to the M=O group,
- hydrogen atom abstraction that may occur theoretically either from methyl or methylene group, leading to n-propyl or iso-propyl radical.

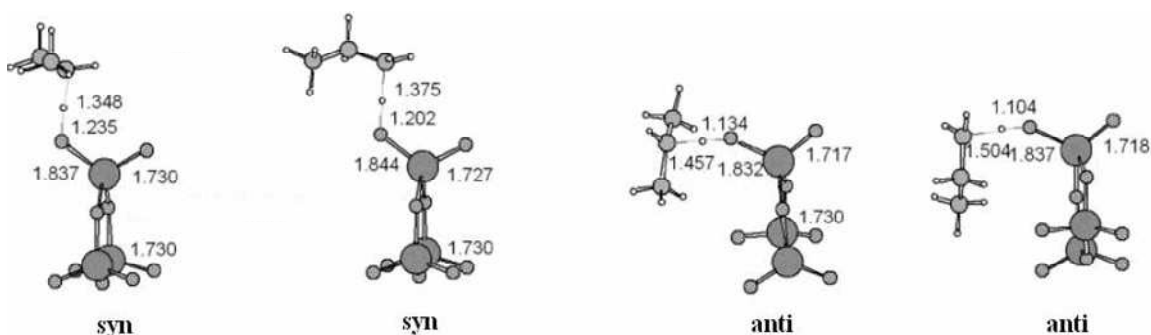


**Figure 1.2.3.** Some examples of the possible transitional states of hydrogen atom abstraction according to [18]. The numbers on the figures correspond to the calculated bond lengths.

17 different transitional states were taken into account. The free enthalpy of activation for each case ( $\Delta G^\ddagger$ ) was estimated at 688 K and the rate constants were evaluated according to the Eyring equation. In order to compare directly the calculated and the experimental findings of the isotopic tracer studies reported by Chen et al. [15], the kinetic isotopic effect for each considered reaction pathway was also estimated using the transitional state theory.

The hydrogen abstraction pathways were considered to be one electron processes, leading to radicals. The energy barriers for these pathways were found to be the lowest among the considered ones. This indicated that the probability of hydrogen atom abstraction is much higher, than the occurrence of other two-electron processes. The propane molecule may approach the Mo=O group in *syn* or *anti* position (Figure 1.2.3). Only one of the terminal Mo=O group is involved in the process, the another one is a spectator group.

The calculated activation enthalpy values revealed that the *anti*-modes are favored against the *syn*-modes, by 25.1-29.3 kJ/mol (Table 1.2.2).

**Table 1.2.2.** The calculated thermodynamic quantities of the supposed hydrogen atom abstraction pathways, in comparison with the experimentally determined values [18].

Type of C-H cleavage	$\Delta H^\ddagger$ (kJ/mol)	$\Delta S^\ddagger$ (J/mol·K)	$\Delta H_r$ (kJ/mol)
-CH <sub>2</sub> - <i>syn</i>	164.0	-105.9	133.5
-CH <sub>3</sub> <i>syn</i>	180.3	-100.4	154.4
<b>-CH<sub>2</sub>- <i>anti</i></b>	<b>135.1</b>	<b>-119.7</b>	133.5
-CH <sub>3</sub> <i>anti</i>	154.8	-123.0	154.4
<b>-CH<sub>2</sub>- experimental</b>	<b>117.2</b>	<b>-121.8</b>	-

It was also pointed out that breaking the methylene C-H bond is more favorable, than breaking of the methyl C-H bond. The difference of 16.3-19.7 kJ/mol in the activation enthalpy could be assigned to the differences in bond strengths. The reasonable agreement between the calculated and experimental activation parameters corresponding to the methylene C-H bond suggests that the theoretical description of the experimental observation is good. It is also notable that the calculation overestimated the kinetic isotopic effect compared to the experimental data reported by Chen et al. [15], but some indications were found that both methyl and methylene hydrogen atoms are involved.

### 1.2.3. The direct oxidation of propane to acrylic acid

#### 1.2.3.1. Generalities

Different types of catalysts were tested for the activation of propane. The most efficient catalyst class is represented by the systems based on reducible (typically transition) metal oxides.  $V_2O_5$  and  $MoO_3$  are versatile catalysts for organic compound oxidation, because they lose oxygen reversibly [19]. The most investigated catalytic materials within this class are vanadium phosphorous oxides (VPO), heteropoly compounds (HPCs), and multi-component mixed oxides (MMOs) [2-4]. The performance of these catalysts in terms of propane conversion, selectivity and yield to acrylic acid is summarized in the Table 1.2.3.

**Table 1.2.3.** Optimized catalytic performance of VPO, HPC and MMO catalyst systems for oxidation of propane to acrylic acid, as summarized based on references [2] and [4].

Catalyst		T(°C)	X <sub>C3</sub> (%)	S <sub>AA</sub> (%)	Y <sub>AA</sub> (%)
VPO	VPO (P:V=1:1)	420	46	32	14.7
	VPO (P:V=1:1)	400	23	48	11.2
	0,01% Ce – VPO	390	28	68	18.8
HPC	H <sub>2</sub> (VO) <sub>0,5</sub> (2,2-bipy)PMo <sub>12</sub> O <sub>40</sub>	400	50.4	21.5	10.8
	Nb(pyridine)-PMo <sub>11</sub> VO <sub>40</sub>	380	21	49	10.3
	20% H <sub>x</sub> Cu <sub>0,6</sub> Cr <sub>0,6</sub> PMoV <sub>2</sub> AsO <sub>40</sub> /SiO <sub>2</sub>	390	38	39	14.8
MMO	MoV <sub>0,3</sub> Te <sub>0,23</sub> Nb <sub>0,12</sub> O <sub>n</sub>	380	84	63	53
	MoV <sub>0,3</sub> Te <sub>0,23</sub> Nb <sub>0,12</sub> O <sub>n</sub>	380	80	60	48

Table 1.2.3 indicates that the highest conversions of propane and the highest selectivities for acrylic acid were achieved on MoVTeNbO<sub>x</sub> catalysts, originally patented by Mitsubishi [20, 21]. This catalyst is also active and selective for propane ammoxidation; suggesting that there are some common steps in the partial oxidation and ammoxidation reactions [2-4].

### 1.2.3.2. Identification of propane selective oxidation pathways

The early ideas about the mechanism of the propane selective oxidation reaction were summarized by Bettahar et al. [12]. The theoretical network of reaction steps in selective oxidation of propane is shown in Figure 1.2.4. This reaction network was supported mainly by thermodynamic considerations. However, the thermodynamic calculations on the reaction enthalpy were performed at normal conditions and not reaction conditions. Too less catalytic and kinetic evidences were known for this reaction network.

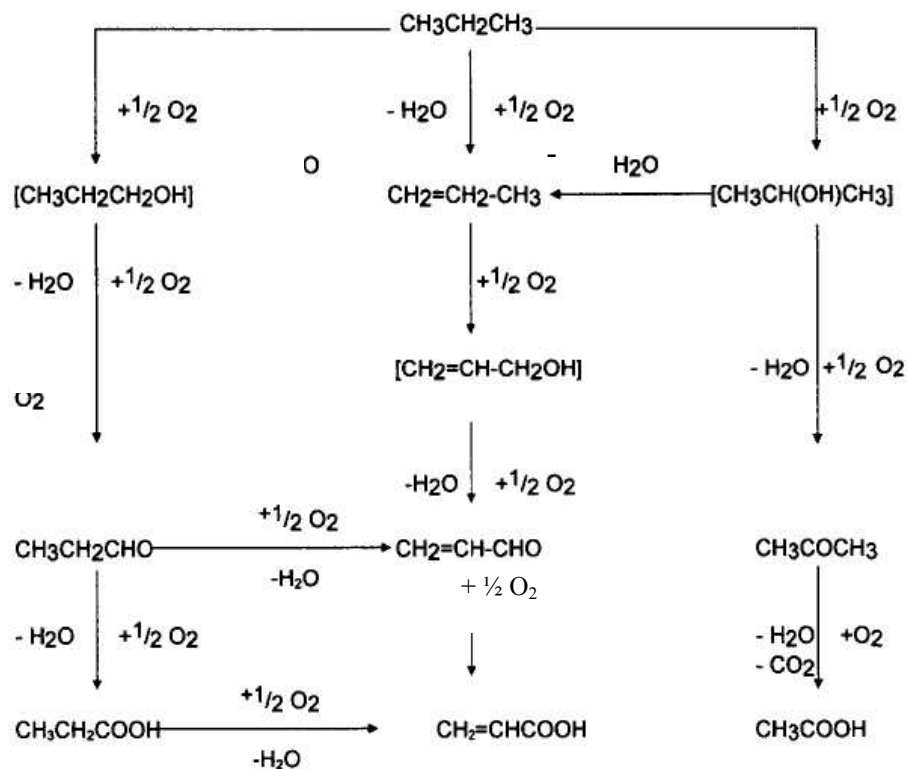
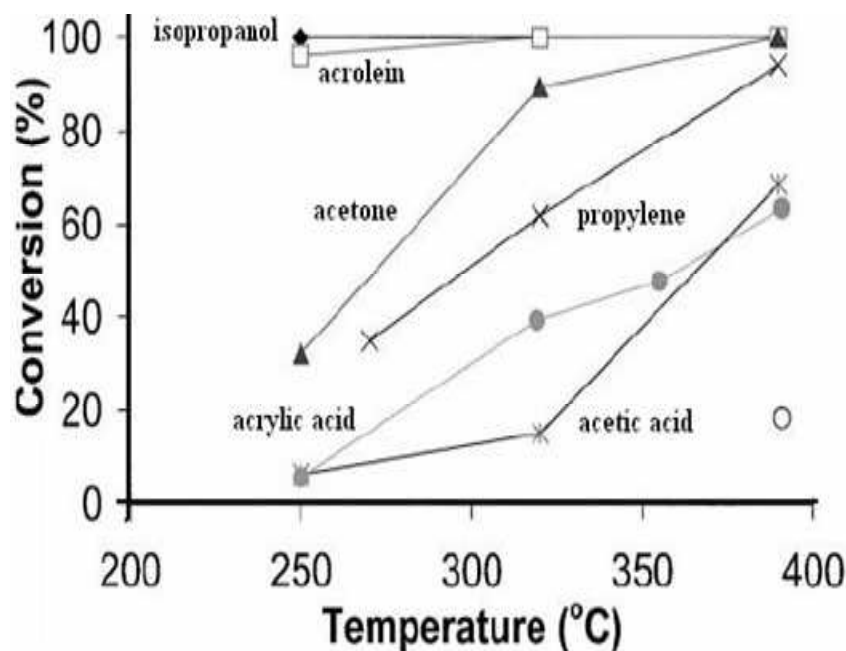


Figure 1.2.4. Reaction network of propane oxidation according to Bettahar et al. [12].

Lin et al. studied the reaction pathways of the selective oxidation of propane over a  $\text{MoVTeNbO}_x$  catalyst [22]. They prepared the catalyst according to the method described in the patent literature [20, 21]. The catalyst characterization indicated the following composition:  $\text{MoV}_{0.25}\text{Te}_{0.18}\text{Nb}_{0.09}\text{O}_x$  (bulk composition, determined by XRF) and  $\text{MoV}_{0.3}\text{Te}_{0.19}\text{Nb}_{0.15}\text{O}_x$  (surface composition determined by XPS). The BET surface area

was  $3.6 \text{ m}^2/\text{g}$ , while the mean pore diameter was found to be  $180 \text{ \AA}$ . The SEM images revealed primary sub-micron particles and their aggregates. XRD peaks were found at  $2\cdot\Theta=22.4^\circ$ ;  $28.6^\circ$ ;  $36.6^\circ$ ;  $45.4^\circ$  and  $50.4^\circ$ , respectively, which are in accordance with the peaks reported by Ushikubo [20, 21]. The catalytic test was carried out at the reaction temperature of  $391^\circ\text{C}$ , with initial feed composition  $\text{C}_3\text{H}_8$ : air:  $\text{H}_2\text{O} = 3$ : 50: 47 vol%, at  $\text{GHSV}=1200 \text{ h}^{-1}$ . Under these conditions, 18% propane conversion was attained, the selectivity for acrylic acid was 26%, and  $\text{CO}_x$ , acetic acid and acetone were produced with 54, 8 and 1% selectivity, respectively. The presence of propylene and acrolein in the outflow gas mixture was not observed.

In order to elucidate the propane oxidation pathways, the relative reactivities of oxidation products and of potential intermediates were studied (Figure 1.2.5). The ranking order of the reactivity was found to be: propane  $\ll$  acetic acid  $\approx$  acrylic acid  $<$  propylene  $<$  acetone  $<$  acrolein  $\approx$  isopropanol.



**Figure 1.2.5.** The relative oxidative stability of several intermediates at different temperatures [22].

The acrolein, acetone, isopropanol and propylene were found to be very reactive at around  $390^\circ\text{C}$ . Based on this observation the authors argued that this is the reason why these intermediates can not be detected during the partial oxidation of propane to acrylic

acid. It is to be noted, that the real reactivity of the isopropanol, acrolein and acetone can not be observed from the above plot, because the conversions reach 100% at around 390°C.

The product distribution upon oxidation of the above compounds was the following. The acetone oxidation over the catalyst produced acetic acid at lower temperatures and CO<sub>x</sub> at higher temperatures. The oxidation of acrolein produced acrylic acid and CO<sub>x</sub>. At higher temperatures, a small amount of acetic acid was also detected. The acetic acid was believed to be a product of the oxidative degradation of acrylic acid.

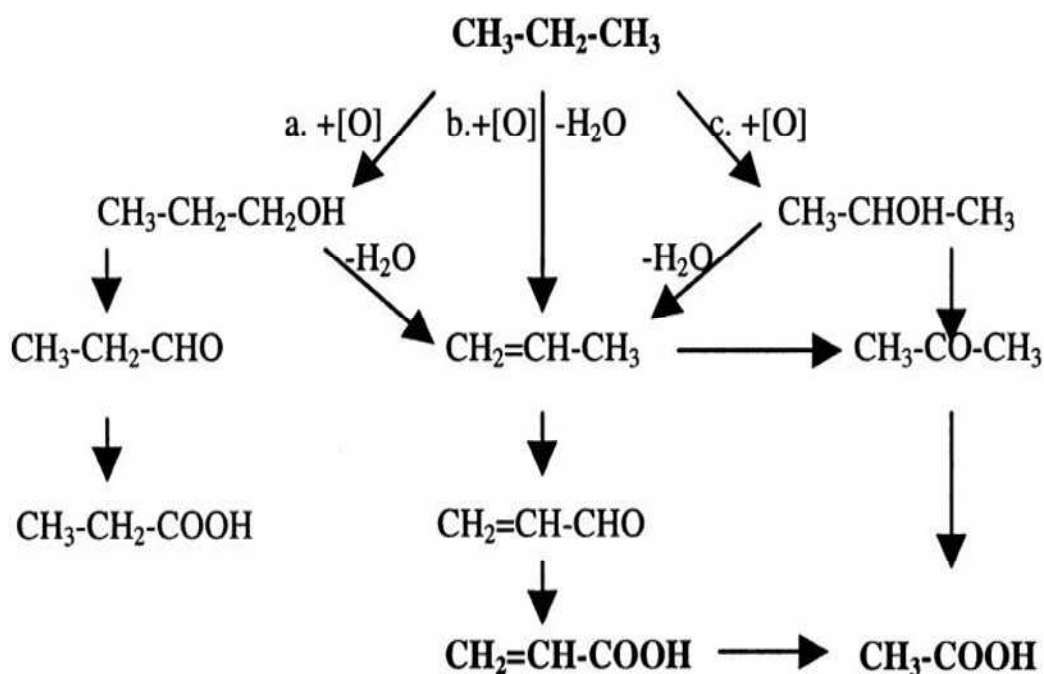


**Figure 1.2.6.** Oxidation pathways of propane according to [22].

A more complicated profile consisting of parallel and consecutive steps was found for propylene oxidation: at higher temperatures the propylene→acrolein→acrylic acid was favored, while at lower temperatures acetone and subsequently acetic acid were produced in larger amounts.

The isopropanol reacted also via two competing pathways: the dehydration lead to propylene, while the oxidation produced acetone. At higher temperatures, the propylene pathway was found to be favored, and the selectivity to acrylic acid was higher in this case.

The product of oxidative degradation of acrylic acid was found to be acetic acid and  $\text{CO}_x$  as also shown by Vitry et al. [23]. During the oxidation of acetic acid, only carbon oxides were detected.

Based on these observations, a reaction scheme of propane oxidation was proposed (Figure 1.2.6). The pathways (a) and (c) leading to n-propanol and isopropanol are in conflict with the experimental and theoretical findings [12-16]. These alcohols were believed to undergo dehydration to propylene and oxidation to the corresponding carbonyl compounds and carboxylic acids, respectively, according to the above scheme. During the catalytic oxidation of propane, however, n-propanol, propionaldehyde and propionic acid were not detected at all. Therefore, path (a) was regarded as not to be probable. Path (b) is a direct oxidative dehydrogenation of propane to propylene, followed by oxidation to acrylic acid through acrolein. The latter pathway was regarded to be more likely, because the product distribution patterns of propane and propylene oxidation are similar, while that of isopropanol are significantly different.

Similar reactivity studies were undertaken by Luo et al., including the oxidation of n-propanol and propanal as potential intermediates [24]. Basically, the same reaction pathway was proposed as the one shown above (Figure 1.2.6).

Based on gas phase analysis at different residence times the reaction sequence propane→propene→acrolein→acrylic acid has also been proposed on  $\text{MoVSbNbO}_x$  catalysts [25]. The acetic acid obtained on these catalysts was assumed to be formed via propene→acetone. The main function of water on  $\text{MoVSbNbO}_x$  catalysts was assigned to its role in preserving the metals in a partially reduced oxidation state [26].

Kinetic studies on the partial oxidation of propane to acrylic acid over egg-shell type  $\text{MoV}_{0.33}\text{Te}_{0.22}\text{Nb}_{0.11}\text{O}_x$  catalysts containing 10 to 20% active mass on spherical steatite have been performed by Balcells et al. and Griftede [27, 28]. From the characteristic shapes of the selectivities vs. propane conversion plots, propene was considered to be the only primary product, which is in agreement with the previous studies. The low propylene concentrations observed in the gas phase was regarded to be the indication that

the oxidative dehydrogenation of propane is the rate determining step. A simple system of differential equations containing first order rate expressions with respect to the organic compounds was set up. However, the carbon monoxide, carbon dioxide and acetic acid were considered as three carbon atom containing pseudo-products and merged under the term “byproducts”. Although the calculated results were in a good agreement with the experimental data, the model proposed by Griftede seems to be too abstract, because it assumes that the three byproducts are formed in a coupled reaction step.

The reaction scheme of propene on the same catalyst was found to be more complex, including acrolein, acetone and acetic acid as detectable intermediates/by-products. The model proposed for propylene oxidation was based the same assumption as the model proposed for propane oxidation. The influence of temperature, oxygen concentration and water content on propane oxidation was studied. Only a small influence of the oxygen concentration was observed. Concerning the reactor operation, a steam content of about 20-30 vol-% was recommended.

The reaction network of selective oxidation of propene on mixed oxide catalysts (MoVNbO, MoVSbO and MoVTeNbO) was also investigated by Concepción et al. [29]. FTIR measurements of propylene adsorption/desorption over these catalysts suggested three different intermediates:

- a symmetric  $\pi$ -allylic species, which is formed if  $\alpha$ -hydrogen abstraction sites (i.e.  $\text{Sb}^{3+}$  or  $\text{Te}^{4+}$ ) are present. The  $\pi$ -allylic species represent the intermediate in the selective oxidation of propylene to acrylic acid by a redox mechanism,
- an enolic-type intermediate in the hydration/oxidation of the olefin to form acetone and acetic acid on Brønsted acid sites,
- a  $\pi$ -bonded propylene species interacting with Lewis acid sites, which is regarded as a precursor in the deep oxidation of propylene.

Fushimi et al. has carried out catalytic studies on  $\text{MoV}_{0.3}\text{Te}_{0.23}\text{Nb}_{0.17}\text{O}_x$  over a wide range of temperatures, feed compositions and contact times [30]. Steady-state (space velocity

and temperature variation) and non steady-state experiments (pulse-response temporal analysis of the products) were carried out. The temperature variation experiment was done by increasing the reaction temperature up to 400°C followed by a controlled cooling. In this temperature programmed reaction, complete oxygen conversion was observed at around 400°C. More important, a hysteresis phenomenon of the product yields was observed during the cooling when using stoichiometric and reducing feed compositions. The hysteresis phenomenon was accounted for the effect of nonlinearity of the kinetics and adsorption-desorption of the intermediates and products. However, no hysteresis was observed when using net oxidizing feed. The apparent activation energies of acrylic acid formation were determined to be 73 and 186 kJ/mol, depending on feed composition and contact time, respectively.

Based on transient experiments, a complicated reaction network was proposed. The main reaction pathway consists of propane→propylene→acrolein→acrylic acid→CO+CO<sub>2</sub> steps. The TAP experiments indicated that water reacts with the adsorbed acrolein to form acrylic acid. The unselective pathways corresponding to total oxidation of propylene, allylic intermediate and acrylic acid were proposed for the production of CO, CO<sub>2</sub> and acetic acid. Since no differentiation was made between the pathways leading to these products, the model has the same restrictions like the one proposed by Griβtede [27, 28].

The effect of CO<sub>2</sub> initial concentration added to the initial feed was also studied in the interval between 0 and 50 vol% (Figure 1.2.7). The results revealed an approximately linear increase of the acrylic acid yield with the initial CO<sub>2</sub> content in the feed. Without experimental evidence, the positive effect of the higher CO<sub>2</sub> concentrations was accounted for the adsorption of CO<sub>2</sub> on the active sites and/or formation of an intermediate that favors the selective pathway.

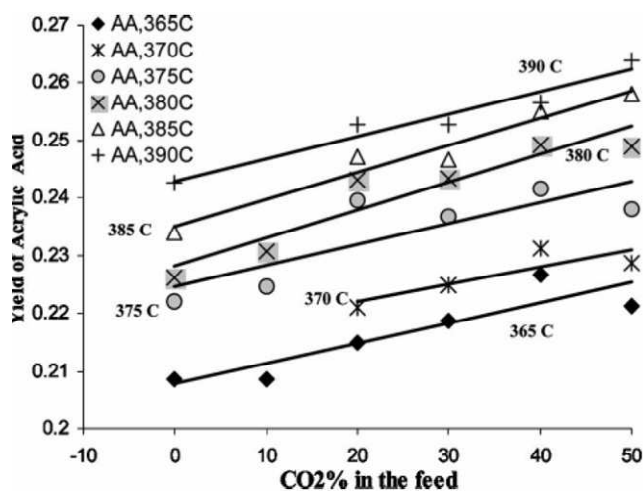


Figure 1.2.7. Effect of CO<sub>2</sub> on the acrylic acid yield [30].

Redox pulse experiments on MoVTeNbO<sub>x</sub>, carried out by Grasselli et al. in absence of O<sub>2, (gas)</sub> revealed that the oxidation of the propane occurs even under this condition. The catalyst remained in the reduced state without a structural collapse. The reduced catalyst could be re-oxidized in presence of O<sub>2</sub>. The authors claimed this finding as a confirmation of the direct involvement of lattice oxygen in (amm)oxidation process [31].

### 1.2.3.3. Active sites on MoVTeNbO<sub>x</sub> catalysts

MoVTeNbO<sub>x</sub> catalysts are generally composed of two crystalline phases [32]:

- an orthorhombic, active and selective phase (M1)
- an orthorhombic, much less active but selective phase (M2)

Propane activation and high selectivities towards acrylic acid are generally attributed to the presence of the orthorhombic M1 phase [33, 34].

A synergistic effect in activity and selectivity for (amm)oxidation of propane was claimed for the nano-scale mixture of M1 and M2. The synergistic effect was not observed for physical mixtures of the phases (Table 1.2.4) [2, 9, 31]. However, it is to be noted that the selectivities were compared at very different propane conversions. Moreover, the M2 catalyst was tested at 410°C, while the M1 and the phase mixture at

380°C. It is well known that the selectivity depends on the conversion of propane. Therefore, the conclusions concerning the synergistic effect are questionable.

**Table 1.2.4.** Catalytic effect of the individual phases of the mixture in the propane partial oxidation [2].

Catalyst	T(°C)	X <sub>C3</sub> (%)	S <sub>AA</sub> (%)
M1	380	27.9	52
M2	410	0.6	22
M1+M2	380	34.9	53

The function of the individual catalysts components has been assigned by López-Nieto according to the schema given in Figure 1.2.8 [35]. The transformation of propane to propylene was suggested to occur on the V=O adjacent to Mo or Nb-sites. The further oxidation of propylene to acrolein was believed to occur on Te-sites, while the oxidation of acrolein to acrylic acid on the V- or Nb-sites adjacent to Mo-site. However, the model does not explain the formation of acetic acid, CO and CO<sub>2</sub>. It is also notable that the catalyst used by López-Nieto was a phase mixture [35].

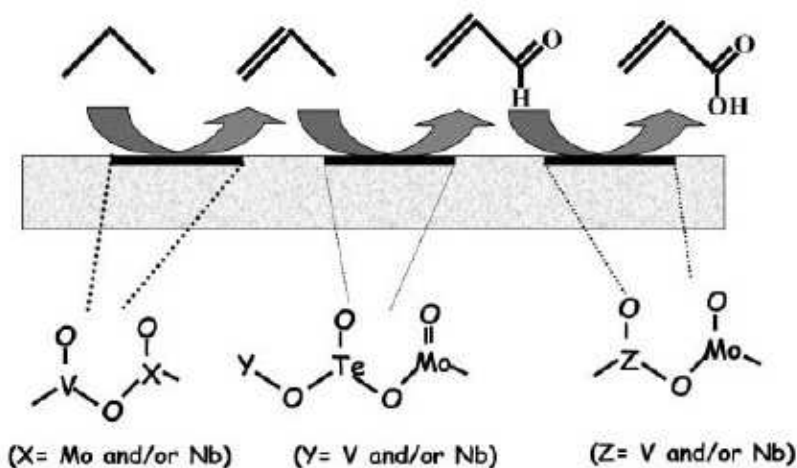


**Figure 1.2.8.** Reaction steps and nature of active and selective sites in the oxidation of propane to acrylic acid on MoVTeNbO<sub>x</sub> catalysts [35].

Three single-phase M1 catalysts having different elemental compositions,  $\text{MoVO}_x$ ,  $\text{MoVTeO}_x$  and  $\text{MoVTeNbO}_x$ , have been prepared hydrothermally by Ueda et al. [34]. On the basis of the catalytic results in propane oxidation, it was concluded that

1. crystallinity seems to be necessary for selective oxidation of propane to acrylic acid,
2. the propane molecule is oxidized to propene over surface active sites composed of octahedrally coordinated Mo and V units located in the unique heptagonal arrangement of the M1 structure,
3. when Te is incorporated into the network, the resulting catalyst becomes selective for the formation of acrylic acid without changing intrinsic oxidation activity of Mo and V sites,
4. Nb prevents the over-oxidation of acrylic acid by its site isolation effect.

Without experimental evidence, the propane activating property of the M1 phase was assigned by Grasselli et al. to  $\text{V}^{5+}$  centers which favor the radical-type H-atom abstraction, leading to a secondary propyl-radical [9, 31]. The second H-atom abstraction occurs on the  $\text{Te}^{4+}$ -center next to the  $\text{V}^{5+}$ -center. The  $\text{Nb}^{5+}$ -center stabilizes the primary active centers and separates them spatially from each other. The formed olefin coordinates to the  $\text{Mo}^{6+}$ -center, where the O or N atom is inserted via another H-atom abstraction on the adjacent  $\text{Te}^{4+}$ -center of the M2 phase. Therefore the M2 phase is considered to contribute to the selective olefin conversion toward the desired product. Because  $\text{V}^{5+}$  centers are not available in M2 phase, it cannot activate propane. On the other hand, the excellent performance of propylene conversion of the M2 phase is accounted for the rather high number of  $\alpha$ -H-atom abstracting  $\text{Te}^{4+}$ -sites. However, the presence of active centers is not sufficient; the catalytic performance depends in a crucial manner on the surface geometry of the active sites and the redox properties of the catalyst.

Gulians et al. has studied the catalytic performance of a nano-crystalline Mo-V-O M1 phase [36]. The original Mo-V-O was practically unselective in propane oxidation; however a significant improvement in selectivity was observed when Te-, Nb- and Sb-oxides were supported on the surface at sub-monolayer coverage. Low-energy ion

scattering (LEIS) study of the submonolayer coverage indicated that Nb species were preferentially located at the topmost surface, while the subsurface Te- and Sb concentrations declined gradually into the bulk. The highest selectivity was observed when both Nb and Te (or Sb) oxide species were present at the surface. In general, the selectivity was comparable to those observed on bulk MoVMO<sub>x</sub> catalysts (M=Te, Nb, or Sb).

**Table 1.2.5.** Activation energy of propane partial oxidation on different surface-promoted catalysts [36].

Promoter	E <sub>A</sub> (kJ/mol)	Promoter	E <sub>A</sub> (kJ/mol)
none	74	Nb	72
Te	125	Nb+Te	108
Sb	62	Nb+Sb	79

The effect of temperature and space velocity was studied on the conversion, selectivity and yield. The apparent activation energies of propane conversion were determined (Table 1.2.5). Interestingly, only the inclusion of Sb led to a decrease, while promotion by Te led to a net increase in the apparent activation energy. The niobium barely had any effect on the activation energy. The inclusion of Nb besides Te led to a catalyst on which the apparent activation energy of propane was still considerably higher than for the unpromoted and the Nb-modified catalyst. Even though Nb and Sb promotion alone decreased slightly the activation energy, the simultaneous presence of Nb and Sb led to a slight increase of the activation energy.

Zhu et al. modified selectively the V<sup>5+</sup>/V<sup>4+</sup> ratio in the MoVTeO catalyst by adjusting the acidity of the precursor solution [37]. The solutions were evaporated and calcined at 873 K in N<sub>2</sub> stream, to obtain the catalyst. XPS measurements suggested that the number of surface V<sup>5+</sup> were preferentially enhanced by addition of pH adjustors in the precursor solution. The high number of surface V<sup>5+</sup> sites (<sup>5+</sup>V=O groups) was claimed to be responsible for propane activation, while the bulk V<sup>4+</sup> was suggested to play a significant role in promoting electron- and oxygen atom transfer during the reaction. The authors

claimed that the bulk  $V^{5+}/V^{4+}$  ratio is also important, as higher number of  $V^{4+}$  sites facilitate the total oxidation, while less  $V^{4+}$  sites resulted in a high selectivity to acrolein.

#### 1.2.3.4. The effect of acid-base character of the catalyst

Besides the redox properties of the transition metal oxide catalysts, the acidity/basicity also plays a significant role in the oxidation reactions. The ideal surface structure of an oxide, as generated by cutting the crystal at a specific crystal plane, is composed by an array of cations (Lewis acid site) and lattice oxygen anions (basic site). The acidic character of the cations and the basicity of lattice oxygen depend on the ionic character of the metal-oxygen bonds [38].

The metal-oxygen bond in oxides of transitional metals with high oxidation state ( $Mo^{6+}$ ,  $V^{5+}$ ) is rather covalent, thus they are acidic oxides. On the other hand, the same elements in the lower oxidation state have more ionic character and they behave as basic oxides.

The acid-base characteristics of the oxide have a major effect on the activation of the reactants, the relative rates of the competitive pathways, and the rate of adsorption/desorption of the reactants and products. The relatively weak Lewis acidity is a key parameter that determines the oxygenate formation. The Brønsted acidity is important in propane activation; however, strong Brønsted acidity favors the hydration of propylene to isopropanol which may be oxidized to acetone and acetic acid. Controlling the Lewis/Brønsted acidity of the catalyst is also connected with the effect of steam on the catalyst activity. In general it is stated that by blocking Brønsted acid sites with water or ammonia the over-oxidation is reduced and favors acrylic acid formation [2, 3].

Many attempts to correlate the catalyst activity with the redox and acid-base properties were reported in the literature. Due to the fact, that that the redox and acid-base characteristics are not independent, Novakova et al. and Centi pointed out that these correlations are not generally valid [2, 3]. A careful study of these characteristics on the individual reaction steps rather than on the global behavior of the whole reacting system was recommended [3].

### 1.2.3.5. The effect of steam

The introduction of steam in the feed mixture inhibits the oxidative dehydrogenation of propane over  $ZrO_2$  supported  $MoO_x$  and  $VO_x$  catalysts [14-16].

In contrast to that, the presence of steam in the feed was noted to be essential for the formation of acrylic acid from propane over Mo and V based catalysts [26, 27, 28, 39].

Novakova et al. noted that the steam content affects on the kinetics of propane oxidation over a phase mixture  $MoVNbSbO_x$  catalyst [26]. The rate of acrylic and acetic acid formation increases strongly in the steam content interval between 0 and 20 vol%, and the rates leveled off above 20 vol% steam content. It was also noted that the presence of steam influences the apparent activation energy of propane consumption. At a steam content of 25 vol% a value of 50 kJ/mol was determined, while in dry feed the apparent activation energy was found to be 68 kJ/mol. It was observed that in absence of steam an irreversible phase change occurs, accompanied by deactivation of the catalyst: upon addition of steam after performing the experiment in dry feed, neither the original phase composition nor the initial catalytic activity was attained. It was noted that the deactivation was a relatively fast process, which completed in ca. 50 minutes.

Griβtede has carried out a kinetic study on the steam effect on propane oxidation over  $MoV_{0.33}Te_{0.25}Nb_{0.17}O_x$  catalyst deposited on steatite balls [27, 28]. It was found that in the presence of 50 vol% steam the rate constant of propane consumption increased by a factor of 2.4, while the propylene further oxidation rate constant increased by a factor of 4.4 compared to the experiment performed in dry feed. The selectivity to acrylic acid was only 50%, while the oxidative stability (i.e. the ratio between the formation and further oxidation rate constants) of acrylic acid was found to be 13 in dry feed. Upon introducing 50 vol% steam in the feed, the selectivity increased to 80% and the oxidative stability was also improved to 32. Similarly to the results given by Novakova [26], the conversion and selectivity increased in the steam concentration interval between 0 and 20 vol% and leveled off at concentrations higher than 20 vol%. The positive effect of the steam on the productivity was accounted for the faster desorption rate of the product. However, no experimental evidence was given for this assumption. On the other hand, as a second

possibility the modification of the phase composition in presence of steam was highlighted. This possibility was speculated based on the observation that the pretreatment of the catalyst in the reactor using steam containing a gas mixture (50 vol% H<sub>2</sub>O and 50 vol% N<sub>2</sub> at 140°C for 24 hours) lead to a better performances (S<sub>AA</sub>=80%) compared to the experiment in which the reaction was started without pretreatment. When the catalyst was pretreated with a 10 vol% steam containing mixture, the highest acrylic acid selectivity was found to be only 40%. However, the catalyst was not characterized by XRD either before or after the pretreatment or catalytic experiment in order to support the assumption concerning the phase change.

Dubois et al. patented a method for preparation of acrylic acid by selective oxidation of propane over MoVTe(Sb)Nb(Ta)SiO<sub>x</sub> catalysts in fluidized bed without steam in the feed [40]. They noted that the presence of steam favored the formation of acetone, acetic acid and propanoic acid, however the latter was produced in very small amounts (below 1%). The catalyst activity was not decreased after 24 h on stream, in contrast to the deactivation phenomenon noted by Novakova et al. The conversion was below 30% in all cases, while the highest selectivity toward acrylic acid was about 40%.

Landi et al. studied the effect of water on propane oxidation over (VO)<sub>2</sub>P<sub>2</sub>O<sub>7</sub> catalyst [41-43]. The catalytic testing was started using dry feed at 430°C, the acrylic acid selectivity was very low. When stable catalytic operation was reached, the temperature was decreased to 400°C and, 20 vol% steam was introduced in the feed. The propane conversion decreased in presence of steam, while the acrylic acid selectivity increased compared to the steam free feed. Stable operation in steam containing feed was reached in about 40 hours time on stream. Steady-state and dynamic experiments carried out at different steam contents revealed that the activity and selectivity changed reversibly with the steam content, but stable operation was reached in 6-12 hours time on stream. The propane conversion decreased monotonically with the steam content, while the maximum acrylic acid selectivity was attained at 15 vol% steam content.

The characterization of the catalyst lead to the conclusion that the presence of steam

enhances the crystallinity, promotes the disappearance of  $V^{5+}$  containing phase and reduces the number and strength of surface acid sites.

Based on the literature records, the possible effect of steam can be summarized as follows:

Physical interaction of water with the catalyst:

- competitively adsorbs with  $C_3H_8$  and intermediates on the active sites and/or blocks the Lewis acid sites or modifies the ratio of Lewis/Brønsted acidity [3, 39, 41-45]
- enhances the desorption of oxygenates [28, 39, 46-50].

Chemical interaction of water with the catalyst:

- changes the oxidation state/composition of the M1 MoVTaNbO<sub>x</sub> catalyst [51],
- increases the number of Brønsted acid sites [46]
- increases the number of surface hydroxyl groups [14, 15, 45, 52]
- induces phase change [26, 52, 53], enhances the crystallinity [41-43, 53].

Chemical interaction of water with the adsorbed reaction intermediates:

- the water could act as both a nucleophilic and oxidizing reactant in the formation of the acrylic acid from the acrolein [3, 30]
- in presence of water, different reaction pathways are possible, i.e. the propylene intermediate may undergo hydration to 2-propanol on the acid sites, followed by oxidation to acetone and acetic acid [3, 54].

#### **1.2.3.6. The effect of redox potential of gas phase and oxygen species**

The redox potential of the gas mixture depends on the propane:oxygen ratio. Due to the stoichiometry of the propane to acrylic acid reaction, the ratio of 1:2 is defined as stoichiometric. When the propane:oxygen ratio is smaller than 1:2 the gas mixture is

rather reducing. Finally, if this ratio is higher than 1:2, the feed is net oxidizing. In the literature various feed compositions were used from reducing ( $C_3H_8/O_2=6,5/10$ ) [33, 34, 36], stoichiometric [20, 21, 51] to strongly oxidizing ( $C_3H_8/O_2$  ratio ranging from 0,8/31,4 to 2,6/97,4) [47, 48]. However, only a few studies were concentrated on finding out the effect the redox potential on the catalytic properties.

Grißtede has carried out a kinetic study on the effect of oxygen using the  $MoV_{0.33}Te_{0.25}Nb_{0.17}O_x$  catalyst. Only oxidizing feed compositions were used ( $C_3H_8/O_2$  equal to 2/6, 2/9 and 2/20 vol%, respectively) [28]. The concentration profiles, conversion and selectivities were found to be the same irrespectively on the oxygen concentration. From this observation it was argued that the reaction is 0th order with respect to oxygen. In connection to the steam effect it was also argued that the steam does not enhance the reoxidation rate becausee of the 0th order kinetics involving the oxygen.

Zheng et al. studied the effect of oxygen concentration on propane oxidation over  $MoV_{0.31}Te_{0.23}Nb_{0.12}O_x$  catalyst [39]. The  $C_3H_8/O_2$  ratio was varied from 1/1 to 1/5, therefore reducing, stoichiometric and net oxidizing feed compositions were used at a space velocity of  $1800\text{ h}^{-1}$  and  $400^\circ\text{C}$ . The conversion was steadily increasing with the oxygen concentration, while the selectivity and consequently the yield passed through a maximum at the  $C_3H_8/O_2$  ratio of 1/3.

The selective partial oxidation of alkanes to oxygenates and the oxidative dehydrogenation reactions as well imply chemical reaction on saturated hydrocarbon molecules and oxygen species. The hydrocarbon molecules possess a closed shell electronic structure; therefore they are in a singlet state. The oxygen species activate of the C-H bonds or eventually the C-C bonds to form the desired product(s) and the  $CO_x$ , respectively. The bonding and electronic structure of oxygen species are reviewed here.

The oxygen atom has 8 electrons; the electron configuration is the following:  $1s^2 2s^2 2p_x^2 2p_y^1 2p_z^1$ . Upon molecule formation, the atomic orbital of two oxygen atoms are hybridized. The oxygen molecule in its ground state has an open-shell electronic structure. There is one unpaired electron on each of the  $\pi_x^*$  and  $\pi_y^*$  degenerated antibonding orbitals. The electronic configuration of the oxygen molecule in the ground-

state is:  $KK(\sigma_{2s})^2(\sigma_{2s}^*)^2(\sigma_{2pz})^2(\pi_{2px})^2(\pi_{2py})^2(\pi_{2px}^*)^1(\pi_{2py}^*)^1$ , where K denotes the closed molecular orbital formed by the 1s atomic orbitals.

The presence of the unpaired electrons has two consequences: (a) the gas phase oxygen in the ground state is a triplet diradical, noted with the term symbol of  $^3\Sigma_g^-$ ,

(b) the oxygen molecule is the only paramagnetic species among the diatomic gases with even number of electrons.

The bond order – defined as the half of the difference between the number of electrons in the bonding orbitals and the numbers of electrons that occupy antibonding orbitals – is equal to two [55, 56].

Due to spin constraints, no reaction happens between a singlet (e.g. hydrocarbon) and a triplet species (e.g. molecular oxygen in ground state). This explains that there is no reaction between the alkanes and oxygen at low temperatures and without a catalyst. However, there are a number of excited or ionized oxygen species which are much more reactive.

Upon excitation of the ground state  $O_2$  by 94.72 kJ/mol energy, the spin of one of the unpaired electron on the antibonding  $\pi$  orbital will be inverted, leading to a singlet species  $^1\Delta_g$ . However, the electron configuration and the bond order of the  $^1\Delta_g$  is the same as in the case of the ground state oxygen molecule. When the ground state oxygen molecule is excited by 157.85 kJ/mol, the two unpaired electrons are getting paired on one antibonding  $\pi$  orbital. The resulting species is “the other singlet” with the term symbol of  $^1\Sigma_g^+$ , and the same bond order with the first excited state  $^1\Delta_g$  and the ground state  $^3\Sigma_g^-$  species. However the electronic configuration is different from the  $^1\Delta_g$  and  $^3\Sigma_g^-$  states:  $KK(\sigma_{2s})^2(\sigma_{2s}^*)^2(\sigma_{2pz})^2(\pi_{2px})^2(\pi_{2py})^2(\pi_{2px}^*)^2$ .

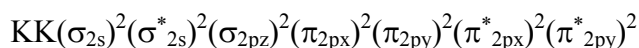
In heterogeneous catalysis, however, the redox catalysts involve ionic oxygen species which are the following:  $O^-$  and  $O^{2-}$  (oxide anion),  $O_2^-$  (superoxide anion),  $O_2^{2-}$  (peroxide anion).

The  $O^-$  anion contains one more electron than the oxygen atom. The electronic configuration of  $1s^2 2s^2 2p_x^2 2p_y^2 2p_z^1$  shows that this species is a mono-radical anion. Because the total electron spin angular momentum is  $1/2$ , the degeneracy is equal to 2. This doublet oxygen species gives a single ESR signal, without hyperfine splitting.

The orbitals of the doubly ionized  $O^{2-}$  are fully occupied. The electronic configuration of this species is  $1s^2 2s^2 2p_x^2 2p_y^2 2p_z^2$ . The total electron spin angular momentum is zero; therefore this ion is a singlet species which does not give a signal in the ESR spectrum.

The superoxide ion ( $O_2^-$ ) is formed by monoelectronic ionization of the oxygen molecule, the extra electron being located on one of the antibonding  $\pi$  orbitals. The electron configuration of  $KK(\sigma_{2s})^2(\sigma_{2s}^*)^2(\sigma_{2pz})^2(\pi_{2px})^2(\pi_{2py})^2(\pi_{2px}^*)^2(\pi_{2py}^*)^1$  displays a mono-radical feature. As a doublet species, the superoxide anion gives a single ESR signal. Because the antibonding orbital is more populated compared to the molecular oxygen, the bond order is reduced from 2 to 1.5.

In the peroxide anion ( $O_2^{2-}$ ) both antibonding  $\pi$  orbitals are fully occupied, which leads to a bonding order of one.



Upon population of the antibonding orbitals with electrons, the O-O bond length increases and the bond energy decreases in the  $O_2$ ,  $O_2^-$  and  $O_2^{2-}$  series. Similarly to the  $O^{2-}$  anion, the peroxide anion is a singlet.

Since the formation of all these ionic oxygen species is exothermic, they are activated species. Upon ionization, however, the degeneracy also decreases from triplet to doublet and singlet, respectively. The reaction between the hydrocarbon and singlet oxygen anion on the catalyst surface is not spin forbidden anymore, therefore the alkane oxidation reaction may take place at a reasonable temperature.

However the reactivity of these species is different and often controls the selectivity of the process. The electrophilic species are represented by  $O^-$ ,  $O_2^-$  and  $O_2^{2-}$ , respectively. They are electron deficient and react with the electron rich regions of the hydrocarbon molecule, such as C=C bonds. The nucleophilic  $O^{2-}$  anion is often identified as lattice oxygen. Because its orbitals are fully occupied by electrons, this species is expected to react with electron poor regions of the molecule, such as C-H bonds [55, 57, 58].

The selectivity control also depends on the reaction type. In the alkane oxidative dehydrogenation or oxidation to unsaturated aldehydes or acids, the selective pathway is associated to C-H bond activation. The attack of electrophilic species on the C=C bond leads to peroxo-complexes or epoxides which decompose by C-C bond cleavage and gives total oxidation products. Other examples of nucleophilic oxidation are: oxidative

dehydroisomerization, and dehydrocyclization, oxidation of alkylaromatics to aldehydes without aromatic ring rupture, ammoxidation, oxidation of aldehydes to acids, oxidation of aromatics to anhydrides.

On the other hand, in the case of electrophilic oxidation reactions the C=C bond activation is desired, because the C-H bond activation by nucleophilic oxygen leads to unselective pathways. Such reactions are the epoxidation, oxidation and oxyhydration of alkenes to saturated ketones, oxidation of aromatics to anhydrides and acids with ring rupture [57, 58].

#### **1.2.4. Reactor designs, operation modes**

##### **1.2.4.1. Conventional laboratory scale reactors**

In heterogeneous catalysis different reactor types and designs are employed [59, 60]. The most important and frequently used ones are described here.

Based on the operation mode, two types can be distinguished: batch and continuous reactors. The batch reactor is a closed system, with a fixed mass of catalyst and volume of reactant. The volume or density of the reacting mixture may change as the reaction proceeds, while the temperature can be kept constant. The concentration of reactants and products change with the reaction time. The reaction rate involving the reactant A can be easily determined from the change of number of moles divided by the volume of the reactor (Equation 1.2.1). If the volume of the reacting mixture is kept constant, the reaction rate is defined as the first order derivative of the concentration with respect to reaction time.

$$r_A = -\frac{1}{V} \cdot \frac{dn_A}{dt} \quad (\text{Equation 1.2.1})$$

The continuous reactors are open systems. These can be further classified based on the flow characteristics in total backmixing reactors (gradientless or continuous flow stirred tank reactor, CSTR) and plug-flow reactors. The CSTR consists of a vessel equipped with an efficient stirrer. The reacting mixture flows in with a continuous rate. The

concentrations are the same in any volume element and any time of the vessel because of the stirring. Moreover, the concentrations at the outlet are the same as in the reactor. The difference between the inlet and outlet concentration resembles a step-function. For a system with constant density, the reaction rate can be calculated by dividing the concentration difference by the mean residence time ( $\bar{t}$ ) (Equation 1.2.2). The mean residence time is defined as the ratio between the volume of the reactor and the volumetric feed flow rate. The most important advantage of a CSTR is indeed the fact that there are no concentration gradients in the catalyst bed; the chemical potential is equal at any volume element of the reactor.

$$r_A = -\frac{c_{A,inlet} - c_{A,outlet}}{\bar{t}} = \frac{\Delta c_A}{\bar{t}} \quad (\text{Equation 1.2.2})$$

The plug-flow reactor (PFR) consists of a tube which contains the catalyst in the form of packing or a fixed bed. The reacting mixture passes through the reactor tube. Two constraints are to be fulfilled by this type of reactor:

- No axial mixing (i.e. in the direction of flow) of fluid in the inside of the tube.
- Complete radial mixing (i.e. perpendicular to the direction of flow) of fluid in the reactor tube.

When the reactor is operated in steady-state and there is no or negligible change of the density, the reaction rate is the first derivative of the concentration with respect to the contact time ( $\tau$ ) (Equation 1.2.3):

$$r_A = -\frac{dc_A}{d\tau} \quad (\text{Equation 1.2.3})$$

The most widely employed reactor type for laboratory-scale experiments in heterogeneous catalysis is the PFR. Using this reactor permits testing for screening the best performing catalyst in a given series. More importantly, the study of the effect of

operation variables (initial concentration of reactants, reaction temperature, and contact time) for kinetic purposes.

Two different regimes are distinguished:

- Differential regime, when the reactor is operated at low educt conversion. This can be determined experimentally, by plotting the conversion of the educt against the contact time. The upper limit of the conversion for the differential regime is that point where the plot deviates from linearity. The educt consumption rate can be determined from the slope of the concentration – contact time plot for the differential regime.
- Integral regime, when the reactor is operated at high conversions. The integral regime extends between the upper conversion limit of the differential regime and full conversion.

For industrial applications, the maximum performance is usually attained in the integral regime. For this purpose, it is often not enough to carry out experiments only in the differential regime. However, strictly speaking, the reaction rates can be defined only for the differential regime. Therefore, kinetic modeling is needed to fit the curves with integrated rate equations derived from a proposed reaction network. The fitting parameters are the rate constants, which do not depend on the extent of the reaction.

#### **1.2.4.2. Catalytic membrane- and multi-stage reactor designs**

In partial oxidation reactions the high yield for the desired product is often difficult to achieve, because the intermediate(s) and the product are thermodynamically less stable than the educt. In those cases when the intermediate(s) and product are oxidatively not stable over a given catalyst, the excess of oxygen in the feed favors the total oxidation, which results in low productivity [39, 61]. For this reasons, different reactor designs (such as catalytic membrane- and multi-tubular reactors) were applied for the dosing of the oxidant to avoid high oxygen concentrations and to change the local kinetics along the reactor tube.

The catalytic membrane reactor is a tubular reactor, but the tube is made of a semi-permeable membrane instead of quartz or metal. The reactant is fed in the tube like in the case of a conventional fixed bed reactor, while the oxidant is fed through the membrane. The membrane acts as a distributor of the oxygen along the catalytic bed. Therefore, the local oxygen concentration is lower than in the case of the conventional plug-flow reactor. The local oxygen concentration influences the local reaction rate, also the rate of total combustion. By changing the local oxygen concentrations, a better performance may be achieved in the catalytic membrane reactor compared to the conventional reactor designs [61].

However, it is to be noted that complete radial mixing is needed, in order to avoid the radial concentration gradients. Otherwise, high oxygen concentrations at around the walls of the reactor which would favor total oxidation, while in the middle of the reactor tube the mixture would be rather reducing.

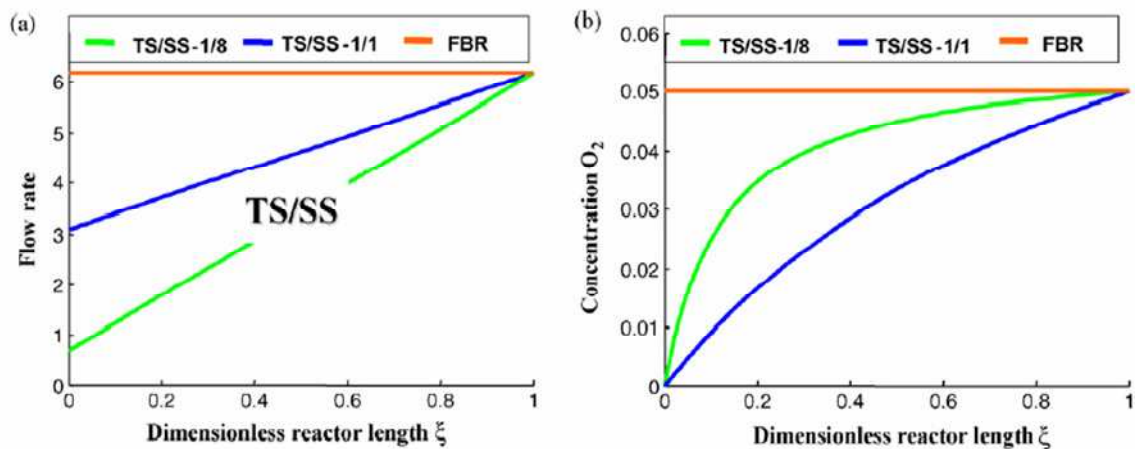


**Figure.1.2.9.** The flow rate (left) and concentration distribution of oxygen (right) in the catalytic membrane reactor without reaction taking place. The blue and green curves correspond to different reactor geometries (aspect ratios). The profile corresponding to fixed bed reactor (FBR) is indicated by orange line [61].

In contrast to the plug flow reactors operated in steady-state, the feed total flow rate increases along the catalytic bed (Figure 1.2.9). Therefore, the space velocity also increases along the tube. Without catalytic reaction taking place, the oxygen concentration also increases along the reactor tube [61].

Some examples of applications of such reactor designs are briefly reviewed below.

Oyama et al. employed a catalytic membrane reactor for the epoxidation of propylene in presence of hydrogen over Au/TS-1 catalyst. In this reactor the formation rate of propylene epoxide could be improved by 100-200% compared to the conventional fixed bed reactor [62]. This is due to the fact that high oxygen concentrations could be used in the catalytic membrane reactor, which are not accessible in a conventional reactor for safety reasons.

Campanelli et al. studied the oxidative dehydrogenation of propane over  $\text{VO}_x/\gamma\text{-Al}_2\text{O}_3$  and  $\text{VO}_x/\text{ZSM-5}$  in catalytic membrane reactor. The performance of this reaction was found to be higher than the conventional fixed bed reactor [63, 64].

The reactor system developed by Hamel et al. is a combination between the multi-stage reactors and catalytic membrane reactors. Three catalytic membrane reactors were connected in series. In this arrangement, increasing, decreasing and constant oxygen concentrations were achievable along the reactor cascade as well as different temperatures in the different reactor units [61].

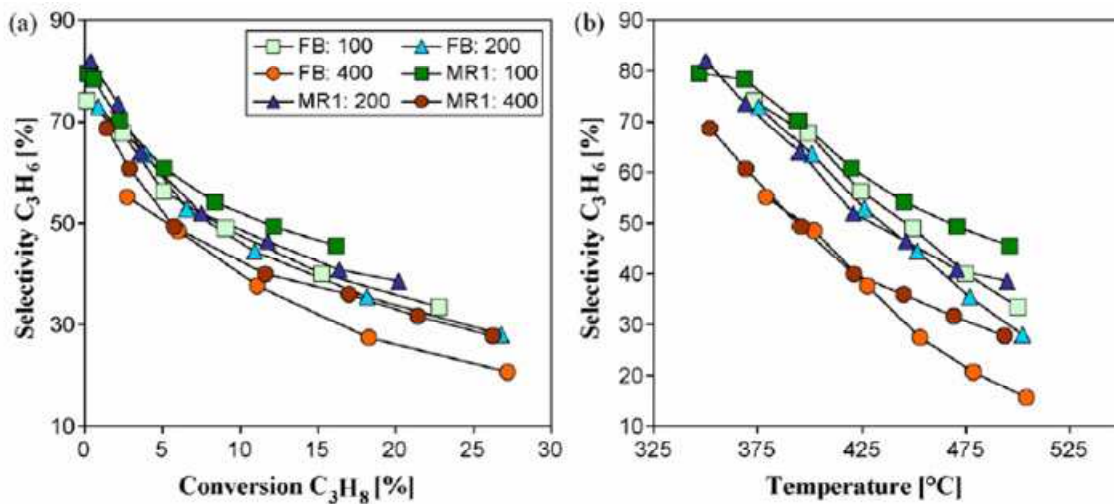


**Figure 1.2.10.** (a) Selectivity of propylene vs. propane conversion, (b) selectivity of propylene vs. temperature. Conditions:  $x_{\text{C}_3\text{H}_8}^{\text{in}}=1\%$ ,  $\text{O}_2/\text{C}_3\text{H}_8=1$  and  $\text{WHSV}=100$  and  $400 \text{ kg}/\text{m}^3$  [61].

The ethane and propane oxidative dehydrogenation was performed in this system using  $\text{VO}_x/\gamma\text{-Al}_2\text{O}_3$  catalyst. The catalytic results from the membrane (MR) reactor were better compared to the experiments carried out in a conventional fixed bed (FB) reactor almost under any conditions (Figure 1.2.10).

O'Neill et al. used a dual-bed membrane reactor as oxygen distributor for the oxidation of propane to acrolein [65]. The first bed contained propane oxidative dehydrogenation catalyst (0.5 g  $\text{V}_2\text{O}_5/\text{MgO}$  at a reaction temperature of  $500^\circ\text{C}$ , while the second bed consisted of bismuth-molybdate for the further oxidation of propylene to acrolein produced in the first reactor tube (2.0g at a reaction temperature of  $475^\circ\text{C}$ ).

Catalytic studies were conducted with both catalysts separately, then in the dual-bed configuration. In these separated experiments, the maximum selectivity to propylene and acrolein was observed for stoichiometric feed, while the selectivity declined in both cases when oxygen excess was used. The dual bed experiments were performed under the optimal conditions determined in the single-bed separated catalytic membrane reactors. Using the dual bed configuration, the selectivity to acrolein could be improved by 21% compared to the experiment when the catalytic membrane reactors were used separated. However, it was also found that the separate membrane reactor performance was only marginally higher (by a few %) compared to the conventional fixed bed reactor.

Fang et al. used a modified fixed bed reactor design equipped with an oxygen distributor tube [66]. The reactor setup permitted experiments with a single- as well as dual catalytic bed. The reacting mixture was fed at the top of the reactor, and in the dual bed operation mode additional oxygen was supplied through the distributor tube which ended up between the two catalyst beds.  $\text{NiZrO}_x$  catalyst was used for oxidative dehydrogenation of propane, while in the second bed cobalt containing bismuth molybdate catalyst was used for oxidation of propylene to acrylic acid. Both of these catalysts showed low activity in a single-bed arrangement: the conversion over  $\text{NiZrO}_x$  catalyst was below 10% and selectivity around 2 %, while on the modified bismuth molybdate catalyst the conversion and acrylic acid selectivity were below 1% at the temperature of  $380^\circ\text{C}$ . The

combination of the catalyst beds lead to a conversion of about 10%, while the selectivity was around 25%. The addition of oxygen via the distributor tube increased significantly the yield of acrylic acid, to about 12%.

Summarizing the advantages of catalytic membrane and multi-tubular reactors, it can be stated that

- These systems permit the variation of the local concentration of the oxidant. The local concentration has a direct effect on the local kinetics and reaction rate, thus the total oxidation may be prevented.
- Different amounts of catalysts may be loaded in the individual reactor tubes. Therefore, different contact times are achievable in the reactor tubes. The contact time in each reactor can also be an operational variable in these systems.
- The temperature of each reactor tube can be set individually, which is important if the product is oxidatively unstable.

As shown by the above presented examples, the optimization of the additional operational variables in catalytic membrane and multi-tubular reactors, the performance may be improved compared to the conventional reactor systems used for basic research.

### **1.2.5. Reaction kinetics**

The heterogeneously catalyzed reactions consist of 7 serial steps as follows [67]:

- Diffusion of the reactant species in the fluid phase towards the surface of the solid catalyst.
- Internal diffusion of the reactant in the pores of the catalyst particle.
- Adsorption of the reactant molecule on the surface.
- Chemical transformation of the reactant into product.

- Desorption of the product.
- Diffusion of the products in the pores of the catalyst.
- Diffusion of the product towards the fluid phase.

The first two and the last two steps are transport phenomena and as such, physical phenomena. The reaction conditions and operation mode can be chosen in such a way that the mass transport does not limit the chemical reaction on the surface.

The reaction mechanism is ultimately the set of elementary steps, which explains how the bonds are split and formed during the chemical transformation. However, besides the description of all elementary reactions, the postulated reaction mechanism should contain information concerning the chemical and electronic structures of the transition state for each elementary step [75]. In applied heterogeneous catalysis such a description is seldom achieved, even though in many literature sources the elucidation of reaction mechanism is claimed.

### 1.3. Motivation

Upon reviewing the literature about the selective oxidation of propane to acrylic acid on Mo and V based mixed oxides it was found that predominantly the studies were performed using phase mixture catalysts. The understanding of the role of the individual phases and active sites in the propane oxidation reaction is still under debate [2, 9, 29, 34, 36, 70-72], in spite of the claims given by Grasselli et al. [31] and López-Nieto et al. [35]. Their conclusions were assigned based on disproportionately few catalytic and kinetic data compared to the structural characterization data.

In contrast to this, very limited information exists about the catalytic properties of phase-pure materials in propane oxidation reaction. Furthermore, the following open questions and conflicting conclusions were identified:

- The bulk structural stability of the MoVTeNbO<sub>x</sub> catalyst under various conditions (dry, reducing, stoichiometric and oxidizing feed) was not evidenced [27, 28]. On the other hand, it was reported that the phase composition of the not phase pure

MoVSbNbO<sub>x</sub> catalyst is irreversibly altered when exposing to dry feed conditions, accompanied by the irreversible drop of the catalytic performance.

- The detailed kinetic study of the operational variables (reaction temperature, steam content, redox potential) was not described on a phase-pure M1 MoVTeNbO<sub>x</sub> catalyst.
- The reaction pathways are under debate. The early versions were proposed mainly based on thermodynamic considerations [4, 12] and a very limited number of integral catalytic data [2, 12, 22, 30, 47, 48] but only very few systematic kinetic studies were carried out. Typically, these studies were performed using phase mixture catalysts [24-28, 73, 74].
- The common feature of the proposed pathways is that the total oxidation product (CO and CO<sub>2</sub>) formation is either not explained at all [12, 24, 35], or they are merged together as CO<sub>x</sub>=CO+CO<sub>2</sub> produced by the total oxidation of acrylic and acetic acids [2, 4, 22, 24, 25, 47, 48, 71, 74]. Lintz et al. and Fushimi et al. continued the simplification by merging the CO, CO<sub>2</sub> and acetic acid under a three carbon atom containing pseudo-byproduct [27, 28, 30, 71]. The mechanism proposed by Grasselli et al. does not explain at all the formation of these byproducts [9, 31, 35, 70]. However, a postulated mechanism should contain all the contributing elementary reactions as well as the description of electronic and chemical structures of the transition state for each elementary reaction [75].

The experimental work presented this thesis is centered around the kinetic study of propane selective oxidation to acrylic acid on MoVTeNbO<sub>x</sub> catalyst. Due to the fact that the role of the individual phases is not yet fully understood, a phase-pure MoVTeNbO<sub>x</sub> catalyst was used. The experiments were designed to answer some of the above outlined open questions:

- The bulk structural stability of the phase-pure M1 MoVTeNbO<sub>x</sub> catalyst under real reaction conditions (T=400°C and GHSV=5000 h<sup>-1</sup>, whereby maximum acrylic acid selectivity is attained in fixed bed reactor) was addressed in an in situ XRD experiment. The steam content and redox potential was varied during this experiment, the conditions covered steam containing-, dry-, stoichiometric-,

- oxidizing-, reducing- and strongly reducing ( $C_3H_8$  in  $N_2$ ) feed compositions, respectively.
- The kinetic study on the temperature, steam- and oxygen concentration was carried out in a conventional fixed bed reactor. The oxidation of the intermediates (propylene and acrolein) was also carried out in the temperature interval corresponding to the propane oxidation in order to determine the relative reactivities. For unraveling the source of  $CO_2$  in the  $C_3H_8$  and  $C_3H_6$  and acrolein oxidation reactions (i.e. is  $CO_2$  produced from the total oxidation of the organics or the further oxidation of CO), a separate CO oxidation and water gas shift reaction was envisaged.
  - A two-stage reactor design was employed for the stage-wise addition of the oxidant ( $O_2$ , and  $N_2O$ ), reducing gases ( $C_3H_6$ , CO) and the thermodynamically stable end product ( $CO_2$ ). The  $O_2$  addition was performed in order to check whether the multi-stage arrangement improves the catalytic performance similarly to the literature sources. In the literature, the nitrous oxide was reported to be an alternative and more efficient oxidant than molecular oxygen in ODH reactions [77, 78]. Therefore the potential applicability of this oxidant was also checked in the two-stage reactor system. The addition of  $C_3H_6$ , CO and  $CO_2$  was performed in order to observe whether these products competitively adsorb on the active sites of the catalyst or not.
  - The product distribution analysis corresponding to the propane oxidation and the catalytic data obtained for propylene, acrolein and CO oxidation reactions in both the single-tube and the two-stage reactor setups are considered in the proposed reaction network [76].

### References Chapter 1

1. J. P. Lange, Economics of alkane conversion, Chapter 3 in E. G. Derouane et al. (Eds.) Sustainable strategies for the upgrading of natural gas: fundamentals, challenges and opportunities, Springer 2005, 51-83
2. E.K. Novakova, V. C. Védrine, Propane Selective Oxidation to Propene and Oxygenates on Metal Oxides in J.L.G. Fierro, Metal Oxides, Chemistry and Applications, CRC Press, 2006, 414-455.

3. G. Centi, F. Cavani, F. Cavani, F. Trifiro, *Selective Oxidation by Heterogeneous Catalysis*, Kluwer Academic/Plenum Publishers, 2001, 363-384.
4. M. M. Lin, *Appl. Catal. A*, 207 (2001) 1–16.
5. [www.icis.com](http://www.icis.com), retrieved on 02.03.2011
6. [www.oilenergy.com](http://www.oilenergy.com), retrieved on 02.03.2011
7. R.K. Grasselli, J.D. Burrington, *Adv. Catal.* 30 (1981) 133.
8. J.D. Burrington, C.T. Kartisek, R.K. Grasselli, *J. Catal.* 81 (1983) 489.
9. R.K. Grasselli, J.D. Burrington, D.J. Buttrey, P. DeSanto, Jr., C.G. Lugmair, A.F. Volpe, Jr., T. Weingand, *Topics in Catal.* 23 (2003) 5.
10. R.K. Grasselli, *Topics in Catal.* 15 (2001) 93.
11. M. Egishara, K. Matsuo, S. Kawaga, T. Seiyama, *J. Catal.* 58 (1979) 409.
12. M. M. Bettahar, G. Costentin, L. Savary, J. C. Lavalley, *Appl. Catal. A*, 145 (1996) 1-48.
13. Y. H. Jang, W. A. Goddard III, *J. Phys. Chem. B*, 106 (2002) 5997-6013.
14. K. Chen, A. T. Bell, and E. Iglesia, *J. Phys. Chem. B*, 104 (2000) 1292-1299.
15. K. Chen, E. Iglesia, A. T. Bell, *J. Phys. Chem. B*, 105 (2001) 646-653.
16. K. Chen, A. Khodakov, J. Yang, A. T. Bell, E. Iglesia, *J. Catal.* 186 (1999) 325-333.
17. B. Y. Jibril, *Int. J. Chem. Kinet*, 38 (2003) 176-183.
18. G. Fu, X. Xu, X. Lu, and H. Wan, *J. Phys. Chem. B*, 109 (2005) 6416-6421
19. N.N. Greenwood, A. Earnshaw, *Chemistry of the Elements*, 2<sup>nd</sup> Edition, Butterworth Heinemann, 1997, 981-987, 1007-1017.
20. T. Ushikubo, H. Nakamura, Y. Koyasu, S. Wajiki, US Patent 5 380 933 (1995) to Mitsubishi Kasei Corporation
21. T. Ushikubo, I. Sawaki, K. Oshima, K. Inumaru, S. Kobayakawa, K. Kiyono, US Patent 5 422 328 (1995) to Mitsubishi Kasei Corporation.
22. M. Lin, T. B. Desai, F. W. Kaiser, P. D. Klugherz, *Catal. Today*, 61 (2000) 223–229.
23. D. Vitry, Y. Morikawa, J.L. Dubois, W. Ueda, *Applied Catalysis A: General* 251 (2003) 411–424.
24. L. Luo, J.A. Labinger, M.E. Davis, *J. Catal.* 200 (2001) 222–231.
25. E.K. Novakova, J.C. Vadrine, E.G. Derouane, *J. Catal.* 211 (2002) 235-243.
26. E.K. Novakova, J.C. Vadrine, E.G. Derouane, *Catal. Lett.* 83 (2002) 177.
27. E. Balcells, F. Borgmeier, I. Grißtede, H.-G. Lintz, F. Rosowski, *Appl. Catal. A* 266 (2004) 211-221.
28. I. Grißtede, *Die partielle Oxidation von Propan zu Acrylsäure, Bestimmung der Reaktionskinetik und in-situ Charakterisierung des Katalysators unter Betriebsbedingungen*, Dissertation, Universität Karlsruhe, 2004, Universitätsverlag Karlsruhe, ISBN 3-937300-17-1
29. P. Concepcion, P. Botella, J. M. Lopez Nieto, *App. Catal. A*, 278 (2004) 45–56.
30. R. Fushimi, S. O. Shekhtman, A. Gaffney, S. Han, G. S. Yablonsky, J. T. Gleaves, *Ind. Eng. Chem. Res.* 44, (2005) 6310-6319.
31. R. K. Grasselli, D. J. Buttrey, J. D. Burrington, A. Andersson, J. Holmberg, W. Ueda, J. Kubo, C. G. Lugmair, A. F. Volpe, *Top. Catal.*, 38 (2006) 7-16.
32. P. DeSanto, D. J. Buttrey, R. K. Grasselli, C. G. Lugmair, A. F. Volpe Jr., B. H. Toby, T. Vogt, *Z. Kristallogr.* 219 (2004) 152-165

33. M. Baca, A. Pigamo, J.L. Dubois, and J.M.M. Millet, *Top. Catal.*, 23 (2003) 39-46
34. W. Ueda, D. Vitry, T. Katou, *Catal. Today* 96 (2004) 235–240
35. P. Botella, J. M. López-Nieto, B. Solsona, A. Mifsud, and F. Márquez, *J. Catal.* 209 (2002) 445-455
36. V. V. Gulians, R. Bhandari, B. Swaminathan, V. K. Vasudevan, *J. Phys. Chem. B*, 109 (2005) 24046-24055.
37. Y. Zhu, W. Lu, H. Li, H. Wan, *J. Catal.*, 246 (2007) 382-389
38. G. Busca, *Phys. Chem. Chem. Phys.* 1 (1999) 723-736.
39. W. Zheng, Z. Yu, P. Zhang, H. Fu, X. Zhang, Q. Sun, X. Hu, *J. Natural Gas Chem.* 17 (2008) 191-194
40. J. L. Dubois, D. Garrait, A. Le Gall, G. Bazin, S. Serreau, FR patent, WO 2006/072682 A1, 2006
41. G. Landi, L. Lisi, J. C. Volta, *Chem. Commun*, 9, 4 (2003) 492-493
42. G. Landi, L. Lisi, J.-C. Volta, *J. Mol. Catal. A*, 222 (2004) 175-181
43. G. Landi, L. Lisi, J. C. Volta, *Catal. Today*, 91-92 (2004) 275-279
44. T.V. Andrushkevich, *Catal. Rev. Sci. Eng.*, 35 (1993) 213-259
45. E. M. Erenburg, T. V. Andrushkevich, G. Ya. Popova, A. A. Davidov, V. M. Bondareva, *React. Kinet. Catal. Lett.* 12, 1 (1979) 5-11
46. E.M. Erenburg, T. V. Andrushkevich, V. I. Bibin, *Kinet. Catal.*, 20, 3 (1979), 680.
47. M. Ai, *J. Catal.* 101 (1986) 389
48. M. Ai, *Catal. Today*, 42 (1998) 297
49. A. C. Kaddouri, C. Mazzochia, E. Tempesti, *Appl. Catal. A* 180 (1999) 271
50. J. Barrault, C. Batiot, L. Magaud, M. Ganne, *Stud. Surf. Sci. Catal.*, 110 (1997) 375
51. A. C. Sanfiz, T. W. Hansen, D. Teschner, P. Schnorch, F. Girgsdies, A. Trunschke, R. Schlogl, M. H. Looi, S. B. A. Hamid, *J. Phys. Chem. C*, 114, 4 (2010) 1912-1921
52. J. C. Vadrine, J. M. M. Millet, J. C. Volta, *Catal. Today*, 32, 1-4, (1996) 115-123
53. R. Recknagel, *Chemische Technik*, 46, 6 (1994) 324-331
54. Moro-oka, *Appl. Catal. A: General*, 181 (1999) 323-329
55. Z. Sojka, E. Giamello, M. C. Paganini, *Radicals in Catalysis – Heterogeneous*, in I. T. Horváth (Ed.), *Encyclopedia of Catalysis*, Vol. 5, Wiley-Interscience, 2003, 738-768,
56. N.N. Greenwood, A. Earnshaw, *Chemistry of the Elements*, 2<sup>nd</sup> Edition, Butterworth Heinemann, 1997, [13] P. Mars, D. W. Krevelen, *Chem. Eng. Sci.*, 3, 1954, 41.
57. S. T. Oyama, Factors affecting selectivity in catalytic partial oxidation and combustion reactions, in B. K. Warren, S. T. Oyama (Eds.), *Heterogeneous Hydrocarbon Oxidation*, ACS Symposium Series 638, 2-20, J. Haber, *Selectivity in heterogeneous catalytic oxidation of hydrocarbons*, B. K. Warren, S. T. Oyama (Eds.), *Heterogeneous Hydrocarbon Oxidation*, ACS Symposium Series 638, 20-36
58. J. Haber, *Selective oxidation – Heterogeneous*, in I. T. Horváth (Ed.), *Encyclopedia of Catalysis*, Vol. 6, Wiley-Interscience, 2003, 141-187

59. R. W. Missen, Ch. A. Mims, B. A. Saville, Introduction to Chemical Reaction Engineering and Kinetics, John Wiley and Sons, 1999, 25-41
60. J. M. Berty, Experiments in catalytic reaction engineering, Studies in surface science and catalysis, Vol. 124, Elsevier, 1999, 29-45
61. C. Hamel, Á. Tóta, F. Klose, F. Tsotsas, A. Seidel-Morgenstern, Chem. Eng. Res. and Design, 86 (2008) 753-764
62. S.T. Oyama, X. Zhang, J. Lu, Y. Gu, T. Fujitani, J. Catal., 257 (2008) 1-4
63. A. Bottino, G. Campanelli, A. Comite, J. Membr. Sci., 197, 1-2 (2002) 75-88
64. G. Campanelli, E. Carosini, F. Cavani, O. Monticelli, F. Trifiro, Chem. Eng. Sci., 51, 10 (1996) 1817-1826
65. C. O' Neill, E. E. Wolf, Catal. Today, 156 (2010) 124-131
66. W. Fang, Q. J. Ge, J. F. Yu, H. Y. Xu, Ind. Eng. Chem. Res., 50, 4 (2011) 1962-1967
67. J. B. Butt, Reaction kinetics and reactor design, Chapter 7, Chapter 1, Marcel Dekker, 2000, 1-104, 457-571
68. R. A. van Santen, J. W. Niemantsverdriet, Chemical kinetics and catalysis, Fundamental and Applied Catalysis, Plenum Press, 1995, Chapter 2, 21-66
69. N. A. Bhore, M. T. Klein, K. Bishoff, Ind. Eng. Chem. Res., 29 (1990) 313-316
70. R. K. Grasselli, C. G. Lugmair, A. F. Volpe, Top. Catal., 50 (2008) 66-73
71. H.-G. Lintz, S. P. Müller, Appl. Catal. A: General 357 (2009) 178-183
72. R. Schlögl, Top. Catal., 54 (2011) 627-638
73. Lin Luo, PhD Thesis, California Institute of Technology, Pasadena, California, 2001
74. F. N. Naraschewski, A. Jentys, J. A. Lercher, Top. Catal. 54 (2011) 639-649
75. K. A. Connors, Chemical kinetics, VCH Publishers, 1990, 1-10
76. R. Naumann d'Alnoncourt, L. I. Csepei, Yu. V. Kolen'ko, A. Trunschke, R. Schlögl, manuscript in preparation.
77. E. V. Kondratenko, M. Cherian, M. Baerns, D. Su, R. Schlögl, X. Wang, I. E. Wachs, J. Catal. 234 (2005) 131-142
78. E. V. Kondratenko, A. Brückner, J. Catal. 274 (2010) 111-116

## **Chapter 2. Experimental methods**

### **2.1. Physico-chemical characterization of the catalysts**

In this section those methods are described which were employed to characterize the catalyst. Routine measurements (determination of the surface area, recording the X-ray diffractogram for checking the phase purity, imaging by SEM/TEM and elemental analysis by EDX) were done for each sample, while XPS and microcalorimetric experiments on the adsorption of propane was performed for selected samples.

#### **2.1.1. Nitrogen physisorption**

The nitrogen physisorption was carried out on a Quantachrome 6B setup at  $-196^{\circ}\text{C}$ . Prior to the measurement, an outgassing procedure was performed at  $150^{\circ}\text{C}$  for 2 hours. The specific surface area was calculated using the multipoint Brunauer-Emmett-Teller method applied to the data collected in the relative pressure interval between 0.05 and 0.3 of the adsorption isotherms. The total pore volume was estimated from the volume of the physisorbed nitrogen at the relative pressure of 0.95.

#### **2.1.2. X-Ray Diffraction**

The powder X-ray diffraction patterns were recorded using a Stoe STADI-P transmission diffractometer and a Bruker D8 ADVANCED diffractometer, both equipped with a  $\text{Cu K}_{\alpha 1}$  radiation source.

The in-situ XRD study was performed using the Bruker D8 ADVANCED diffractometer. The gas mixture of propane, oxygen, and helium was supplied by mass flow controllers and, while a bubbler connected to a HAAKE<sup>®</sup> thermostat was employed for introducing the steam. Catalytic reaction was carried out at a temperature of  $400^{\circ}\text{C}$ , the reaction was followed by an on-line mass spectrometer.

### **2.1.3. Scanning Electron Microscopy (SEM/EDX) and Scanning Transmission Electron Microscopy (STEM)**

The SEM-EDX analysis was performed using a Hitachi S-4800 scanning electron microscope operated at 10 kV accelerating voltage. The STEM measurement was done in Titan CS 80-300 TEM setup operated at 300 kV. The spatial resolution was ca. 1.3 Å.

### **2.1.4. X-Ray Photoelectron Spectroscopy (XPS)**

The XPS experiments were carried out using the monochromatic radiation of the ISIS (Innovative Station for In Situ Spectroscopy) at the synchrotron facility BESSY II of the Helmholtz Zentrum Berlin. The measurements were carried out at a pressure of 0.25 mbar oxygen, in order to avoid reduction of tellurium. The core level spectra of O 1s, V 2p, Mo 3d, Te 3d, Nb 3d and C 1s were recorded at 150 eV constant kinetic energy of the incident photon beam. This corresponded to the inelastic mean free path of approximately 0.6 nm, therefore, the setup was operated in the surface sensitive mode. The normalization of the spectra was done with respect to the storage ring current and the incident photon flux determined by using a gold foil. The data analysis was done in CASA software using Shirley baseline subtraction.

### **2.1.5. Microcalorimetry**

The differential heats of adsorption were determined using an MS70 Calvet Calorimeter (SETRAM). Details about the experimental setup consisting of the gas dosing system, calorimeter and the custom-designed high-vacuum system were described in detail before [1]. The catalyst sample was investigated in the same sieve fraction as used for the catalytic experiments (250-355 µm). The pretreatment of the sample prior to the calorimetric experiment was performed in vacuum (at  $3 \cdot 10^{-8}$  mbar) at 150°C. The propane and propylene adsorption experiment was performed at 40°C. The pressure change and the heat signal were recorded at every dosing step of the probe molecules. The adsorption isotherm was derived from the dosed amount of probe molecule and the

equilibrium pressure. The signal area was converted into heat by means of the calibration factor of the calorimeter determined in advance. The heat was divided by the number of molecules adsorbed in the respective dosing step [2].

## **2.2. The experimental setup for propane oxidation**

For catalytic and kinetic experiments a home built fixed bed reactor system was used (Figure 2.2.1). The propane oxidation setup (denominated as PropOx 1) consisted of three modules:

- Gas dosing system
- Reactor system
- On-line gas analytics.

In the following sections the design features and details of the modules are given.

### **2.2.1. The gas dosing system**

On Figure 2.2.1 the scheme of the reactor system is shown. The gas dosing system consisted of 3+2 mass flow controllers (MFC) as follows:

- O<sub>2</sub>, ( Bronkhorst, type EL-FLOW, max. flow rate 5 mln/min)
- C<sub>3</sub>H<sub>8</sub> (Bronkhorst, type EL-FLOW, max. flow rate 2.5 mln/min)
- N<sub>2</sub> (Bronkhorst, type EL-FLOW, max. flow rate 70 mln/min)
- N<sub>2</sub> (Bronkhorst, type EL-FLOW, max. flow rate 100 mln/min). This was used in the steam content variation experiment, when the feed was switched from steam containing feed to dry feed. Additionally, this flow controller was used for the purging of the second reactor tube with a mixture of N<sub>2</sub>+H<sub>2</sub>O when the two-stage reactor system was operated in a single-tube mode.
- O<sub>2</sub> (Bronkhorst, type EL-FLOW, max. flow rate 5 mln/min, not shown on Figure 2.2.1), this was used for the addition of oxygen and other gases (C<sub>3</sub>H<sub>6</sub>, N<sub>2</sub>O, CO, CO<sub>2</sub>) in the two-stage reactor system. The two-stage reactor system is described in section 2.2.3.

For the study on the effect of steam it was necessary to vary the steam content between 40 and 0 vol%. The steam was introduced via a syringe pump (Harvard Apparatus, Model 22 with a double syringe holder) equipped with a 5.0 ml gas tight syringe made of quartz (provided by Hamilton) and an evaporator. The home-built evaporator was a stainless steel vessel surrounded by a heater (nominal power of 600W) heated up to 97°C. The cavity of the vessel was filled up with SiC (particle size between 200 and 400 microns). The liquid water entered the vessel through a 1/16 inch size tubing. Nitrogen was used as carrier gas for steam through the evaporator. Even though the evaporation temperature was experimentally optimized, oscillations in the steam concentration were noticed, which induced oscillations in the concentration of all the other components. Therefore a Swagelok stainless steel pressure vessel of 150 ml was installed in the heated oven as a buffer volume, in order to minimize the fluctuations of the concentrations.

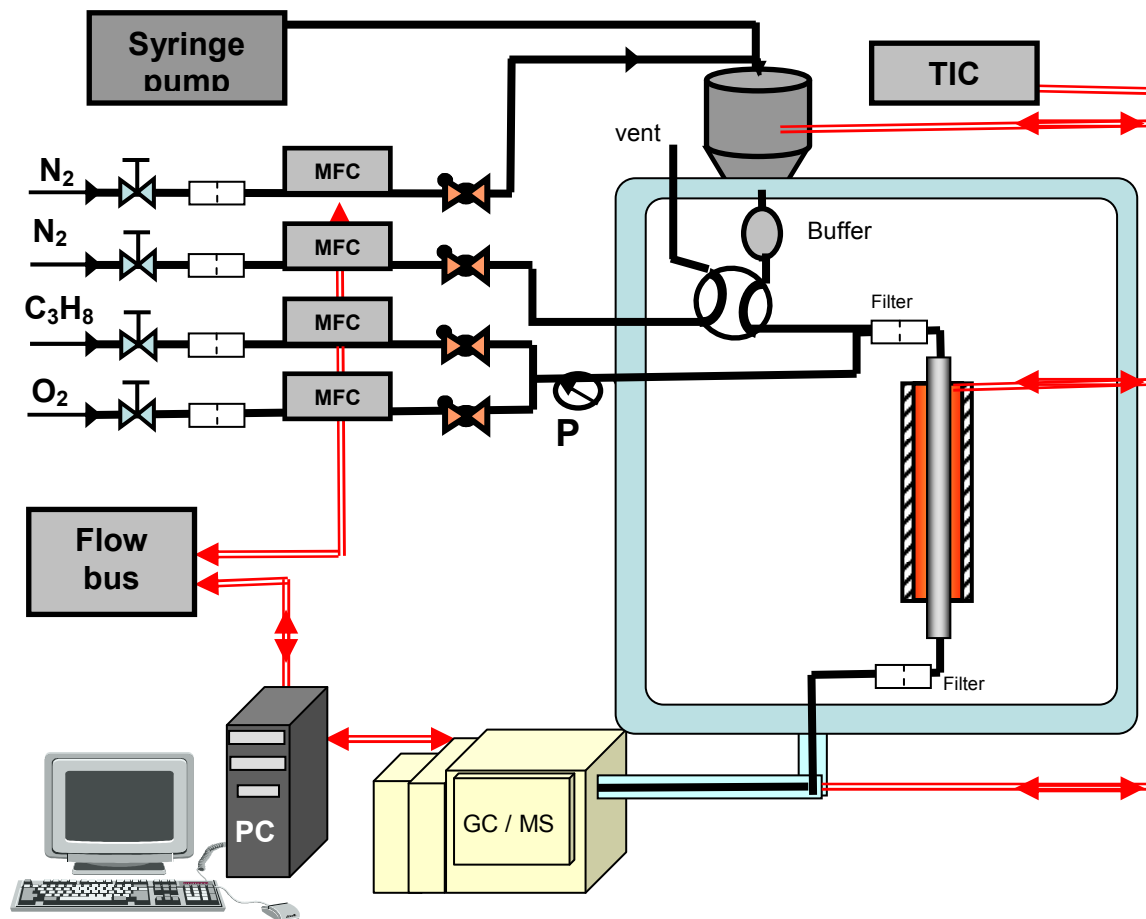


Fig. 2.2.1. The experimental setup denominated as PropOx-1.

A Swagelok four-way valve installed in the heated oven permitted to switch immediately between a steam containing feed and dry feed and back. When the four way valve was in the position indicated by Figure 2.2.1., the  $N_2$ +steam mixture was added to the  $C_3H_8+O_2$  mixture. On the other hand, when the valve was turned in the other position, pure nitrogen was added to the  $C_3H_8+O_2$  mixture for the experiments carried out under steam free conditions. The  $N_2$ +steam mixture was produced continuously, but it was purged by the valve to the vent.

For re-measuring the catalytic properties with the steam containing feed, the four way valve was turned back in the position indicated by Figure 2.2.1.

The necessity of above described arrangement and procedure is due to the fact that the replacement of the steam containing feed by dry feed by switching off the syringe pump is not fast enough. Both the evaporator and the pressure vessel has a relatively large volume and it would have taken more than an hour to replace the steam containing feed by dry feed and vice versa. However, by using this valve system, the time resolution of the measurement on the steam effect was reduced to the time resolution of the analytical setup (ca. 17 min), permitting to observe if the catalyst is deactivating fast or not in absence of steam.

A Swagelok filter (2 microns) was installed between the T-junction where the  $N_2$ +steam and the  $C_3H_8+O_2$  mixtures were unified in order to ensure complete mixing.

The 4 way valve, buffer volume, the reactor tube and the gas lines were housed in a Heraeus oven heated up to 140°C. The transfer line between the oven and the heated oven and the analytical setup was heated to the same temperature by means of heating tapes.

### **2.2.2. Reactor tube characteristics**

A quartz tube was used as reactor with an outer diameter of 9.7 mm and inner diameter of 6.8 mm. The reactor tube was surrounded by a tubular heating cartridge (Figure 2.2.1) and placed in the heated oven. The oven was heated up to 140°C in order to avoid condensation of the steam and reaction products (acrylic acid and acetic acid).

For finding out the isothermal zone of the reactor, the oven was heated up to 140°C, while the temperature of the reactor heating cartridge was set to 400°C. A gas mixture containing 40 vol% steam and 60 vol% N<sub>2</sub> was flown through the empty reactor with a flow rate of 50 mln/min. The thermocouple was moved by 0.5-1.0 cm along the tube from bottom towards the top and the temperature was measured at each position. The temperature profile is given in Figure 2.2.2. A plateau is observed between 8 and 13 cm of the reactor length. For a better estimation, a standard deviation of less than 1°C was considered as an objective criterion for the length of the isothermal zone.

The isothermal zone started at 8.5 cm and ended at 12.5 cm, therefore the length is 4 cm. Within this zone the average temperature was found to be 400,1°C, with a standard deviation of 0.7°C and a confidence interval of 0.2°C. The absolute difference between the maximum and minimum temperatures ( $\Delta T = T_{\max} - T_{\min}$ ) was 1.5°C within this interval. The difference of  $T_{\max} - T_{\text{average}}$  was 0.7°C which is in good agreement with the standard deviation of the temperature profile curve in the isothermal zone. Therefore, it can be stated that the catalytic reaction was carried out under isothermal conditions.

An isothermal volume of 1.45 ml was calculated from the inner diameter of the reactor tube and the length of the isothermal zone. This was the maximum volume of the catalyst which could be loaded in the isothermal zone.

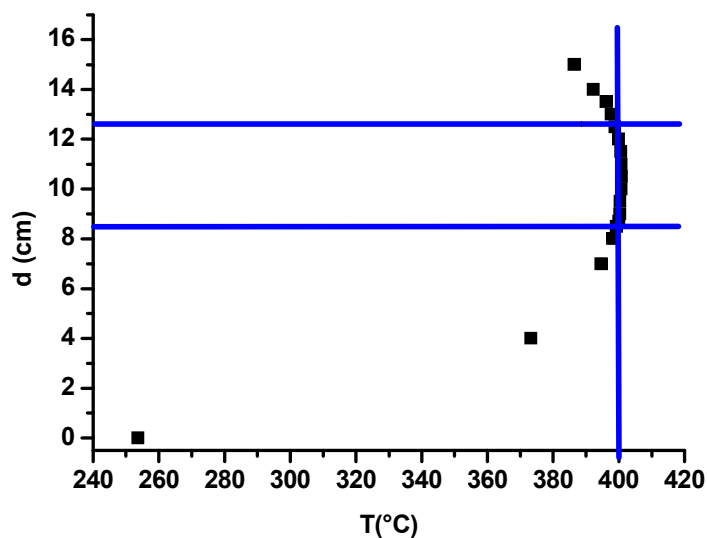


**Figure 2.2.2.** The temperature profile of the reactor tube. Zero centimeter corresponds to the bottom of the heating cartridge. The delimitation of the isothermal zone is marked by blue lines.

The catalyst was used as a sieve fraction between  $d_{p,\min}=250$  and  $d_{p,\max}=355$  microns. The ratio between the reactor diameter ( $d_r$ ), length of the isothermal zone ( $L_{\text{isoth}}$ ) and the particle size are given by the equation 2.2.1-2.2.3. The ratio between the reactor diameter and particle size should be at least 10 (Equation 2.2.1). The length of the isothermal zone should exceed at least 50 times the particle size (Equation 2.2.2). The dimensionless criterion concerning the reactor geometry is that the length of the isothermal zone should be at least 5 times larger than the diameter. The numerical values of these ratios exceed the minimum criteria (Equations 2.2.1-2.2.3), therefore no axial diffusion (back-mixing), no radial gradient in concentrations, temperature and reaction rate occurs [3].

$$\frac{d_r}{d_{p,\max}} = \frac{6.8}{0.355} = 19,2 \quad \frac{d_r}{d_{p,\min}} = \frac{6.8}{0.250} = 27.2 \quad (\text{Equation 2.2.1})$$

$$\frac{L_{\text{isoth.}}}{d_{p,\max}} = \frac{40}{0.355} = 112,7 \quad \frac{L_{\text{isoth.}}}{d_{p,\min}} = \frac{40}{0.250} = 160,0 \quad (\text{Equation 2.2.2})$$

$$\frac{L_{\text{isoth.}}}{d_r} = \frac{40}{6.8} = 5.9 \quad (\text{Equation 2.2.3})$$

In order to avoid hot-spots or temperature gradient formation, the catalyst was mixed with SiC (particle size between 315 and 400 microns) prior to filling in the reactor tube. Usually 0.25-0.30 ml catalyst was mixed up with 1.15-1.2 ml SiC. This corresponds to a dilution ratio between 3.8 and 4.8. The SiC does not only act as a diluent between the catalyst particles, but also improves the reaction heat transfer. The heat conductivity of SiC is 2-3 order of magnitude higher compared to the heat conductivity of molybdenum and vanadium based oxides ( $\lambda_{\text{SiC}}=1.2\text{-}2.5 \text{ W/cm}\cdot\text{K}$  [4],  $\lambda_{\text{MoVOx}}=2.5\cdot 10^{-3} \text{ W/cm}\cdot\text{K}$  [5]).

A slightly different SiC sieve fraction was used (315-400  $\mu\text{m}$ ) compared to the catalyst particle size (250-355  $\mu\text{m}$ ) in order to facilitate the separation of the catalyst after catalytic experiment. When the loading was taken out from the reactor, the solid mixture was sieved using a 315 micron sieve. The catalyst particles between 250 and 315 micron fell in the collection plate, while the catalyst particles and SiC above 315 microns remained in the sieve. The collected catalyst was not always free of small fraction of SiC

(less than 1%). Therefore, sometimes the post-catalytic XRD patterns contained reflections of SiC as well.

The loading of the reactor was performed according to the following procedure: a quartz wool plug was inserted in the tube to the lower end of the isothermal zone. Then the catalyst and SiC physical mixture was poured in the tube using a glass funnel to a level which was 2 mm below the upper end of the isothermal zone. At the end, ca. 2 mm of SiC layer was added to the top of the bed. The reactor tube was inserted in the heating cartridge. A K-type thermocouple that measured the temperature in the catalytic bed was fixed in such a way that it touched only the SiC on the top. Therefore, this arrangement permitted to avoid cross contamination of one catalytic bed to another by the particles which eventually might stick to the surface of the thermocouple.

For the downstream tubing and transfer line between the reactor and the analytical setup, a PEEK tubing was used which is chemically more inert than stainless steel. The employment of PEEK was necessary in order to minimize the adsorption of products and polymerization of acrylic acid on the walls of the tubing. On the downstream tubing from the reactor, a second filter (Swagelok, 2 micron) was installed in order to prevent the solid particles to enter into the valve system and/or columns of the analytical setup.

### 2.2.3. Estimation of the Weisz-number and the Thiele modulus and effectiveness factor

For the estimation of whether mass transport limitation plays a role in the reaction, the Weisz-number ( $\Psi$ ) and the Thiele modulus ( $\Phi$ ) was calculated according to the equations:

$$\Psi = L_c^2 \cdot \frac{n+1}{2} \cdot \frac{r_{C_3H_8} \cdot \rho_{cat.}}{D_{eff} \cdot c_{C_3H_8,0}} \quad (\text{Equation 2.2.4})$$

$$\Phi = L_c \cdot \sqrt{\frac{k_{C_3H_8} \cdot c_s^{n-1}}{D_{eff}}} \quad (\text{Equation 2.2.5})$$

$$\eta = \frac{\tanh \Phi}{\Phi} \quad (\text{Equation 2.2.6})$$

Since the propane oxidation reaction was found to be first order with respect to propane ( $n=1$ , see section 4.2.3), the  $(n+1)/2$  term becomes equal to one. Similarly, the term involving the surface concentration of propane on the  $(n-1)^{\text{th}}$  power becomes equal to one in the equation 2.2.5 for  $n=1$ .

The characteristic length ( $L_c$ ) was calculated from the particle diameter assuming spherical particles. The catalyst density ( $\rho_{\text{cat}}$ ) of 1.12 g/ml was determined by weighting 1,0 ml sieve fraction. The effective diffusion coefficient of propane ( $D_{\text{eff}}=0.018 \text{ cm}^2/\text{s}$ ) was taken from [6]. The integral reaction rate of propane consumption was calculated at the highest reaction temperature of 400°C. The rate constant of propane consumption ( $k_{\text{C}_3\text{H}_8}=0.870 \text{ gs/ml at } 400^\circ\text{C}$ ) was determined from the fitting of the rate equation to the experimental data points (section 6.5). Finally, the effectiveness factor ( $\eta$ ) was calculated according to the equation 2.2.6. Because the particle size was between 250 and 355 microns, the values were calculated for both extremes (Table 2.2.1) .

**Table.2.2.1.** The  $\Psi$ ,  $\Phi$  and  $\eta$  dimensionless numbers corresponding to propane oxidation reaction.

<b>Dimensionless number</b>	<b><math>d_p=250 \text{ mm}</math></b>	<b><math>d_p=355 \text{ mm}</math></b>
$\Psi$	0.05	0.10
$\Phi$	0.29	0.41
$\eta$	0.97	0.95

As it is demonstrated by Table 2.2.1, the Weisz-number and Thiele modulus are below one. The effectiveness factor (the ratio between the actual rate and the highest possible rate) approaches one. Therefore it can be concluded that the pore diffusion is negligible and the reaction rate is kinetically controlled.

#### **2.2.4. The two stage reactor system**

A reactor cascade consisting of two reactor tubes with identical diameter was constructed. These were equipped with the same type of heating cartridge. The isothermal zone was determined also for the second reactor tube according to the previously described procedure (section 2.2.2).

The reactor tubes were connected in series according to the Figure 2.2.3. In order to permit experiments in one reactor tube only, a six port valve was used for the connection of the tubes.

When the position of the six port valve was according to the left side of Figure 2.2.3, the feed mixture was flowing only through the reactor 1. The gas mixture which was leaving this reactor is transferred to the analytical setup (indicated by green lines). Therefore, this corresponds to a single-tube reactor operation mode. In the meantime, the second reactor was purged continuously with a mixture of steam and nitrogen, using the second nitrogen line and the second syringe of the syringe pump.

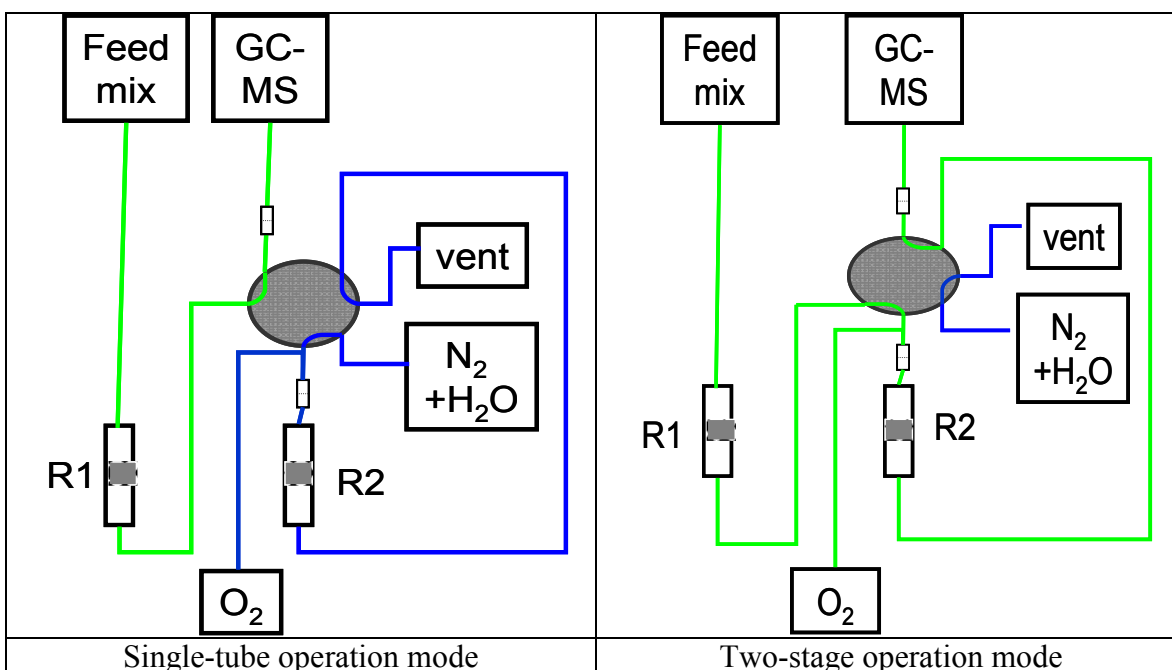


**Figure 2.2.3.** The gas tubing connection of the two stage reactor.

The steam and nitrogen mixture which left the second reactor tube was purged to the vent (indicated by the blue lines). In this configuration, the optional oxygen mass flow controller was not in use.

On the other hand, when the six port valve was turned in the position indicated by the right side of Figure 2.2.3, the feed mixture went through both reactor tubes and then analyzed by the GC-MS (green lines). This corresponds to the two-stage operation mode. Addition of oxygen or other gas was possible through the T-junction installed between

the six port valve and the second reactor. The steam+N<sub>2</sub> mixture was continuously generated but purged to the vent (blue lines).

The addition of gases between the two reactors increased the total flow rate in the second reactor tube. Therefore it influenced slightly both the concentrations and the space velocity. The change of the concentration was corrected by means of the dilution ratio (i.e. the ratio between the total flow rates leaving the second and the first reactor tube). The corrected concentrations were used for the selectivity and rate calculations. The space velocity in the second reactor was calculated based on the loaded amount of catalyst and the total flow rate.

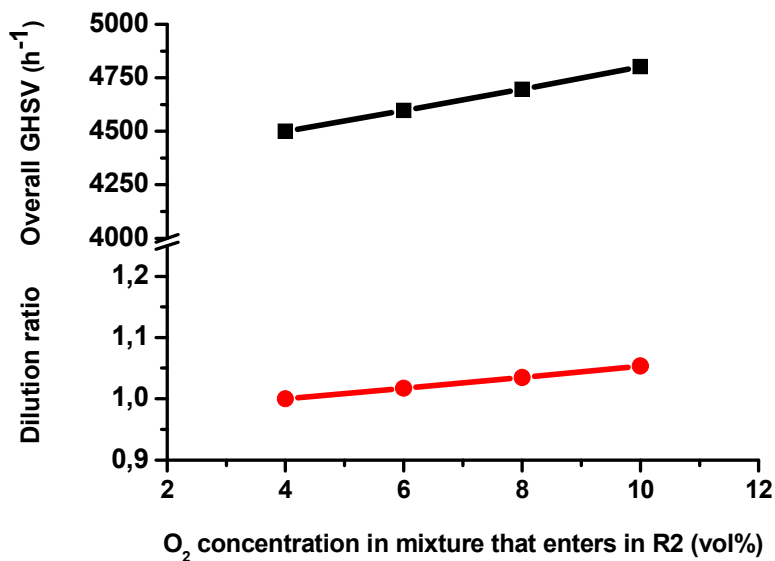


**Figure 2.2.4.** The dilution ratio in the second reactor (red dots) and the overall space velocity (black squares) change upon oxygen addition in the two-stage reactor system.

An example for the change of these parameters in function of the added oxygen gas concentration is shown by Figure 2.2.4. For the calculation of rates, the corrected concentrations were divided by the overall contact time. Therefore, the rate data are more appropriate for the assessment of the effect of added gases than conversion-selectivity data which are not corrected with respect to the change of contact time.

### 2.2.5. The analytical system

For the on-line analysis of the reaction mixture, a GC-MS was used. This setup consisted of five columns, three valves and two detectors (MSD and TCD, respectively) (Agilent 6890 N gas chromatograph, Agilent Technologies 6957 B inert MSD).

The configuration of the columns and the detectors are as follows:

1. 15 m long DB-1 guard-column + 60 m long analytical DB-1 column connected to the MSD. Helium was used as carrier gas at 2.0 ml/min flow rate. The chromatographic method was developed in such a way to separate the oxygenates on the DB-1 columns (Figure 2.2.5). The MSD was operated in Solvent Delay mode until 4 minutes in order to protect the filament and electron-multiplier damage caused by the oxygen and high steam content of the analyzed gas mixture. Therefore, the part of the chromatogram below 4 minutes was not shown on the MSD.
2. 1 m long HaysepQ guard column + 30 m long Plot Q analytical column + 30 m long Plot Molesieve analytical column. The molesieve column could be bypassed by means of a switching valve in order to avoid that polar compounds enter in this column. The detector was a TCD. Helium was used as carrier gas at 7.0 ml/min constant flow rate.

The method was developed in such a way to enable separation and quantitation of C<sub>3</sub>H<sub>8</sub>, C<sub>3</sub>H<sub>6</sub>, H<sub>2</sub>O, N<sub>2</sub>, CO and CO<sub>2</sub> (Figure 2.2.6). The critical separations were the C<sub>3</sub>H<sub>6</sub>-C<sub>3</sub>H<sub>8</sub> and the O<sub>2</sub>-N<sub>2</sub> peak pairs, respectively. The peak resolution of the critical separations was calculated based on Equation 2.2.7 [7]:

$$R_s = \frac{2 \cdot (t_{R,i+1} - t_{R,i})}{\omega_{i+1} + \omega_i} \quad (\text{Equation 2.2.7})$$

The criterion for baseline separation is that the resolution is higher than 1,5 ( $R_s > 1.5$ ) [7]. The resolution of the C<sub>3</sub>H<sub>6</sub>-C<sub>3</sub>H<sub>8</sub> and O<sub>2</sub>-N<sub>2</sub> is higher than the limit of 1.5 (Table 2.2.2). Therefore the above method is good with respect to peak resolution.

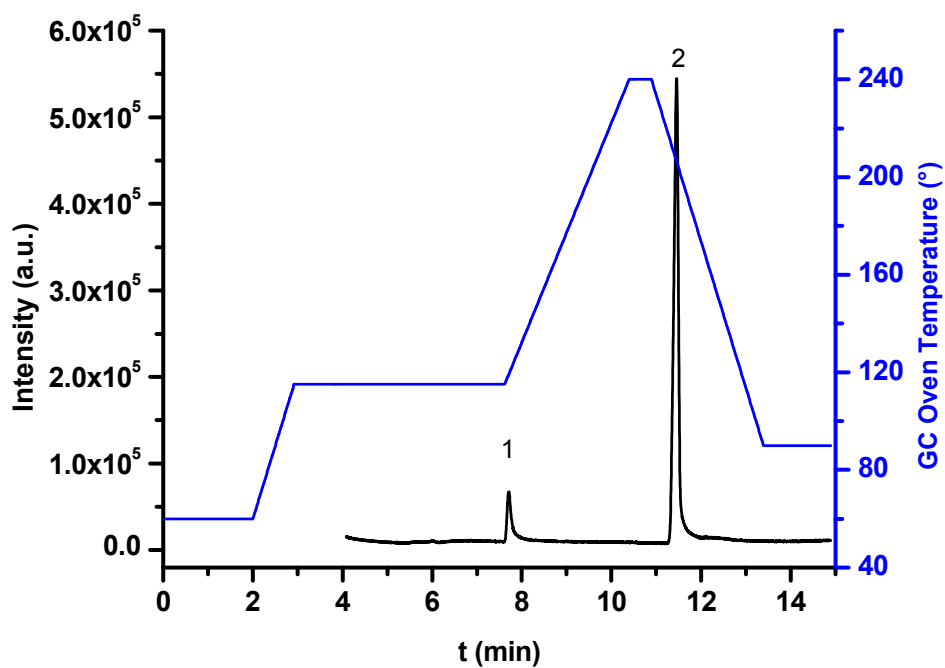


Figure 2.2.5. Detection at the MSD. 1: acetic acid, 2: acrylic acid.

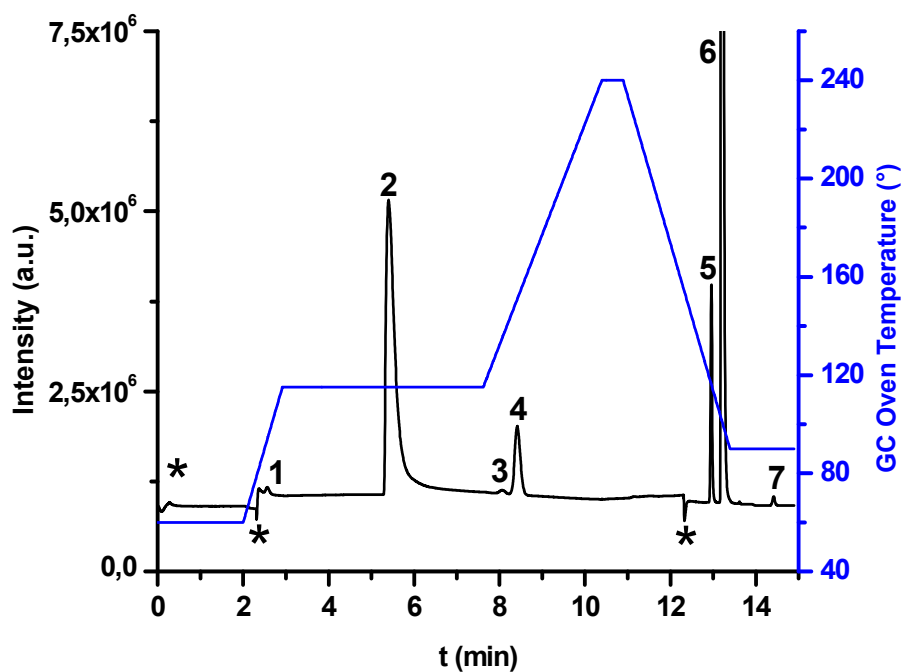


Figure 2.2.6. Detection at the TCD. 1: carbon-dioxide, 2: water, 3: propylene, 4: propane, 5: oxygen, 6: nitrogen, 7: carbon-monoxide, \* : valve switching.

**Table 2.2.2.** The resolution for the peak-pairs which elute close to each other.

<b>Peak-pair number</b>	<b>Peak-pair</b>	<b>R<sub>s</sub></b>
3-4	C <sub>3</sub> H <sub>6</sub> -C <sub>3</sub> H <sub>8</sub>	2.5
5-6	O <sub>2</sub> -N <sub>2</sub>	5.3

The total length of the analysis time was 15 minutes. Gas sampling was performed at every 17 minutes. Therefore the method was satisfactory with respect to the sampling frequency (3.5/h). In case of the acrolein and CO oxidation experiments (sections 4.2.6 and 4.2.7) the number of components were less, therefore the analysis time could be further reduced (to 10 and 8 minutes, respectively).

### **2.2.6. Calibration of the GC-MS**

For the calibration with C<sub>3</sub>H<sub>8</sub> and O<sub>2</sub>, the pure gases (supplied by Westfalen, 99.95%) were mixed with nitrogen (Westfalen, 99.95%). For the calibration with products (C<sub>3</sub>H<sub>6</sub>, CO, CO<sub>2</sub>) and low concentrations of C<sub>3</sub>H<sub>8</sub> and O<sub>2</sub>, gas mixtures with certified concentrations were used (supplied by Westfalen). The composition of calibration mixture 1 was the following: 1.05 vol% C<sub>3</sub>H<sub>8</sub>, 1.03 vol% C<sub>3</sub>H<sub>6</sub>, balance N<sub>2</sub>. The calibration mixture 2 consisted of 1.04 vol% CO, 1.02 vol% CO<sub>2</sub>, 1.06 vol% O<sub>2</sub>, 46.3 vol% N<sub>2</sub> and balance He.

These mixtures were dosed via mass flow controller and diluted further with nitrogen. The resulting gas mixtures were analyzed by the GC-MS. The peaks were integrated and the peak areas were represented with respect to the concentrations (Figure 2.2.7). Weighted linear regression was performed in order to determine the sensitivity (the weighting factor being given by the standard deviation of the repeated measurements).

For the calibration of oxygenates, a saturator was used to saturate a gas stream of nitrogen. The acetic acid and acrylic acid was used with a p.a. quality solutions supplied by Merck. Ca. 15 ml of liquid was poured in the saturator and nitrogen was bubbled through it with a flow rate of 15 mln/min. The temperature of the bubbler was controlled by a HAAKE<sup>®</sup> thermostat. The vapor pressures of these acids at different temperatures are shown in the Table 2.2.3.

**Table.2.2.3.** Vapor pressures of acetic- and acrylic acid at around room temperature [11].

T(°C)	p <sub>HAc</sub> (bar)	p <sub>AA</sub> (bar)
15	0.0079	0.0017
20	0.0109	0.0025
25	0.0149	0.0036

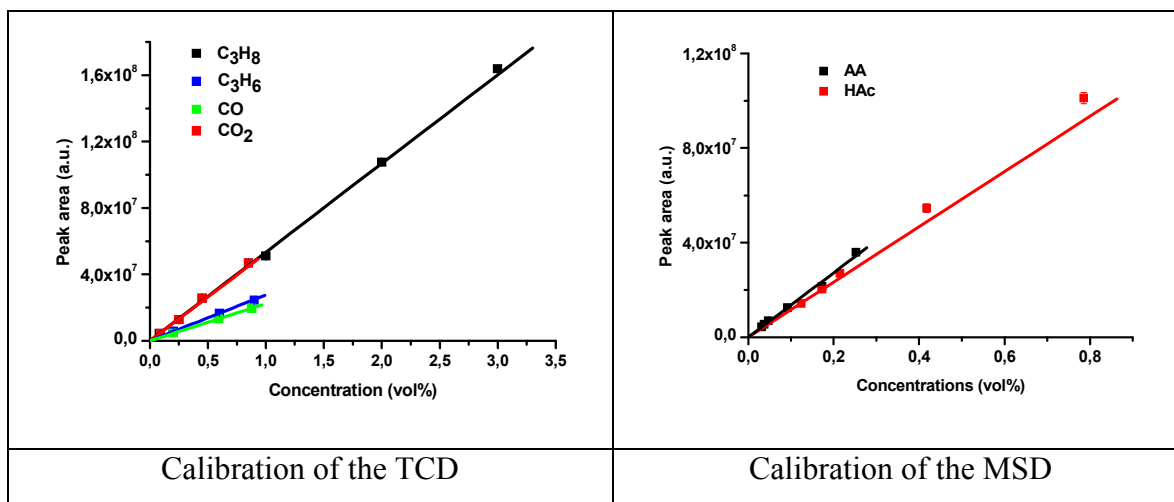


**Figure 2.2.7.** Calibration graphs.

The vapor pressure of these oxygenates are too high at temperatures above 20°C compared to that observed usually in the catalytic experiments. On the other hand, both acids freeze at around 13°C, therefore lower concentrations are not achievable only by using the saturator. Therefore, in order to avoid extrapolations, the mixture was further diluted with nitrogen using the second nitrogen line. The calibration graphs of the oxygenates are shown in Figure 2.2.7.

The sensitivity of the TCD is known to be stable over a relatively long time (months), but the MSD is much less stable. Therefore, the TCD was recalibrated every 3-4 months, while much frequent (weekly) recalibration was needed for the MSD. In order to take into account the daily variation of the MSD sensitivity, every day a solution of 0.5 vol% acetic acid in acetonitrile solvent was injected using the liquid injector port of the GC (Agilent Technologies 7683 B Series Injector). The relative sensitivity was determined every day with respect to the sensitivity determined from the multi-point calibration

described above. For the calculation of the concentration of oxygenates, the actual relative sensitivity was also taken into account.

### 2.2.7. Data analysis

The gas hourly space velocity (GHSV) was calculated based on the volume of the catalyst ( $V_{cat}$ ) loaded in the reactor and the feed total flow rate ( $\dot{V}_{tot.}$ ) (Equation 2.2.8). Whenever the density of the catalyst was not determined with the sufficient precision, the weight hourly space velocity was used (WHSV) which is calculated based on the mass of the catalyst and the total flow rate of the feed. The contact time (W/F or  $\tau$ ) is the reciprocal value of the weight hourly space velocity. The volumetric flow rates were considered at normal conditions (mln).

$$GHSV = \frac{\dot{V}_{tot.}}{V_{cat}} \quad (h^{-1}) \quad (\text{Equation 2.2.8})$$

$$WHSV = \frac{\dot{V}_{tot.}}{m_{cat}} \left( \frac{ml}{g \cdot h} \right) \quad (\text{Equation 2.2.9})$$

$$W / F = \tau = \frac{m_{cat}}{\dot{V}_{tot.}} \left( \frac{g \cdot s}{ml} \right) \quad (\text{Equation 2.2.10})$$

For primary data analysis the conversion, selectivity and yield was calculated under every condition. The educt conversion ( $X_{Educt}$ ) was defined as the ratio between the consumed amount of educt and the initial concentration (Equation 2.2.11). The product selectivities ( $S_{P,i}$ ) were calculated by dividing the amount of formed product by the amount of transformed educt (Equation 2.2.12). The product yield ( $Y_{P,i}$ ) was calculated as the product between the conversion and the selectivity (Equation 2.2.13), while the carbon balance (C-balance) as the ratio between the initial concentration of the educt and the sum of the concentrations of the carbon containing species measured at the reactor outlet (Equation 2.2.13).

$$X_{Educt} = \frac{C_{Educt,0} - C_{Educt}}{C_{Educt,0}} \cdot 100 (\%) \quad (\text{Equation 2.2.11})$$

$$S_{P,i} = \frac{\frac{n_{P,i}}{n_{Educt}} \cdot c_{P,i}}{\sum_{i=1}^n \frac{n_{P,i}}{n_{Educt}} \cdot c_{P,i}} \cdot 100 (\%) \quad (\text{Equation 2.2.12})$$

$$Y_{P,i} = X_{Educt} \cdot S_{P,i} (\%) \quad (\text{Equation 2.2.13})$$

$$C - \text{balance} = \frac{\sum_{i=1}^n \frac{n_{P,i}}{n_{Educt}} \cdot c_{P,i}}{C_{Educt,0}} \cdot 100 (\%) \quad (\text{Equation 2.2.14})$$

The consumption and formation reaction rate was determined as:

$$r_i = \left| \frac{c_{i,0} - c_i}{\tau} \right| \quad \left( \frac{\mu\text{mol}}{\text{g} \cdot \text{s}} \right) \quad (\text{Equation 2.2.15})$$

The apparent activation energy ( $E_a$ ) and the preexponential factor ( $\ln A$ ) were determined from the linearized Arrhenius-equation:

$$\ln r_i = \ln A - \frac{E_a}{R \cdot T} \quad (\text{Equation 2.2.16})$$

The activation enthalpy ( $\Delta H^\ddagger$ ) and activation entropy ( $\Delta S^\ddagger$ ) were calculated based on the linearized Eyring-Polanyi equation:

$$\ln \frac{r_i}{T} = \left( \ln \frac{k_B}{h} + \frac{\Delta S^\ddagger}{R} \right) - \frac{\Delta H^\ddagger}{R \cdot T} \quad (\text{Equation 2.2.17})$$

### 2.3. Catalyst synthesis and characterization

This section describes the preparation of the catalysts which were used for catalytic and kinetic studies reported in chapter 4. Besides the description of the preparation method, the results of physico-chemical characterization are also reported here.

#### 2.3.1. The synthesis of phase pure M1 MoVTeNbO<sub>x</sub> catalyst

The phase-pure M1 MoVTeNbO<sub>x</sub> catalyst was prepared in a relatively large batch (ca. 50 g) according to the procedure developed by detail by Kolen`ko et al [8 ]. This method is adapted from Ushikubo et al. [9] which lead to M1+M2 phase mixture. The phase-pure M1 material was obtained by the washing route described by Baca et al. [10].

92.86 mmol ammonium-heptamolybdate (AHM, (NH<sub>4</sub>)<sub>6</sub>Mo<sub>7</sub>O<sub>24</sub>·4H<sub>2</sub>O) and 195.00 mmol NH<sub>4</sub>VO<sub>3</sub> was dissolved in 1500 ml MQ water at 80°C. The solution was cooled to 40°C and 149.50 mmol solid Te(OH)<sub>6</sub> was added to it and dissolved. 81.25 mmol NH<sub>4</sub>[NbO(C<sub>2</sub>O<sub>4</sub>)<sub>2</sub>]·xH<sub>2</sub>O was dissolved in 500 ml MQ water at 40°C. The two solutions were mixed up and diluted to a total volume of 2500 ml by MQ water, giving a solution with a nominal metal ion concentrations normalized to molybdenum equal to: Mo/V/Te/Nb=1/0.30/0.23/0.125. This solution was stirred for 30 min at 40°C, then spray-dried in a Büchi B-191 spray-dryer. The resulting solid material was calcined at 275 °C for 1 h in synthetic air flow of 100 mln/min, followed by annealing in a Xerion rotary tube furnace 600 °C for 2 hours in Ar flow (100 mln/min) [2, 8]. A crystalline phase mixture was produced (internal identification number 6057) consisting of 63% M1 and 37% M2 phase. The BET surface area was found to be 5 m<sup>2</sup>/g, while the SEM indicated large spherical aggregates. The M2 phase was dissolved by treatment with 15% H<sub>2</sub>O<sub>2</sub> solution and stirring for 24 hours. After washing by distilled water and drying, the remaining solid (internal identification number 6058) was a phase pure M1 material with a surface area of 19 m<sup>2</sup>/g. The SEM revealed rod-like morphology, while aggregate formation was not characteristic to this sample. The shape of the *ab* plane is ill defined and rather porous. Finally, the washed sample was activated at 600°C for 2 hours in the rotary tube furnace under argon flow.

**Table 2.3.1.** The properties of the phase-pure M1 catalysts #6059, #6902 and #8947.

	<b>#6059</b>	<b>#6902</b>	<b>#8947</b>
BET SA (m <sup>2</sup> /g)	8.8	7.5	10.2
Phase comp.	M1	M1	M1
Unit cell parameters (Å)	$a=21.1255(2)$ $b=26.6145(2)$ $c=4.0137(2)$	$a=21.1201(1)$ $b=26.6088(2)$ $c=4.015342)$	$a=21.1462(2)$ $b=26.6312(3)$ $c=4.01454(3)$
Pba2 (no. 32)			
Elem. Comp.	MoV <sub>0.26</sub> Te <sub>0.10</sub> Nb <sub>0.22</sub> O <sub>x</sub>	MoV <sub>0.23</sub> Te <sub>0.10</sub> Nb <sub>0.24</sub> O <sub>x</sub>	--

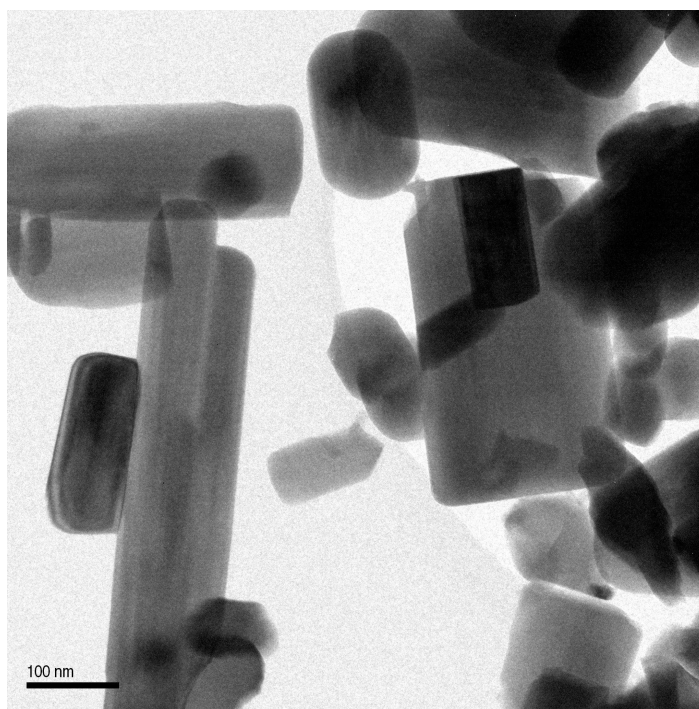


**Figure 2.3.1.** The TEM image of the catalyst #6059.

The resulting material (internal identification number #6059) exhibited a BET surface area of 9 m<sup>2</sup>/g. The nitrogen adsorption isotherm is of type III, characteristic to a macroporous material (isotherm not shown). Because there are no meso- or micropores, internal mass transport limitation is not expected to occur. In the section 2.2.3 it is shown that the effectiveness factor is above 0.95 which proves that the internal mass transport limitation is indeed negligible.

In the XRD pattern the reflections corresponded to the phase-pure M1 material (ICSD 55097) (Figure 2.3.2). The degree of crystallinity was found to be ca. 85%, using rutile TiO<sub>2</sub> SRM 674b as internal standard. The lattice parameters were determined after Rietveld refinement (Table 2.3.1).

The TEM images revealed rod-like morphology (Figure 2.3.1).

A second batch activated from sample #6058 got the internal identification number of #8947. This showed very similar XRD pattern and catalytic properties to that of #6059.

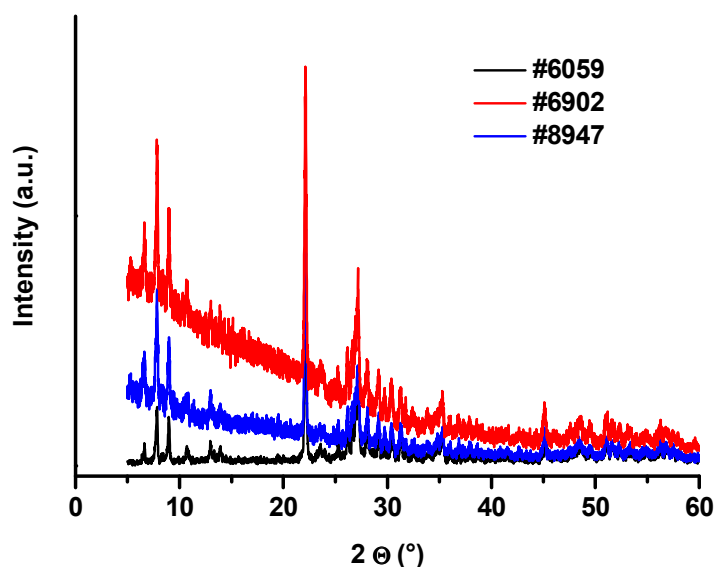


Figure 2.3.2. The XRD pattern of #6059, #6902 and #8947.

A repeated synthesis gave the sample #6902, with a similar physico-chemical and catalytic properties with the #6059 sample. This suggests the reproducibility and reliability of the relatively large scale synthesis method reported by Kolen'ko et al [8].

## References Chapter 2

1. L. C. Jozefowicz, H. G. Karge, E. N. Coker, *J. Phys. Chem.*, 98 (1994) 8053
2. M. Hävecker, S. Wrabetz, J. Kröhnert, L. I. Csepei, R. Naumann d'Alnoncourt, Yu. V. Kolen'ko, F. Girgsdies, R. Schlögl, A. Trunschke, *J. Catal.*, submitted
3. M. Baerns et al. *Technische Chemie*, Wiley-VCH, 2006, 145-193
4. E. A. Burgermeister, W. von Muench, E. Pettenpaul, *J. Appl. Phys.*, 50, 9 (1979) 5790-5794

5. M. Baerns, H. Hofmann, A. Renken, Chemische Reaktionstechnik, Lehrbuch der Chemie, Volume 1, Georg Thieme Verlag, 3<sup>rd</sup> Edition, 1999
6. I. Grißtede, Die partielle Oxidation von Propan zu Acrylsäure, Bestimmung der Reaktionskinetik und in-situ Charakterisierung des Katalysators unter Betriebsbedingungen, Dissertation, Universität Karlsruhe, 2004, Universitätsverlag Karlsruhe, ISBN 3-937300-17-1
7. R. L. Grob, E. F. Barry, Modern practice of gas chromatography, 4<sup>th</sup> Ed., 2004, 25-65, A. Braithwaite, Chromatographic methods, 5<sup>th</sup> Ed., Kluwer Academic Publishers, 1999, 17-40
8. Yu. V. Kolen'ko, W. Zhang, R. Naumann d'Alnoncourt, F. Girgsdies, T. W. Hansen, T. Wolfram, R. Schlögl, A. Trunschke, submitted, ChemCatChem, 2011.
9. T. Ushikubo, K. Oshima, A. Kayou, M. Hatano, X. Can Li, Stud. Surf. Sci and Catal. 112 (1997) 473-480
10. M. Baca, J. M. M. Millet, Appl. Catal. A: General, 279 (2005) 67-77
11. [www.fluidat.com](http://www.fluidat.com)

## **Chapter 3. Structural stability of the M1 MoVTaNbO<sub>x</sub> catalyst under propane oxidation conditions**

### **3.1. Abstract**

In this section the details and results of the in-situ XRD experiment are described, in which the bulk structural stability of the phase-pure M1 MoVTaNbO<sub>x</sub> under real reaction conditions catalyst was addressed. XRD diffractograms were recorded during the long term catalytic experiment on propane oxidation reaction whereby different conditions (steam containing and steam free, net reducing, stoichiometric, and net oxidizing feed compositions). The evaluation of the XRD patterns revealed that the catalyst phase purity was not affected under any of the conditions. Therefore, the bulk structure of the catalyst is stable and constant during the propane oxidation reaction.

### **3.2. Introduction**

Upon reviewing the literature of propane oxidation on Mo and V based oxides only a few studies were found which addressed the question of bulk structural stability of the catalyst under working conditions. However, the information concerning structural stability under reaction conditions is an absolute prerequisite for proper catalytic, kinetic and structure-activity relationship studies.

The stability of the catalyst might be influenced by different factors:

- The temperature is one of the most important ones. Upon the catalyst formulation, usually the thermal treatment or activation is the last step, when the desired crystal structure is developed. The activation is usually carried out at higher temperature than the reaction temperature. Therefore it is not expected that under reaction conditions the temperature plays a role in the stability provided that the reaction is carried out isothermally and hot-spots do not form on the catalyst surface. However, because the activation is carried out in inert atmosphere (argon or helium) and it is not evident that the catalyst is stable in presence of feed at

- reaction conditions even if the reaction temperature is inferior to the activation temperature.
- The redox potential. When a reducing feed is used, the catalyst might be reduced, which leads to change in the composition and in severe cases to the transformation of the crystal structure. On the other hand, when oxidizing feed is used and if the constituting metal ions are not in the highest oxidation state, these ions may be oxidized which also may induce phase change if the structure is not flexible enough. Grasselli et al. carried out redox pulse experiments using a phase-pure M1  $\text{MoV}_{0.25}\text{Te}_{0.11}\text{Nb}_{0.12}\text{O}_x$  catalyst. By applying 120 pulses consisting of  $\text{C}_3\text{H}_8$  and  $\text{NH}_3$ , the catalyst could be reduced as deep as 70 atomic layers of the lattice and then reoxidized by oxygen without structural collapse [1]. This showed the stability of the catalyst bulk structure under reducing conditions. Of course, under reducing conditions the product distribution changed and the propylene formation prevailed. However, it was not shown whether the reoxidized catalyst shows the same conversion and selectivity or not. Zenkovets et al. has also shown that the  $(\text{MoVW})_5\text{O}_{14}$  may be reduced by hydrogen without structural transformation [2].
  - The presence or absence of steam in the feed. Water is a reaction product of oxidation catalysis. However, frequently a high steam content (20-40 vol%) is needed to introduce in the feed for optimal catalytic performance. Novakova et al. observed that in absence of the steam, the catalytic performance of the  $\text{MoV}_{0.3}\text{Sb}_{0.25}\text{Nb}_{0.08}\text{O}_x$  (mixture of  $(\text{MoV/Nb})_5\text{O}_{14}$   $(\text{MoV})_5\text{O}_{14}$ ,  $\text{MoNbO}_x$  and  $\text{SbVO}_x$  phases) drops and the phase composition also changes [3]. Upon re-introducing the steam in the feed, neither the initial phase composition nor the catalytic performance was established. Grißtede noted that the pretreatment of the  $\text{MoV}_{0.33}\text{Nb}_{0.17}\text{Te}_{0.25}\text{O}_x$  catalyst at  $140^\circ\text{C}$  for 24 hours in the reactor using a gas mixture consisting of 50 vol% steam and 50 vol% nitrogen is necessary to achieve high selectivity (69%). When the pretreatment was done with a mixture containing only 10 vol% steam, the highest selectivity was around 40%. Without evidences from XRD measurements it was assumed that the steam promotes the formation of the selective phase [4]. Recknagel also supposed that the better

catalytic performance in acrolein oxidation to acrylic acid is due to phase change induced by steam [5].

- Grißtede noted that when propane was switched to propylene in the feed, the conversion and selectivities reached the steady state only after 72 hours time on stream. Without further experimental evidences (e.g. XRD), this observation was also accounted for the altering of the phase composition.
- The formation of the selective VPO phase (documented by XRD study) was described under propane oxidation conditions, by feeding propane and oxygen at 430°C, then decreasing the temperature to 400°C and introducing steam [6-8].

As shown in the above enlisted literature sources, there is not enough information concerning to the

- bulk structural stability of the phase pure Mo and V based oxide catalysts under various reaction conditions (steam containing and dry feed, low and high oxygen content, and switching from propane to propylene as educt).
- eventual coupling between kinetics of the solid state transformation and the kinetics of the surface catalyzed reaction.

Therefore, within this work, foremost the above open questions were addressed. In order to find out whether under real reaction conditions phase transformation occurs or not, an in-situ XRD experiment was carried out at different steam contents and oxygen concentrations. In the section 3.3 the results of this experiment are summarized.

For the study of the effect of steam and oxygen content on the stability under reaction conditions, experiments were carried out to vary these parameters in the fixed bed reactor as well. The catalytic performance was found to be constant over the time at any steam content (including dry feed) and any initial oxygen concentration (sections 4.2.2 and 4.2.4). The reaction was followed for relatively long time (up to 4 hours at every space velocity), and neither deactivation in time nor change in the selectivity was observed. The conversion measured in dry feed was found to be lower compared to the steam containing feed. Upon switching back from dry feed to the steam containing feed, the catalytic

properties were found to be the same as before (section 4.2.2). Therefore, in contrast to the finding of Novakova et al. [3] reported for the MoVSbNbO<sub>x</sub> catalyst, the catalytic properties of MoVTeNbO<sub>x</sub> are reversible when exposing it to dry feed.

When the reaction was operated under reducing conditions, the propane conversion was found to be lower than in the case of stoichiometric or net oxidizing feed. After performing the reaction under reducing conditions, stoichiometric feed was used again. The conversion and selectivity was comparable to that measured under reducing conditions, but it converged slowly to the value measured before exposing the catalyst to reducing conditions (section 4.2.4 and 4.3.1).

### **3.3. In-situ XRD study on the effect of steam and oxygen**

The experiment was carried out using a STOE Stadi P type diffractometer in a theta-theta arrangement, equipped with a Cu K<sub>α1</sub> radiation source (wavelength=1,54060 Å) and a scintillation detector. A mass of 0.2107 g catalyst was placed in the sample holder of the XRD setup. The feed consisting of steam, propane, oxygen and balance helium was supplied via heated stainless steel tubing in order to avoid condensation of the steam. For the introduction of the steam a bubbler attached to a HAAKE<sup>®</sup> thermostat was used. The total flow rate was always 17.6 mln/min, giving a gas hourly space velocity of 5000 h<sup>-1</sup>. The rationale behind choosing this space velocity is that the maximum productivity in the fixed bed reactor experiments was observed between 4500 and 9000 h<sup>-1</sup> space velocity (described in detail in sections 4.2.1, 4.2.2). Therefore the bulk structure was envisaged to be probed by XRD under the highest performance of the catalyst. The gas mixture leaving the XRD cell was analyzed by an Omnistar<sup>™</sup> mass spectrometer. The following fragments were monitored in time: 12, 13, 14, 16, 17, 18, 28, 29, 30, 31, 32, 40, 41, 42, 43, 44, 45, 56, 60 and 72.

XRD scans were performed under every condition as follows:

1. in helium (100%) at room temperature,
2. in helium (100%) at 400°C
3. C<sub>3</sub>H<sub>8</sub>/O<sub>2</sub>/H<sub>2</sub>O/He=3/6/20/71 vol%, 400°C
4. C<sub>3</sub>H<sub>8</sub>/O<sub>2</sub>/H<sub>2</sub>O/He=3/3/0/94 vol%, 400°C
5. C<sub>3</sub>H<sub>8</sub>/O<sub>2</sub>/H<sub>2</sub>O/He=3/4.5/0/92.5 vol%, 400°C
6. C<sub>3</sub>H<sub>8</sub>/O<sub>2</sub>/H<sub>2</sub>O/He=3/6/0/91 vol%, 400°C
7. C<sub>3</sub>H<sub>8</sub>/O<sub>2</sub>/H<sub>2</sub>O/He=3/9/0/88 vol%, 400°C
8. C<sub>3</sub>H<sub>8</sub>/O<sub>2</sub>/H<sub>2</sub>O/He=3/12/0/85 vol%, 400°C
9. C<sub>3</sub>H<sub>8</sub>/O<sub>2</sub>/H<sub>2</sub>O/He=3/12/5/80 vol%, 400°C
10. C<sub>3</sub>H<sub>8</sub>/O<sub>2</sub>/H<sub>2</sub>O/He=3/0/5/92 vol%, 400°C
11. C<sub>3</sub>H<sub>8</sub>/O<sub>2</sub>/H<sub>2</sub>O/He=3/0/0/97 vol%, 400°C
12. C<sub>3</sub>H<sub>8</sub>/O<sub>2</sub>/H<sub>2</sub>O/He=3/0/0/97 vol%, 400°C, scan performed after long time on stream (24 hours) under this strongly reducing condition
13. in helium (100%) at room temperature.

Repeated scans were performed at every condition in order to be able to observe if eventually slow solid state transformation occurs. The second reason for repeated acquisition of the patterns is that to improve the data quality for the Rietveld refinement. The total length of the experiment was 2 weeks.

First, scans were made at room temperature and 400°C as well in pure helium (condition 1 and 2). Then a measurement was performed using stoichiometric feed and 20 vol% steam (condition 3). In the next step both the oxygen and steam was changed to 3 and 0 vol %, respectively (condition 4). In the next four conditions (5, 6, 7 and 8) the oxygen content was increased from 4,5 (reducing) to 6 (stoichiometric) to 9 and 12 (net oxidizing), in dry feed. In the next condition 5 vol% steam was introduced while keeping the initial oxygen concentration at 12 vol%. The condition 10 corresponds to strongly reducing feed (0 vol% O<sub>2</sub>) in presence of 5 vol% steam, while in the last condition (11) the feeding of steam was also stopped. The scanning was continued while exposing the catalyst to this extreme condition (12) for long time (ca. 24 hours). After this, the propane was switched off and the final scans were recorded at room temperature in helium flow.

The XRD patterns shown in Figure 3.3.1 indicated that under reaction conditions from 3 to 11, no new peak appeared, i.e. no new phase was developed, irrespective of the steam content or the redox potential of the gas mixture. Only slight changes were observed in the peak intensities and positions. More pronounced decrease in the peak intensity was observed upon exposing the catalyst to extreme reducing condition (propane in helium) for long time, but the absence of a new peak suggested that no new phase was formed. The XRD patterns were evaluated quantitatively as well. Rietveld refinement showed that all the patterns correspond to phase-pure  $M1\text{ MoVTeNbO}_x$ , therefore phase transformation during all the above conditions could be ruled out. The lattice parameters are shown in Figure 3.3.2.

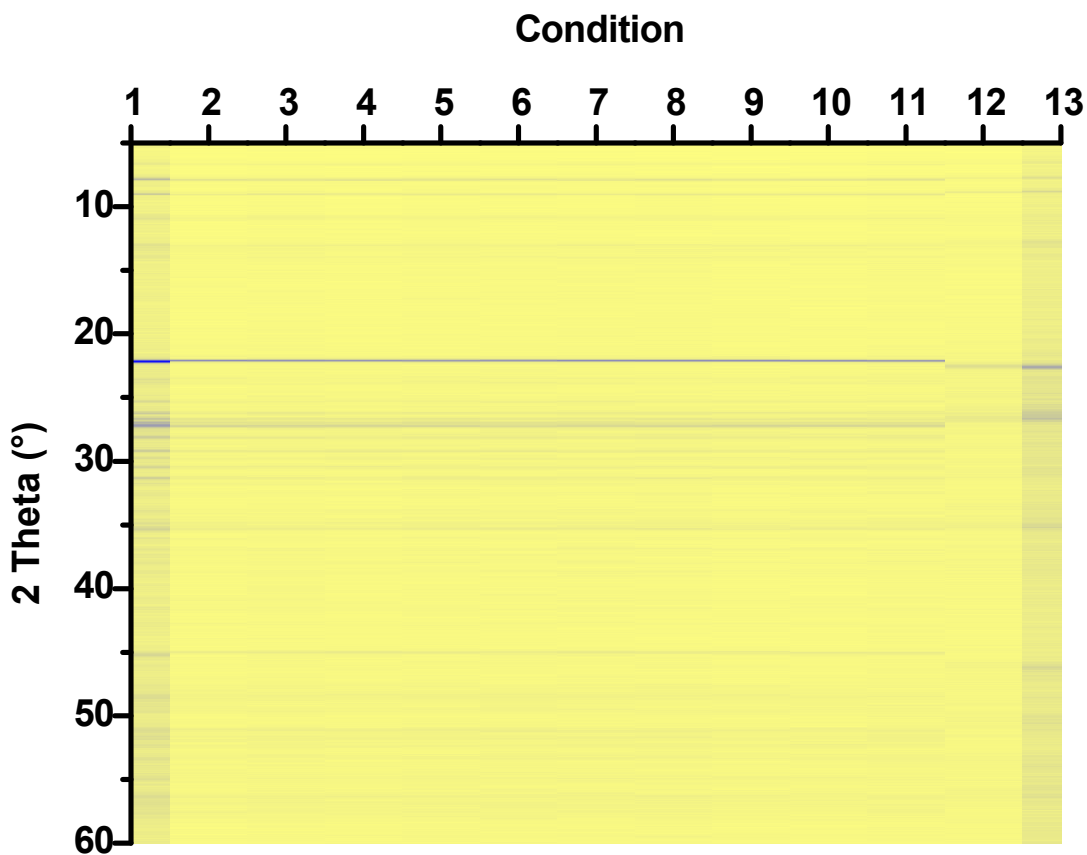


**Figure 3.3.1.** The XRD patterns recorded under different reaction conditions.

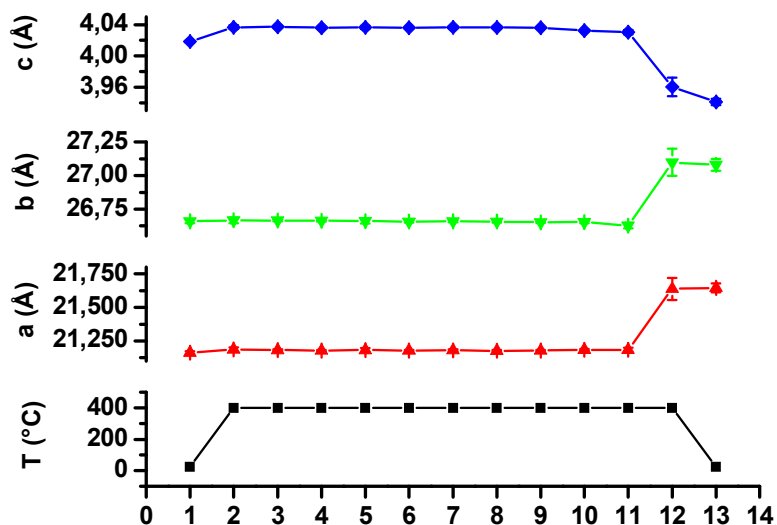
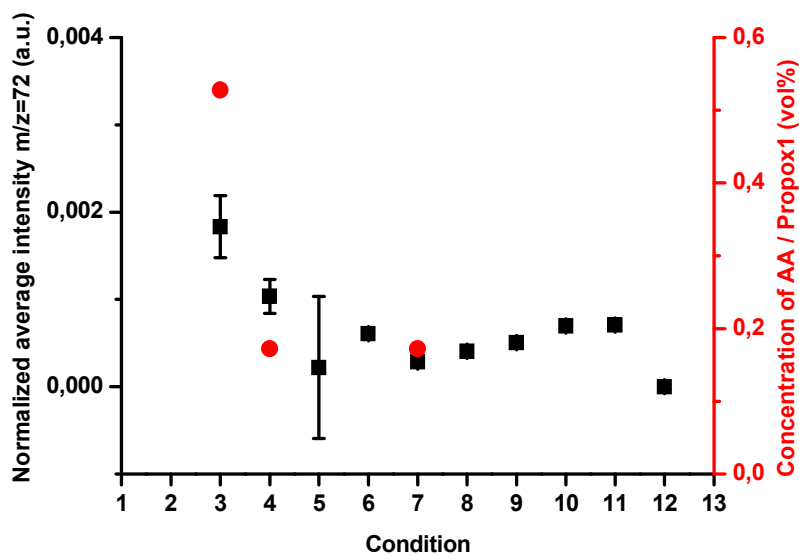


Figure 3.3.2. The lattice constants determined for every condition.

First it can be seen that upon heating up the catalyst in helium, anisotropic lattice expansion occurs, i.e. the thermal expansion occurred preferentially along the  $c$  and  $a$  axis, while the  $b$  lattice parameter was unaffected. Under reaction conditions ranging from 3-11 no change was observed in any of the lattice constants, irrespectively of the steam content or the redox potential. However, upon exposing the catalyst to extreme reducing conditions for long time, the  $a$  and  $b$  lattice constants were increasing, while the  $c$  was decreasing. Finally, anisotropic contraction along the  $c$  axis was observed also upon cooling down the catalyst in inert atmosphere.

The mass spectrometric data recorded during the in-situ XRD experiment was also evaluated. Because the sensitivity of a mass spectrometer changes over the time, the conversion and selectivity data could not be determined with the usual precision obtained at the PropOx-1 fixed bed reactor setup. Therefore, the current of  $m/z=72$  fragment corresponding to the acrylic acid was normalized with respect to helium. The signal was averaged over the time for every condition (Figure 3.3.3). For comparison, the concentration of the acrylic acid determined in PropOx-1 setup, corresponding to three of the conditions is shown in the same graph. It can be observed that the results are

comparable. The differences may be accounted to the fact that the MS data is only semi-quantitative, while the GC-MS data is quantitative (section 2.2). Furthermore, the other reason might be that the sample holder cell of the in-situ XRD setup has a very different geometry compared to the PropOx-1 setup described in the section 2.2.



**Figure 3.3.3.** The normalized average intensity corresponding to acrylic acid during the in-situ XRD experiment monitored by on-line MS (black squares). The concentration of acrylic acid determined in the PropOx-1 fixed bed reactor (blue dots).

### 3.4. STEM analysis of the catalyst before and after the in-situ XRD experiment

The catalyst sample was analyzed by means of scanning transmission electron microscopy (STEM) before and after the in-situ XRD experiment. The elemental analysis was performed by EDX at selected spots.

The STEM images are shown in Figure 3.4.1. It can be observed that the particle size was not affected by the reaction. However, the images corresponding to the post-catalytic sample revealed pitting-like holes on the particles. The occurrence of the voids is statistically distributed and the void size is approximately the same. This suggests that the transformation from the initial to the final state of the catalyst is not a topotactic transformation (i.e. no reaction front can be observed).

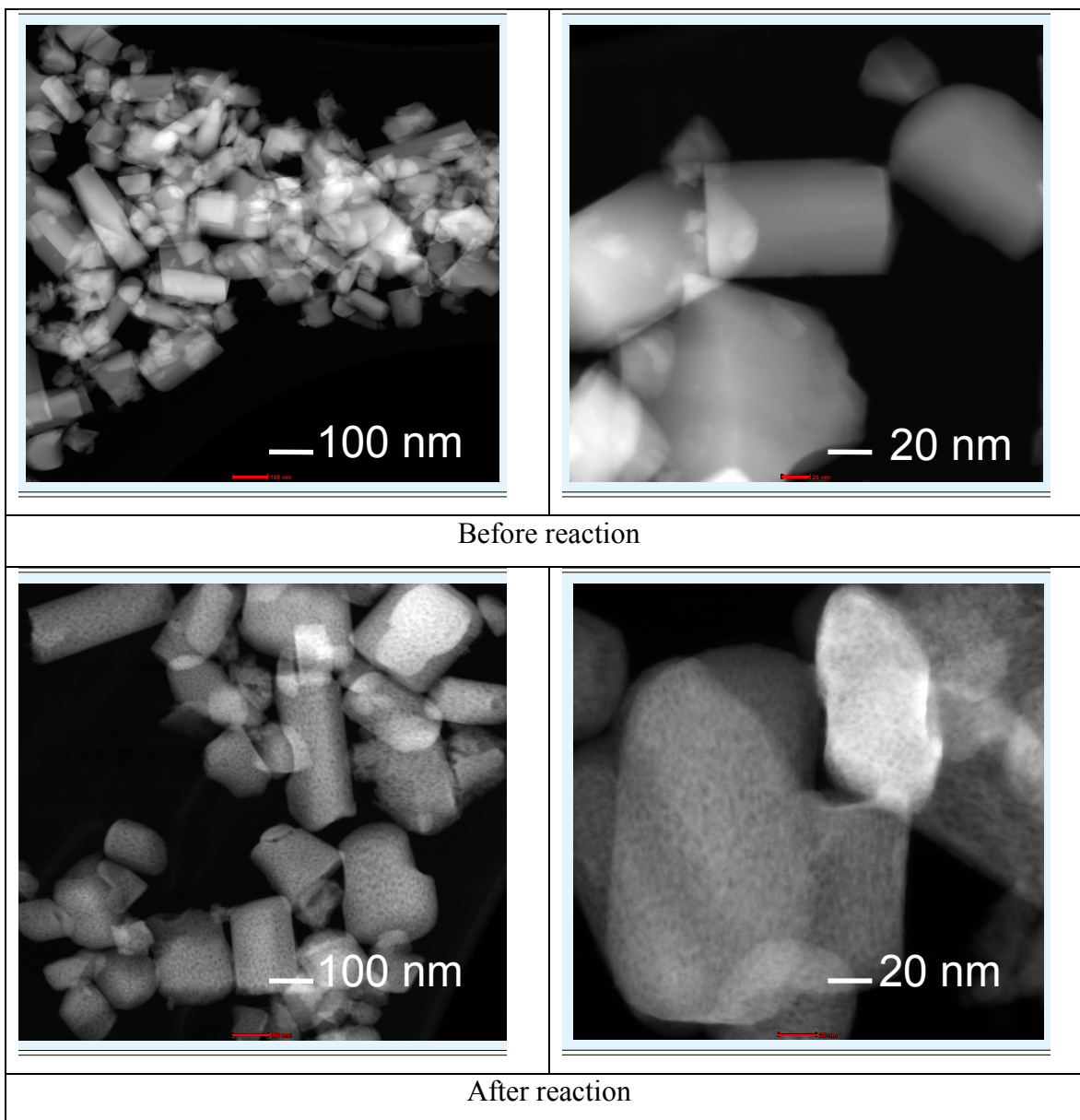


**Figure 3.4.1.** STEM images of the catalyst before and after the in-situ XRD experiment.

The elemental mapping of the particles before reaction showed homogeneous distribution of all the constituting elements (Figure 3.4.2). In contrast to this, the post catalytic sample showed a very heterogeneous distribution of the oxygen, supporting the fact that the catalyst was indeed reduced. Depletion of the tellurium content was also observed in the spots marked with red crosses in the Figure 3.4.3.

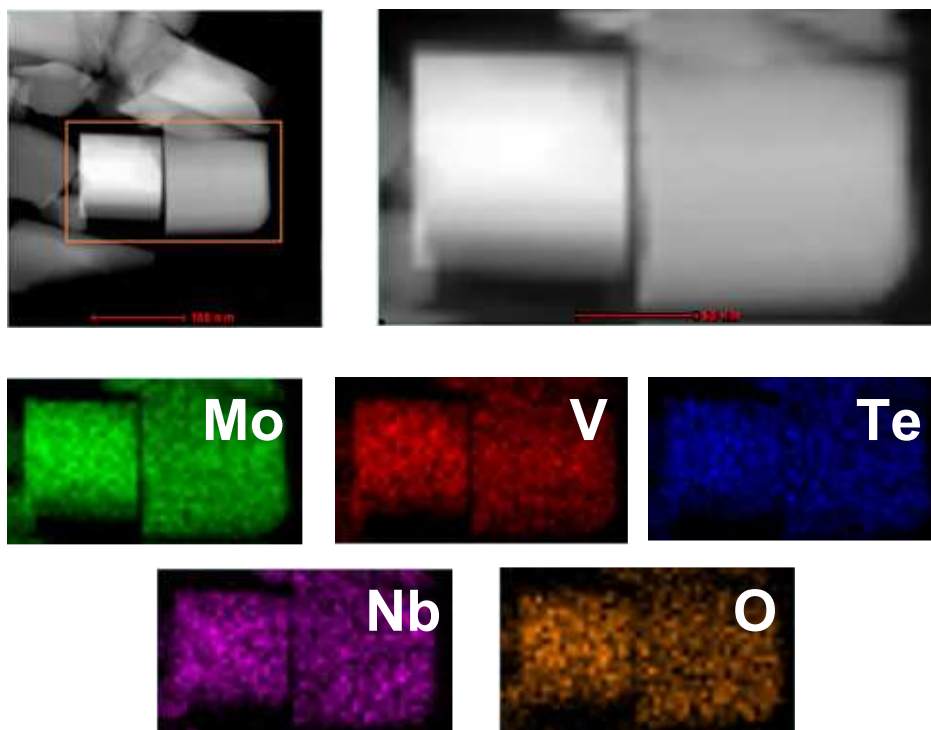


**Figure 3.4.2.** The elemental mapping of the catalyst before reaction.

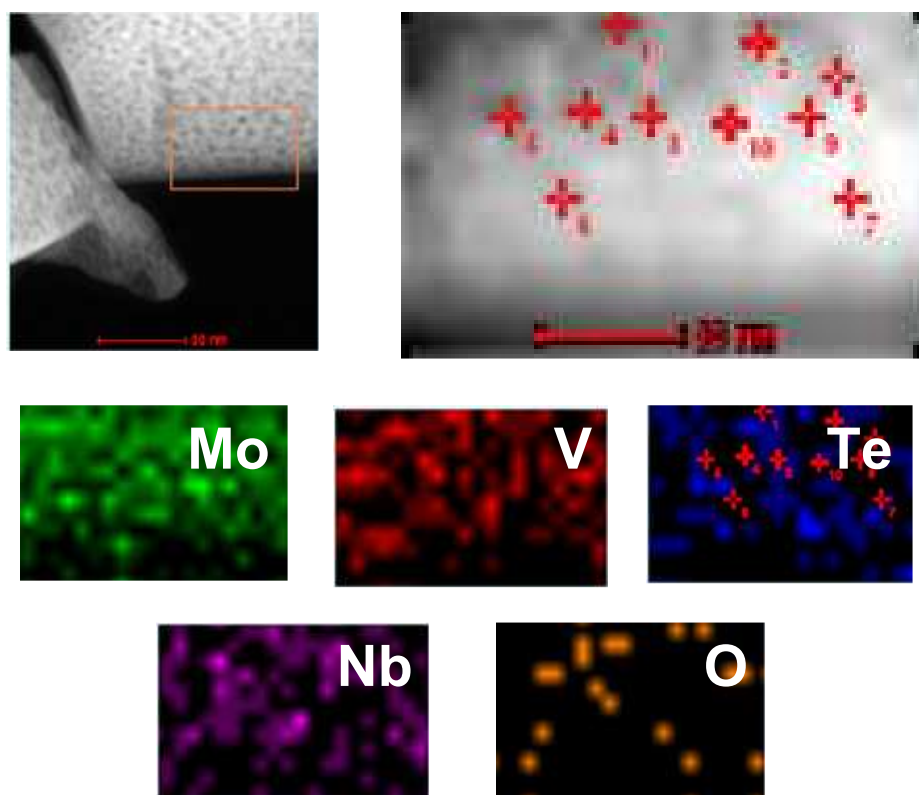


**Figure 3.4.3.** The elemental mapping of the catalyst after reaction.

### 3.5. Conclusions

Upon reviewing the literature dealing with selective oxidation of propane to acrylic acid, it was found that the information concerning the structural stability or instability of the catalyst is seldom reported. Novakova et al. has shown that the deactivation of the MoVSbNbO<sub>x</sub> phase mixture in dry feed is irreversible and it is a consequence of irreversible change in the phase composition. Grißtede also reported the decay of the catalytic performance over the MoVTeNbO<sub>x</sub> catalyst, but no information was provided about the phase composition either before or after the catalytic experiments.

The motivation for the work presented in this section is the fact that the structural stability of a catalyst under various reaction conditions is a criterion for the proper catalytic and kinetic study.

In-situ XRD study was performed on the effect of steam and the oxygen concentration using a phase-pure MoVTeNbO<sub>x</sub> catalyst. The measurements were done at the space velocity corresponding to the maximum productivity of the catalyst. The steam content was varied between 20 and 0 vol%, while the redox potential of the feed between net oxidizing, stoichiometric, moderately reducing conditions. Neither the XRD patterns nor the lattice parameters were changing significantly under these conditions, suggesting that the catalyst bulk structure is robust enough to withstand the variation of the parameters in such a broad interval. At the end, very strongly reducing feed (3 vol% propane and 97 vol% helium) was applied for long time on stream as well. No new peak appeared in the XRD pattern, indicating that no new phase appeared, but the lattice constants changed under this extreme condition. Additionally, the STEM/EDX analysis of the spent catalyst revealed that pitting-like holes appeared on the catalyst particles, and depletion of the tellurium content was also noted.

However, the bulk structure of the used phase-pure M1 MoVTeNbO<sub>x</sub> catalyst is stable under conditions relevant to catalytic applications. Therefore, the kinetics of the heterogeneously catalyzed reaction is not coupled with any solid-state transformation.

The next chapter reports the catalytic and kinetic study of propane oxidation over the phase-pure M1 MoVTeNbO<sub>x</sub> catalyst.

### References Chapter 3

1. R. K. Grasselli D. J. Buttrey, J. D. Burrington, A. Andersson, J. Holmberg, W. Ueda, J. Kubo, C. G. Lungmair, A. F. Volpe, *Top. Catal.*, 38 (2006) 7-16
2. G. A. Zenkovets, G. N. Kryukova, V. Yu. Gavrilov, S. V. Tsybulya, V. A. Anufrienko, T. A. Larina, D. F. Khabibulin, O. B. Lapina, E. Rödel, A. Trunschke, T. Ressler, R. Schlögl, *Materials Chemistry and Physics*, 103 (2007) 295-304
3. E. K. Novakova, J. C. Védrine, E. G. Derouane, *Catalysis Letters*, 83, 3-4 (2002) 177-182
4. I. Grißtede, Die partielle Oxidation von Propan zu Acrylsäure, Bestimmung der Reaktionskinetik und in-situ Characterisierung des Katalysators unter Betriebsbedingungen, Dissertation, Universität Karlsruhe, **2004**, Universitätsverlag Karlsruhe, ISBN 3-937300-17-1
5. R. Recknagel, *Chemische Technik*, 46, 6 (1994) 324-331
6. G. Landi, L. Lisi, J. C. Volta, *Chem. Commun*, 9, 4 (2003) 492-493
7. G. Landi, L. Lisi, J.-C. Volta, *J. Mol. Catal. A*, 222 (2004) 175-181
8. G. Landi, L. Lisi, J. C. Volta, *Catal. Today*, 91-92 (2004) 275-279

## **Chapter 4. Kinetic studies of propane oxidation to acrylic acid on a phase-pure MoVTeNbO<sub>x</sub> catalyst**

### **4.1. Abstract**

A detailed kinetic study is presented for the phase pure M1 MoVTeNbO<sub>x</sub> catalyst. Kinetic studies including the effect of temperature, steam-, propane- and oxygen content variation were performed. The oxidation of propylene, acrolein, carbon monoxide and water gas shift reaction gave important additional information concerning the reactivity of the intermediates and reaction pathways, respectively. Catalytic experiments were performed also in a two-stage reactor system consisting of two reactor tubes connected serially.

### **4.2. Kinetic studies on phase-pure M1 MoVTeNbO<sub>x</sub>**

According to the motivation of the present work, a phase-pure and structurally stable MoVTeNbO<sub>x</sub> catalyst was envisaged for detailed kinetic study in the propane oxidation reaction. The exceptional stability of the phase-pure M1 MoVTeNbO<sub>x</sub> catalyst under catalytically relevant reaction conditions was evidenced in the Chapter 3. In this chapter the results of the kinetic and catalytic experiments are presented. The temperature, propane-, oxygen- and steam contents were varied. Furthermore, the reactivity of the oxidation in propylene intermediate was carried out in the temperature interval corresponding to propane oxidation reaction (360-400°C) and high space velocity (typically 20000 and 80000 h<sup>-1</sup>). The effect of steam on propylene oxidation was also studied.

Acrolein oxidation was carried out in the typical temperature interval corresponding to propane oxidation and very high space velocity (GHSV=250000 h<sup>-1</sup>).

CO oxidation and water gas shift reaction was carried out in the temperature interval of propane oxidation for revealing the secondary pathways that CO might be involved in. On the other hand, the CO oxidation activity was used as a proxy for the amount of electrophilic oxygen species on the catalyst surface.

A two-stage reactor system was used for studying the effect of stage-wise addition of different gases (O<sub>2</sub>, N<sub>2</sub>O, C<sub>3</sub>H<sub>6</sub>, CO and CO<sub>2</sub>).

The oxygen addition in the two-stage reactor design revealed that the acrylic acid yield can be increased, in contrast to the oxygen content variation in the conventional single-tube fixed bed reactor.

Nitrous oxide addition showed no effect on the reactivity. Moreover, the nitrous oxide conversion was found to be zero under every condition, suggesting that the phase pure M1 MoVTenNbO<sub>x</sub> catalyst is not reoxidized by N<sub>2</sub>O.

The product distribution upon propylene addition in the two-stage reactor revealed that acrylic acid, acetic acid, carbon monoxide and carbon dioxide are formed from propylene.

Upon addition of CO in the two stage reactor, no change in the catalytic activity was observed. CO was not further oxidized, which suggests that this is an inert end product besides the CO<sub>2</sub>. Furthermore, this experiment indicated a very low abundance of the electrophilic oxygen species during propane oxidation reaction.

The addition of CO<sub>2</sub> in the two-stage reactor showed also no influence on the product distribution of propane oxidation reaction.

#### **4.2.1. Variation of the contact time and temperature**

For the kinetic study, the contact time was varied up to 2.02 gs/ml by changing the flow rate and the catalyst mass. The experiments were performed at 360, 380 and 400°C. The feed composition was kept constant at C<sub>3</sub>H<sub>8</sub>/O<sub>2</sub>/H<sub>2</sub>O/N<sub>2</sub>=3/6/40/51 vol%.

The dimensionless concentration profiles corresponding to all the detectable compounds (propane, propylene, acrylic and acetic acid, CO and CO<sub>2</sub>, respectively) are presented in the Figure 4.2.1. The normalization of the concentrations was done by dividing the actual concentrations with the initial concentration of propane. By numerical differentiation of the concentration-contact time curves it is possible to obtain the rates of propane consumption and the rates of product formation, respectively. Strictly speaking, the rates can be obtained only in the differential regime, because by definition, within the differential regime the concentrations change linearly with the contact time. In the integral regime the curves deviate from linearity, therefore the rates depend on the extent of the reaction. Highly nonlinear concentration profiles can be observed for the reaction

products above 0,1 gs/ml contact time. Though, for the qualitative description of the kinetic curves, the rate of propane consumption and product formation is considered, irrespective of the integral or differential mode.

The highest acrylic acid productivity is observed in the integral regime. For this reason, in order to find out the effect of operational variables (temperature, redox potential and the steam content) and optimize the acrylic acid yield, it was necessary to carry out the experiment also in the integral mode.

In this section, the effect of temperature on the catalytic properties and kinetic rate constants are presented.

Qualitatively the concentration profiles can be described as follows:

The propane consumption rate increases with temperature.

Propylene is the first intermediate of the reaction, as indicated by a curve that passes through a maximum.

The CO<sub>2</sub> and CO formation rate increases with the temperature. However the CO formation rate was found to be higher than the CO<sub>2</sub> formation rate. Thermodynamically, the carbon monoxide may be further oxidized to CO<sub>2</sub>. This could mean that possibly CO is formed first, and in a consecutive step it may be oxidized to the thermodynamically favored product, CO<sub>2</sub>. If CO would be readily further oxidized to CO<sub>2</sub>, a maximum would be observable in the CO concentration profile. However in the studied contact time interval, the CO concentration profile does not show a maximum at any temperature. Measurements at higher contact times were avoided because of complete oxygen conversion. Therefore from these data the CO oxidation can neither be stated nor refuted. The reactivity in CO oxidation over MoVTeNbO<sub>x</sub> catalyst was addressed in a separate series of experiments. The results are presented in detail in subchapter 4.2.7. As it is shown there, the CO oxidation and water gas shift activity is negligible under the reaction conditions relevant for the selective oxidation reactions. Therefore, CO and CO<sub>2</sub> are formed in independent pathways during the propane, propylene and acrolein oxidation reactions.

The acetic acid is a minor byproduct, which appears at contact times higher than 0.1 gs/ml. No maximum can be observed on the concentration profile, though it can not be stated whether it is a relatively stable end product or it is further oxidized to CO or CO<sub>2</sub>.

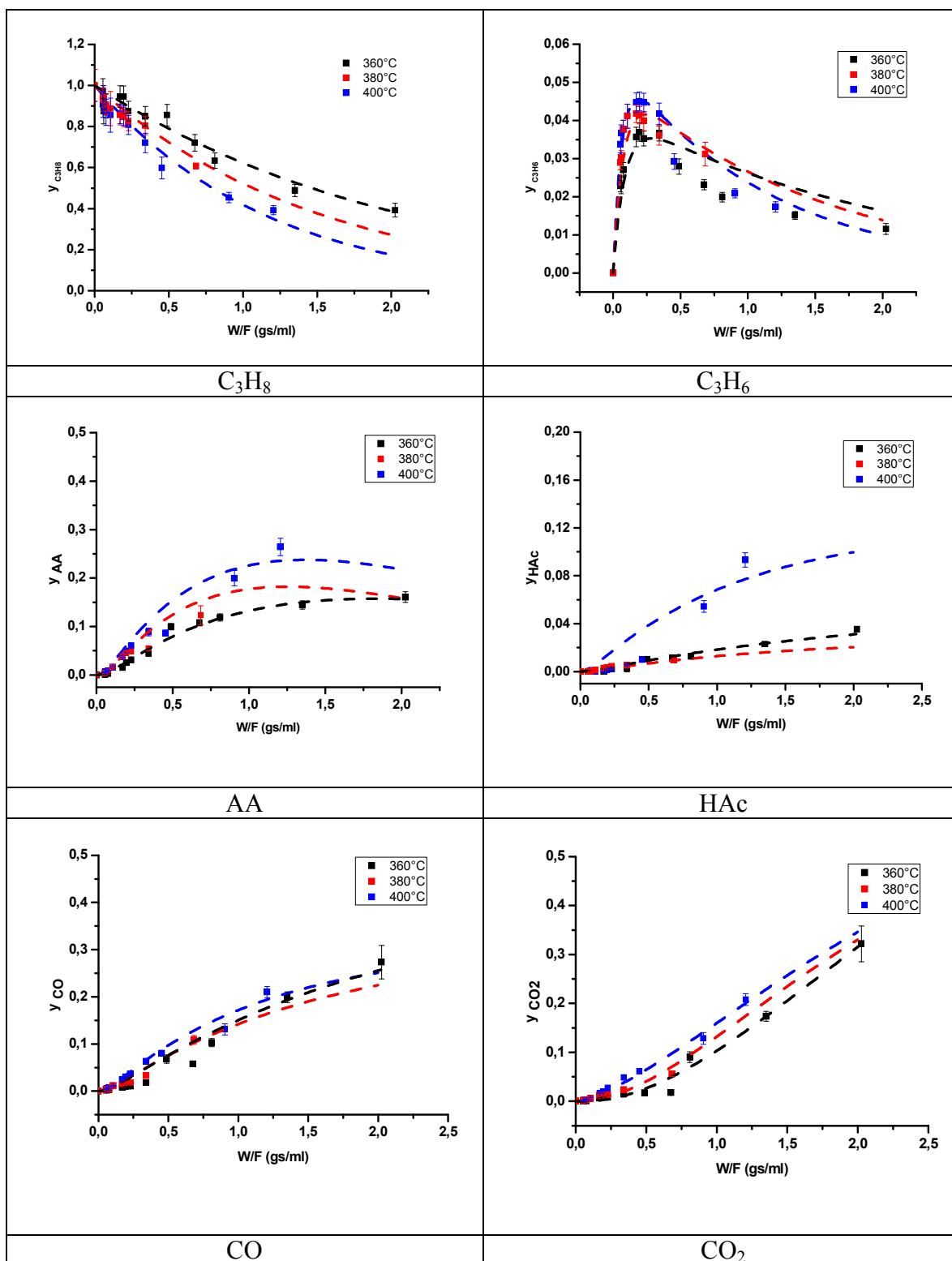


**Figure 4.2.1.** The evolution of concentrations with the residence time at different temperatures. Squares – experimental data, dashed curves – fitted kinetic curves based on reaction model 1 (for modeling see section 6.4.). Feed composition:  $C_3H_8/O_2/H_2O/N_2=3/6/40/51$  vol%, Catalyst ID=6059.

The acrylic acid is the desired product of the reaction. Its concentration – therefore its formation rate as well – increase with the contact time and reaction temperature.

However, above 1.5 gs/ml contact time, the conversion of oxygen approaches 100%, which leads to a high redox potential gradient along the reactor. High oxygen conversions were avoided, because the catalyst particles in the bottom of the catalytic bed are reduced and the kinetics may change with the reduction degree of the catalyst surface. The maximum acrylic acid yield was 25-30%, depending on the temperature.

#### **4.2.2. Variation of the steam content**

The steam content variation was performed in the interval between 0 and 40vol% and for a contact time up to 0.90 gs/ml (GHSV=4500 h<sup>-1</sup>). The feed consisted in every case of 3 vol% propane and 6 vol% oxygen. The steam content was decreased from 40 to 0 vol% by steps of 10 vol%, the balance being N<sub>2</sub>, at a reaction temperature of 400°C.

The experiments presented here were started up with steam containing feed (40 vol%), then the steam content was then reduced by 10 vol%. The catalytic properties were measured for relatively long time in dry feed in order to be able to observe if deactivation occurs. Subsequently, the catalytic performance was re-measured using 20 vol% steam containing feed.

The “reasonably long term stability” of the catalytic properties in steam free feed is demonstrated in Figure 4.2.2. The adjective of reasonability in the context of long term stability is related here to the time resolution of the used analytical methods. As shown in the Experimental part (section 2.2.5.), the gas chromatographic setup has a time resolution of one injection/17 minutes. On the other hand, in situ XRD experiments were carried out on the effect of oxygen and steam (Chapter 3). The time resolution of the XRD setup is several hours/scan.

As shown by Figure 4.2.2, the stability in time of the catalytic performance exceeds satisfactorily the gas chromatographic analysis time. Neither catalyst deactivation nor change in the selectivity was observed within the studied time on stream intervals up to 4 hours at different space velocities. The stability of catalytic performance makes possible to perform the kinetic study of propane oxidation also under steam free feed conditions.

It has to be emphasized that even if no steam is fed in the reactor, water is produced by the reaction, on the active sites of the catalyst. Therefore, it would be improper to state that the experiments were carried out under dry conditions. Moreover, there is a gradient of produced water concentration along the catalytic bed. Indeed, the chromatographic analysis of the reactor effluent gas showed a detectable amount of water. However due to highly asymmetric peak shape and low peak area, the quantification of the formed water was difficult.

It is important to notice that at a contact time of 0.227 gs/ml (GHSV=18000 h<sup>-1</sup>), the conversion is low, and at the limit of the differential operation mode. The most abundant product is propylene with a selectivity of ca. 50%. The acrylic acid selectivity is quite low, and acetic acid is not produced at all.

At lower space velocities, the conversion increases, and the selectivity to acrylic acid becomes higher than the propylene selectivity. Additionally, acetic acid appears as byproduct. Below the space velocity of 9000 h<sup>-1</sup> the selectivity to acrylic acid decreases due to total oxidation. In every case, however, the selectivity to CO was higher than the selectivity to CO<sub>2</sub>.

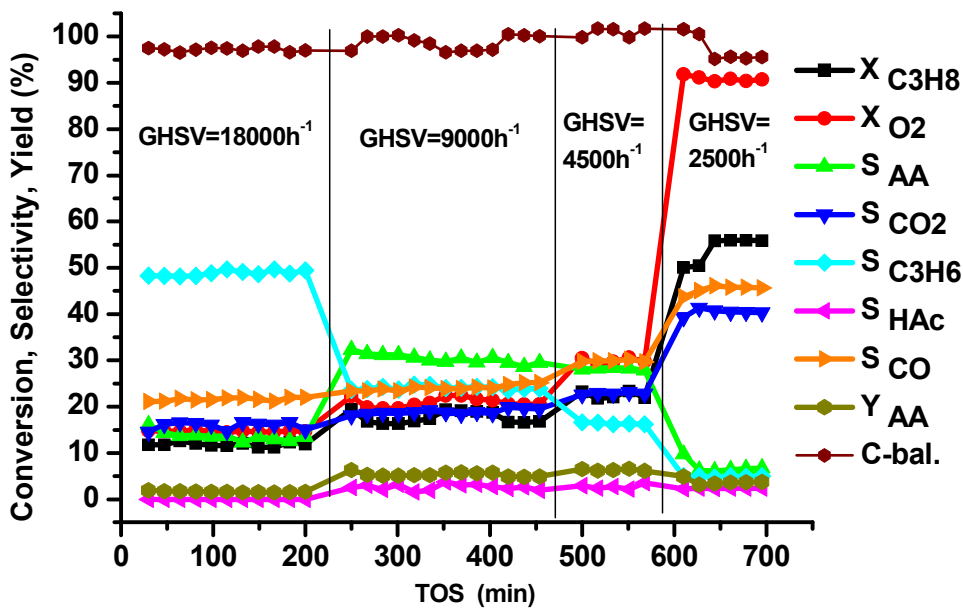
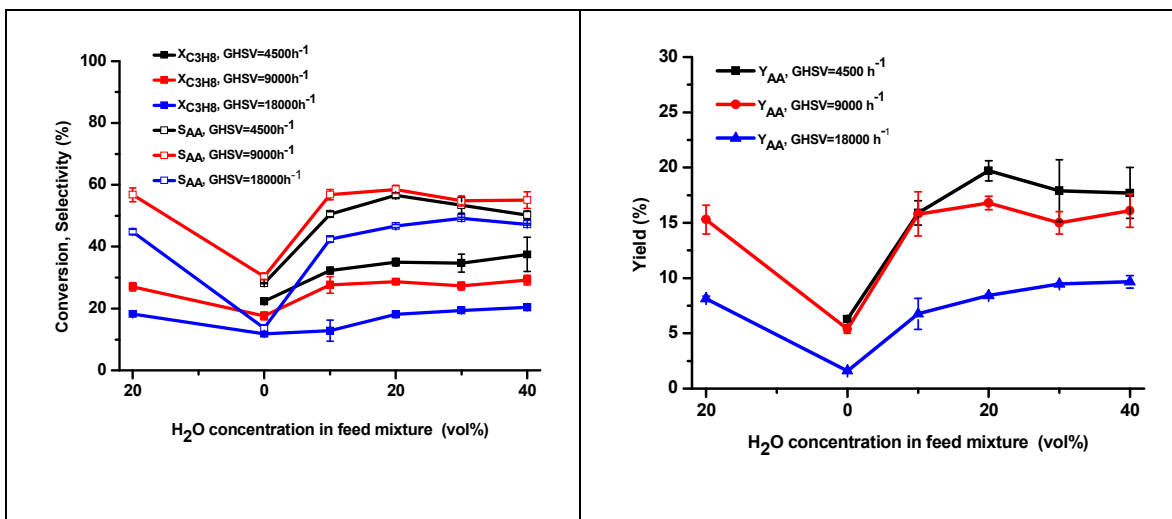


Figure 4.2.2. The stability of catalytic performance in steam-free feed.

After performing the catalytic performance in dry feed, the catalytic properties were re-measured using a feed mixture containing 20 vol% steam. Upon immediate switching from dry feed to steam containing feed, the conversions and selectivities were found to be constant over the time on stream, within experimental errors. Moreover, the catalytic performance was the same as before exposing the catalyst to dry feed (Figure 4.2.3.). This suggests that the catalyst responds dynamically to the changes of the steam content in the feed. The changes are completely reversible and faster than the gas chromatographic analysis time of 17 minutes. The productivity of the catalyst expressed in terms of conversion of propane, the selectivity and yield to acrylic acid is displayed on Figure 4.2.3 at a space velocity of 18000, 9000 and 4500 h<sup>-1</sup> (W/F=0.228, 0.455 and 0.904 gs/ml, respectively).

In the concentration interval between 20 and 40 vol%, the catalytic performance is not influenced significantly by the steam.

Below a steam content of 20 vol%, both the conversion and selectivity drops dramatically. Nevertheless, in contrast to the observation reported by Novakova et al. [1], this drop is reversible: after switching back to the feed containing 20 vol% steam, the conversions and selectivities were comparable to those determined before exposing the catalyst to dry feed.



**Figure 4.2.3.** The effect of steam on the acrylic acid productivity at GHSV=4500, 9000 and 18000 h<sup>-1</sup>.

The temperature variation between 360 and 400°C using reaction mixtures containing 0, 10 and 40 vol% steam was also performed. The catalytic properties expressed in terms of propane conversion, acrylic acid selectivity and yield are summarized in the Figure 4.2.4. Similarly to the trend demonstrated in Figure 4.2.3, the conversion of propane and the selectivity to acrylic acid is positively influenced at every temperature (Figure 4.2.4). Although the conversion rises, and the selectivity decreases slightly, the yield to acrylic acid levels off at around 380°C.

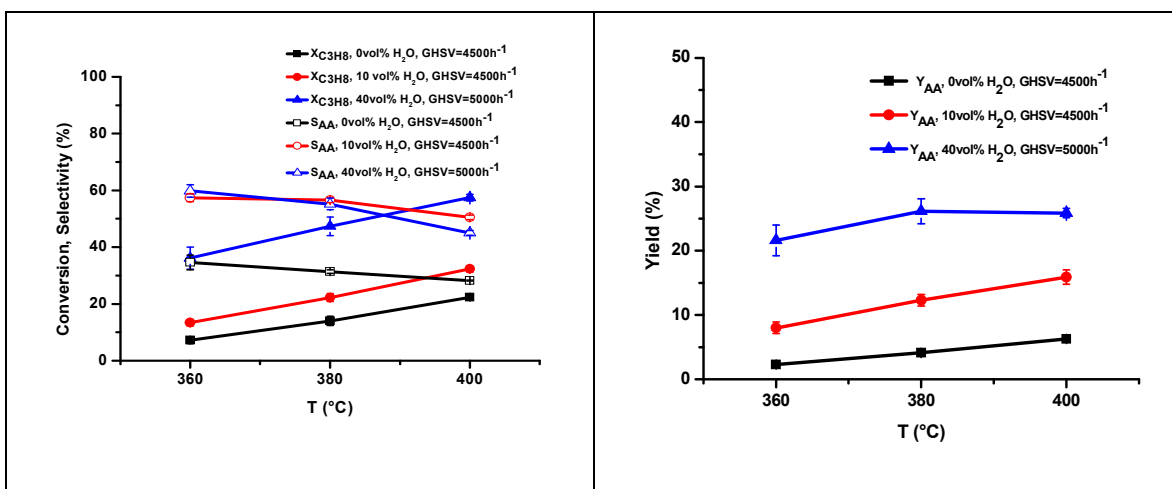


**Figure.4.2.4.** The effect of temperature on the catalytic performance at 0, 10 and 40 vol% steam content. Catalyst #6059.

The activation parameters (apparent activation energy, logarithm of the pre-exponential factor, activation enthalpy and entropy, respectively) were calculated using the linearized form of the Arrhenius- and Polanyi-Eyring equations. The numerical values of these activation parameters are summarized in Table 4.2.1.

It can be observed that in the presence of steam the apparent activation energy is reduced significantly, by a factor of 2,4 when 40 vol% steam is present in the feed mixture. The logarithm of the pre-exponential factor and the activation entropy decreases as well, indicating that in presence of steam both the number of collisions per unit surface and also the structure of the activated complex is influenced. On the other hand, the activation enthalpy is larger when steam is present in the feed.

**Table 4.2.1.** The activation parameters of propane consumption at different steam contents.

<b>Activation parameter C<sub>3</sub>H<sub>8</sub> consumption</b>	<b>0 vol% H<sub>2</sub>O</b>	<b>10 vol% H<sub>2</sub>O</b>	<b>40 vol% H<sub>2</sub>O</b>
E <sub>a</sub> (kJ/mol)	95 ± 13	76 ± 7	39 ± 8
lnA	20 ± 2	17 ± 1	11 ± 1
ΔH <sup>#</sup> (kJ/mol)	-89.70 ± 0.02	-70.26 ± 0.01	-33.49 ± 0.01
ΔS <sup>#</sup> (J/molK)	-92.58 ± 0,03	-118.36 ± 0.02	-168.22 ± 0.02

A decreasing trend in the apparent activation energy of propane oxidation on MoVSbNbO<sub>x</sub> catalyst was reported by Novakova et al. In dry feed the apparent activation energy was found to be 68 kJ/mol, while only 50 kJ/mol at 25 vol% steam content [1]. However, in the work reported by Novakova et al. the MoVNbSbO<sub>x</sub> catalyst was deactivating and the bulk structure was altered irreversible in steam-free feed. Therefore, the apparent activation energy of 68 kJ/mol was probably not determined under steady-state conditions.

The concentration profiles from contact time variation at different steam concentrations are presented in Figure 4.2.5. In the following, the qualitative information arising from these plots are summarized.

The propane consumption rate depends on the steam content of the feed. The lowest consumption rate was observed in a steam free feed. The presence of steam enhances the consumption rate; however this positive effect levels off above the concentration of 20 vol%.

This observation is in accordance with the trends reported by Novakova et al. and Grißtede [1-4].

The propylene concentration profile is similar at all steam contents. However, the contact time ( $W/F_{\max}$ ) corresponding to the maximum propylene concentration shows the following dependence on the steam content: 0.272 gs/ml at 0 vol% steam, 0.227 gs/ml at 10 vol% steam and 0.185 gs/ml for 20, 30 and 40 vol% steam. The value of  $W/F_{\max}$  is related to the formation and consumption rate constant of propylene. In case of the first

order consecutive reactions the  $W/F_{\max}$  is equal to the logarithmic average of the rate constants of the steps involving the intermediate product.

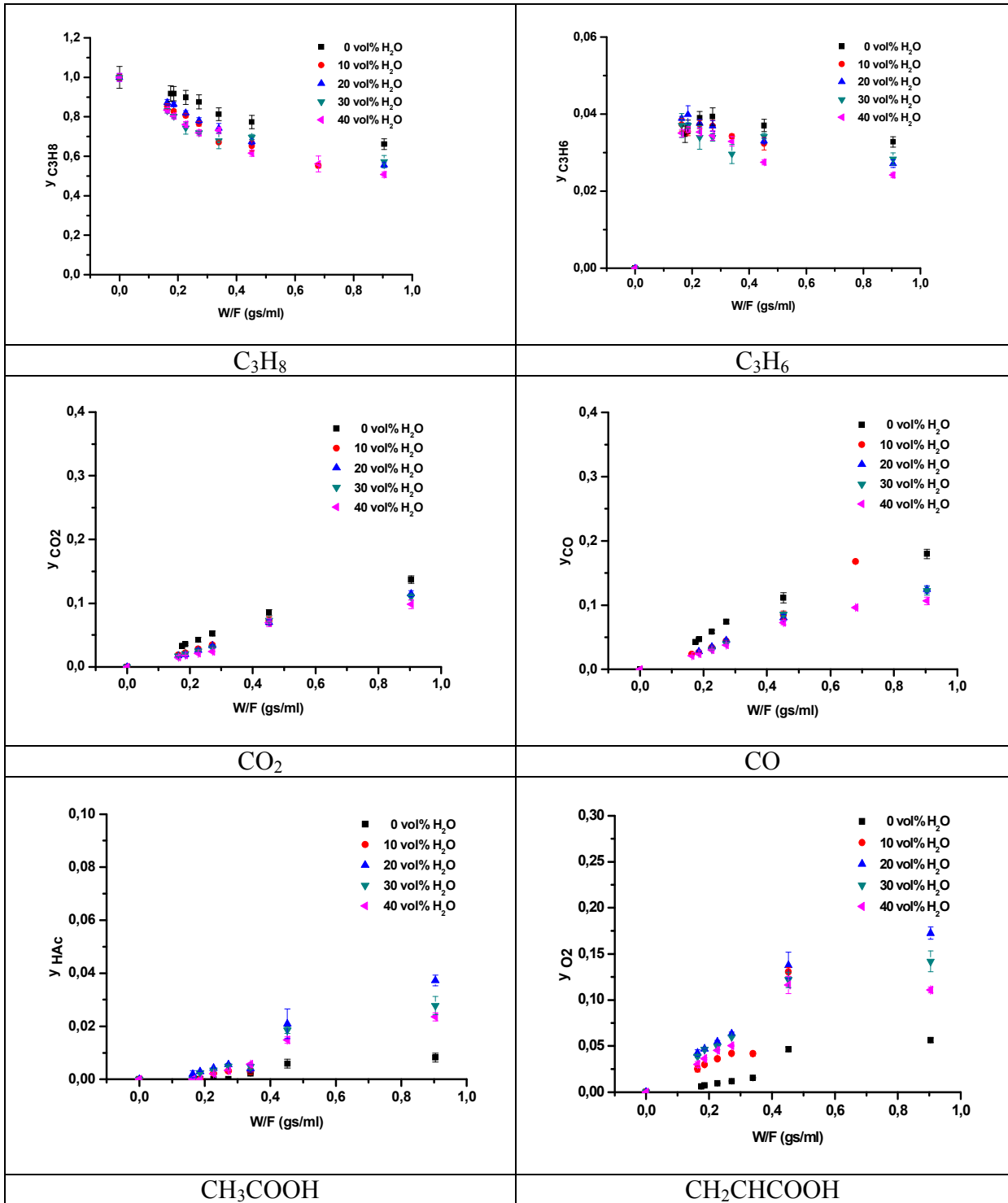


Figure 4.2.5. The effect of steam on the concentration profiles.

The decrease of  $W/F_{\max}$  suggests that presence of steam increases the increase of the ratio between the consumption and the formation rate constant of propylene. On the other hand, not only the position of the maximum is related to the formation and consumption rate constants, but the actual concentration of the intermediate product as well. At high contact times, the decay of propylene concentration is more enhanced in presence of steam. This also suggests that steam increases the rate constant of further oxidation of propylene [5].

The CO and CO<sub>2</sub> concentration profiles share the same qualitative features: compared to the dry feed, both the CO and CO<sub>2</sub> formation rates are reduced already in the presence of 10 vol% steam.

A further increase of steam concentration does not further reduce the rates of CO and CO<sub>2</sub> formation. It is also notable that the rate of CO formation is higher than CO<sub>2</sub> formation rate, under every condition. Nevertheless, the concentration profile does not reveal more information about the steps by which these total oxidation products are formed. Therefore, it could not be established whether CO was formed as a first total oxidation product and then further oxidized to CO<sub>2</sub>, or they are products of parallel and independent steps. This issue was addressed and elaborated in subchapters 4.2.7 and 4.3.3, where results concerning the CO oxidation, water gas shift reaction and addition of CO in the two-stage reactor are presented, respectively.

The formation rate of acrylic acid and acetic acid is enhanced significantly in presence of steam in the feed, in accordance with the observations of Grißtede [2, 3], Novakova et al. [1], Dubois et al. [6] and Zheng et al. [7]. The maximum formation rates are observed at 20 and 30 vol% steam concentration. At 40 vol% water content the acetic and acrylic acid concentrations are slightly lower compared to those determined at 20 and 30 vol% steam content, especially at contact times close to 1.0 gs/ml.

Neither the acetic acid nor the acrylic acid concentration passes a maximum in the studied contact time interval. The only exception is the measurement carried out without steam in the feed, in this measurement the concentration profiles of acetic acid and acrylic acid are flattened at high contact times, but no net decay can be observed. This shows that both acids are relatively stable against further oxidation.

### 4.2.3. Variation of the propane content

The propane concentration variation was performed in the interval between 1 and 3 vol% for the determination of the partial order with respect to propane. For this purpose the concentration of oxygen and steam was kept constant at 6 and 40 vol%, respectively, the nitrogen making up the balance (Figure 4.2.6).

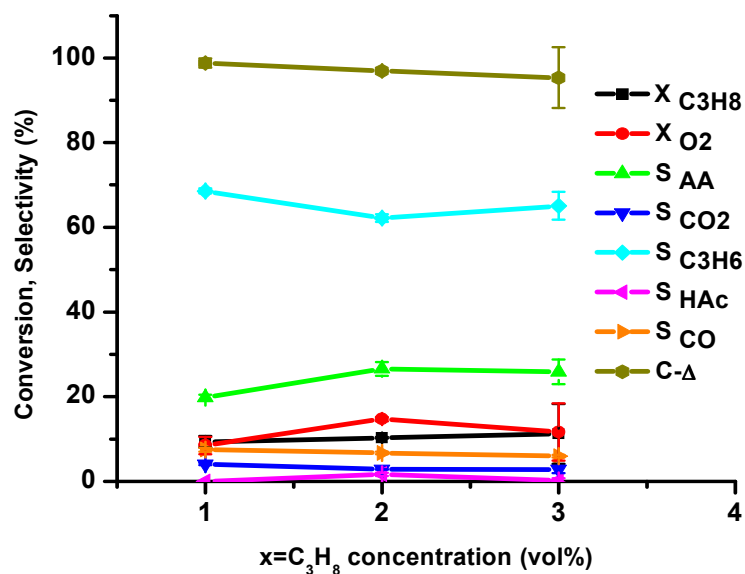


**Figure 4.2.6.** The effect of the propane concentration on the catalytic performance.  $C_3H_8/O_2/H_2O/N_2=x/6/40/(54-x)$  vol%,  $T=400^\circ C$ . GHSV= 34280  $h^{-1}$ ,  $W/F=0.11$  gs/ml. Catalyst: #6059.

Because the propane concentration was varied at constant oxygen concentration, the redox potential was stoichiometric with respect to the propane to acrylic acid reaction (in the case of the feed  $C_3H_8/O_2=3/6$  vol%), and net oxidizing (in the case of  $C_3H_8/O_2=2/6$  and  $1/6$  vol% feeds, respectively). The experiment was performed at  $400^\circ C$  and a contact time of 0.11 gs/ml.

The propane conversion is relatively independent on the initial propane concentration. Propylene is the main product, while other products in the order of abundance are acrylic acid, CO, CO<sub>2</sub> and acetic acid. In case of slightly oxidizing feed ( $C_3H_8/O_2=2/6$  vol%) the selectivities were very similar to that obtained for stoichiometric feed, while in case of

strongly oxidizing feed (6-fold excess of oxygen) the propylene selectivity increased slightly at the expense of acrylic acid selectivity.

For kinetic modeling, the partial order with respect to reactants, propane and oxygen were determined using a power rate equation. This power rate equation contains two independent variables, the concentrations of propane and oxygen, respectively (Equation 4.2.1). Because of this, the reaction order with respect to both components can be obtained by partial derivation of the rate equation if both concentrations are varied simultaneously in the experiments (Equations 4.2.2 and 4.2.3). On the other hand, if the concentration of one component is kept constant, the rate law is simplified. Since the initial oxygen concentration was 6 vol% in all the experiments, the two constant terms on the right hand side of the power law can be contracted into a single apparent rate constant  $k'$  (Equation 4.2.4). Then the power law will contain only one variable. The reaction order  $m$  can be determined from the slope of the straight line of the double-logarithmic plot according to the linearized equation 4.2.5 (Figure 4.2.7) [8, 9].

$$r = k \cdot c_{C_3H_8,0}^m \cdot c_{O_2,0}^n \quad (\text{Equation 4.2.1})$$

$$m = \frac{\partial \ln r}{\partial \ln c_{C_3H_8,0}} \quad (\text{Equation 4.2.2})$$

$$n = \frac{\partial \ln r}{\partial \ln c_{O_2,0}} \quad (\text{Equation 4.2.3})$$

$$r_{C_3H_8} = k' \cdot c_{C_3H_8,0}^m \quad (\text{Equation 4.2.4})$$

$$\ln r_{C_3H_8} = \ln k' + m \cdot \ln c_{C_3H_8,0} \quad (\text{Equation 4.2.5})$$

The slope of the above plot shown below is equal to  $1.10 \pm 0.01$ , and consequently the reaction is first order with respect to propane.

The application of the integral method supported that the reaction is first order with respect to propane: the simulated concentration profile based on the integrated rate equations containing a first order step with respect to propane is in good agreement with the experimentally determined profile over a wide contact time interval (Figure 4.2.1). This is an indication that first order kinetics is valid under both differential and integral regimes [8].

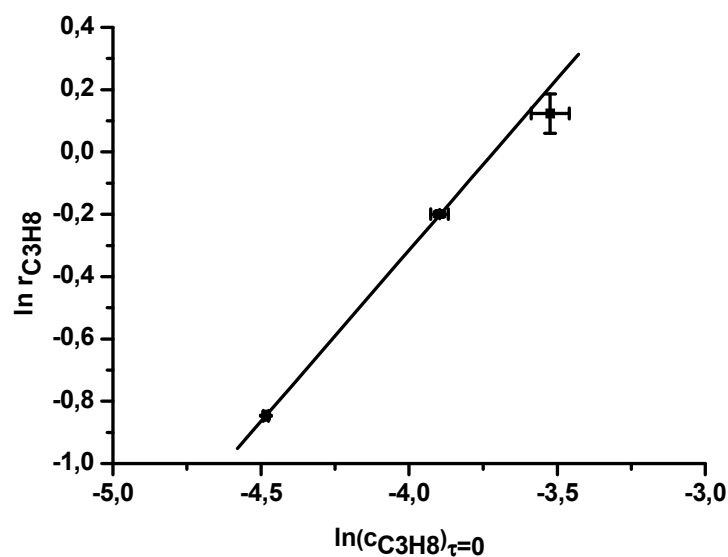
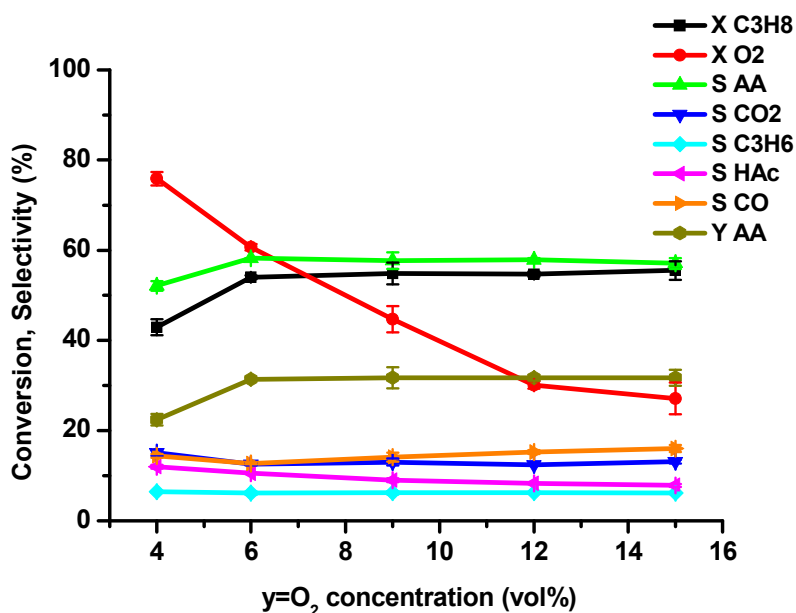


Figure 4.2.7. Determination of the reaction order with respect to propane.

#### 4.2.4. Variation of the oxygen content

The effect of the initial oxygen concentration was also studied. The initial oxygen concentration was varied in the interval from 4 to 15 vol%, keeping the initial propane concentration constant at 3 vol%. Thus, the catalytic experiments were performed under three redox potentials of the gas mixture:

- i) reducing, at 4 vol% O<sub>2</sub>,
- ii) stoichiometric, at 6 vol% O<sub>2</sub> and
- iii) net oxidizing at 9, 12 and 15vol% O<sub>2</sub>, respectively.



**Figure 4.2.8.** The effect of the oxygen concentration on catalytic performance.  $C_3H_8/O_2/H_2O/N_2=3/y/40/(57-y)$  vol%,  $T=400^\circ C$ . GHSV= 4500  $h^{-1}$ , W/F=0,904 gs/ml, catalyst: #6059.

The redox potential in terms of reducing, stoichiometric and oxidizing feed was defined with respect of the stoichiometry of 1:2 with respect to propane and oxygen, corresponding to the propane to acrylic acid transformation.

Under reducing conditions, both the conversion and selectivity to acrylic acid were found to be slightly lower compared to the catalytic performance observed at stoichiometric and oxidizing conditions. However, the conversion, selectivity and consequently also the yield to acrylic acid levels off at 6 vol% O<sub>2</sub>, as demonstrated in Figure 4.2.8. The fact that the propane conversion does not depend on the initial oxygen concentration under stoichiometric and oxidizing conditions suggests that the O<sub>2</sub> activation is not rate limiting.

For the determination of the reaction order with respect to oxygen, the power rate law was considered:

$$r_{O_2} = k' \cdot c_{O_2,0}^n \quad (\text{Equation 4.2.6})$$

$$\ln r_{O_2} = \ln k' + n \cdot \ln c_{O_2,0} \quad (\text{Equation 4.2.7})$$

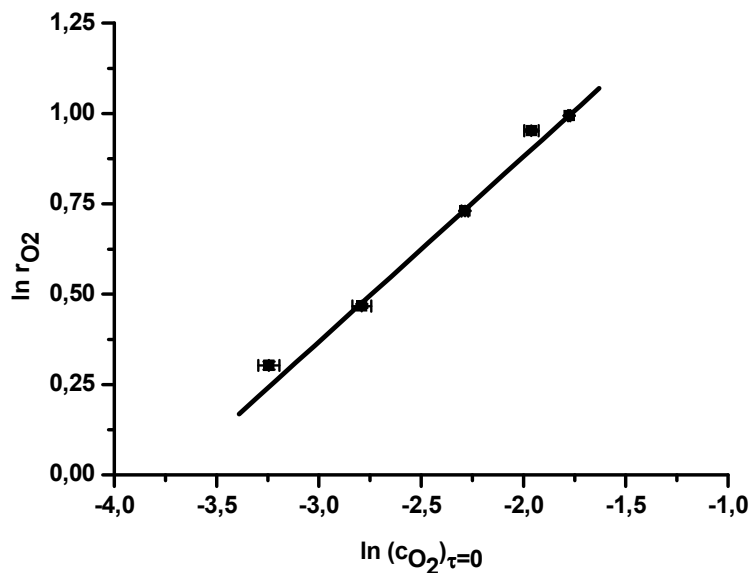


**Figure 4.2.9.** Determination of the reaction order with respect to oxygen. Cat: #6059.

Since the initial propane concentration was constant at 3 vol% in all the experiments, the first two terms in the right hand side of the power law were contracted into a single apparent rate constant  $\hat{k}$ . The reaction order was determined from the slope of the straight line of the double-logarithmic plot (Figure 4.2.9) according to the linearized equation 4.2.7.

The integral oxygen consumption rate was calculated as the product between the fractional conversion ( $x_{O_2}$ ) and the molar flow of oxygen in the feed ( $u_{O_2}$ ) expressed in  $\mu\text{mol/g.s}$ . Weighted linear regression of the double-logarithmic plot gave a reaction order with respect to oxygen equal to  $n_{O_2}=0.512\pm 0.002$ .

Griβtede and Balcells et al. reported similar catalytic properties to that shown on Figure 4.2.8 [2, 3]. Under net oxidizing conditions ( $C_3H_8/O_2$  ratio ranging from 2/6 to 2/20), the propane conversion and product selectivities were the same for every oxygen concentration and contact time [2, 3, 10]. Balcells et al. used reducing, stoichiometric and oxidizing feed, the  $C_3H_8/O_2$  ratio being between 1/1.5 and 1/4. The propane consumption rate and acrylic acid formation rate leveled off at the molar ratio of  $C_3H_8/O_2=1/2$  [2].

In contrast, Zheng et al. noted an increase in the propane conversion with the  $C_3H_8/O_2$  molar ratio varied between 1/1 and 1/5. The highest selectivity and yield of acrylic acid was observed at a molar ratio of 1/3 [7].

#### 4.2.5. Propylene oxidation

Upon analyzing the concentration–residence time plot, propylene presents the first maximum. This means that it is an intermediate in the direct oxidation of propane to acrylic acid. The application of the delplot technique (section 6.4.) also supported that propylene is an intermediate. At higher contact times, where the acrylic acid selectivity is higher, the propylene selectivity is low, usually less than 10%. On the other hand, propylene is known to be more reactive in oxidation reactions.

The selective oxidation of propylene is usually carried out at lower temperatures (325-350°C) than propane oxidation [11]. For these reasons, the authors stated that the oxidative dehydrogenation is the rate determining step in propane oxidation to acrylic acid, arguing that once the propylene is formed, it reacts readily further to acrylic acid and byproducts. Griβtede also reported the propylene oxidation over M1 and M2 phase mixture  $MoVTenbO_x$  on steatite balls. The reaction was performed at a lower temperature interval (310-330°C) because at higher temperature the propane conversion was nearly 100%. Kinetic experiments on propylene oxidation were done at 360°C. However, it may be inappropriate to extrapolate the reactivity and reaction kinetic data from 310-360° to 360-400°C [3].

A possible strategy for unraveling the pathways and kinetics of a complex reaction such as propane oxidation is the bottom to top approach. According to this approach, catalytic reaction is carried out using the reaction products and intermediates as educts. The product distribution gives information concerning the reaction pathways, while the rates show the relative reactivity of all the compounds. However, the reaction conditions (temperature, redox potential) should be chosen in such a way to approach those of the one-step propane oxidation conditions, in order to avoid an unjustifiable extrapolation.

In order to explain the reactivity difference in propylene oxidation, the results of two sets of experiment are presented here:

(a) at low GHSV of  $5000 \text{ h}^{-1}$  ( $W/F=0.72 \text{ g}\cdot\text{s}/\text{ml}$ ) and in a low temperature interval (230-270°C) (Figure 4.2.10, top),

(b) at higher GHSV of  $20000 \text{ h}^{-1}$  ( $W/F=0.018 \text{ g}\cdot\text{s}/\text{ml}$ ) and in the temperature interval between 360 and 400°C (Figure 4.2.10, bottom).

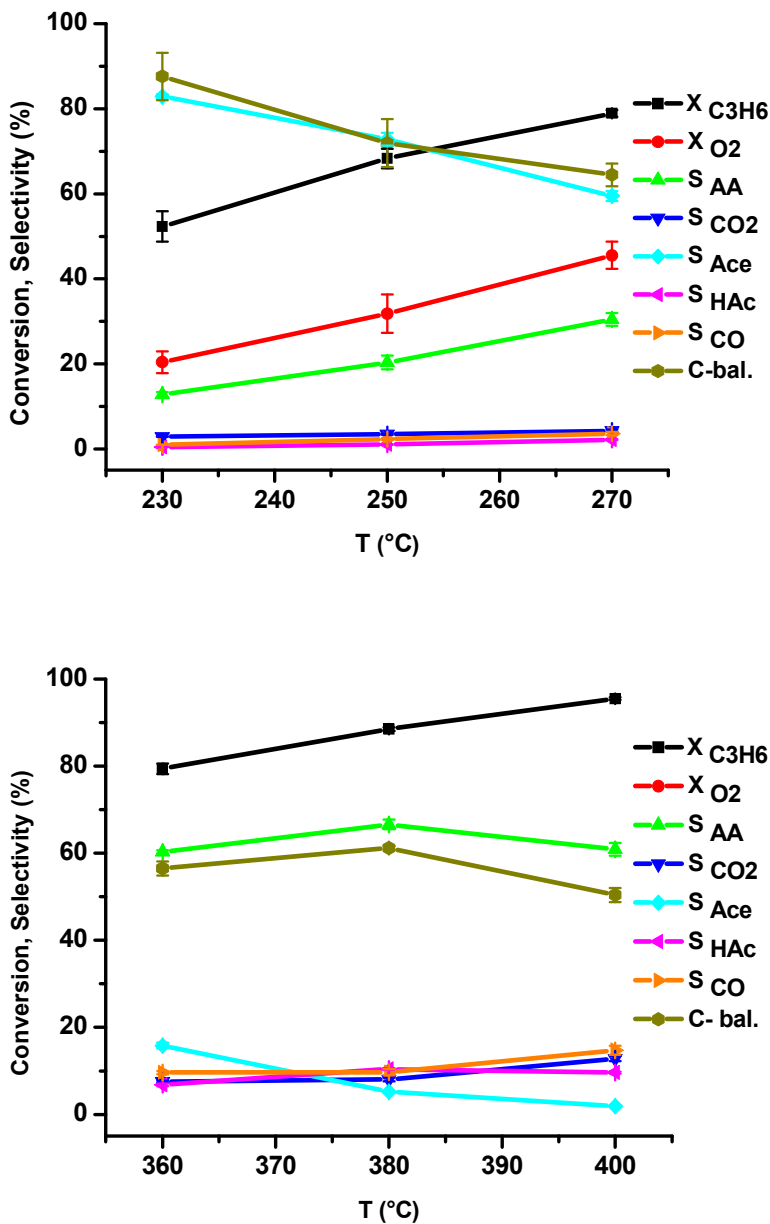


**Figure 4.2.10.** Propylene oxidation with #6902. Feed composition:  $\text{C}_3\text{H}_6/\text{O}_2/\text{H}_2\text{O}/\text{N}_2=3/6/40/51 \text{ vol}\%$ . Top: GHSV= $5000 \text{ h}^{-1}$ , bottom: GHSV= $20000 \text{ h}^{-1}$ . Catalyst: #6902.

In both experiments, the feed composition was the following:  $C_3H_6/O_2/H_2O/N_2=3/6/40/51$  vol%. The oxygen and steam contents were chosen to be equal with that of the feed for propane oxidation on this catalyst.

In the case (a) the propylene conversion was high despite of the low temperature, suggesting the high activity of the catalyst. The main product was acetone; its substantial selectivity dropped approximately linearly with the temperature. The selectivity of acrylic acid - the second most abundant product - showed an increasing trend with the temperature.

The  $CO_2$ , CO and acetic acid were found to be minor products, the maximum selectivities being 4.3; 3.6 and 2.3, respectively. Surprisingly, maleic anhydride was also produced in quite significant amounts, as identified on the chromatogram by the mass spectrometric detector.

However, the quantification of this product was not possible, because of the very broad and irreproducible peak shape in the chromatogram. One reason for the scarce reproducibility is that the maleic anhydride is a larger molecule and more polar than acrylic acid. The second difficulty is related to the fact that maleic anhydride hydrolyzes to maleic acid in presence of the high steam content of the feed. Hydrolysis may happen in the downstream tubing of the reactor system, as well as in the DB-1 column gas chromatograph, causing broad peaks with irreproducible peak areas.

The temperature interval in case (b) was identical with that used for the propane oxidation reaction. Almost complete propylene conversion was achieved at a relatively high space velocity of  $20.000\text{ h}^{-1}$ . In contrast to the low space velocity – low temperature experiment, in this case the acrylic acid is the most abundant product, with a maximum selectivity at a reaction temperature of  $380^\circ\text{C}$ .

A small amount of acetone is also produced during the reaction, but its selectivity sinks strongly with increasing reaction temperature.  $CO_2$ , CO and acetic acid are produced in a higher amount than in the experiment carried out at low space-velocity and low temperature. An inversion can be observed in the selectivity ratio between the  $CO_2$  and CO, compared to the experiment done in the low temperature interval with five times longer contact time.

It is notable, that a substantial amount of maleic anhydride was also produced, but the quantification problem was more severe than in case (a). Therefore, the maleic acid selectivity was not calculated in any of the above two cases, which led to a systematic error in the carbon balance, as shown in the Figure 4.2.10. Nevertheless, the formation of maleic acid, a four carbon atom containing product from propylene is indeed not straightforward. One possible explanation is that hydrogen radical was removed from the methyl group of propylene. Then two allyl radicals recombined to benzene, which finally was oxidized to maleic acid.

Because the propylene conversion at 270°C, GHSV=5000h<sup>-1</sup> and 360°C, 20000h<sup>-1</sup> are very similar, the selectivities obtained under these two conditions can readily be compared. It is to be observed, that the product distribution is very different. In the low space velocity–low temperature experiment, acetone is the most abundant product; followed by acrylic acid, while in the higher space velocity–higher temperature experiment, these selectivities were inverted. On the other hand, during propane oxidation reaction acetone is not produced in detectable amounts, even if propylene is an intermediate product. Also the CO and CO<sub>2</sub> selectivity ratio is inverted in the low temperature interval.

Therefore, this experiment exemplifies that the catalytic and kinetic experiments of propylene and other intermediate oxidation should be performed in the temperature interval which is identical to that used for propane oxidation.

The effect of steam on the catalytic performance of propylene oxidation over phase pure MoVTeNbO<sub>x</sub> was also investigated (Figure 4.2.11). The steam content variation was performed using the same procedure as in the case of propane oxidation. The steam content was reduced from 40vol% to 0 vol% by 10 vol% steps. No deactivation was observed in absence of steam. After exposing the catalyst to dry feed, the catalytic performance was re-measured at 20 vol% steam content.

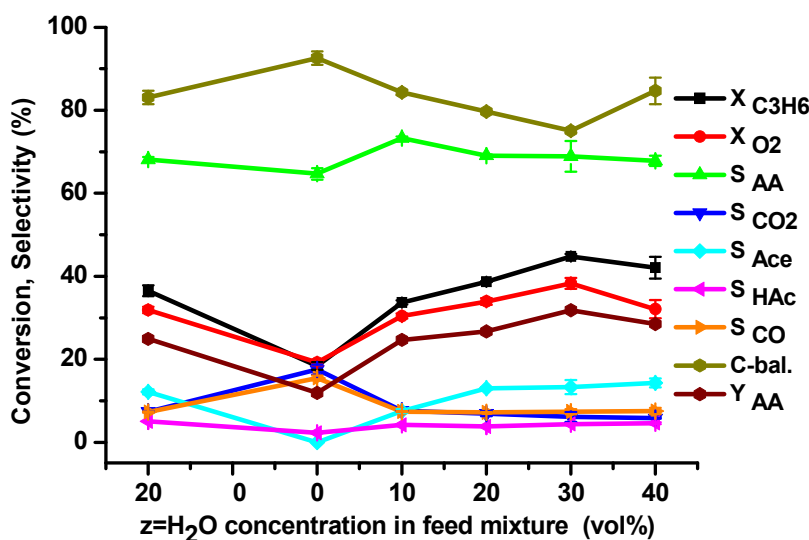


**Figure 4.2.11.** The effect of H<sub>2</sub>O on propylene oxidation. Feed composition: C<sub>3</sub>H<sub>6</sub>/O<sub>2</sub>/H<sub>2</sub>O/N<sub>2</sub>=3/6/z/(91-z) vol%, GHSV=80000 h<sup>-1</sup>, T=400°C. Catalyst: 6902.

The reaction temperature was set to 400°C, which is identical with the temperature where the steam content variation for propane oxidation was carried out. Since in the temperature variation at a space velocity of 20000 h<sup>-1</sup> almost 100% propylene conversion was observed at 400°C, the steam content variation was carried out at a space velocity of 80000 h<sup>-1</sup> (W/F= 0.045 g·s/ml). At this high space velocity the highest conversion was approximately 40%, between 20 and 40 vol% steam content.

Similarly to the observations for the steam content variation in the propane oxidation, the conversion decreased continuously below 30 vol% steam content, while a significant drop below 20 vol% steam concentration also for propylene oxidation. The acrylic acid selectivity did not change significantly upon decreasing the steam content of the feed. However, the acetone selectivity decreased dramatically; at 0 vol% steam content no detectable amount of acetone was formed. This suggests the involvement of steam in acetone formation according to the oxy-hydration pathway [12-16].

It is notable that in absence of co-fed steam, the selectivity to total oxidation products increased, and the ratio between the CO/CO<sub>2</sub> selectivities was inverted compared with experiments carried out in the steam-containing feed. Since the propylene conversion was relatively low, maleic anhydride formation was also lower, which led to a better carbon balance than that reported for the space velocity of 20000 h<sup>-1</sup>.

Upon re-measuring the catalytic performance in 20 vol% steam, the catalytic performance was found to be identical with the one determined before measuring in a dry feed. The reversibility of both the conversion and selectivity with the steam content is similar to that observed in the case of propane oxidation.

#### 4.2.6. Acrolein oxidation

Propylene was found to be the first intermediate in propane selective oxidation. It is supposed that the oxidation of propylene to acrylic acid proceeds through allyl alcohol and acrolein intermediates. This assertion was supported by the fact that the oxidation of propylene to acrylic acid in a single elementary step is not probable, because such a transformation would require the elimination of two hydrogen atoms and insertion of two oxygen atoms.

Postulated reaction pathways take into consideration acrolein and sometimes allyl-alcohol formation as well, although only in a few studies is their detection reported under catalytic conditions [16-21].

Concepción et al. reported the detection of a  $\pi$ -allylic intermediate ( $\text{CH}_2=\text{CH}-\text{CH}_2-\text{O}-$ ) by means of FTIR spectroscopy on  $\text{MoVTeNbO}_x$  catalyst [22]. It was suggested that this surface intermediate of the propylene oxidation is transformed to acrylic acid by a redox mechanism, via acrolein. However, in the gas phase no acrolein was detected.

In the propane and propylene oxidation experiments described above, neither allyl alcohol, nor acrolein was formed at any space velocity and/or feed composition in the temperature interval between 360 and 400°C.

The purpose of this experiment was to determine the reactivity and product distribution in acrolein oxidation over the phase-pure  $\text{MoVTeNbO}_x$  catalyst.

For the catalytic experiment, a feed with the following composition was used: acrolein/ $\text{O}_2$ / $\text{H}_2\text{O}$ / $\text{N}_2$ =3/6/0/91vol%, at a weight hourly space velocity of 250000 ml/gh ( $W/F=0.014$  gs/ml). The temperature was varied between 360 and 400°C (Figure 4.2.12).

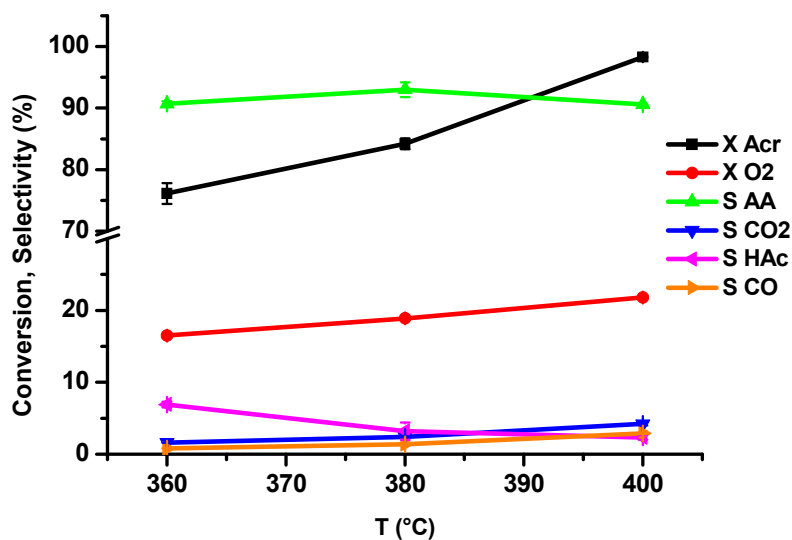


**Figure 4.2.12.** The effect of temperature on acrolein oxidation. Catalyst #6059.

As seen in Figure 4.2.13, the catalyst is very active in acrolein oxidation even at very high space velocity. The highest acrylic acid selectivity was attained at 380°C, while the highest yield of 89% at 400°C.

Acetic acid was found to be a by-product, its selectivity decreased with increasing temperature. Literature sources also reported the production of acetic acid during the oxidation of acrolein. Without experimental evidence, Lin et al. explained the appearance of acetic acid byproduct as due to oxidative degradation of acrylic acid at temperatures close to 400°C [23]. However, both the acrolein and acrylic acid contain only  $sp^2$  carbon atoms, while acetic acid contains a  $sp^3$  carbon atom as well. This would imply that the C=C bond is saturated upon oxidation of acrylic acid (i.e. the formal charge of -2 is reduced to -3). Such saturation (reduction) is uncommon in oxidation reactions. A possible explanation might be the intra-molecular transposition of a hydrogen atom from the carbonyl- or carboxyl group to the methylene group.

An increasing trend was observed for CO and CO<sub>2</sub>, the latter total oxidation product being produced in larger amount than CO.

From the Arrhenius- and Eyring-Polanyi plots, the activation parameters of acrolein and oxygen consumption were determined (Table 4.2.2.).

**Table 4.2.2. The activation parameters of acrolein oxidation on #6059 catalyst.**

Parameter	Acrolein	Oxygen
$E_a$ (kJ/mol)	$25.5 \pm 1.4$	$24.9 \pm 2.0$
$\ln A$	$9.15 \pm 0.2$	$7.5 \pm 0.4$
$\Delta H^\ddagger$ (kJ/mol)	$-20.129 \pm 0.002$	$-183.617 \pm 0.003$
$\Delta S^\ddagger$ (J/molK)	$-183.617 \pm 0.003$	$-197.160 \pm 0.003$

#### 4.2.7. CO oxidation and water gas shift reaction

As observed at the kinetic study of propane oxidation (4.2.1 and 4.2.2 subchapters), the CO formation rate was always higher than the CO<sub>2</sub> formation rate in the studied contact time interval, independently of the temperature and steam content. This raised the question whether first the CO is produced, which upon further oxidation is converted to CO<sub>2</sub>. The delplots indicate that both CO and CO<sub>2</sub> are mainly second rank products (Section 6.4). However the delplot technique relies on extrapolation of the dependent variable to zero propane conversion. This implies that, strictly speaking, the rank order is valid only in the differential regime.

The CO concentration profile steadily increased in the studied contact time interval, without showing a maximum characteristic to an intermediate product (Figure 4.2.1 and 4.2.5). Because of these reasons, it was not possible to state or to refute whether CO is further oxidized. On the other hand, the oxidation of CO by water, known as water gas shift reaction, could neither be confirmed nor denied based on the kinetic data of propane oxidation.

To answer the above questions, CO oxidation experiments were carried out. In order to get more insights in the reaction kinetics, possible reaction pathways and oxygen species on the catalyst surface, the reactivity of CO oxidation was screened in the following order:

- i) CO oxidation in absence of steam, using stoichiometric and oxidizing feed (CO/O<sub>2</sub>/N<sub>2</sub>=3/1.5/95.5 vol% and CO/O<sub>2</sub>/N<sub>2</sub>=3/6/91 vol%, respectively),
- ii) Water-gas shift reaction with a feed containing 40 vol% steam (CO/O<sub>2</sub>/H<sub>2</sub>O/N<sub>2</sub>=3/0/40/54 vol%),

- iii) CO oxidation in absence of steam, using oxidizing (CO/O<sub>2</sub>/H<sub>2</sub>O/N<sub>2</sub>=3/6/40/51 vol%) feed.

The steam-free feed resembles to propane oxidation carried out in absence of water. The choice of CO/O<sub>2</sub>=3/1.5 and 3/6 covers a wide range of redox potentials, which occur under propane oxidation conditions.

In the presence of oxygen and water, the CO oxidation by oxygen and the water gas shift reaction may occur simultaneously.



This would lead to an ambiguity in deciding which reaction is actually taking place. On the other hand the contribution of each to the overall CO oxidation reactivity is also difficult, because the above mentioned parallel reaction steps involve the same educt and the same product. Therefore, it was necessary to perform separately the water gas shift reaction and the CO oxidation reaction in presence of steam. The conditions of these two reactions were also chosen in such a way to cover the relevant conditions of propane oxidation reaction.

Since the CO oxidation and water gas shift activity of MoVTeNbO<sub>x</sub> mixed metal oxide catalysts was not reported up to now, the reactivity screening started with an exploratory measurement performed in a wide range of temperature (from 150 to 400°C) and two space velocities (3000 h<sup>-1</sup> and 12000 h<sup>-1</sup>, respectively) in dry feed. The product appeared only at temperatures higher than 250°C at low space velocity (Figure 4.2.14). However, the highest conversion of CO was only 1%. At the space velocity of 12000 h<sup>-1</sup> no reactivity was observed below 350°C.

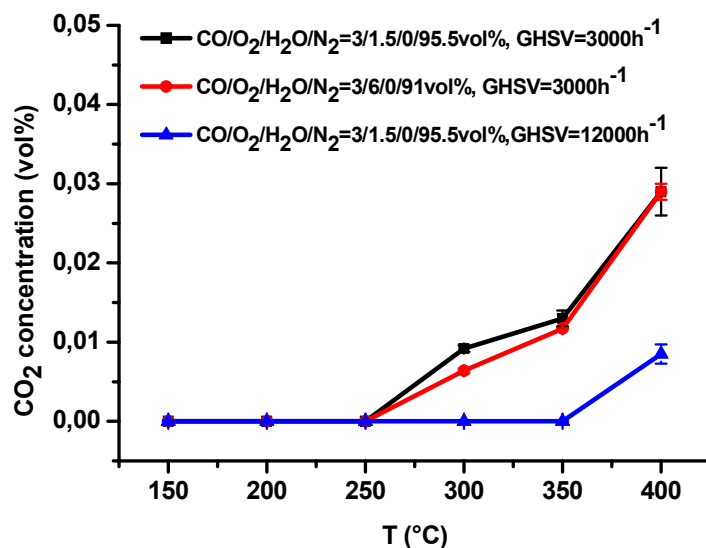


**Figure 4.2.13.** CO oxidation at different temperatures, space velocities in stoichiometric and oxidizing feed. Catalyst: #8947.

The activation parameters of CO oxidation reaction have been determined based on the linearized Arrhenius- and Polanyi-Eyring plots. The results are summarized in Table 4.2.3.

**Table 4.2.3.** The activation parameters of CO oxidation in dry feed.

Feed	Stoichiometric	Oxidizing
	CO/O <sub>2</sub> =2/1	CO/O <sub>2</sub> =1/2
lnA	7.5±1.2	9.2±1.2
E <sub>a</sub> (kJ/mol)	41±7	52±2
ΔH <sup>#</sup> (kJ/mol)	-36±7	-46±2
ΔS <sup>#</sup> (J/molK)	-197±10	-183±3

After performing the above exploratory experiment, the space velocity variation was carried out for CO oxidation in dry feed, for the water gas shift reaction and CO oxidation in presence of steam. The catalytic data are summarized in Figure 4.2.14. This plot reveals the least reactivity in the water gas shift reaction, the highest CO conversion being 0,5% in the studied contact time interval.

The CO oxidation activity in dry feed was higher than the water gas shift reaction. For the CO oxidation in dry feed, the CO conversion was found to be the same, independently on whether the feed was stoichiometric or oxidizing.

The highest activity was observed in the case of CO oxidation in presence of 40 vol% steam. It should be mentioned that the reactivity in this latter reaction is not a simple algebraic sum of the CO oxidation in dry feed and the water gas shift reactions.

However in all these reactions, the conversion of CO to CO<sub>2</sub> is far below 2%. These observations show that the CO oxidation and water gas shift reaction are negligible reaction steps under the propane oxidation reaction conditions. It is also to be mentioned, that the kinetic study of propane oxidation was carried out in the space velocity interval between 66000-4500 h<sup>-1</sup> (W/F=0,05-0,90 gs/ml).

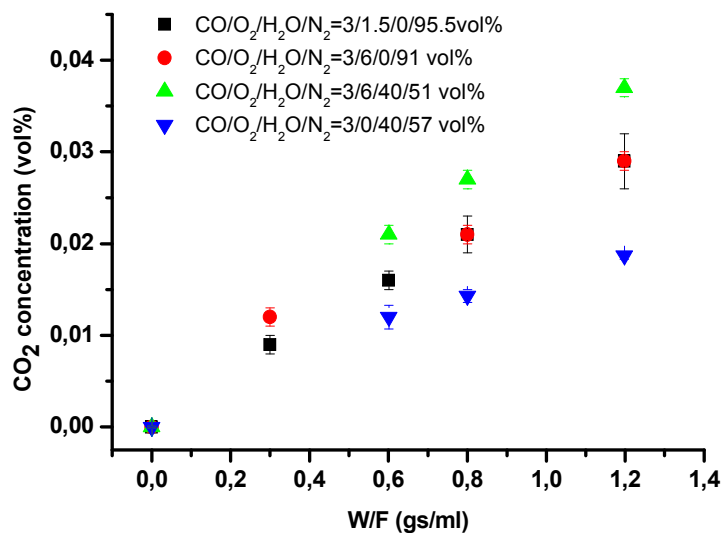


Figure 4.2. 14. Space velocity variation for CO oxidation and water gas shift reaction.

The low reactivity in CO oxidation reaction has two implications with respect to the propane oxidation.

The first is related to the reaction pathways involving CO and CO<sub>2</sub>. The above experiments revealed that the CO is not further oxidized to CO<sub>2</sub> under any conditions. This suggests that in the propane oxidation reaction, CO and CO<sub>2</sub> are formed in two different and independent pathways.

The second implication is related to the nature of oxygen species. As it was described in the introduction, the CO oxidation activity is related to the presence of the electrophilic oxygen species on the catalyst surface [24].

Although quantitative correlations were not done because of the lack of calibration standards, based on the negligible CO oxidation activity it can be stated that the electrophilic oxygen species are not abundant on the phase-pure MoVTeNbO<sub>x</sub> catalyst under propane oxidation conditions.

#### **4.2.8. Comparison of the reactivity of propane, propylene, acrolein and carbon monoxide oxidation reactions**

The activity of phase pure MoVTeNbO<sub>x</sub> catalyst in propane, propylene, acrolein and carbon monoxide oxidation is summarized and presented on Figure 4.2.15. Because the reactivity of propylene and acrolein is higher, the space velocity was adjusted in such a way that the conversion is below 100%. Therefore, the propylene oxidation was carried out at a space velocity of 20000 h<sup>-1</sup>, while in the case of acrolein oxidation a much higher space velocity of 250000 h<sup>-1</sup> was used.

Because the conversions at different space velocities are difficult to compare, the consumption rates of the four educts were calculated and plotted versus the reaction temperature.

The reactivity increases in the following order: carbon monoxide << propane < propylene << acrolein. The reactivity ranking order of propane, propylene and acrolein is similar to that reported by Ai [19] and Lin et al. [23]. However, in these literature sources the reactivity ranking order was established by performing the reactions at the same space velocity and varying the reaction temperature.

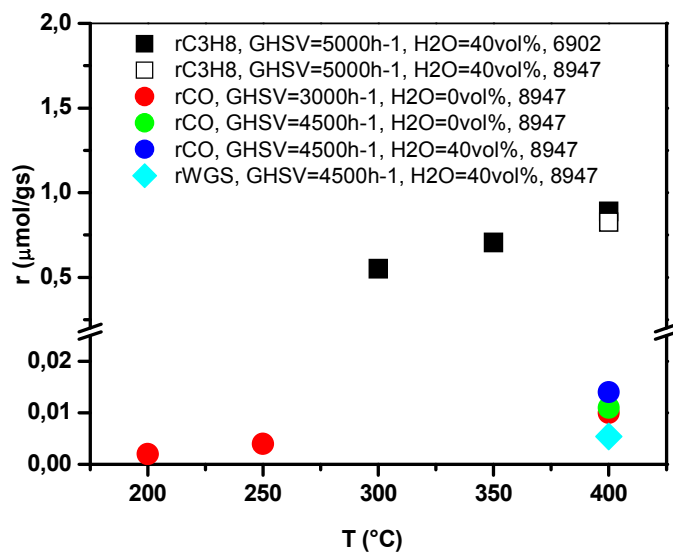
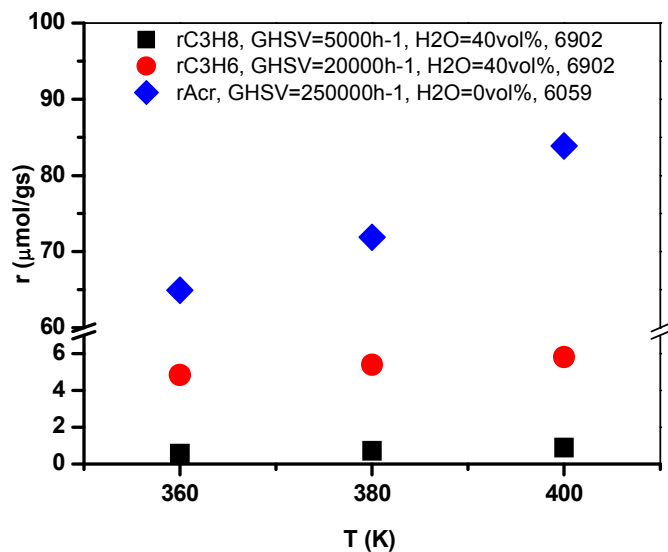


**Figure 4.2.15.** Comparison of the propane, propylene, acrolein (top), propane, CO oxidation and water gas shift activity (bottom) of the catalyst.

As Figure 4.2.16 indicates, the reaction rates span over four orders of magnitude. The relative rate of propylene consumption with respect to propane consumption is equal to 6.6 at the reaction temperature of 400°C. On the other hand, the relative rate of acrolein oxidation at 400°C is 94.4. The relative rate of CO oxidation with respect to propane was

0.016 and 0.011 in dry feed and 40 vol% steam containing feed, respectively. The lowest relative rate of 0,006 was observed for the water gas shift reaction on the MoVTeNbO<sub>x</sub> catalyst.

### 4.3. Two-stage reactor used as a distributor of oxidizing and reducing gases

The dosing of oxygen in catalytic membrane reactors and multi-tubular reactors were reported to give better catalytic performance compared to the conventional single tube fixed bed reactor design [25-31]. The ODH of propane and ethane was extensively studied by Seidel-Morgenstern et al. [31]. The ODH and selective oxidation reaction to acrylic acid share the same steps of propane activation to propylene; therefore qualitatively these two reactions are similar. The oxidation of propane to acrolein [32] and acrylic acid [33] was reported by employing a dual-bed system, whereby in the first reactor ODH proceeded while in the second reactor the propylene was further oxidized.

In contrast to these above mentioned catalyst systems, the MoVTeNbO<sub>x</sub> is able to oxidize directly the propane to acrylic acid. Therefore in the present section the selective oxidation of propane is reported over a phase-pure M1 MoVTeNbO<sub>x</sub> catalyst in a two-stage reactor.

The stage-wise addition of oxygen and other gases was performed in a system consisting of two reactor tubes connected serially (two-stage reactor, TSR). The addition of gases was technically realized by means of a T-junction installed on the tubing that connects the two reactor tubes (section 2.2.4, Figure 2.2.3).

The reactors were loaded with the same amount of catalyst phase-pure M1 MoVTeNbO<sub>x</sub> catalyst (0,2400 g or 0,2667 ml sieve fraction of sample #6059), mixed with SiC diluent. The initial concentration of the feed components entering the first reactor was kept constant (C<sub>3</sub>H<sub>8</sub>/O<sub>2</sub>/H<sub>2</sub>O/N<sub>2</sub>=3/6/40/51 vol%), while different gases (O<sub>2</sub>, N<sub>2</sub>O, C<sub>3</sub>H<sub>6</sub>, CO and CO<sub>2</sub>) were added to the gas mixture entering the second reactor tube. The temperature of both reactors was set to 400°C. A total flow rate of 40 mln/min corresponds to a space velocity of 9000 h<sup>-1</sup> in each reactor tube, while the overall space velocity is 4500 h<sup>-1</sup>.

### 4.3.1. Addition of O<sub>2</sub> and N<sub>2</sub>O

The variation of oxygen concentration in a single tube reactor revealed that the catalytic performance is neither enhanced nor reduced by up to a five-fold oxygen excess compared to the stoichiometric feed. The effect of the redox potential was studied also in the two-stage reactor setup.

Additionally, the potential applicability of N<sub>2</sub>O as an oxidant was examined. The motivation for this was the numerous reports in the literature about the successful application of nitrous-oxide as oxidant instead of molecular oxygen in heterogeneously catalyzed reactions (i.e. the industrial oxidation of benzene to phenol over FeZSM-5 catalyst, alkane oxidative dehydrogenation, propylene epoxidation, hydroxylation of chlorobenzene, fluorobenzene, phenol, biphenyl [34]). Also, N<sub>2</sub>O was found to be an applicable oxidant in propane oxidative dehydrogenation on VO<sub>x</sub> on MCM-41 [35], SiO<sub>2</sub> and  $\gamma$ -Al<sub>2</sub>O<sub>3</sub> [36] supports. Markedly higher propylene selectivity was reported when N<sub>2</sub>O was using as oxidant, compared to the catalytic data obtained with O<sub>2</sub>. This was explained by the slower reoxidation kinetics observed in case of N<sub>2</sub>O. More recently, Kondratenko et al. reported two different surface species, as probed by in-situ EPR spectroscopy, and postulated two different reoxidation mechanisms of the VO<sub>x</sub>/MCM-41 catalyst by O<sub>2</sub> and N<sub>2</sub>O, respectively. In the case of reoxidation by O<sub>2</sub>, the V<sup>n+</sup>...O<sup>-</sup> species was identified, which was assumed to give rise to O<sup>-</sup> electrophilic species, leading to total oxidation [37].

However, no reports were found about the potential application of N<sub>2</sub>O in the oxidation of propane to acrylic acid.

The staged addition of oxygen was performed as follows. First, the propane oxidation reaction was performed at a space velocity of 9000 h<sup>-1</sup> using the feed of C<sub>3</sub>H<sub>8</sub>/O<sub>2</sub>/H<sub>2</sub>O/N<sub>2</sub>=3/6/40/51 vol% in a single-tube operation mode. The oxygen content of the effluent mixture was found to be 4 vol%. Therefore, in the two-stage operation mode the initial oxygen concentration in the second reactor tube is equal to 4 vol% without addition of oxygen.

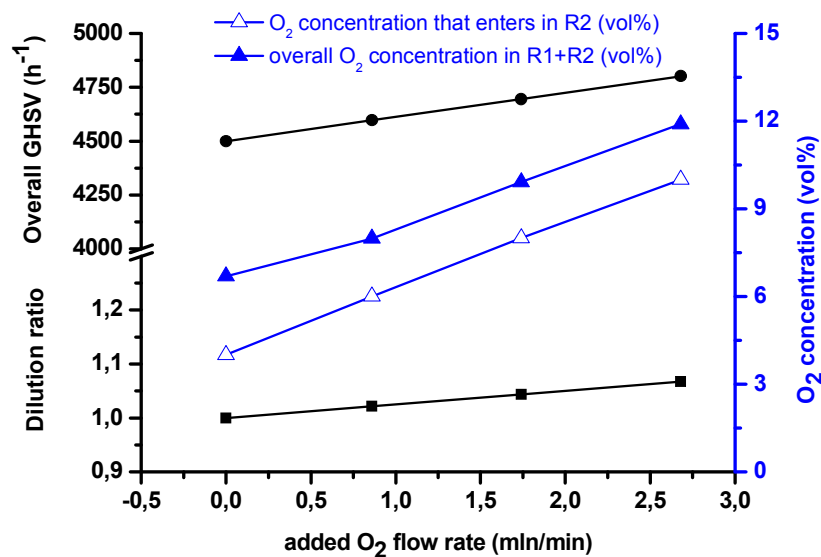


**Figure 4.3.1.** The dilution ratios (black squares), overall space velocities (black dots) and the oxygen concentrations (empty and full blue triangles) in function of the flow rate of the added oxygen.

To the effluent gas mixture leaving the first reactor tube, pure oxygen gas was added through the T-junction, in order to achieve initial oxygen concentrations of 6, 8 and 10 vol% O<sub>2</sub> in the second reactor tube.

The overall oxygen concentration in the two reactor tubes was 6, 8, 10 and 12 vol%, respectively. Because of the oxygen addition, the total flow rate increased in the second reactor tube and in the same time, the reaction mixture was diluted. The dilution factor, the overall space velocity, the oxygen concentration at the inlet of the second reactor tube and the overall oxygen concentration in the two-stage reactor in function of the flow rate of added oxygen gas is displayed in Figure 4.3.1. The dilution factor and the space velocity change were taken into account for the calculation of the conversion, selectivity and reaction rates.

The reaction rates obtained at a space velocity of 4500 h<sup>-1</sup> in the single-tube mode and two-stage mode without addition of oxygen between the two reactor tubes were very similar (Figure 4.3.2). In contrast to the oxygen content variation experiments performed in the single tube reactor (Figure 4.2.8 in subchapter 4.2.4), the staged addition of oxygen in relatively high concentration positively influenced the catalytic properties.

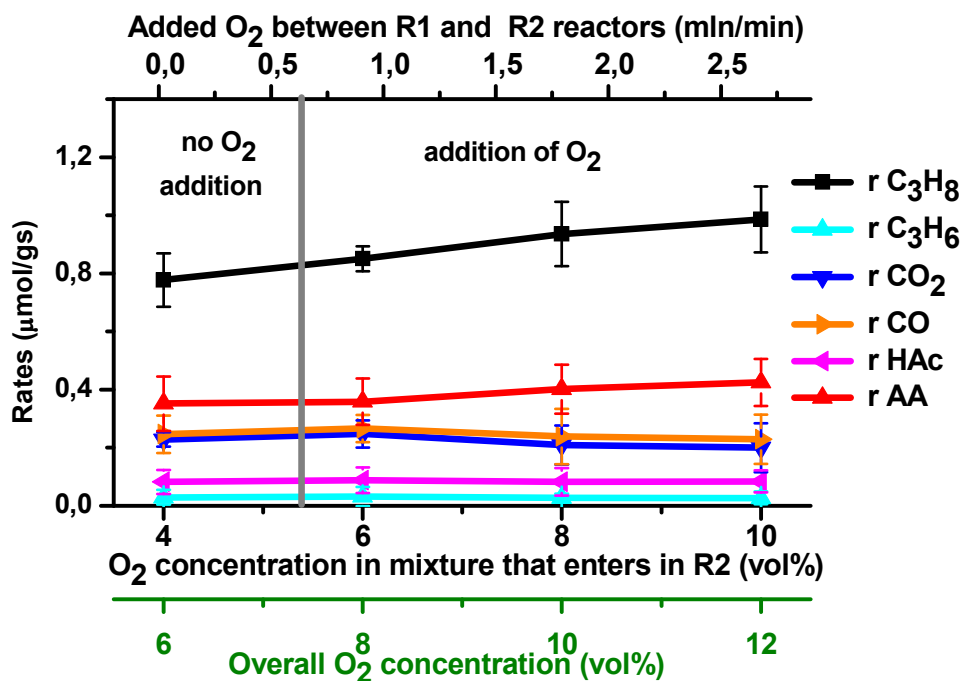


Figure 4.3.2. The effect of oxygen addition in the two-stage reactor.

.At the oxygen content of 8 and 10 vol% in the second reactor (10 and 12 vol% overall oxygen content), the overall rate of propane consumption increased slightly compared to measurements with lower oxygen concentrations (Figure 4.3.2).

The rate of acrylic acid formation was observed to increase at 8 and 10 vol% oxygen concentrations in the second reactor. The rate of CO and CO<sub>2</sub> production increased only marginally upon oxygen addition, while the rate of propylene and acetic acid formation was not influenced by the oxygen concentration.

When the catalytic properties obtained in the two-stage reactor and single-tube reactors were compared in terms of conversion, selectivity and yield, two cases could be distinguished (Figure 4.3.3). Both reactor systems performed similarly at 6 and 8 vol% overall oxygen concentration. However, the catalytic performance in the two-stage reactor is superior to the single-tube reactor above 8 vol% overall oxygen content. A net increase of 1.1% in the propane conversion and an increase of 4.7% in the acrylic acid selectivity was determined at an overall oxygen content of 10 vol% compared to the

single-tube reactor experiment. Therefore by employing the two-stage reactor, the acrylic acid yield could be increased by 5.3%.

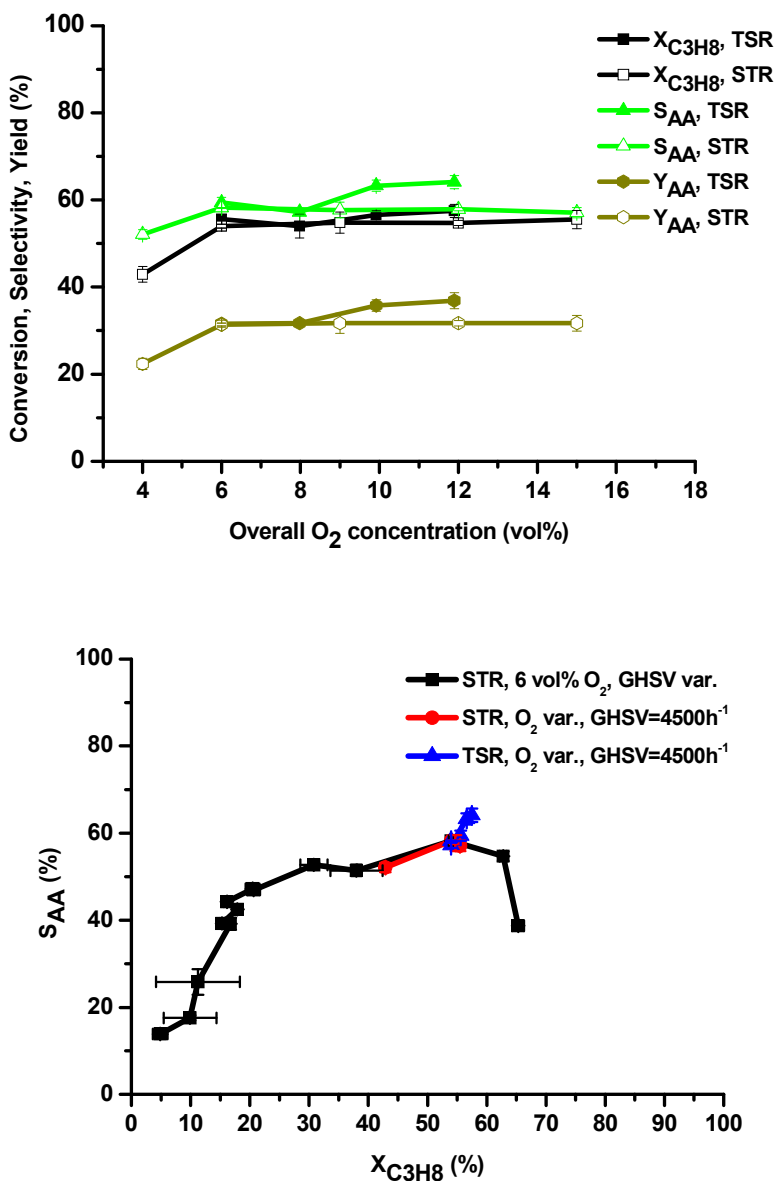


Figure 4.3.3. Comparison of the catalytic performance in the single-tube reactor (STR) and two-stage reactor (TSR).

As already mentioned above, the oxygen addition diluted the reacting gas mixture and also increased the space velocity. However the conversion and selectivity also depends on the space velocity. Firstly, it can be ruled out that the slight enhancement of propane

conversion is due to the increase of space velocity from oxygen addition, because the conversion decreases with increasing space velocity.

In order to rule out that the positive effect of oxygen addition on the selectivity is an artifact due to the minor increase of space velocity, a conversion-selectivity plot was constructed displaying all the STR and TSR data (Figure 4.3.3, bottom). On this plot the selectivity to acrylic acid determined at 6 vol% initial oxygen concentration in the STR, passed through a maximum at a conversion of ca. 55%. Despite varying the oxygen content variation in the STR operation mode, the selectivity could not be improved. On the other hand, upon oxygen addition in the TSR, both the conversion and the selectivity increased, the data points were above the maximum of the conversion-selectivity curve corresponding to the conventional STR system. This revealed that the increase in the selectivity is not an artifact due to the change of the space velocity by oxygen addition.

The feasibility of application of  $N_2O$  as an oxidant was also studied in the two-stage reactor. The  $N_2O$  concentration was varied from 0.5 vol% up to 4.0 vol% in the second reactor, keeping constant the gas mixture composition of  $C_3H_8/O_2/H_2O/N_2=3/6/40/51$  vol% in the first reactor. The catalytic properties were found to be the same in the presence of  $N_2O$ , irrespective of its concentration (Figure 4.3.4). Moreover, the  $N_2O$  conversion was found to be zero, indicating that  $N_2O$  has no effect on the reaction when dioxygen is also present in the gas mixture. Then the initial oxygen concentration fed in the first reactor was reduced from 6.0 to 4.0 vol% and in the same time, 4 vol%  $N_2O$  was fed in the second reactor, respectively (Figure 4.3.4, condition noted with \*). Under this condition, total  $O_2$  consumption was observed, accompanied by a slight decrease of the propane conversion and a significant decrease of the acrylic acid selectivity. At the same time, the propylene, acetic acid and carbon dioxide selectivities are increasing slightly.

Under reducing condition, the  $N_2O$  conversion was also found to be zero, similarly for the catalytic runs performed in presence of dioxygen. In terms of oxygen atoms, 4 vol%  $N_2O$  is equivalent with 2 vol%  $O_2$ . Therefore, feeding 4 vol% oxygen and 4 vol%  $N_2O$  in the two-stage reactor is equivalent to 6 vol% oxygen with respect to oxygen atoms. The fact that the  $N_2O$  conversion was zero throughout all the above described conditions led

to the conclusion that  $N_2O$  does not reoxidize the phase-pure  $MoVTeNbO_x$  catalyst under propane oxidation conditions. The explanation for this observation could be that either the  $N_2O$  does not adsorb on the surface of the catalyst or the catalyst is unable to activate the N-O bond, while there is no such a constraint in dioxygen adsorption and the activation of the O=O bond.

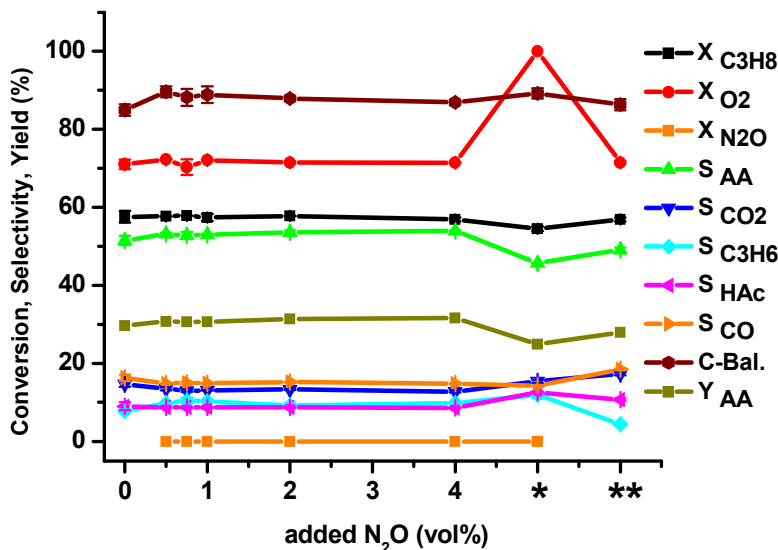


**Figure 4.3.4.** Addition of  $N_2O$  in the two-stage reactor. Conditions noted with stars: \* - 4,0 vol%  $O_2$  introduced in R1 reactor and 4,0 vol%  $N_2O$  in R2 reactor ; \*\* - 6 vol%  $O_2$  introduced in R1 reactor and 0,0 vol%  $N_2O$  in R2 reactor.

Nitrous oxide may undergo thermal dissociation leading to  $N_2$  and  $O\cdot$ . The oxygen free radicals may induce radical homogeneous reactions under propane oxidation conditions. Although, as it is shown above, the product distribution is independent on the concentration of added  $N_2O$ , it was necessary to assess the amount of the highly reactive oxygen radical, the new oxygen species introduced in the system by the addition of  $N_2O$ . Based on the kinetic data published by Allen et al. [38] on thermal dissociation of  $N_2O$ , the maximum concentration of the gas phase oxygen radical was found to be  $5.4 \cdot 10^8$  radicals $\cdot cm^{-3}$  (in the order of  $10^{-15}$  mol radical $\cdot cm^{-3}$ ). The calculated conversion of  $N_2O$  towards  $N_2$  and  $O\cdot$  was extremely low, in the order of magnitude of  $10^{-8}$  %. This is in accordance with the observed zero conversion of  $N_2O$  during the addition experiments.

Therefore this calculation proves that the thermal dissociation of  $N_2O$  and the appearance of oxygen radicals are negligible under propane oxidation conditions.

After the  $N_2O$  was switched off and 6 vol%  $O_2$  was fed in the first reactor, in the beginning the conversion of propane and the selectivity of acrylic acid were as low as in the case of 4 vol%  $O_2$  in the first reactor and 4 vol%  $N_2O$  in the second reactor.

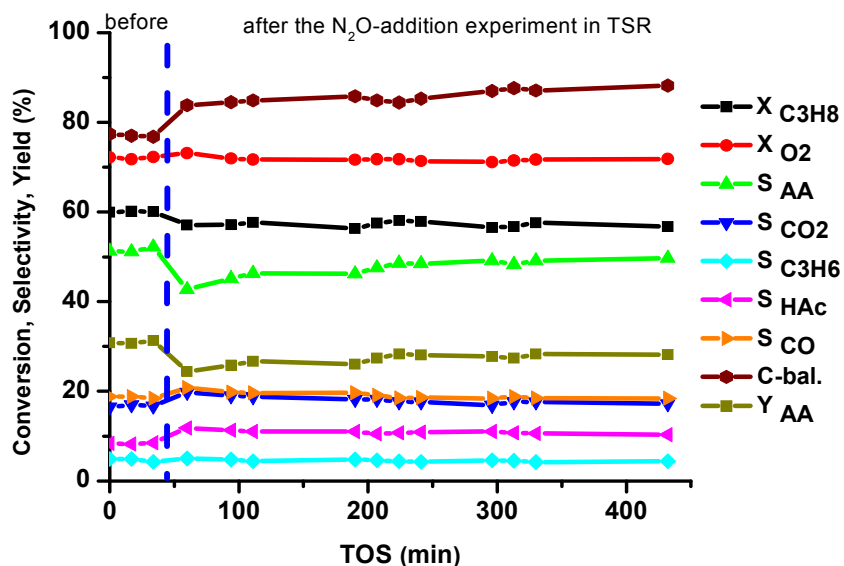


Figure 4.3.5. Reactivation of the catalyst after exposing to reducing conditions.

The catalytic properties converged slowly (in ca. 8 hours time on stream) to the initial values (“reactivation during catalytic reaction”) (Figure 4.3.5). This suggests the reversibility of the decay in catalytic performance when operating the reaction under reducing conditions for short time on stream (1 hour).

### 4.3.2. Addition of propylene

In the previous section it was shown that the staged addition of the oxygen can increase the catalytic performance. The effect of added reducing agents was also studied.

The reducing agent was chosen based on the following considerations:

i) the added compound should neither produce compounds which may poison the catalyst nor react in homogeneous or heterogeneous pathways with the intermediates or products of propane oxidation reaction,

ii) it should present a reasonably high reduction potential, and  
iii) it should not introduce additional complexity in the reaction pathways of propane oxidation.

Hydrogen was not applied, because of the i) and ii) criteria. Firstly, it may hydrogenate the propylene and acrylic acid at 400°C. Secondly, the onset temperature of H<sub>2</sub>-TPR of the catalyst was at around 370°C, with the peak maximum at 450°C (data not shown), therefore is not a very strong reducing agent. Ethylene, the C1-C3 alcohols and aldehydes were excluded based on the iii) criterion, because all of these compounds are oxidized to aldehydes or acids and undergo total oxidation pathways as well. The remaining options were propylene and carbon monoxide.

However, both of these compounds are also reaction products in the propane oxidation reaction. Being an intermediate, propylene is further oxidized to acrylic acid, acetic acid and carbon oxides.

In the following, the addition of propylene in the two-stage reactor is presented (Figure 4.3.6). Upon addition of 0.50 and 0.75 vol% propylene between the two reactors, the global rate of propane consumption was constant within experimental errors. However, the propylene concentration monitored at the outlet of the second reactor was constant, irrespective of the added amount of propylene between the two reactors. The global rate of propylene formation was constant in spite of addition. This means that the whole amount of added propylene completely was completely consumed. The oxidation of the added propylene was well reflected in the enhancement of the global rates of acrylic acid, acetic acid and carbon monoxide and carbon dioxide formation. It is notable, that upon propylene addition in the two-stage reactor, no other product (i.e. acetone) was detected by the GC-MS setup, like in the case of propylene oxidation.

The significant increase of the oxygen consumption rate attests that the added propylene indeed acts as a strong reducing agent. Addition of propylene in higher concentration than 0.75 vol% was avoided in order to keep the oxygen conversion below 100%.

Upon switching off the propylene addition, the catalytic properties were remeasured. Because the catalyst was not exposed to very reducing conditions ( $X_{O_2} < 100\%$ ), the catalytic performance was found to be constant over time (i.e. no “reactive reactivation” was observed like in the case shown on Figure 4.3.6). The rates of propane consumption

and the product formation were found to be very similar to the values determined before the addition of propylene (Figure 4.3.6.). This also supports the observed reversibility of the catalytic properties after operating the reaction under reducing conditions.

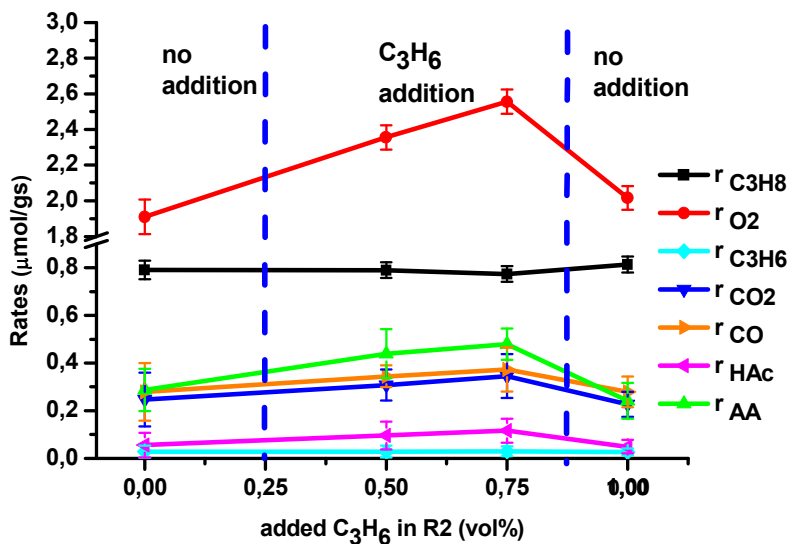


Figure 4.3.6. The effect of C<sub>3</sub>H<sub>6</sub> addition of in the two-stage reactor.

A very slight decrease of the propane consumption rate was observed upon propylene addition. This may suggest that there is a slight competition between propane and propylene on the adsorption sites. Microcalorimetric experiments on propane and propylene adsorption showed that a larger amount of propylene can be adsorbed compared to propane at the same equilibrium pressure [39]. On the other hand, the additional propylene may be adsorbed on the sites which are energetically less favored for propane adsorption.

In turn, the results may be interpreted as there are two active sites. One of them is performing the oxidative dehydrogenation of propane, while the other one oxidizes further the propylene. The slight reduction of the propane consumption rate may be a consequence of the higher reduction degree of the catalyst surface.

### 4.3.3. Addition of CO

In the 4.2.7 section it is shown that CO oxidation reactivity over MoVTeNbO<sub>x</sub> catalyst is negligible, even though CO is known to be a reducing compound. This can be attributed to low abundance of electrophilic oxygen species on the surface.

However, because of the very low reactivity in CO oxidation, the surface redox property of the MoVTeNbO<sub>x</sub> catalyst certainly does not change significantly during one catalytic cycle. On the other hand the catalyst showed ca. 80 times higher reactivity in propane oxidation (Figure 4.2.15), therefore in this reaction the reduction degree is expected to be changed more significantly during one catalytic cycle [40]. Upon such significant changes of the oxidation states, the nature and the abundance of the surface oxygen species might be different. Because the CO oxidation reaction is suitable for semi-quantitative estimation of the electrophilic oxygen species, the CO addition in the two-stage reactor was performed in order to probe the changes of the abundance of active oxygen species during propane oxidation reaction.

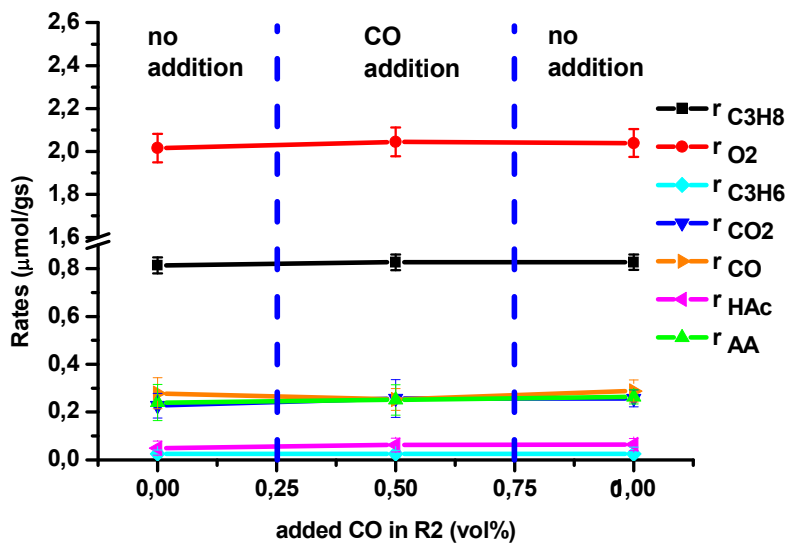


Figure 4.3.7. The effect of CO addition in the two-stage reactor.

Upon addition of 0.5 vol% CO to the mixture that enters the second reactor, no change in the propane and oxygen consumption was observed (Figure 4.3.7). This suggests that CO

does not compete with propane for adsorption sites and is not further oxidized to CO<sub>2</sub>. The added CO concentration was subtracted from the concentration measured at the outlet of the second reactor. The resulting value was found to be identical with the CO concentration measured without addition. Moreover, the CO<sub>2</sub> formation was also not affected by the CO addition. These latter observations also support the fact that the CO oxidation during propane selective oxidation reaction is negligible, independent of the surface redox potential changes of the catalyst in the catalytic cycle.

The formation of propylene, acetic acid and acrylic acid was also not affected by the CO addition, revealing that the CO is an inert end-product.

This experiment confirmed that the electrophilic oxygen species are not abundant on the catalyst surface under working conditions.

#### 4.3.4. Addition of CO<sub>2</sub>

Carbon dioxide is the thermodynamically favored end product of the propane oxidation reaction. Although it is often considered to be an inert product, CO<sub>2</sub> may play different roles in heterogeneous catalysis:

- competitively adsorb with educt or intermediates on the active sites,
- it was reported to increase the conversion in the dehydrogenation reaction of isobutane [41]
- the presence of CO<sub>2</sub> was found to be beneficial for propane oxidation reaction over MoVTeNbO<sub>x</sub> catalyst. The obtained catalytic results revealed a linear increase of yield of acrylic acid with the CO<sub>2</sub> content in the feed [42].

The microcalorimetric experiment on CO<sub>2</sub> adsorption revealed that the density of sites interacting with CO<sub>2</sub> is higher than the density of sites available for propane adsorption. On the other hand, the initial differential heat of adsorption of CO<sub>2</sub> was found to be ca. 30 kJ/mol, while for propane adsorption a value of 40 kJ/mol was determined on catalyst #6059 after propane oxidation reaction. The heat profile corresponding to the CO<sub>2</sub> adsorption on the used catalyst indicated a relatively homogeneous distribution of the surface basic sites.

CO<sub>2</sub> addition in the two-stage reactor system was performed in order to find out whether it competitively adsorbs with propane on the active sites of the catalyst. Up to 2.0 vol% CO<sub>2</sub> was added to the gas mixture leaving the first reactor tube (Figure 4.3.8).

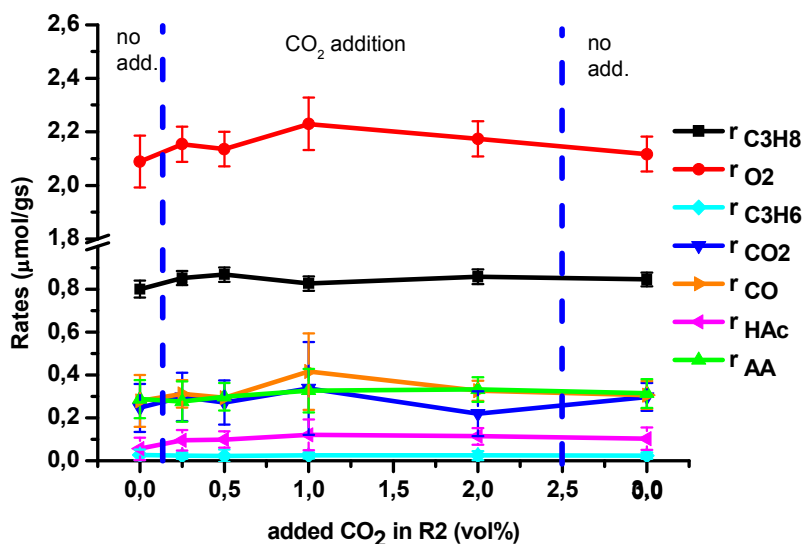


Figure 4.3.8. The effect of CO<sub>2</sub> addition in the two-stage reactor.

Because the added CO<sub>2</sub> is a non-reactive gas added to the mixture, a mass balance equation was set in order to calculate the amount of CO<sub>2</sub> produced in the reaction. Figure 4.3.8 displays the rates of educt consumption and product formation as a function of the concentration of the added CO<sub>2</sub>. No significant changes could be observed in the propane and oxygen consumption rate.

The propylene and acrylic acid formation rate is insensitive to the addition of CO<sub>2</sub>. This suggests that carbon dioxide does not adsorb competitively either with propane, or with propylene on the active sites of the catalyst. A slight increase in the CO formation rate could be observed when 1.0 vol% CO<sub>2</sub> was added to the reacting mixture. On the other hand, CO<sub>2</sub> formation rate was slightly reduced when 2.0 vol% CO<sub>2</sub> was added, while acetic acid formation was slightly enhanced by the presence of carbon dioxide.

#### 4.4. Conclusions

Catalytic and kinetic studies on propane oxidation to acrylic acid were carried out using a high performing phase-pure M1 MoVTeNbO<sub>x</sub> catalyst. The reaction temperature, redox potential of the gas phase and the steam content of the feed was varied. The highest acrylic acid yield of ca. 30% was attained at 400°C and stoichiometric feed containing 40 vol% steam. A reversible drop of the catalytic performance was observed when the steam concentration was decreased to 0 vol%. Neither the conversion nor the selectivity was increased or decreased in oxidizing feed (up to five-fold excess of oxygen).

The oxidation of intermediates (propylene and acrolein) and CO over the phase-pure M1 catalyst was also performed at the same temperature interval where propane oxidation is carried out, in order to establish the reactivity ranking, product distribution and to probe the reaction pathways.

The catalyst was found to be ca. 6 times more active in propylene oxidation compared to propane oxidation at a temperature of 400°C, the main product being acrylic acid. The acrolein oxidation rate was ca. 100 times higher compared to the propane oxidation at 400°C, while the acrylic acid yield was over 90%. On the other hand, the rate of CO oxidation and water gas shift reaction was found to be ca. 100 times lower compared to the propane oxidation. The low reactivity in CO oxidation suggested low abundance of electrophilic oxygen species. Additionally, this finding suggested that the CO and CO<sub>2</sub> are produced in independent pathways during the propane, propylene and acrolein oxidation reactions.

Staged addition of oxidizing and reducing agents (O<sub>2</sub>, N<sub>2</sub>O, C<sub>3</sub>H<sub>6</sub>, CO and CO<sub>2</sub>) was performed in a setup consisting of two serially connected reactor tubes. The oxygen content variation in this arrangement lead to increase in the propane conversion and acrylic acid selectivity, giving an improvement of the acrylic acid yield by 5% compared to the conventional fixed bed reactor. Additionally it was found that N<sub>2</sub>O is an inert gas in the propane oxidation reaction. This lead to the conclusion that the phase-pure MoVTeNbO<sub>x</sub> catalyst is unable to activate the N<sub>2</sub>O molecule.

Upon addition of propylene, the formation rate of acrylic acid, acetic acid, CO and CO<sub>2</sub> products increased.

The addition of CO did not influence the consumption rate of propane and oxygen and the formation rate of any product. This suggested that the CO does not adsorb competitively with propane or any intermediates on the active sites. Additionally, this experiment proved that the CO oxidation activity is very low during propane oxidation reaction, therefore indirectly also proved that the CO<sub>2</sub> is produced independently from CO in the propane oxidation reaction. The observation concerning the low abundance of electrophilic oxygen species, irrespectively on the degree of reduction of the catalyst surface within one catalytic cycle was also supported by the results of this experiment. The CO<sub>2</sub> addition in relatively low concentration also did not influence the rates significantly, suggesting that the thermodynamically favored end product does not adsorb competitively with the educt or intermediates on the active sites of the catalyst.

#### References Chapter 4

1. E. Novakova, E. G. Derouane, J. Védrine, *Catal. Lett.* 83, 3-4 (2002) 177-182
2. E. Balcells, F. Borgmeier, I. Grißtede, H-G. Lintz, *Catal. Lett.* 87 (2003) 195
3. I. Grißtede, Die Partielle Oxidation von Propan zu Acrylsäure, Bestimmung der Reaktionskinetik und in-situ charakterisierung des Katalysators unter Betriebsbedingungen, Dissertation, Universität Karlsruhe, 2004, Universitätsverlag Karlsruhe, ISBN 3-937300-17-1; E. Balcells,
4. F. Borgmeier, I. Grißtede, H.-G. Lintz, F. Rosowski, *Appl. Catal. A: General*, 266 (2004) 211
5. J. B. Butt, *Reaction kinetics and reactor design*, 2<sup>nd</sup> Ed., Marcel Dekker Inc., 2000, pp. 25-35
6. J. L. Dubois, D. Garrait, A. Le Gall, G. Bazin, S. Serreau, FR Patent, WO 2006/072682 A1, 2006
7. W. Zheng, Zh. Yu, P. Zhang, Y. Zhang, H. Fu, X. Zhang, Q. Sun, X. Hu, *J. Natural Gas Chemistry*, 17 (2008) 191-194
8. Ch. G. Hill, *An Introduction to Chemical Engineering, Kinetics and Reactor Design*, John Wiley and Sons, 1977, 24-74
9. R. W. Missen, Ch. A. Mims, B. A. Saville, *Introduction to Chemical Reaction Engineering and Kinetics*, John Wiley and Sons, 1999, 49-55
10. I. Grißtede, H-G. Lintz, *Catal. Lett.* 87 (2003) 195
11. G. Centi, F. Cavani, F. Trifiro, *Selective oxidation by heterogeneous catalysis*, Kluwer Academic/Plenum Publishers, 2001, 363-384
12. M. Ai, *J. Catal.*, 101 (1986) 473-483
13. Y. Moro-oka, *Appl. Catal. A: General*, 181 (1999) 323-329
14. L. Luo, PhD thesis, California Institute of Technology, Pasadena, California, 2001
15. J. C. Védrine, E. K. Novakova, E. G. Derouane, *Catal. Today*, 81 (2003) 247-262
16. H-G. Lintz, S. P. Müller, *Applied Catal. A: General*, 357 (2009) 178-183

17. M. M. Lin, *Appl. Catal. A*, 207 (2001) 1-16
18. E. K. Novakova, J. C. Védrine, Propane selective oxidation to propene and oxygenates on metal oxides, in *Metal Oxides - Chemistry and applications*, J.G.L. Fierro (Ed.), 2006, CRC Press, pp. 414-461
19. M. Ai, *Catal. Today*, 13 (1992) 679-684
20. M. Ai, *J. Catal.*, 101 (1986) 389-395
21. J. C. Védrine, E. K. Novakova, E. G. Derouane, *Catal. Today*, 81 (2003) 247-262
22. P. Concepción, P. Botella, J. M. López Nieto, *Appl. Catal. A: General*, 278 (2004) 45-56
23. M. Lin, T. B. Desai, F. W. Kaiser, P. D. Klugherz, *Catal. Today*, 61 (2000) 223-229
24. J. Hermann, *Catal. Today*, 112 (2006) 73-77
25. S.T. Oyama, X. Zhang, J. Lu, Y. Gu, T. Fujitani, *J. Catal.*, 257 (2008) 1-4
26. G. Campanelli, A. Bottino, D. Romano, O. Montinelli, A. Servida, F. Cavani, S. Rossini, *Stud. in Surf. Sci. and Catal.* 119 (1998) 423-428
27. A. Bottino, G. Campanelli, A. Comite, *J. Membr. Sci.*, 197, 1-2 (2002) 75-88;
28. G. Campanelli, E. Carosini, F. Cavani, O. Monticelli, F. Trifiro, *Chem. Eng. Sci.*, 51, 10 (1996) 1817-1826
29. J. A. Dalmon, A. Cruz-Lopez, D. Farruseng, N. Guilhaume, E. Iojoiu, J.-Ch. Jalibert, S. Miachon, C. Mirodatos, A. Pantazidis, M. Rebeilleau-Dassonneville, Y. Schuurman, A. C. van Veen, *Appl. Catal. A: General*, 325, 2, 15 (2007) 198-204
30. H.-G. Lintz, A. Reitzmann, *Catalysis Reviews: Science and Engineering*, 49, 1, (2007) 1-32
31. C. Hamel, Á. Tóta, F. Klose, F. Tsotsas, A. Seidel-Morgenstern, *Chem. Eng. Res. Design*, 86 (2008) 753-764; C. O'Neill, E. E. Wolf, *Catal. Today*, 156 (2010) 124-131 ; W. Fang, Q.-J. Ge, J.-F. Yu, H.-Y. Xu, *Ind. Eng. Chem. Res.*, 50 (2011) 1962-1967
32. C. O'Neill, E. E. Wolf, *Catal. Today*, 156 (2010) 124-131
33. W. Fang, Q.-J. Ge, J.-F. Yu, H.-Y. Xu, *Ind. Eng. Chem. Res.*, , 50 (4) (2011) 1962-1967
34. V. N. Parmon, G. I. Panov, A. Uriarte, A. S. Noskov, *Catal. Today*, 100 (2005) 115-131
35. E. V. Kondratenko, M. Cherian, M. Baerns, D. Su, R. Schlögl, X. Wang, I. E. Wachs, *J. Catal.* 234 (2005) 131-142
36. E. V. Kondratenko, M. Cherian, M. Baerns, D. Su, R. Schlögl, X. Wang, I. E. Wachs, *J. Catal.* 234 (2005) 131-142
37. E. V. Kondratenko, A. Brückner, *J. Catal.* 274 (2010) 111-116
38. M. T. Allen, R. A. Setter, F. L. Dryer, *Int. J. Chem. Kinet*, 27 (1995) 883-909
39. M. Hävecker, S. Wrabetz, J. Kröhnert, L. Csepei, R. Naumann, Yu. V. Kolen'ko, F. Girgsdies, R. Schlögl, A. Trunschke, *J. Catal.*, submitted
40. J. M. López-Nieto, B. Solsona, P. Concepción, F. Ivars, A. Dejoz, M. I. Vázquez, *Catal. Today*, 157 (2010) 291-296
41. J. Ogonovski, E. Skrzynska, *Cat. Comm.*, 11 (2009) 132-136
42. R. Fushimi, S. O Sekhtman, A. Gaffney, S. Han, G. Yablonsky, J. T. Gleaves, *Ind. Eng. Chem. Res.* 44 (2005) 6310-6319

## Chapter 5. Post synthesis treatment of the phase-pure M1 MoVTeNbO<sub>x</sub> catalyst

### 5.1.1. Abstract

Post-synthesis treatment of the phase-pure M1 MoVTeNbO<sub>x</sub> catalyst with different aqueous solutions at room temperature is presented in this chapter. The modifying agents were selected in such a way to cover all the chemical effects (neutral, acidic, basic, oxidizing and reducing, respectively). Catalytic experiments on propane and propylene oxidation showed that the chemical treatment of the phase-pure M1 MoVTeNbO<sub>x</sub> sample with neutral, acidic, basic and reducing solution leads to a marginal improvement in the activity, while the acrylic acid yield is not significantly influenced. On the other hand, the treatment with oxidizing solution leads to a very dramatic decrease in activity and selectivity and alters the homogeneous energetic distribution of propane adsorption sites probed by adsorption microcalorimetry. The acrylic acid selectivity at the same propane conversion was found to correlate with the surface Te content and Te/V ratio. The phase purity was not affected either by the chemical treatment or the catalytic reaction of propane and propylene oxidation, suggesting the exceptional bulk structural robustness of the M1 MoVTeNbO<sub>x</sub> catalyst.

### 5.1.2. Introduction

The as prepared mixed metal oxide catalysts are seldom phase pure materials. The synthesis of MoVTeNbO<sub>x</sub> catalyst often leads to M1+M2 phase mixtures.

In the patent literature several methods are claimed for the selective removal of the M2 phase. The Japanese Laid-Open Patent Application No. 10-330343 claimed a single and a dual stage washing procedure using aqueous oxalic acid, ethylene glycol and hydrogen-peroxide solutions, aiming at modification of the crystalline phase composition of MoVSb based oxide catalysts. Treatments of the same oxide catalyst with organic acid, alcohol, inorganic acid and hydrogen peroxide are claimed as well [1].

Washing of MoVTeNbO and related oxide catalysts using organic acids, alcohols, inorganic acids and hydrogen peroxide has been claimed by the patent literature for selective removal of the M2 phase [2, 3]. Oxalic acid and ethylene diol were claimed to

be the most effective agents in removal of the M2 phase. None of the listed inorganic acids was highlighted as preferred washing agent. Higher temperatures were suggested to be favorable for faster removal of the M2 phase. However the results concerning the phase composition are described only qualitatively by the term “substantially free of hexagonal phase”. Changes in the bulk and/or surface elemental composition were not monitored and the results of catalytic experiments are completely missing.

Gulians et al. reported that the treatment of phase pure  $\text{MoVO}_x$  catalyst by anhydrous 2-propanol leads to significant change in the surface elemental composition, as probed by LEIS study [4]. The as prepared material exhibited a surface composition of  $\text{MoV}_{0.19}\text{O}_x$ , while in case of the treated sample the enrichment of vanadium was observed, the composition being  $\text{MoV}_{0.69}\text{O}_x$ . On the other hand the bulk composition and M1 phase was unaffected by the treatment. The 2-propanol treated sample however showed an improved selectivity to acrylic acid and a lower propane apparent activation energy compared to the as prepared  $\text{MoVO}_x$  catalyst.

Baca et al. reported complete removal of M2 phase by washing with 15% hydrogen-peroxide containing solution from a M1+M2 phase mixture [5].

Due to the lack of any quantitative data reported in the patent literature, it is not known whether the claimed positive effect of solution treatment applied to a phase mixture is due exclusively to the selective dissolution of the M2 phase or it might be related to the possible change in the surface composition as well, similarly to the data reported by Gulians et al. [4].

Therefore, in this chapter the effect of different selected solutions (neutral, acidic, basic, complexing, oxidizing and reducing) on the phase pure M1  $\text{MoVTenbO}_x$  catalyst is addressed in order to sort out their effect on the

- Bulk structure, phase purity
- Surface/bulk composition
- Catalytic properties.

## 5.2. Modifying agents and procedure

The starting material (called also parent sample) was a phase-pure M1 MoVNbO<sub>x</sub> catalyst with the internal identification number #6902. This was subjected to modification procedure by washing in solutions. The synthesis and characterization of the original sample is described in detail in chapter 2.3.

Modification procedure: 2.0 g of parent sample was dispersed in 50 ml of the solutions listed below. The suspension was shaken at room temperature for 3 hours. Then the solid sample was separated from the liquid by vacuum filtration. Finally, the sample was dried in a vacuum desiccator. Although, in the literature a heat treatment step is also recommended after performing the modification procedure, in the present study the final calcination was not performed. The reason for avoiding heat treatment is the evidence of surface reconstruction of a hydrogen-peroxide treated sample, given by Kolen'ko et al. [6].

The modifying solutions were as follows:

1. Distilled water. Chemical effect: neutral. The rationale of using pure water was that to sort out the effect of the solvent on the catalyst, since all the other modifying agents were used as aqueous solutions. The distilled water treated sample got the internal identification number of #7797.

The pH of the filtrate solution was 1.9. Since the catalyst does not contain hydrogen ions bound in the structure, the surprisingly high pH change of 5.1 was a consequence of metal ion leaching. The metal ions leached out from the sample may undergo hydrolysis and form hydroxides and oxo-ions. The consumption of hydroxyl ions in the hydrolysis is reflected in the drop of the pH.

2. 0.1M phosphoric acid, H<sub>3</sub>PO<sub>4</sub>. This compound has acidic and complexing properties. The pH of the 0,1 M H<sub>3</sub>PO<sub>4</sub> solution was 1.7, while the pH of the filtrate after treatment was 2.7. Even though phosphoric acid is a relatively strong acid, the pH of the filtrate is higher by 1.8 compared to the pH of the filtrate from the water treated sample. This might be due to the fact that the leached metal ions form complexes with phosphate ions and hydrolysis is suppressed. To the phosphoric acid solution treated sample the internal number of #7798 was assigned.

3. 0.1 M tetramethylethylenediamine,  $(\text{CH}_3)_2\text{NCH}_2\text{CH}_2\text{N}(\text{CH}_3)_2$  (TMEDA). This compound has basic (pH=10.9) and complexing effects. Upon treating the  $\text{MoVTeNbO}_x$  with this solution, the pH of the filtrate decreased to 4.1. The solid sample after treatment got the number of #7799.

4. 0.1 M sodium bromate,  $\text{NaBrO}_3$ . The bromate ion presents oxidizing properties which potentially may oxidize the elements of the sample in the intermediate oxidation states. The pH change of the solution was from 6.9 to 3.0. The sample was got the internal identification number of #7798.

5. 0.1 M hydrazine,  $\text{N}_2\text{H}_4 \cdot \text{H}_2\text{O}$ . This compound with reducing properties was selected in order to try to reduce some elements in the highest or intermediate oxidation states. The initial pH of the 0.1 M  $\text{N}_2\text{H}_4$  solution was 9.8, while the pH of the filtrate was found to be 9.3. The hydrazine treated sample got the internal identification number of #8113.

In the liquid filtrate four types of equilibria involving the leached metal ions may proceed. One of them is hydrolysis and precipitation formation. From the literature only limited information is available about the solubility of the molybdenum, vanadium, tellurium and niobium hydroxides. The solubility product of  $\text{VO}(\text{OH})_2$  is  $5.9 \cdot 10^{-23}$ , while of  $\text{Te}(\text{OH})_4$  is equal to  $3 \cdot 10^{-54}$  [8]. The calculated pH of a solution that contains  $\text{Te}(\text{OH})_4$  in equilibrium is 3.3, while hydrolysis of vanadyl ion leads to a solution with pH of 6.6. None of these pH values matches with the pH of the filtrate resulting from the water treated #6902 sample, suggesting a complicated hydrolysis/precipitation equilibrium. Based on the Pourbaix-diagrams of Mo-, V-, Nb- and Te-species [7-10], in aqueous solution at the pH of 1,9 the following species are stable:  $\text{MoO}_3$ ,  $\text{VO}_2^+/\text{VO}^{2+}/\text{V}^{3+}$  (depending on redox potential),  $\text{Nb}_2\text{O}_5$ ,  $\text{HTeO}_2^-/\text{Te}_2^{2-}/\text{TeO}_3 \cdot 3\text{H}_2\text{O}/\text{TeO}_3^{2-}/\text{H}_2\text{TeO}_4/\text{HTeO}_2^+$  (depending on the redox potential).

The second equilibrium is condensation of hydrated metal ions and formation of oligo- and polymetallates.

The third equilibrium is the complex formation involving the leached metal cations and the inorganic/organic ligands ( $\text{H}_3\text{PO}_4$ , TMEDA and  $\text{N}_2\text{H}_4$ , respectively) from the washing solutions.

Finally, the fourth equilibrium is the redox reaction between the redox active transitional metal ions with bromate and hydrazine.

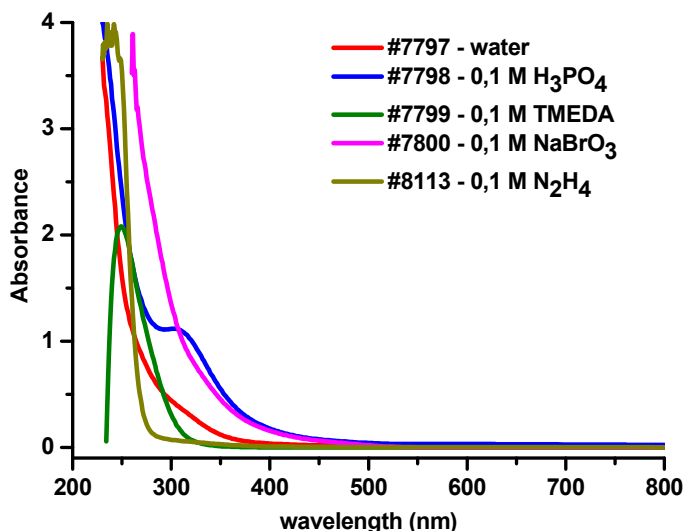


**Figure 5.2.1.** The UV-Vis spectra of the filtrate solutions.

As a result of these equilibria, a multitude of cationic and anionic transitional metal containing species may exist in the filtrate solutions. The UV-Vis spectra of the filtrate solutions were found to be different from each other, indicating that different species are present in all the solutions (Figure 5.2.1). Because of the complexity of the reactions that may occur in the liquid phase and consequently, the formation of large number of species, it was not possible to assign directly the bands to the species.

However, the composition and catalytic properties of the solid material after the liquid treatment is more important, rather than the qualitative and quantitative identification of the ions leached out upon the above described liquid treatments. Therefore, the next sections are focused on the characterization of the solid material after the liquid treatment. Furthermore, catalytic data are presented on propane and propylene oxidation using the modified samples. The reaction pathway analysis of propane oxidation was performed. Different pathways were found; therefore a preliminary kinetic analysis of the propane and oxygen partial order and consumption rate constant was

evaluated. Furthermore, the rate constant of propylene consumption was also determined for every modified catalyst.

### 5.3. Characterization of the modified samples

#### 5.3.1. N<sub>2</sub> physisorption

The nitrogen adsorption isotherms determined at the temperature of liquid nitrogen are shown in Figure 5.3.1.

**Table 5.3.1.** The BET surface area of the samples.

Sample number	Treatment	BET surface area (m <sup>2</sup> /g)
#6902	None	7.5
#7797	H <sub>2</sub> O	12.8
#7798	H <sub>3</sub> PO <sub>4</sub>	11.3
#7799	TMEDA	5.5
#7800	NaBrO <sub>3</sub>	5.0
#8113	N <sub>2</sub> H <sub>4</sub>	11.6

In case of the water treated sample the surface area increased by about 70%, while upon phosphoric acid and the hydrazine treatment the surface area increased by about 50%. On the other hand, in the case of the tetramethylethylenediamin and bromate treatment the surface area decreased by about 30% compared to the parent sample.

#### 5.3.2. X-ray diffraction

The parent and the as prepared modified samples were subjected to XRD measurements between  $2\cdot\Theta=2^\circ$  and  $2\cdot\Theta=80^\circ$ . XRD measurements were performed on samples after the catalytic experiments on propane and propylene oxidation.

Rietveld refinement performed on the patterns showed that the phase purity was not affected, irrespective of the nature of the chemical treatment. The quantitative Rietveld analysis was obtained using the crystal structure of M1 MoVTeNbO<sub>x</sub> (ICSD, 55097) [11]. This observation suggests that the bulk structure of the phase-pure MoVTeNbO<sub>x</sub> catalyst is robust enough to withstand treatment with the above listed solutions. No phase change has happened under propane and propylene oxidation reaction conditions, in

contrast to the phase alteration when switching from propane to propylene educt, speculated by Griřtede [12].

**Table 5.3.2.** The lattice parameters of the catalysts before and after catalytic oxidation of propane and propylene.

<b>Catalyst ID Latt. const.</b>		<b>#6902</b>	<b>#7797</b>	<b>#7798</b>	<b>#7799</b>	<b>#7800</b>	<b>#8113</b>
Before reaction	a (Å)	21.146	21.138	21.126	21.127	21.143	21.143
	b (Å)	26.641	26.630	26.615	26.615	26.640	26.633
	c (Å)	4.0161	4.0169	4.015	4.0153	4.018	4.0151
	V (Å <sup>3</sup> )	2262.4	2261.2	2257.6	2257.7	2262.8	2260.9
After reaction	a (Å)	21.139	21.142	21.145	21.134	21.162	21.144
	b (Å)	26.628	26.631	26.640	26.632	26.654	26.632
	c (Å)	4.0146	4.0123	4.013	4.010	4.013	4.0133
	V (Å <sup>3</sup> )	2259.8	2259.0	2260.7	2257.0	2263.5	2259.9

The lattice constants were extracted for all the samples before and after catalytic reaction. They are listed in Table 5.3.2. It can be observed that by treatment the lattice constants are only slightly affected. The lattice parameters are also slightly changing during the propane and propylene oxidation reaction.

### 5.3.3. SEM/EDX

The SEM images of the parent and modified samples are shown in Figure 5.3.1.

The SEM micrograph of the parent sample is a homogeneous material, but consists of irregularly shaped rod-like particles with length up to 500 nm and diameter between 50 and 100 nm.

Water treatment leads to a wider distribution of particle diameter, but the predominant rod-like shape of the parent sample is conserved.

Upon phosphoric acid treatment the particles loose their rod-like shape and their size is reduced. Aggregates of particles with ill defined shape can also be observed.

Treatment by tetramethylethylenediamin leads to a rather wide distribution of particle size. The shape varies from plate-like to needles and also particles with aspect ratio close to unity can be observed.

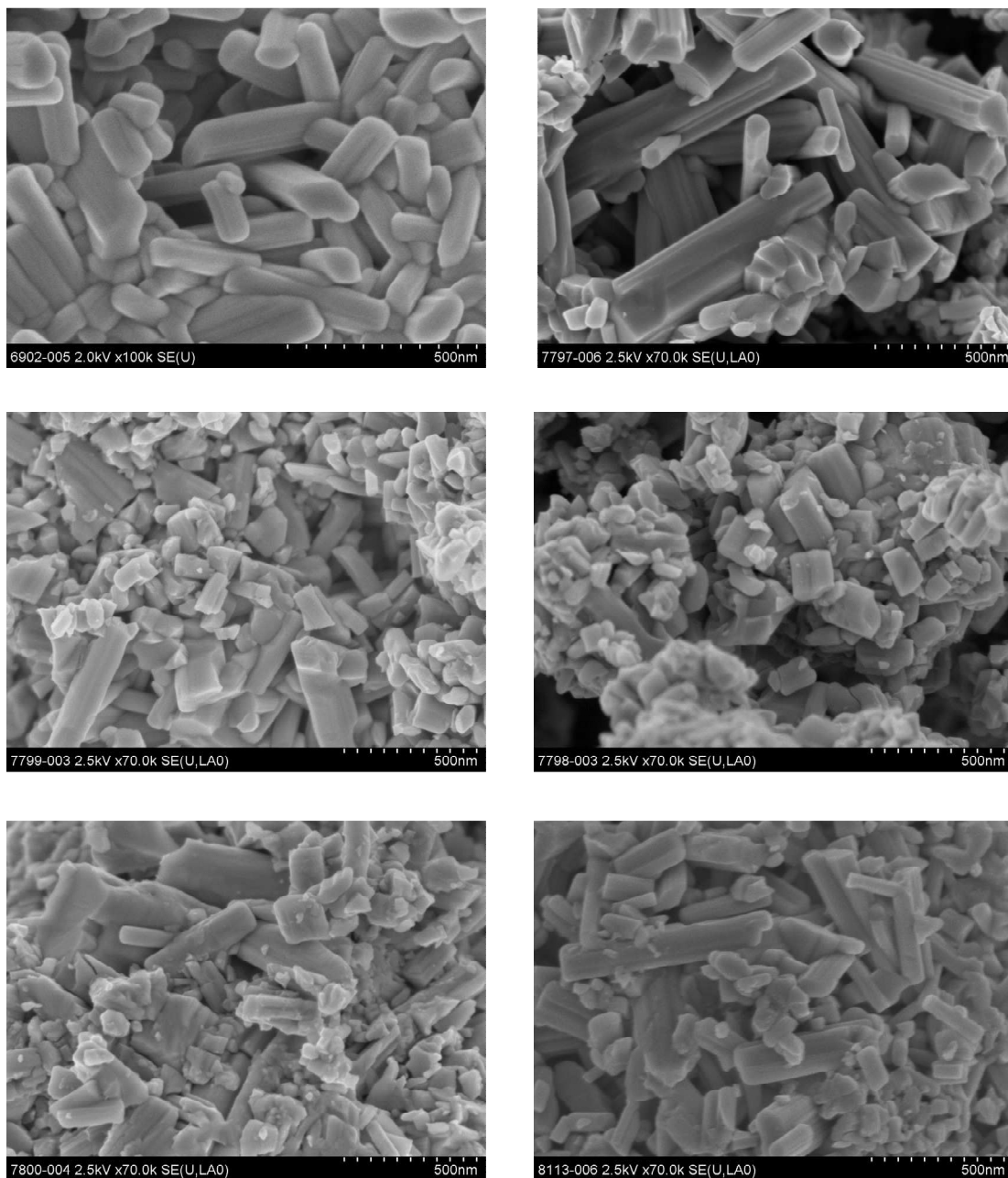


**Figure 5.3.1** The SEM picture of the catalysts. #6902 (parent sample), #7797 (water treated sample), #7798 ( $\text{H}_3\text{PO}_4$  treated sample), #7799 (TMEDA treated sample), #7800 ( $\text{NaBrO}_3$  treated sample), #8113 ( $\text{N}_2\text{H}_4$  treated sample).

Also in the bromate treated sample a broad shape and size distribution can be observed. In the hydrazine treated sample the predominant shape of needle-like morphology from the parent sample is conserved, however particles with not well defined shape between 50-100 nm intervals can also be observed.

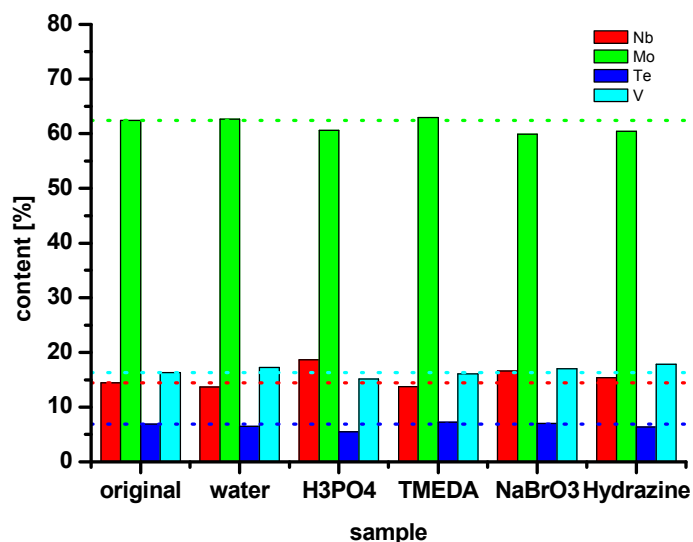


**Figure 5.3.2.** The elemental composition of the original and the modified catalysts as probed by EDX.

The bulk elemental composition of all the samples was determined by means of EDX (Figure 5.3.2). The parent sample (#6902) consists of 62.44 at% Mo, 16.27 at%V, 6.89 at% Te and 14.40 at% Nb, which corresponds to a formula of  $\text{MoV}_{0.26}\text{Te}_{0.11}\text{Nb}_{0.23}\text{O}_x$ .

In the distilled water treated sample (#7797) the enrichment of Mo and V (62.61 at% and 17.28 at%) and depletion of Te and Nb (6.47 at% and 13.65 at%, respectively) was observed, leading to a formula of  $\text{MoV}_{0.28}\text{Te}_{0.10}\text{Nb}_{0.22}\text{O}_x$ .

The phosphoric acid treatment leads to slight decrease of Mo, V and Te content in the sample #7798 (60.64 at%, 15.16 at% and 5.50 at%, respectively) balanced by the enrichment of Nb (18.7 at%).

Upon tetramethylethylenediamine treatment, the Mo and Te content is increasing (to 62.94 at% and 7.27 at%), while the V and Nb content decreases (16.07 and 13.72 at%) giving a sample of #7799 with the formula  $\text{MoV}_{0.26}\text{Te}_{0.12}\text{Nb}_{0.22}\text{O}_x$ .

Bromate treatment leads to the most significant depletion of Mo (to 59.94 at%), while V, Te and Nb are enriched (16.99, 7.04 and 16.63 at%). This sample with number #7800 has the formula of  $\text{MoV}_{0.28}\text{Te}_{0.12}\text{Nb}_{0.28}\text{O}_x$ .

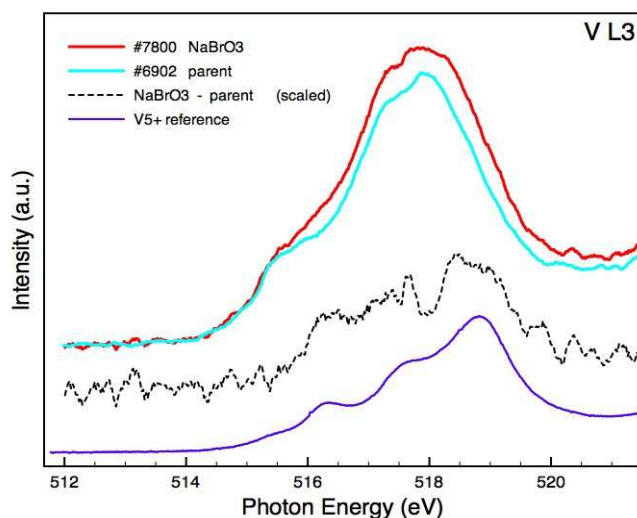
Upon hydrazine treatment, the Mo and Te content decreases (60.45at% and 6.37 at%), while V and Nb are enriched compared to the parent sample (17.84 at% and 15.34at%). The formula of the sample #8113 is  $\text{MoV}_{0.30}\text{Te}_{0.11}\text{Nb}_{0.25}\text{O}_x$ .

### 5.3.4. XAS and XPS

X-ray photoelectron spectroscopy (XPS) spectra were recorded at the synchrotron radiation facility BESSY II for each modified samples. The high pressure XPS spectra were recorded at room temperature and in the presence of about 0.25 mbar oxygen pressure in order to avoid the beam-induced reduction of the tellurium.

No significant difference was observed between the X-ray absorption spectra (XAS) corresponding to the original material, water-, phosphoric acid-, tetramethylethylenediamine- and hydrazine treated samples. This suggests that no significant changes happened in the average oxidation state or coordination geometry of the metals upon treatment with the above named modifiers. On the other hand, the difference spectra between the bromate treated sample (#7800) and the original material corresponding to the vanadium L3 edge showed a similarity with the  $V^{5+}$  reference spectrum (Figure 5.3.5). This suggests that the bromate treatment lead to partial oxidation of the  $V^{4+}$  ions to  $V^{5+}$ .

The survey photoelectron spectra showed that phosphorous-, nitrogen- and bromide containing species are absent in all the samples. This suggests that none of the modifying agents or their eventual reaction products (complexes, reduced or oxidized forms of bromate and hydrazine, respectively) were bound to the catalyst.



5.3.3. NEXAFS spectra of the bromate treated sample( #7800), the parent sample (#6902), the difference spectrum and the  $V^{5+}$  reference spectrum.

Therefore, the contamination of the M1 structure with different molecular or ionic species from the chemical treatment can be ruled out.

Core level photoelectron spectra of O1s, V2p (3/2), Mo3d (5/2), Nb3d (5/2) and Te3d (5/2) were recorded at different kinetic energies. Low kinetic energy (165, 170 and 180 eV) was applied for surface sensitive mode, while higher kinetic energy (465, 470 and 480 eV) for the bulk sensitive mode.

The binding energy (BE) of Mo3d (5/2) are slightly lower compared to the typical value of 232,6 eV reported for MoO<sub>3</sub> standard compound [5, 13, 14]. The Mo3d peak is likely composed of three peaks, corresponding to a binding energy of 231.0, 232.0 and the highest component of 232.6 eV. Therefore the predominant oxidation state of molybdenum is 6+, with minor contribution of 5+ and 4+. The presence of low abundance of Mo<sup>5+</sup> oxidation state has also been reported [14, 15].

**Table 5.3.3.** The binding energies corresponding to every catalyst.

<i>Sample</i>	<i>O1s (eV)</i>	<i>V2p (3/2) (eV)</i>	<i>Mo3d (5/2) (eV)</i>	<i>Nb3d (5/2) (eV)</i>	<i>Te3d (5/2) (eV)</i>
#6902: parent	530.3	516.3	232.1*	206.4	576.2 573.3
#7797: H <sub>2</sub> O	530-530.1	516-516.1	232.0-232.1*	206.3	576-576.2 573-573.2
#7798: H <sub>3</sub> PO <sub>4</sub>	529.9-530.1	516-516.2	232.1*	206.3	576-576.1 573-573.1
#7799: TMEDA	530.1-530.2	516.1- 516.2	~232.2*	206.4-206.5	576-576.1 573
#7800: NaBrO <sub>3</sub>	~530.3	~516.4- 516.2	~232.2*	~206.5	576.4- 576.2 ~573.3
#8113: N <sub>2</sub> H <sub>4</sub> ·H <sub>2</sub> O	530.1- 530.2	516.2- 516.3	232.2*	206.5	576.3 573.3

The binding energy of Nb3d (5/2) was close to the value of 207,2 reported for 5+ oxidation state, while the binding energy of tellurium indicated the oxidation state of 4+. On the other hand, the vanadium oxidation state was found to be 4+. As identified by XAS, in the bromate treated sample a small amount of V<sup>5+</sup> was also present.

The surface and bulk elemental composition was quantified from the spectra obtained at low and high kinetic energy, respectively. The bulk elemental composition showed a good agreement with the values determined by multi-spot EDX analysis.

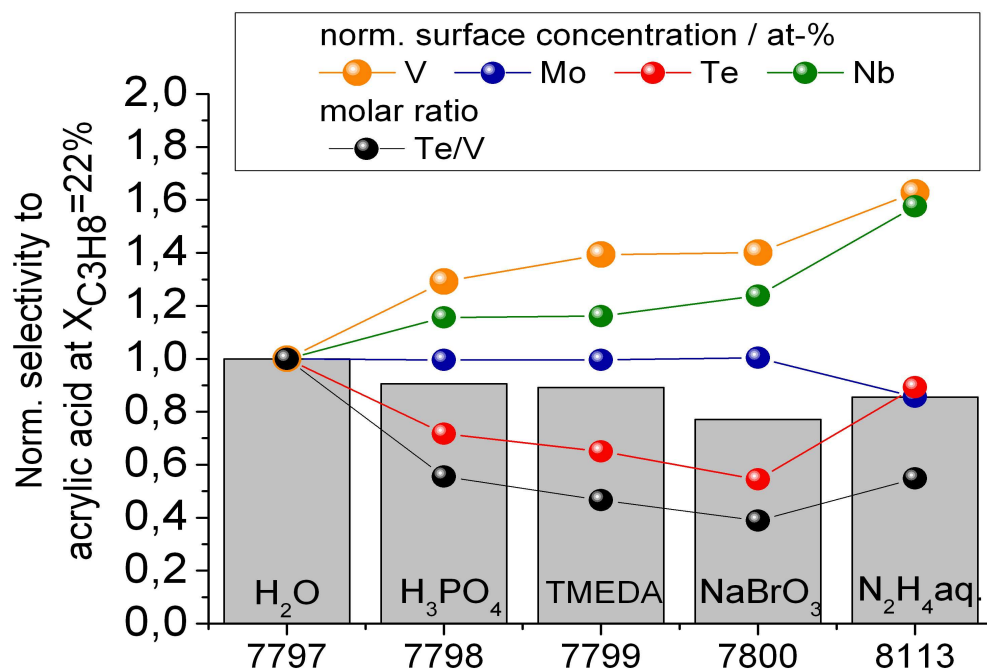


**Figure 5.3.4.** Normalized surface concentrations. Correlation of Te content and Te/V ratio with the normalized selectivity to acrylic acid (bar-graph).

For a correlation between the elemental composition and the elemental composition and the catalytic properties, the surface concentration of the constituents corresponding to every catalyst was normalized to the water treated sample #7797 (Figure 5.3.4). Similarly, the selectivity to acrylic acid determined at a propane conversion of  $22 \pm 2\%$  was normalized to the selectivity of the water treated sample. More detailed description about catalytic oxidation of propane can be found in the subchapter 5.4.1. A good correlation was found between the tellurium and the normalized selectivity. The same trend can be observed for between the tellurium to vanadium ratio and the normalized selectivity. This observation is in accordance with that reported by Hävecker et al. [15].

### 5.3.5. Microcalorimetry

Adsorption microcalorimetry was employed to determine the number, strength and energy distribution of the adsorption sites on the catalyst. Among the possible probe molecules applicable in microcalorimetry, propane and propylene were used to determine the adsorption heat of educt on the catalyst. On the other hand, CO and NH<sub>3</sub> probe molecules were applied in order to characterize the acid-base properties of the sample. The interaction of these latter molecules with the catalyst was monitored also by means of FTIR spectroscopy.

A detailed microcalorimetric experiment using propane and propylene as probe molecules was carried out on the original catalyst (#6059), the results serving as reference for the modified and spent catalysts. The term “spent catalyst” refers to a sample which has been used for catalytic reaction of propane and propylene oxidation. Since the aim of the study was to determine adsorption properties, the temperature was chosen low enough (40°C) to avoid chemical reaction on the catalyst surface.

The Figure 5.3.5 displays the adsorption isotherm and the differential heat of propane adsorption on the original material before and after catalytic reaction.

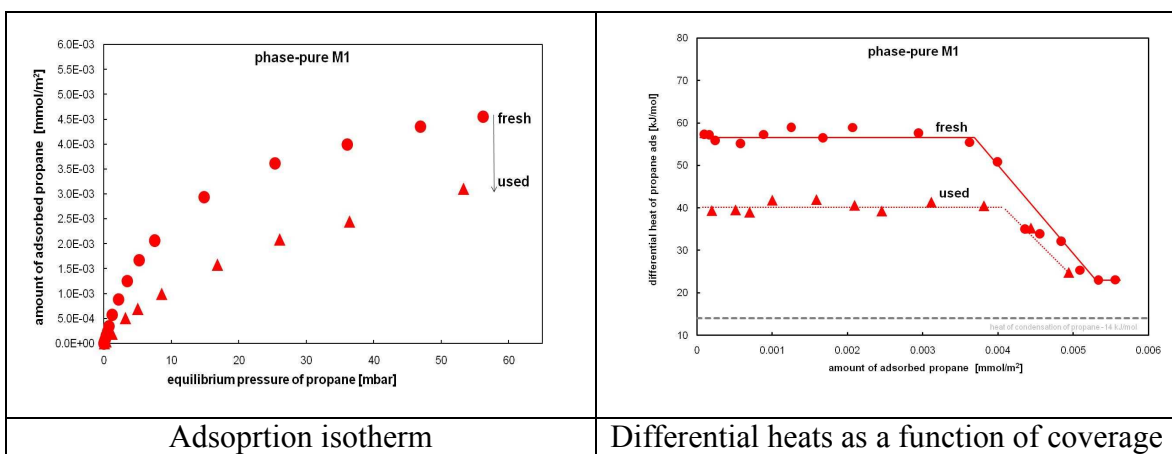


**Figure 5.3.5.** Adsorption of propane (educt of the catalytic reaction) at 313 K on fresh (dots) and used M1 (triangle) activated at 423 K under vacuum.

The adsorption isotherm was fitted with a Langmuir model. A fit up to 25 mbar equilibrium pressure corresponding to the monolayer coverage yielded an adsorption order of 1.06 on the fresh catalyst. The adsorption equilibrium constant was found to be

0.080. On the other hand, the amount of adsorbed propane on the spent catalyst is lower at every equilibrium pressure compared to the fresh catalyst. The Langmuir fit gave an adsorption order of 1.04. The adsorption order close to unity suggests non dissociative adsorption.

The initial differential heat of propane adsorption on the fresh M1 MoVTeNbO<sub>x</sub> is constant at approximately 57 kJ/mol. This indicates homogeneous distribution of energetically uniform adsorption sites. Additionally, FTIR spectroscopy of ammonia adsorption showed the presence of both Brønsted and Lewis acid sites. However the ratio between the Brønsted and Lewis acid sites was found to be equal to 2,34 [15].

The monolayer is completed at 3.5 μmol/m<sup>2</sup> propane coverage, corresponding to an equilibrium pressure of 25 mbar. Above this coverage, the differential heat of adsorption decreases linearly with the amount of adsorbed propane, suggesting the absence of interaction between adsorbed molecules. A saturation value of adsorption is reached at about 5.2 μmol/m<sup>2</sup> and 22 kJ/mol enthalpy.

Upon desorption of propane by evacuation at 40°C, the integral signal of desorption was recorded. The integration of this signal gave the integral heat of desorption. The absolute value of the sum of differential heat of adsorption is comparable to the integral heat of desorption (Table 5.3.4), indicating that the propane adsorption is a reversible process. Additionally, the individual differential adsorption signals did not deviate from the baseline, suggesting that the process is pure adsorption. The time constant of the stepwise adsorption was found to be close to the time constant determined in the calibration of the calorimetric cell (250-350 s). This also supports the absence of an additional process (e.g. chemical reaction) besides the adsorption.

A repeated experiment (re-adsorption after desorption, Table 5.3.4) showed that the isotherm and the differential adsorption heats are reproducible.

**Table 5.3.4.** Adsorption and desorption heats corresponding to different coverages.

Experiment	$\sum_{i=1}^n q_{i,\text{int}(\text{ads.})}$ (J)	$-q_{i,\text{int}(\text{des.})}$ (J)
Adsorption of 0,006 mmol/m <sup>2</sup> C <sub>3</sub> H <sub>8</sub>	7.89	6.56
Re-adsorption of 0,004 mmol/m <sup>2</sup> C <sub>3</sub> H <sub>8</sub>	1.56	1.53

The initial differential heat of propane adsorption was constant also on the spent #6059 catalyst, indicating homogeneous distribution of adsorption sites. Nevertheless, the initial differential adsorption heat determined for on the spent catalyst was lower compared to the fresh catalyst; it is only ca. 40 kJ/mol. Similarly to the fresh catalyst, the monolayer was completed at a coverage of 3.5  $\mu\text{mol}/\text{m}^2$  coverage on the spent catalyst as well. Since the monolayer coverage is the same like on the fresh catalyst, the number of adsorption sites does not change during catalytic reaction, but the strength of the interaction decreases by ca. 30%.

The linear decay of the differential heat of adsorption after completion of the monolayer suggests that there are no significant interaction forces between the adsorbed molecules. The reversibility of the propane adsorption on the spent catalyst was proven by the good agreement between the sum of integral heats corresponding to the individual adsorption steps and the integral heat of desorption.

The propylene adsorption isotherms and heat profiles determined at 40°C, corresponding to the fresh and spent #6059 catalyst are displayed on Figure 5.3.6. For comparison, the propane adsorption isotherms and heat profiles are also included in the plot.

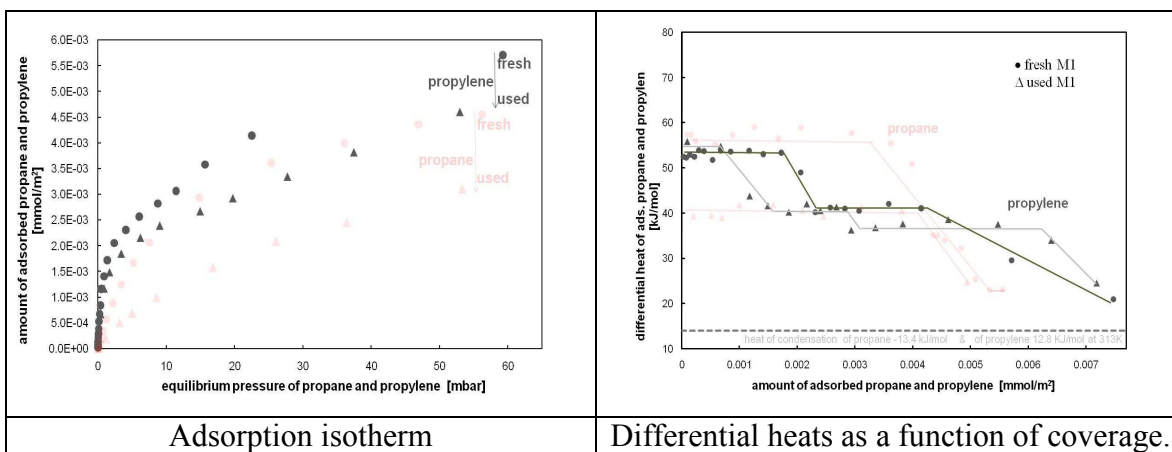


**Figure 5.3.6.** Adsorption of propylene at 313 K on fresh (dots) and used M1 (triangle) activated at 423 K under vacuum.

The propylene adsorption isotherms indicate that a larger amount of propylene can be adsorbed than propane on the fresh and used catalyst at the same equilibrium pressure.

Similarly to propane adsorption, the spent catalyst adsorbs a lower amount of propylene compared to the fresh catalyst.

The heat profile of propylene adsorption on fresh catalyst reflects the formation of two different adsorption complexes due to energetically different adsorption sites. Below the coverage of  $2 \mu\text{mol}/\text{m}^2$  the differential heats are constant at ca.  $54 \text{ kJ}/\text{mol}$ , which is comparable to the propane differential adsorption heat.

The second plateau on the heat profile is between  $2.5$  and  $4.2 \mu\text{mol}/\text{m}^2$ , where the differential adsorption heat is around  $41 \text{ kJ}/\text{mol}$ . Above the coverage of  $4.2 \mu\text{mol}/\text{m}^2$  the differential heat of propylene adsorption decays linearly, indicating no interaction between the adsorbed molecules.

Upon evacuation at  $40^\circ\text{C}$ , the signal corresponding to the propylene desorption was recorded. The integral desorption heat was found to be  $1.0 \text{ J}$ , while the sum of the individual integral heats was  $2.0 \text{ J}$ . The large difference between the adsorption and desorption heats suggests that the propylene adsorption is not a fully reversible process, in contrast to propane adsorption. On the other hand, the time constant was between  $400$  and  $550$  seconds for the low propylene coverage. This exceeds significantly the time constant of  $250$ - $350$  seconds determined for the empty calorimeter, indicating irreversible adsorption. Nevertheless at higher propylene coverage, the time constant of the adsorption was comparable to that determined for the empty calorimeter.

The partial irreversibility of propylene adsorption might be assigned to partial physical blockage of adsorption sites or irreversible changes of these sites. In order to find out which of these possibilities is the reason for the observed irreversibility, the adsorption properties were re-measured with propane as probe molecule.

After desorption of propylene from the fresh #6059 sample, propane was re-adsorbed at  $40^\circ\text{C}$ . The adsorption isotherm of propane re-adsorption performed after propylene adsorption-desorption cycle showed a very significant difference in comparison to the propane adsorption on the fresh #6059 sample (Figure 5.3.8). The amount of re-adsorbed propane was significantly lower at any equilibrium pressure, indicating that the number

of available adsorption sites was reduced during propylene adsorption-desorption experiment.

On the heat profile corresponding to the propane re-adsorption an initial plateau at 57 kJ/mol was observed.

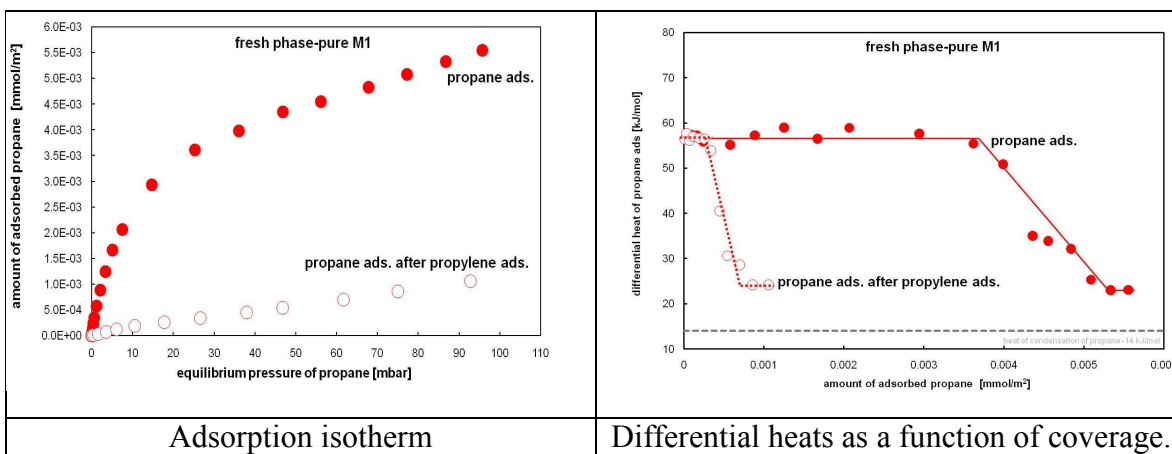


**Figure 5.3.7.** Adsorption of propane at 313 K after propylene adsorption on fresh (open dots) M1 activated at 423 K under vacuum. For comparison, the propane adsorption isotherm and differential heat profile if propane firstly adsorbed on the fresh M1 (dots).

This differential adsorption heat of propane is equal to the value determined on the fresh catalyst, suggesting that the energetics of propane adsorption is the same. The homogeneous distribution of the propane adsorption sites was not altered by the preceding propylene adsorption-desorption process. Nevertheless, the monolayer completion occurred already at around  $0.3 \mu\text{mol}/\text{m}^2$  coverage, indicating that the number of adsorption sites was reduced very significantly, by ca. 90% upon propylene adsorption-desorption. This confirms the observation made by comparing the adsorption isotherms shown on Figure 5.3.6.

The heat profile corresponding to propylene adsorption on the spent catalyst showed three plateaus, which is an indication of three groups of energetically equivalent adsorption sites. The initial differential adsorption heat determined up to  $1 \mu\text{mol}/\text{m}^2$  coverage is 55 kJ/mol. This is identical with the initial adsorption heat on the fresh sample, but also similar to the propane initial adsorption heat on the fresh sample. Between 1 and  $3 \mu\text{mol}/\text{m}^2$  coverage the propylene adsorption heat is 41 kJ, which is

equal to that determined for the fresh catalyst. The third group of energetically equivalent adsorption sites characterized by an adsorption heat of 37 kJ/mol can be observed between 3 and 6  $\mu\text{mol}/\text{m}^2$  coverage.

Propane adsorption experiment was carried out also on the fresh and spent bromate treated M1 sample (#7800). Compared to the original sample, the modified catalyst (#7800) adsorbed a lower amount of propane at any equilibrium pressure. The same trend could be observed upon comparing the adsorption isotherms of the spent original and spent bromate modified (#7800) samples (Figure 5.3.9).

On the heat profile the fresh bromate treated sample shows an initial linear decay of the differential heat of adsorption. The differential adsorption heat is constant at 33 kJ/mol, between 2.2 and 3.5  $\mu\text{mol}/\text{m}^2$  coverage. This plateau indicates the presence of Brønsted acid sites. After the decaying trend, a second plateau can be observed between 4 and 5  $\mu\text{mol}/\text{m}^2$  coverage.

FTIR study on ammonia adsorption supported the presence of both acid sites and revealed a ratio of Brønsted to Lewis acid sites equal to 2.29 [15]. This number is lower compared to that one determined on the original material (2.34), indicating that indeed, and the density of Lewis acid sites is increasing upon bromate treatment.

Additionally, the spent bromate treated sample showed a decaying heat profile with no plateau.

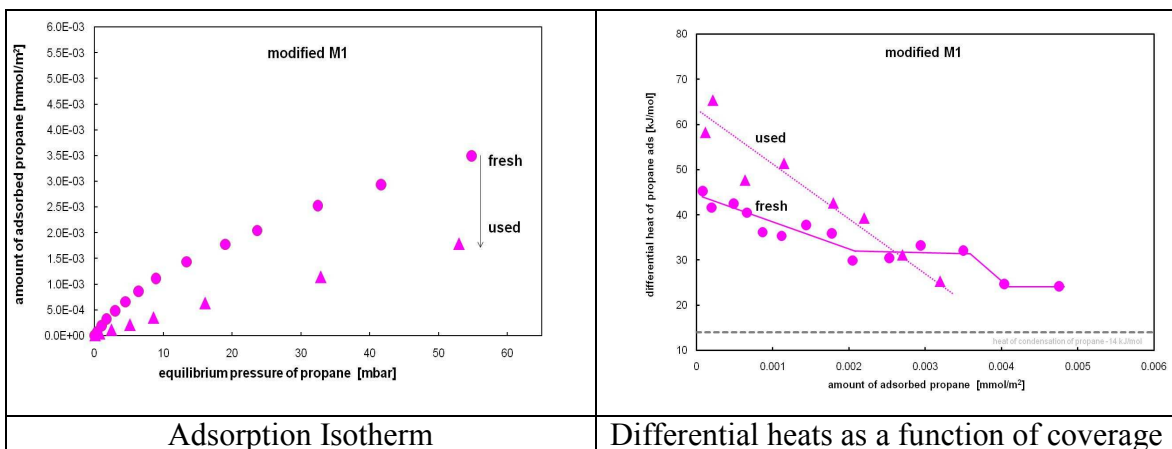


**Figure 5.3.8.** Microcalorimetry on the bromate-treated phase-pure M1 catalyst (#7800) before and after catalytic experiment.

The quantities of propane adsorption determined from the three-variable Langmuir fit (adsorption order  $n$ , monolayer coverage  $N_{\text{mono}}$  and the equilibrium constant of adsorption  $K$ ) are summarized in Table 5.3.5. The propane adsorption equilibrium constant decreases for both catalysts during the reaction.

The surface area available for propane adsorption was calculated based on the monolayer coverage, assuming one-to-one adsorption stoichiometry and propane cross sectional area of  $35,5\text{\AA}^2$ . The surface areas determined by propane and propylene adsorption are in good agreement with the surface area determined by nitrogen physisorption.

**Table 5.3.5.** The adsorption order, monolayer coverage and adsorption constant of propane adsorption for the #6059 and bromate treated sample (#7800).

Probe molecule	Catalyst state	Catalyst ID	$n$	$N_{\text{mono}}$ (mmol/g)	$K$ (hPa <sup>-1</sup> )	Surface area (m <sup>2</sup> /g)	
						Langmuir	BET
C <sub>3</sub> H <sub>8</sub>	Fresh	#6059	1.07(1)	0.0485(8)	0.078(3)	10.4	8.79
		#7800	1.28(4)	0.0561(1)	0.006(2)	13.2	5.04
	Spent	#6059	1.13(6)	0.048(7)	0.022(6)	11.4	n.d.
		#7800	0.99(8)	0.044(3)	0.005(4)	10.3	n.d.

Therefore, the main difference between the original and the bromate treated sample probed by adsorption microcalorimetry are the following:

- the fresh original catalyst exhibits homogeneously distributed energetically equivalent adsorption sites for propane adsorption, while upon bromate treatment energetic heterogeneity.
- the energetic homogeneity of the adsorption sites is conserved for the original material during the propane oxidation reaction, but the reaction induces reduction of the differential adsorption heat compared to the fresh catalyst. In contrast to this, the heat profile of the spent bromate treated material shows a high degree of heterogeneity, the Lewis/Brønsted acid site ratio changes as observed by FTIR study on ammonia adsorption.

## 5.4. Catalytic experiments

### 5.4.1. Propane oxidation

Prior to catalytic tests the samples were pressed with 1,5 tons of force for 1 minute in a pressing tool with 13 mm die. Then the pellet was crushed gently in an agate mortar. A sieve fraction between 250 and 355  $\mu\text{m}$  was used for catalytic experiments. An amount of ca. 0,24 g sieve fraction was mixed with SiC (particle size between 315 and 400  $\mu\text{m}$ ) and loaded in the isothermal zone of the reactor tube.

Constant feed composition was used ( $\text{C}_3\text{H}_8/\text{O}_2/\text{H}_2\text{O}/\text{N}_2=3/6/40/51$  vol%) while the space velocity was varied between 20000 and 3000  $\text{h}^{-1}$  at a reaction temperature of 400°C.

The propane conversion at different space velocities is shown in Figure 5.4.1. The activity of  $\text{H}_3\text{PO}_4$ -,  $\text{H}_2\text{O}$ - and TMEDA treated samples are slightly higher compared to the parent sample. However, the differences are becoming less significant in the integral operation mode, between 30 and 80% conversion. On the other hand, the activity of the bromate treated sample was significantly below the parent- and other modified samples.

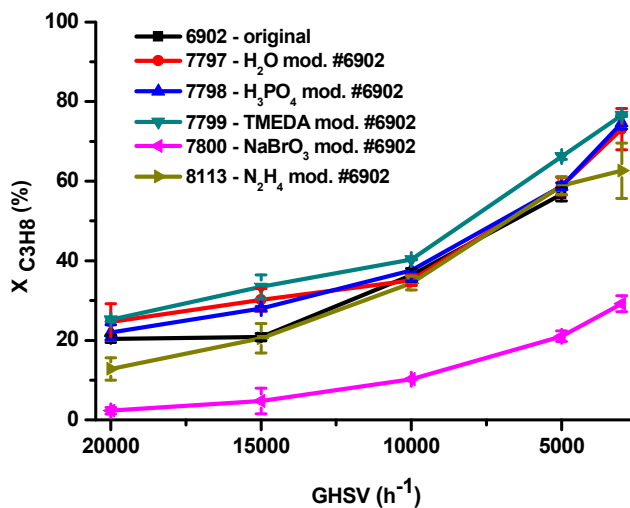


Figure 5.4.1. The activity of the catalysts.

The hydrazine treated sample showed lower activity at a space velocity compared to the parent sample. The activity becomes the same in the space velocity interval between 15000 and 5000  $\text{h}^{-1}$ . At  $\text{GHSV}=3000$   $\text{h}^{-1}$  the oxygen conversion reached 100% for this catalyst and consequently the propane conversion was lower compared to the other

catalysts. After performing the measurement at GHSV=3000 h<sup>-1</sup>, the catalytic properties were re-measured at a space velocity of 5000 h<sup>-1</sup>. These results are summarized in Table 5.4.1. The data show that the catalytic properties are reversible after performing the reaction under partly reducing conditions (100% oxygen conversion). This is in accordance with the observations reported in the subchapter 4.3.1. In case of all the other catalysts the highest oxygen conversion was ca. 95%. The selectivity to acrylic acid of all the catalysts is plotted against the space velocity (Figure 5.4.2, left). The highest selectivity was reached on the parent sample (#6902) at the space velocity of 10.000 h<sup>-1</sup>. Compared to this, the selectivity on H<sub>2</sub>O-, H<sub>3</sub>PO<sub>4</sub> and TMEDA are slightly lower, at space velocities above 10000 h<sup>-1</sup> and more significantly lower below GHSV=10000 h<sup>-1</sup>. The selectivity of the hydrazine and bromate treated samples is significantly below the parent sample.

**Table 5.4.1.** The catalytic performance of the hydrazine treated catalyst (#8113) compared before and after the complete oxygen conversion experiment.

<b>Catalytic Property</b>	<b>GHSV=5000 h<sup>-1</sup></b>	<b>GHSV=3000 h<sup>-1</sup></b>	<b>GHSV=5000 h<sup>-1</sup> remeasured</b>
X <sub>C<sub>3</sub>H<sub>8</sub></sub> (%)	58.9 ± 2.2	65.1 ± 6.1	58.9 ± 4.1
X <sub>O<sub>2</sub></sub> (%)	76.9 ± 2.2	100	77.8 ± 2.0
S <sub>AA</sub> (%)	31.4 ± 1.7	14.9 ± 2.1	27.9 ± 1.1
S <sub>CO<sub>2</sub></sub> (%)	28.6 ± 1.1	38.3 ± 1.7	29.2 ± 2.8
S <sub>C<sub>3</sub>H<sub>6</sub></sub> (%)	4.7 ± 0.4	3.4 ± 0.4	5.5 ± 0.5
S <sub>HAc</sub> (%)	8.8 ± 0.6	10.0 ± 1.3	12.0 ± 1.6
S <sub>CO</sub> (%)	26.5 ± 1.0	33.5 ± 1.5	27.8 ± 2.3
C-bal. (%)	79.0 ± 1.1	90.8 ± 10.6	82.9 ± 4.0

The yield to acrylic acid at every space velocity is shown in Figure 5.4.2 (right). The maximum yield of ca. 26% has been attained on the parent sample and the TMEDA treated sample at the space velocity of 5000 h<sup>-1</sup>. For the H<sub>2</sub>O-, H<sub>3</sub>PO<sub>4</sub> and N<sub>2</sub>H<sub>4</sub> modified samples the maximum yield of ca. 20% was also at the space velocity of 5000 h<sup>-1</sup>. This suggests that the kinetics of the reaction might be similar on these catalysts, though the rate constants may differ slightly.

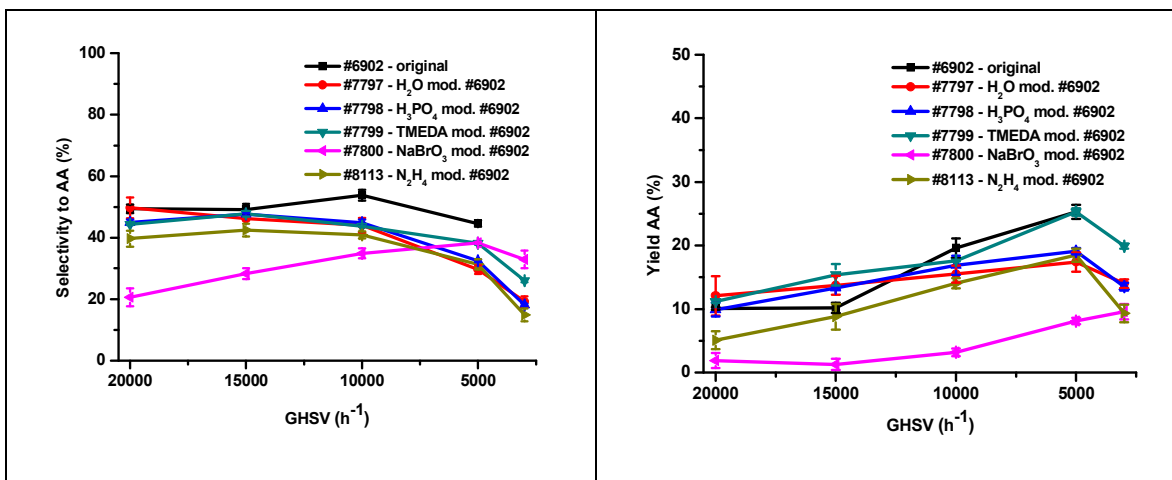


Figure 5.4.2. The selectivity and yield of the catalysts.

The conversion, selectivity and yield profile of the bromate treated sample however differs very much from all the other catalysts, which suggests that the kinetics of propane oxidation is significantly different.

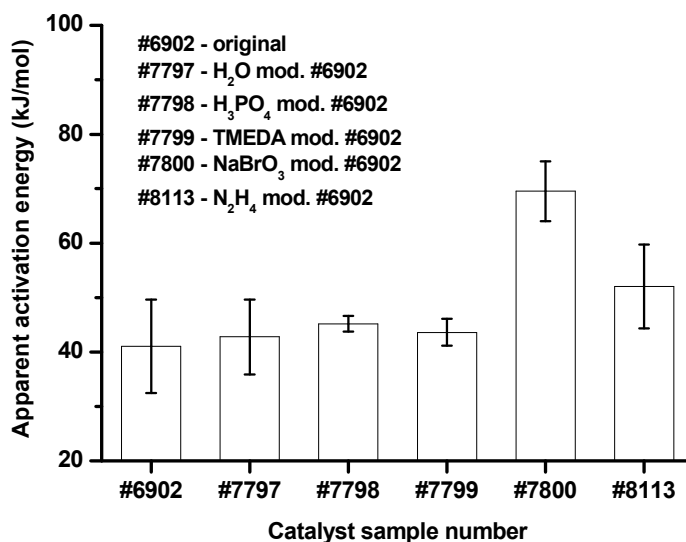


Figure 5.4.3. The apparent activation energy of propane activation over the catalysts.

The temperature variation in 20°C steps between 360 and 400°C was carried out at a space velocity of 5000 h<sup>-1</sup>. The apparent activation energy of propane consumption has been determined from the Arrhenius plots. Similar activation energies have been found for the parent sample and the H<sub>2</sub>O-, H<sub>3</sub>PO<sub>4</sub>-, TMEDA and N<sub>2</sub>H<sub>4</sub> treated samples.

However, the apparent activation energy of propane on the bromate and hydrazine treated sample was significantly higher than for the other samples.

#### 5.4.2. Kinetic analysis of propane oxidation over the modified catalysts

The primary analysis of the activity and selectivity to acrylic acid on different catalysts showed that only the bromate and the hydrazine treated samples are behaving different in propane oxidation reaction. The product rank analysis revealed that the reaction pathways are also different, although in every case the catalyst was M1 MoVTenbO<sub>x</sub> with slightly different surface and bulk elemental composition (Appendix 5.1). In this subchapter the kinetic analysis of propane oxidation is presented.

In section 4.2.3 and 4.2.4 it is shown that the reaction is first order with respect to propane and 0.5<sup>th</sup> order with respect to oxygen. Prior to kinetic modeling, the verification of first order kinetics with respect to propane and half-order kinetics with respect to oxygen was verified using the integral method [16-17]. For this purpose the integrated rate laws were considered (Equations 5.4.1 and 5.4.2).

$$\ln \frac{c_{C_3H_8}}{c_{C_3H_8,0}} = \ln y_{C_3H_8} = -k_{app,C_3H_8} \cdot \tau \quad (\text{Equation 5.4.1})$$

$$c_{O_2}^{0.5} = c_{O_2,0}^{0.5} + 2 \cdot k_{app,O_2} \cdot \tau \quad (\text{Equation 5.4.2})$$

The logarithm of the dimensionless propane concentration was plotted against the contact time, leading to straight lines. This indicates that on every catalyst the reaction order with respect of propane is equal to one. According to the integrated rate law corresponding to oxygen, the square root of the oxygen concentration was represented in function of the contact time. No curvature was observed on the plots, which supports that the reaction order with respect to oxygen is 0.5 for all the catalysts.

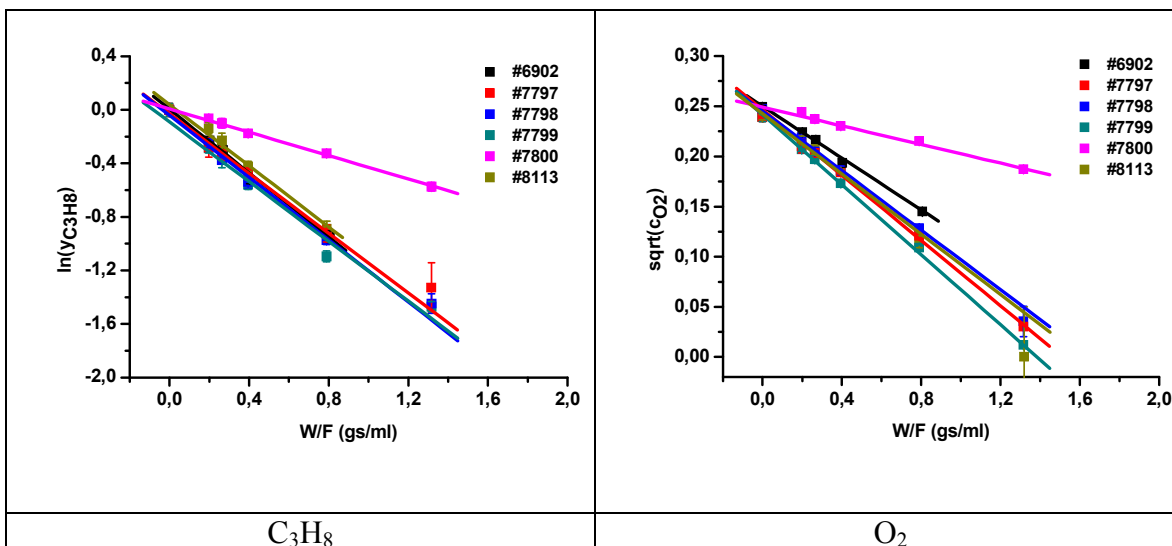


**Figure 5.4.4.** The linear representation of the rate law with respect to propane and oxygen. #6902 – original, #7797 – H<sub>2</sub>O modified, #7798 – H<sub>3</sub>PO<sub>4</sub> modified, #7799 – TMEDA modified, #7800 – NaBrO<sub>3</sub> modified, #8113 – N<sub>2</sub>H<sub>4</sub> modified sample.

The slopes of the linear regressions are collected in the Table 5.4.3. These slopes correspond to the apparent rate constants of propane and oxygen consumption, respectively. The apparent rate constant of propane activation is very similar for all the catalysts, except for the bromate treated sample, which is less active by a factor of 2.7 compared to the parent sample.

**Table 5.4.2.** The apparent rate constants of propane and oxygen consumption.

Catalyst	C <sub>3</sub> H <sub>8</sub>		O <sub>2</sub>	
	-slope (ml/g)	R/N	-slope (ml/g)	R/N
#6902	1.19 ± 0.05	-0.9973 / 5	0.72 ± 0,01	-0.9999 / 5
#7797	1.12 ± 0.09	-0.9955 / 5	0.68 ± 0,01	-0.9993 / 5
#7798	1.16 ± 0.04	-0.9945 / 5	0.60 ± 0,01	-0.9995 / 5
#7799	1.12 ± 0.04	-0.9854 / 5	0.74 ± 0,01	-0.9998 / 5
#7800	0.44 ± 0.02	-0.9971 / 5	0.19 ± 0,01	-0.9901 / 5
#8113	1.14 ± 0.02	-0.9923 / 4	0.80 ± 0,05	-0.9989 / 5

Propylene was found to be an intermediate product. The reaction pathways involving propylene was approximated by the following scheme:



The rate constant of propylene formation is  $k_1$ , while the cumulative rate constant of propylene further oxidation is  $k_2$ . The differential equations corresponding to this scheme are the following:

$$-\frac{dc_{C_3H_8}}{dt} = k_1 \cdot c_{C_3H_8} \quad (\text{Equation 5.4.3})$$

$$\frac{dc_{C_3H_6}}{dt} = k_1 \cdot c_{C_3H_8} - k_2 \cdot c_{C_3H_6} \quad (\text{Equation 5.4.4})$$

By dividing the above two differential equations, the derivative of time ( $dt$  term) is cancelled and resulting differential equation contains only concentrations (Equation 5.4.5). Solving this differential equation leads to the equation involving the dimensionless concentrations of propane and propylene and the dimensionless ratio of the rate constants ( $\kappa=k_2/k_1$ ) (Equations 5.4.6 and 5.4.7).

$$\frac{dc_{C_3H_6}}{dc_{C_3H_8}} = \frac{k_1 \cdot c_{C_3H_8} - k_2 \cdot c_{C_3H_6}}{-k_1 \cdot c_{C_3H_8}} \quad (\text{Equation 5.4.5})$$

$$\frac{c_{C_3H_6}}{c_{C_3H_8,0}} = \frac{k_1}{k_2 - k_1} \cdot \left[ \frac{c_{C_3H_8}}{c_{C_3H_8,0}} - \left( \frac{c_{C_3H_8}}{c_{C_3H_8,0}} \right)^{\frac{k_2}{k_1}} \right] \quad (\text{Equation 5.4.6})$$

$$y_{C_3H_6} = \frac{1}{\kappa - 1} \cdot [y_{C_3H_8} - y_{C_3H_8}^\kappa] \quad (\text{Equation 5.4.7})$$

$$S = \sqrt{\frac{\sum_{i=1}^n (y_{C_3H_6, \text{exp}} - y_{C_3H_6, \text{calcd}})^2}{n}} \quad (\text{Equation 5.4.8})$$

Iterative nonlinear fitting procedure was employed for the determination of the dimensionless rate constant (Figure 5.4.5). A plausible value of  $\kappa$  was chosen, and then the value of  $y_{C_3H_6}$  was calculated. For the objective function of the fitting the standard deviation between the measured and calculated propylene dimensionless concentration has been considered (Equation 5.4.8). The iteration was continued until the minimum of the objective function was found ( $dS/d\kappa=0$ ) (Figure 5.4.5, right).

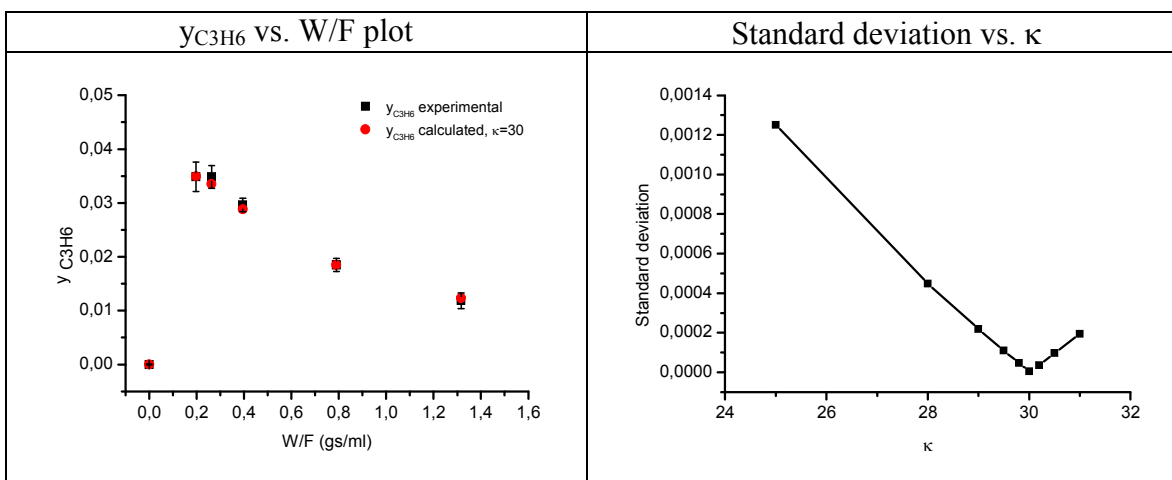


Figure 5.4.5. Plot of the experimental with calculated  $y_{C_3H_6}$  data for catalyst #6902.

The dimensionless rate constant  $\kappa$  for each catalyst was determined using the above described procedure. The numerical values are collected in Table 5.4.3.

Table 5.4.3. The rate constants of propane and propylene consumption.

Catalyst ID	$k_1$ (ml/gs)	$\kappa$	$k_2$ (ml/gs)	$\tau_{max}$ (gs/ml)
#6902	1.19	30.0	35.70	0.10
#7797	1.12	22.5	25.20	0.13
#7798	1.16	23.4	27.14	0.12
#7799	1.12	22.5	25.20	0.13
#7800	0.44	23.2	10.21	0.32
#8113	1.14	22.0	25.08	0.13

The  $\kappa$  values may be compared to literature results.

Griβtede reported a propane consumption rate constant of 0.84 gs/ml, a propylene partial oxidation rate constant to acrylic acid equal to 17 gs/ml and a rate constant of 3.4 gs/ml towards byproducts (CO, CO<sub>2</sub> and acetic acid) formation on a MoV<sub>0.33</sub>Te<sub>0.25</sub>Nb<sub>0.17</sub>O<sub>x</sub> catalyst [12, 18]. The global consumption rate of propylene is therefore 20.4 gs/ml. The ratio of propylene consumption and propane consumption rate is 20.4/0.84=24.3.

López-Nieto et al. reported a value of ca. 24 on a predominantly M1 phase containing MoVTeNbO<sub>x</sub> catalyst [19].

Naraschewski et al. reported a value of 25 for MoVTaNbO<sub>x</sub> catalysts with ten different elemental- and phase compositions [20]. However the fitting was made in case of one of the catalyst, the  $\kappa$  value for each catalyst was not quantified.

From the  $\kappa$  and the  $k_1$  data, the  $k_2$  was also calculated and shown in the Table 5.4.4.

Additionally, the contact time corresponding to the maximum propylene concentration was also calculated (Table 5.4.3).

$$\tau_{\max} = \frac{1}{k_2 - k_1} \ln \frac{k_2}{k_1} = \frac{1}{k_1(\kappa - 1)} \ln \kappa \quad (\text{Equation 5.4.9})$$

It can be seen that the maximum propylene concentration is at around 0.12 gs/ml for most of the catalysts. This low contact time was not covered in the experiments. On the bromate treated sample (#7800) the calculated  $\tau_{\max}$  is equal to 0.32, while the experimental value lies around 0.33, which is in good agreement with the calculated one.

### 5.4.3. Propylene oxidation

Catalytic testing in propylene oxidation reaction has also been carried out using the parent sample and all the modified descendant catalysts.

The feed composition was the following: C<sub>3</sub>H<sub>6</sub>/O<sub>2</sub>/H<sub>2</sub>O/N<sub>2</sub>=3/6/40/51 vol%. According to the reasoning in section 4.2.5, the temperature interval between 360-400°C was chosen, which corresponds to the temperature interval for the propane oxidation. The space velocity was kept at 20000 h<sup>-1</sup> in order to achieve propylene conversions below 100%.

The ranking order of the catalysts in the activity of propylene activity resembles the activity in propane oxidation: the tetramethylethylenediamine treated sample showed the highest activity, followed by the original, the water-, the phosphoric acid, hydrazine and the bromate treated samples. Similarly to the propane oxidation reaction, the propylene conversion was also significantly lower on the bromate treated sample, compared to the other catalysts.

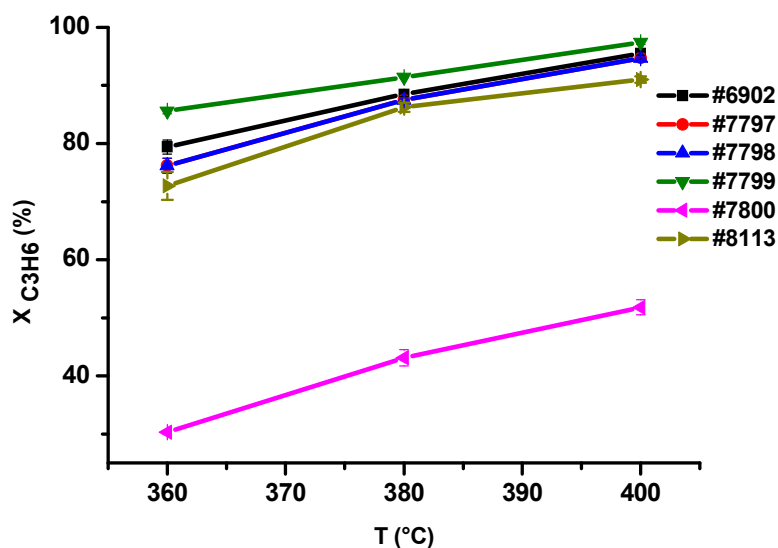


**Figure 5.4.6.** The activity of the catalysts in propane oxidation reaction. #6902 – original, #7797 – H<sub>2</sub>O modified, #7798 – H<sub>3</sub>PO<sub>4</sub> modified, #7799 – TMEDA modified, #7800 – NaBrO<sub>3</sub> modified, #8113 – N<sub>2</sub>H<sub>4</sub> modified sample.

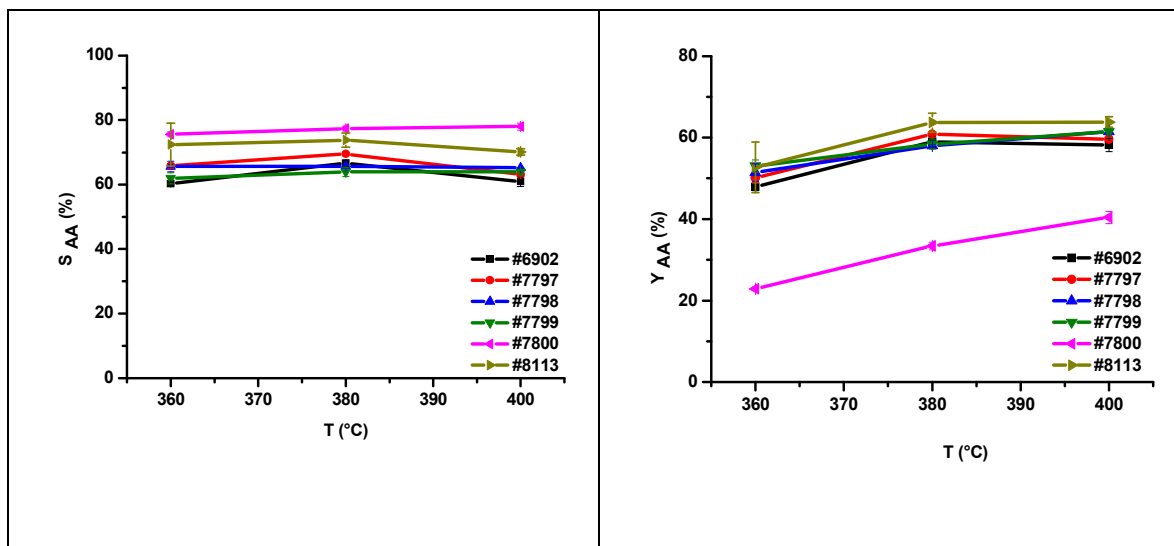


**Figure 5.4.7.** The selectivity and yield of the catalysts in propane oxidation reaction. #6902 – original, #7797 – H<sub>2</sub>O modified, #7798 – H<sub>3</sub>PO<sub>4</sub> modified, #7799 – TMEDA modified, #7800 – NaBrO<sub>3</sub> modified, #8113 – N<sub>2</sub>H<sub>4</sub> modified sample.

The acrylic acid selectivity was found to be the highest on the bromate treated sample followed by the hydrazine treated sample (Figure 5.4.7). The higher selectivity, however, may be attributed to the fact that these catalysts are less active than the others. The

acrylic acid selectivity on other catalysts was lower and similar to each other, with a maximum at 380°C.

When the the acrylic acid yield is compared, the highest performing catalyst is hydrazine treated sample. All the other catalysts show a similar yield at every temperature, except for the bromate treated sample, which has the lowest performance (Figure 5.4.7).

It is notable, that the ratio between the CO and CO<sub>2</sub> selectivity is higher than one for the parent-, H<sub>2</sub>O-, TMEDA- and treated samples, while for the H<sub>3</sub>PO<sub>4</sub>- NaBrO<sub>3</sub> and N<sub>2</sub>H<sub>4</sub>- treated samples this ratio is statistically close to one.

#### 5.4.4. CO oxidation and water gas shift reaction

CO oxidation reaction as a test reaction for electrophilic oxygen species on the catalyst surface was also performed [21]. The reaction was carried out in dry and in 40vol% steam containing feed. Besides this, water gas shift reaction was also carried out using a 40 vol% steam containing feed. The same experimental procedure was applied as it was described in the section 4.2.7.

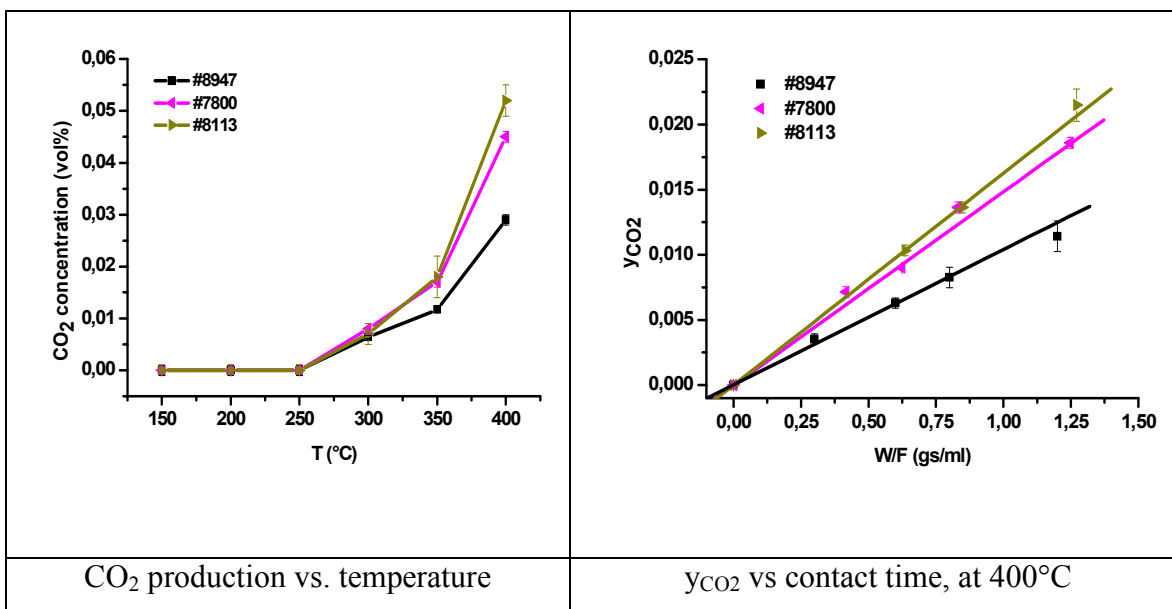


**Figure 5.4.8.** The CO oxidation activity at different temperatures and GHSV=3000 h<sup>-1</sup> (left). The kinetic curves of CO<sub>2</sub> formation at 400°C (right). Conditions: CO/O<sub>2</sub>/H<sub>2</sub>O/N<sub>2</sub>=3/6/0/91 vol%. Catalysts: #8947 – as prepared M1 MoVTeNbO<sub>x</sub>, #7800 – NaBrO<sub>3</sub> treated #6902, #8113 – N<sub>2</sub>H<sub>4</sub> treated #6902.

CO oxidation carried out in steam free oxidizing feed (GHSV=3000h<sup>-1</sup>) at different temperatures revealed that for all the catalysts the onset temperature is between 250 and 300°C. The ranking order in CO oxidation activity at 400°C is the following: hydrazine treated sample (#8113), the bromate treated material (#7800) and original sample (#8947). Therefore the abundance of electrophilic oxygen species is decreasing in this order of the catalysts [26]. It is also notable that the CO conversion was far below the equilibrium conversion for both the CO oxidation and water gas shift reactions (100% and 99.6%, respectively) calculated from the thermodynamic data of CO, CO<sub>2</sub>, H<sub>2</sub> and H<sub>2</sub>O (Table 5.4.5).

**Table 5.4.4.** Activation energy of CO oxidation. Feed composition: CO/O<sub>2</sub>/H<sub>2</sub>O/N<sub>2</sub>=3/6/0/91 vol%, #8947 – as prepared M1 MoVTeNbO<sub>x</sub>, #7800 – NaBrO<sub>3</sub> treated #6902, #8113 – N<sub>2</sub>H<sub>4</sub> treated #6902.

Catalyst ID	E <sub>a</sub> (kJ/mol)
#8947	51 ± 2
#7800	55 ± 7
#8113	54 ± 7

Because the CO conversion is very low (below 3%), all the data are in the differential operation regime. Therefore the rate constant of CO<sub>2</sub> formation is equal to the slope of the straight line of the dimensionless concentration of CO<sub>2</sub> represented in function of the contact time (Figure 5.4.8 and 5.4.9). Since there is no other product than CO<sub>2</sub>, the rate and rate constant of CO consumption is equal to the rate and rate constant of CO<sub>2</sub> formation. The activation energy of CO oxidation determined from the Arrhenius-plot is statistically similar on the three catalysts (Table 5.4.4).

In case of all the three catalysts, the water gas shift reaction had the lowest conversion and rate constant, followed by the CO oxidation in dry feed (Table 5.4.5 and 5.4.6). The highest CO conversion was observed in the case of CO oxidation in presence of 40 vol% steam in the feed. This suggests that CO oxidation and water gas shift reactions are parallel reaction steps. However, it is notable that the CO oxidation activity in presence of 40 vol% steam is less than the algebraic sum of the CO conversions determined in the CO oxidation in dry feed and the water gas shift reaction in presence of 40 vol% steam.

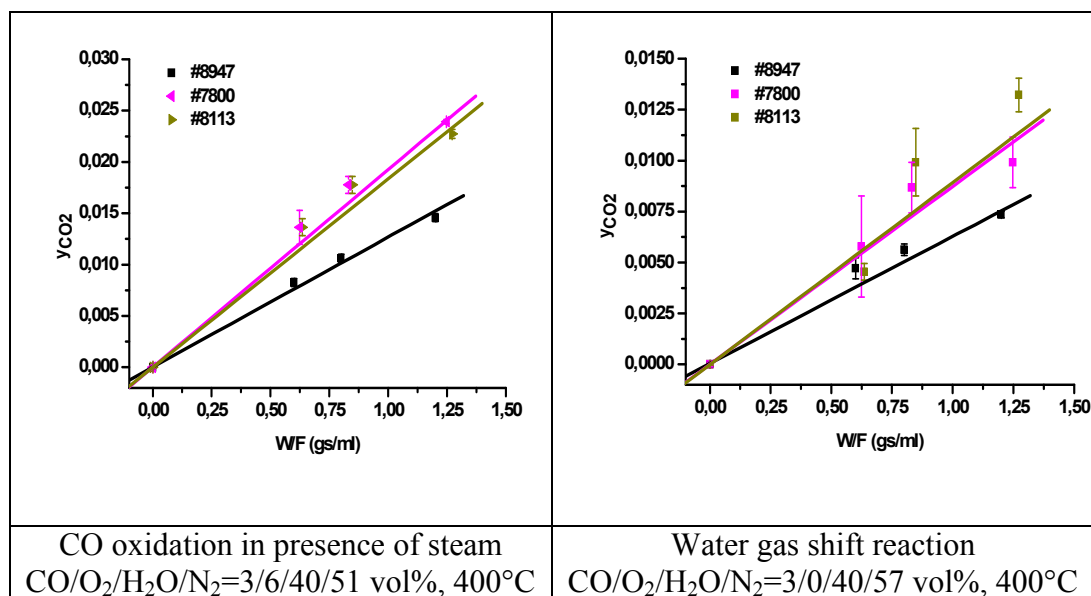


**Figure 5.4.9.** Kinetic curves for CO<sub>2</sub> formation for the CO oxidation in presence of steam and for the water gas shift reactions. Catalysts: #6902 – as prepared M1 MoVTenbO<sub>x</sub>, #7800 – NaBrO<sub>3</sub> treated sample, #8113 – N<sub>2</sub>H<sub>4</sub> treated sample.

**Table 5.4.5.** The CO conversion at GHSV=3000 h<sup>-1</sup> and 400°C.

Catalyst ID.	X <sub>CO</sub> (%) CO oxidation CO/O <sub>2</sub> /H <sub>2</sub> O/N <sub>2</sub> = 3/6/0/91 vol%	X <sub>CO</sub> (%) CO oxidation CO/O <sub>2</sub> /H <sub>2</sub> O/N <sub>2</sub> = 3/6/40/51 vol%	X <sub>CO</sub> (%) water gas shift CO/O <sub>2</sub> /H <sub>2</sub> O/N <sub>2</sub> = 3/0/40/57 vol%
#8947	1.14±0.12	1.46±0.04	0.74±0.04
#7800	1.86±0.04	2.39±0.02	0.99±0.12
#8113	2.15±0.12	2.27±0.04	1.32±0.08
Equilibrium	100	100	99.6

The rate constant of CO oxidation or water gas shift reaction was found to be very low, in the order of magnitude of 10<sup>-2</sup> ml/g.s. The same trends of the rate constant with respect of the catalyst and the feed composition can be observed like in the activity expressed by CO conversion (Table 5.4.6). The difference between the rate constant of CO oxidation in dry feed and the sum of the rate constants CO oxidation in dry feed and the water gas shift reaction suggests that these reactions may run in parallel, but their contribution is not the same.

**Table 5.4.6.** Rate constants of CO<sub>2</sub> formation at 400°C.

Catalyst ID.	k <sub>CO2</sub> (ml/g.s) CO oxidation CO/O <sub>2</sub> /H <sub>2</sub> O/N <sub>2</sub> = 3/6/0/91 vol%	k <sub>CO2</sub> (ml/g.s) CO oxidation CO/O <sub>2</sub> /H <sub>2</sub> O/N <sub>2</sub> = 3/6/40/51 vol%	k <sub>CO2</sub> (ml/g.s) water gas shift CO/O <sub>2</sub> /H <sub>2</sub> O/N <sub>2</sub> = 3/0/40/57 vol%
#8947	$(10.4 \pm 0.4) \cdot 10^{-3}$	$(12.7 \pm 0.3) \cdot 10^{-3}$	$(6.2 \pm 0.2) \cdot 10^{-3}$
#7800	$(14.8 \pm 0.2) \cdot 10^{-3}$	$(19.2 \pm 0.2) \cdot 10^{-3}$	$(8.7 \pm 0.8) \cdot 10^{-3}$
#8113	$(16.4 \pm 0.4) \cdot 10^{-3}$	$(18.4 \pm 0.3) \cdot 10^{-3}$	$(8.9 \pm 0.5) \cdot 10^{-3}$

The very low reactivity in CO oxidation and water gas shift reaction supports the fact that during the propane oxidation, the CO<sub>2</sub> is formed in reaction steps which are independent on the CO formation steps.

## 5.5. Conclusions

The chemical treatment of the phase-pure MoVTeNbO<sub>x</sub> catalyst (referred to as parent or original sample) with distilled water and solutions of phosphoric acid, tetramethylethylenediamin, sodium-bromate and hydrazine was carried out at room temperature. The solutions were chosen in such a way to cover all the chemical effects: neutral, acidic and complexing, basic and complexing, oxidizing and reducing. None of these treatments altered the M1 phase, as probed by XRD. The surface area was only marginally affected by the treatment, as shown by N<sub>2</sub> physisorption.

The morphology did not change significantly upon water treatment of the M1 material. However the treatment by all other solutions changed more significantly the shape of the particles and the aspect ratio. In contrast to the literature evidence [4], not only the surface composition, but also the bulk elemental composition was slightly affected by chemical treatments with different solutions. Nevertheless, the M1 phase was kept intact, which showed that the crystal structure is robust enough to withstand minor changes in the elemental composition upon leaching with the above mentioned solutions. Besides leaching of ions, the oxidation of V<sup>4+</sup> to V<sup>5+</sup> during bromate treatment was also observed. No detectable change of the oxidation states has been observed for the other modified catalysts.

All the modified samples were tested for propane and propylene oxidation reaction. Only marginal improvements were observed in the propane conversion for the H<sub>2</sub>O-, H<sub>3</sub>PO<sub>4</sub> and the TMEDA-treated samples, accompanied by a slight decrease in the acrylic acid

selectivity. On the other hand, the hydrazine treatment reduced slightly, while the bromate treatment reduces significantly both the conversion and the acrylic acid selectivity at any space velocity. For these two latter catalysts the apparent activation energy was found to be higher than for all the other samples. The reaction pathway analysis using the delplot technique revealed that propylene is a first rank product in every case. The acrylic acid, CO, CO<sub>2</sub> and acetic acid were found to be mixed rank products (including primary, secondary and tertiary ranks, the main rank being secondary). The only exception is the hydrazine treated sample, on which all products were found to be of first rank. This sample is the only one which exhibited CO/CO<sub>2</sub> selectivity ratio smaller than one.

The first order kinetics with respect to propane and half order kinetics with respect to oxygen was conserved in all the modified catalysts. The ratio of propylene formation and its further consumption is the highest ( $\kappa=30$ ) for the parent sample. This ratio is lower for the modified catalysts, the lowest value of 22 being determined for the hydrazine treated sample.

The ranking order for catalytic performance of propylene oxidation resembles to the trend observed in propane oxidation.

CO oxidation reaction was carried out on selected catalysts, as a semi-quantitative indicator-reaction for electrophilic oxygen species. The semi-quantitative character of this test reaction is derived from the fact that no standards were used with known abundance of electrophilic oxygen species on the surface, but rather the parent sample was used as a reference catalyst. The CO oxidation activity of the bromate and hydrazine treated samples were determined, because these showed markedly different catalytic behavior both in propane and propylene oxidation reactions. The ranking order in CO oxidation activity showed that the hydrazine treated sample exhibits the highest abundance of electrophilic oxygen species, followed by the bromate treated sample and the original catalyst.

Furthermore, water gas shift reaction and CO oxidation in presence of steam was also carried out on these catalysts. The CO conversion was found to be below 2.5% at the space velocity of 3000 h<sup>-1</sup> and a reaction temperature of 400 °C. The low rate of CO<sub>2</sub> production indicated that under propane oxidation conditions the CO oxidation and water

gas shift reactions are negligible. Therefore, this experiment proved that CO and CO<sub>2</sub> byproducts are formed independently on each other, in different pathways.

The XRD patterns of the samples after propane and propylene oxidation reaction showed that there was no phase change, re-confirming the robustness of the M1 phase under propane and propylene oxidation reaction conditions.

## References Chapter 5

1. Japanese Laid-Open Patent Application No. 10-330343
2. L. E. Bogdan, European Patent 1254707 A1, assigned to Rohm and Haas Company, 2002
- 3.
4. L.E. Bogdan, D. A. Bors, F. A. Pessoa Cavalcanti, M. Bruce Clark, A. M. Gaffney, S. Han US Patent 7326668 B2, assigned to Rohm and Haas Company
5. V. V. Guliants, R. Bhandari, B. Swaminathan, V. K. Vasudevan, H. H. Brongersma, A. Knoester, A. M. Gaffney, S. Han, *J. Phys. Chem. B*, 109 (2005) 24046-24055
6. M. Baca, J. M. M. Millet, *Appl. Catal. A: General*, 279 (2005) 67-77
7. Yu. V. Kolen'ko, T. Wolfram, F. Girgsdies, W. Zhang, T. W. Hansen, D. Su, A. Trunschke, R. Schlögl, *Chem. Cat. Comm.*, accepted for publication
8. I. H. Warren, D.C. Reid, *Chemistry and materials science, Metallurgical and materials transaction B*, Vol. 13, No. 4, 565-570
9. D. Langmuir, P. Chrostowski, R. Chaney, B. Vigneault, Issue Paper on the environmental chemistry of metals, U.S. Environmental Protection Agency, August 2003
10. E. Asselin, T. M. Ahmed, A. Alfantazi, *Corrosion Science*, 49, 2, (2007) 694-710
11. M. Bouroushian, *Electrochemistry of metal chalcogenides, Monographs in Electrochemistry*, (Ed. F. Scholz), Springer 2010, Page 65-69
12. P. DeSanto, D.J. Buttrey, R.K. Grasselli, C.G. Lugmair, A.F. Volpe, B.H. Toby, T. Vogt, *Z. Krist.*, 219 (2004) 152-165
13. I. Grißtede, *Die Partielle Oxidation von Propan zu Acrylsäure, Bestimmung der Reaktionskinetik und in-situ charakterisierung des Katalysators unter Betriebsbedingungen*, Dissertation, Universität Karlsruhe, 2004, Universitätsverlag Karlsruhe, ISBN 3-937300-17-1
14. J. F. Moulder, W. F. Strickle, P. E. Sobol, K. D. Bomben, *Handbook of XPS spectroscopy*, Perkin-Elmer, USA, 1992
15. A. Celaya Sanfiz, T. W. Hansen, D. Teschner, P. Schnörch, F. Girgsdies, A. Trunschke, R. Schlögl, M. H. Looi, S. B. A. Hamid, *Journal of Physical Chemistry C*, 114 (2010) 1912
16. M. Hävecker, S. Wrabetz, J. Kröhnert, L.I. Csepei, R. Naumann d'Alnoncourt, Yu. V. Kolen'ko, F. Girgsdies, R. Schlögl, A. Trunschke, *J. Catal.*, submitted
17. Ch. G. Hill, *An introduction to chemical reaction engineering, kinetics and reactor design*, John Wiley and Sons, 1977, 24-74

18. R. W. Missen, Ch. A. Mims, B. A. Saville, Introduction to chemical reaction engineering and kinetics, John Wiley and Sons, 1999, 49-55
19. E. Balcells, F. Borgmeier, I. Grißtede, H. G. Lintz, F. Rosowski, Appl. Catal. A: General, 266 (2004) 211
20. J. M. López-Nieto, B. Solsona, P. Concepción, F. Ivars, A. Dejoz, M. I. Vázquez, Catal. Today, 157 (2010) 291-296
21. F. N. Naraschewski, C. P. Kumar, A. Jentys, J. A. Lercher, Appl. Catal. A: General, 391, 1-2 (2011) 63-69
22. J. Hermann, Catal. Today, 2006 (112) 73-77

## Chapter 6. Exploratory experiments

### 6.1. Introduction

In the literature many catalyst systems are reported for the selective oxidation of propane to acrylic acid. These can be classified into heteropolyacids and their salts, phosphates and molybdenum based mixed oxides [1, 2]. A strict delimitation between these classes can not be made, because under reaction conditions, the heteropolyacids may transform into oxides or phosphates [3]. In general, the performance of catalysts belonging to the first two classes is rather poor. Ai reported that an acid yield of ca. 12 mol%  $V_2O_5$ - $P_2O_5$  with a P/V ratio equal to 1,00, while the yield decreased strongly with increasing P/V ratio.

Upon incorporation of  $H_3PMo_{12}O_{40}$  heteropoly acid and Te in the  $V_2O_5$ - $P_2O_5$  the yield could be increased. The addition of  $SO_3$  barely had any effect, while in presence of  $H_3PW_{12}O_{40}$ ,  $Nb_2O_5$ ,  $Sb_2O_3$ ,  $SiO_2$  and  $B_2O_3$  the yield decreased significantly [4, 5].

The most prominent catalysts are the molybdenum and vanadium based mixed oxides. Katou et al. reported the hydrothermal synthesis of orthorhombic and amorphous  $MoVO_x$  and  $MoVTeO_x$  catalysts with surface areas up to  $10\text{ m}^2/\text{g}$  [6]. The catalytic experiments were carried out in the narrow temperature interval between 343 and 354 °C. A rather reducing feed with the composition of  $C_3H_8/O_2/H_2O/N_2=6,5/10/45/38,5\text{ vol}\%$  was used. Propane conversions below 30% were reported on these catalysts, at a single space velocity of  $2400\text{ h}^{-1}$ . The products were acrylic acid, propylene, acetic acid, acetone, and carbon oxides. The acrylic acid selectivity was found to be around 6% for the crystalline  $MoVO_x$  catalyst. In comparison to that, the acrylic acid selectivity on the amorphous catalyst was below 4%, even at low propane conversion. The quaternary orthorhombic  $MoVTeO_x$  oxide was found to be the best performing catalyst, a selectivity of 49,3% was reported at a conversion of 25,6%. This led to the conclusion that tellurium promotes the selective pathway towards acrylic acid. The  $CO_2$  selectivity was in every case higher than the  $CO$  selectivity. On the other hand, the acetic acid selectivity was also significant, above 15%. However, the product selectivities were compared at different conversions for each catalyst. Because of the fact that the selectivity depends on the conversion, any kind of comparison or ranking of selectivities made at different conversions might be misleading. Ueda et al. addressed the question of catalytic function of each element of

MoVTeNbO<sub>x</sub> in the selective oxidation of propane to acrylic acid [7, 8]. Catalytic experiments were carried out at different temperatures on hydrothermally prepared single phase orthorhombic MoVO<sub>x</sub>, MoVTeO<sub>x</sub> and MoVTeNbO<sub>x</sub> catalysts, using a more reducing feed (C<sub>3</sub>H<sub>8</sub>/O<sub>2</sub>/H<sub>2</sub>O/N<sub>2</sub>=8/10/45/37 vol%) than that reported by Katou et al. [6]. The propane conversion was found to be very similar over all the catalysts at every temperature below 380°C. Although activation parameters were not calculated, the very similar temperature-conversion curve indicated that the activation energy indeed did not depend on the presence and the quality of the third and fourth element. Based on this fact the authors claimed that Mo and V are the sole elements responsible for propane activation. On the other hand a rather poor selectivity (below 10%) to acrylic acid was reported for MoVO<sub>x</sub> at every temperature, while the incorporation of tellurium lead to a major increase in the selectivity to over 40%. In the presence of niobium, the highest selectivity exceeded 60%, indicating that both tellurium and niobium are indispensable components of a high performing propane oxidation catalyst. The positive effect of tellurium was ascribed to its promoting effect on propylene further oxidation to acrylic acid. On the other hand, the positive effect of niobium was ascribed for preventing the acrylic acid over-oxidation. One possible explanation was given by the site isolation concept, introduced by Grasselli [9]. Without experimental evidence, the modulation of the redox couplings by Nb<sup>5+</sup> in the MoVTeNbO<sub>x</sub> was highlighted as second possibility for the beneficial effect of niobium on the catalytic performance.

Gulians et al. reported the surface promotion of hydrothermally synthesized orthorhombic MoVO<sub>x</sub> catalyst [10]. The tellurium, antimony and niobium promoters lead to increased activity and selectivity to acrylic acid. The mixed Nb+Te and Sb+Nb promoted catalysts showed the highest performance, in accordance with the observations on bulk mixed oxide catalysts.

## **6.2. Propane oxidation reactivity on different Mo and V based catalysts**

In the present study the catalytic testing in propane oxidation reaction to acrylic acid was carried out on different ternary, quaternary and quinary Mo and V based mixed metal oxide catalysts. These are summarized in Table 6.2.1.

In order to compare the catalytic data with literature results, for the ternary and quaternary oxides, the experiments were performed under identical conditions with respect to feed composition and contact time ( $C_3H_8/O_2/H_2O/N_2=6,5/10/45/38,5$  vol%,  $GHSV=2400\text{ h}^{-1}$ ,  $W/F=1,50$  gs/ml) with that used by Katou et al. [6].

**Table 6.2.1.** The used catalysts and reaction conditions. Catalyst preparation methods: SD – spray drying, HT – hydrothermal.

Sample ID.	Composition (EDX analysis)	Prep. Meth.	$C_3H_8/O_2/H_2O/N_2$ (vol%)	GHSV ( $h^{-1}$ )	T ( $^{\circ}C$ )
#1862	$(Mo_{0,93}V_{0,07})_5O_{14}$	SD	3/6/0/91	5000	400- 450
#6142	$MoV_{0,31}O_x$	HT	6,5/10/45/38,5	2400	280- 320
#8103	$MoV_{0,34}O_x$	HT	3/6/40/51	9000- 42000	400
#6274	$MoV_{0,29}P_{0,13}O_x$	HT	6,5/10/45/38,5	2400	320- 360
#6619	$MoV_{0,44}P_{0,05}O_x$	HT	6,5/10/45/38,5	2400	300- 340
#6683	$MoV_{0,3}Te_{0,03}O_x$	HT	6,5/10/45/38,5	2400	300- 340
#6059	$MoV_{0,26}Te_{0,10}Nb_{0,22}O_x$	HT	3/6/40/51	5000- 66000	360- 400

The activities of the catalysts were found to be different under identical space velocity and temperature. Therefore, the temperature was varied in  $20^{\circ}C$  steps in order to achieve similar conversions of propane on the above named ternary and quaternary oxides. In case of #6274 the temperature was varied between 320 and  $360^{\circ}C$ , while in case of #6619 and #6683 the reaction temperatures were between 300 and  $340^{\circ}C$ . Among this set of catalysts, the  $MoVO_x$  #6142 showed the highest activity, thus the temperature was varied between 280 and  $320^{\circ}C$ .

Most of the catalytic studies in propane oxidation are performed under a different condition than that reported by Katou et al. [6]. The typical feed composition is  $C_3H_8/O_2/H_2O/N_2=3/6/40/51$  vol%, and the temperature between 360 and 400°C. For the purpose of comparison, the reactivity of  $MoVO_x$  #8103 catalyst was tested using the latter feed composition at 400°C. In order to achieve different conversion of propane which are comparable to those determined for the previously mentioned catalysts, the contact time was varied between 0,075 and 0,400 gs/ml (GHSV=48000 and 9000h<sup>-1</sup>)

**Table 6.2.2.** Comparison of the catalytic performance of  $MoVTeNbO_x$  (#6059) and  $MoVO_x$  (#8103) samples at 400°C, feed composition:  $C_3H_8/O_2/H_2O/N_2=3/6/40/51$  vol%.

GHSV (h <sup>-1</sup> )	#6059		#8103	
	X <sub>C<sub>3</sub>H<sub>8</sub></sub> (%)	S <sub>AA</sub> (%)	X <sub>C<sub>3</sub>H<sub>8</sub></sub> (%)	S <sub>AA</sub> (%)
9000	38,1 ± 0,4	51,3 ± 1,3	43,6 ± 0,7	0,50 ± 0,02
24000	15,3 ± 0,4	39,2 ± 0,6	23,0 ± 0,5	1,8 ± 0,2

Upon comparing the conversions of propane under identical conditions with respect to the feed composition, temperature and space velocity, it was found that  $MoVO_x$  #8103 is more active than  $MoVTeNbO_x$  #6059 (Table 6.2.1), in contrast to the observation of Ueda et al. [6]. On the other hand, the significantly lower selectivity towards acrylic acid of the  $MoVO_x$  is in accordance with the trend reported by Ueda et al. [6].

For comparison of the catalytic performance of phase-pure M1  $MoVO_x$  and  $Mo_5O_{14}$ -type structure, the  $(Mo_{0,93}V_{0,07})_5O_{14}$  oxide catalyst (#1862) was also tested for propane oxidation. The  $(Mo_{0,93}V_{0,07})_5O_{14}$  catalyst was found to be rather inactive at 400°C and a contact time of 0,72 gs/ml, the conversion being only 0,4% and propylene selectivity of 48%. At a reaction temperature of 450°C a propane conversion of 2,1% was achieved, while the propylene selectivity decreased to 29%. Contrary to the experiment using M1  $MoVO_x$  catalysts, no oxygenates were detected either in steam containing feed, or in dry feed. Under every condition only propylene, CO and CO<sub>2</sub> were produced. Therefore, this oxide acts only as an oxidative dehydrogenation catalyst. This observation indicated that besides the elemental composition, the crystal structure has a decisive role both in propane activation and reaction pathways.

The Mo and V containing M1 catalyst (#8103) was very active at 400°C, while the  $(\text{Mo}_{0,93}\text{V}_{0,07})_5\text{O}_{14}$  structure was much less active. In contrast to the  $\text{MoVO}_x$  M1 structure, the  $(\text{Mo}_{0,93}\text{V}_{0,07})_5\text{O}_{14}$  is unable to insert oxygen in the C-H bond to form oxygenates. The different reactivity of M1  $\text{MoVO}_x$  and  $(\text{Mo}_{0,93}\text{V}_{0,07})_5\text{O}_{14}$  is certainly related to the different termination of the different bulk structures.

The low propane oxidation activity of  $(\text{Mo}_{0,93}\text{V}_{0,07})_5\text{O}_{14}$  (#1862) sample is in accordance with the literature. Baca et al. reported a propane conversion of 0,8% and acrylic acid selectivity of 6% on  $(\text{Mo}_{0,93}\text{V}_{0,07})_5\text{O}_{14}$  at 410°C. On the other hand, the  $(\text{Mo}_{0,93}\text{V}_{0,97})_5\text{O}_{14}$  exhibited a conversion of 26% at 410°C, with 0% selectivity to acrylic acid [11].

For the comparison of the catalytic property of the catalysts, the acrylic acid selectivity was plotted versus the conversion (Figure 6.2.1), which allows a better comparison of the performance, rather than comparing selectivities at different conversions.

The performances of all the ternary and quaternary catalysts were spread in the low conversion-low selectivity quartile of the conversion-selectivity plot. On the other hand, the phase pure  $\text{MoVTeNbO}_x$  catalyst can be found in both the low conversion – high selectivity and the high conversion – high selectivity quartile. Therefore, the rather complex phase pure  $\text{MoVTeNbO}_x$  is the best performing catalyst, since the selectivity is markedly higher than for all the other studied catalysts.

The  $\text{MoVO}_x$  #6142 catalyst exhibited a highest selectivity to acrylic acid of  $2,5 \pm 0,2\%$ , determined at a conversion of propane equal to  $18,5 \pm 2,0\%$ , the maximum yield being  $0,5 \pm 0,1\%$ . The most abundant product at this conversion was CO almost independently on the reaction temperature ( $S=43,5 \pm 0,8\%$ ), followed by  $\text{CO}_2$  with a selectivity of  $25,3 \pm 0,5\%$ . A significant amount of acetic acid was also formed ( $S_{\text{HAc}}=21,7 \pm 0,8\%$ ), while propylene was a relatively minor product, with a selectivity of  $8,0 \pm 0,3\%$ . The selectivity to propylene, acrylic acid and acetic acid decreased with increasing temperature, while the  $\text{CO}_2$  selectivity increased significantly with increasing reaction temperature.

The inclusion of tellurium in the  $\text{MoVO}_x$  structure (#6683) led to a slightly reduced selectivity to acrylic acid compared to the pure  $\text{MoVO}_x$  catalyst. Similarly to the  $\text{MoVO}_x$

catalyst, CO was the most abundant product, with selectivity of ca. 46% and almost independently of the temperature.

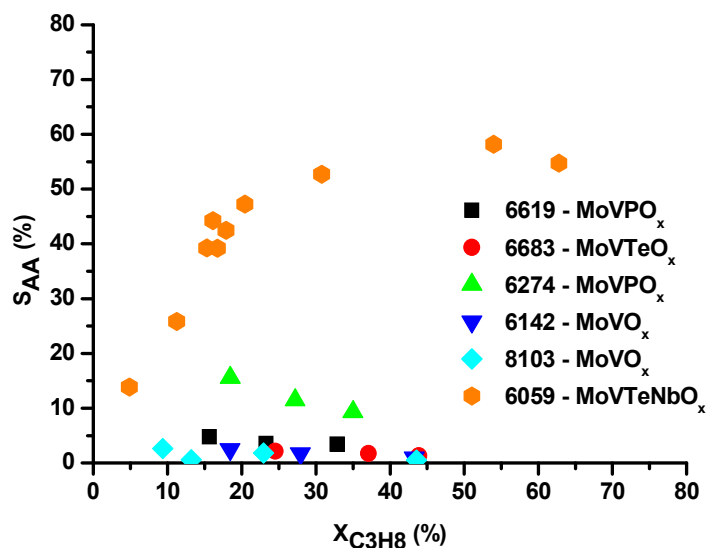


**Figure 6.2.1.** Catalytic performance of different phase-pure Mo and V based oxides.

The second most abundant byproduct was CO<sub>2</sub>. Its selectivity increased with the temperature from 29,0±0,7% to 36,0±0,4%. Acetic acid was formed in quite important amounts (S=15,5±1,6%), while propylene was formed only in 6,8±0,2%.

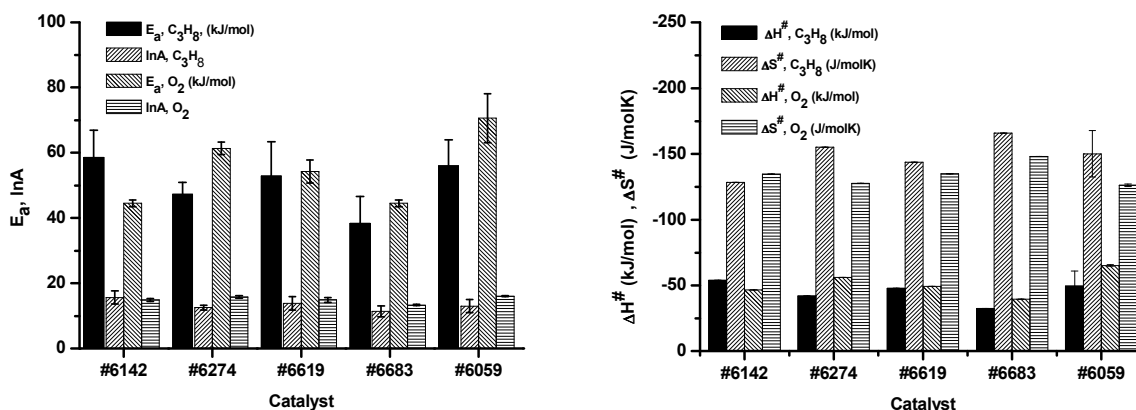
The inclusion of small amount of phosphorous in the MoVO<sub>x</sub> structure (#6619) led to the increase in the selectivity to acrylic acid to 4,7±0,7% measured at the propane conversion of 15,7±3,5%. The main product was CO, its selectivity being over 40%. Carbon dioxide was the second most abundant product with selectivities above 28%. The propylene selectivity was situated between 11,1±0,4 and 6,2±0,4%, while acetic acid between 12,4±1,5 and 10,6±0,7%, depending on the temperature.

A higher phosphorous content in the catalyst #6274 was beneficial for the increase of the selectivity to acrylic to (obtained at 18,1±1,0% propane conversion).

Among the studied ternary and quaternary catalysts, this one exhibited the highest selectivity (15,6±0,3% obtained at a conversion of 18,1±1,0%) and yield of 3,3±0,3%. This yield is higher than the best value reported by Katou et al. [6]. Similarly to the other

catalysts, the total oxidation products are the most abundant ones. The propylene and acetic acid selectivity was  $12,2\pm 0,2\%$  and  $17,6\pm 0,1\%$ , respectively.

The apparent activation parameters (activation energy  $E_a$ , logarithm of the preexponential factor  $\ln A$ , activation enthalpy  $\Delta H^\ddagger$  and activation entropy  $\Delta S^\ddagger$ ) of propane and oxygen conversion were calculated based on the linearized Arrhenius- and Eyring-Polanyi equations. In the literature, the activation enthalpy and entropy is seldom considered, although these quantities also give an important insight into the activation of molecules involved in the reaction.



Activation energy, pre-exponential factor                      Activation enthalpy and entropy  
**Figure 6.2.2.** The activation parameters of the propane and oxygen conversion on the  $MoV(Te)(P)(Nb)O_x$  catalysts.

The highest propane activation energy of ca. 60 kJ/mol was observed for  $MoVO_x$  catalyst. Statistically similar activation energy was determined for the phosphorous containing catalysts. However, in the case of tellurium inclusion, the activation energy of propane is reduced significantly, by ca. 20 kJ/mol, compared to  $MoVO_x$ . This observation is in contradiction with that reported by Ueda et al., namely that the presence of the tellurium and niobium does not affect the propane activation [6-8].

The logarithm of the pre-exponential factor is also different for all the catalysts. The apparent activation energy and the pre-exponential factor of oxygen consumption differ for the individual catalysts. It is remarkable, that the highest oxygen activation energy is associated to the catalyst #6274 with the highest acrylic acid selectivity. However, the

active surface oxygen species are involved in many reaction steps, including the dehydrogenation of propane to propylene, the oxidation of propylene to acrylic and acetic acids, and eventually the combustion steps. Certainly, the global oxygen consumption is the sum of the amount of oxygen species consumed in all these steps.

The negative activation entropy of both propane and oxygen activation suggests that these are involved in associative steps in the formation of the transitional state. More negative activation entropy indicates a more rigid transitional state. The most negative activation entropy was observed on #6683 MoVTeO<sub>x</sub>, while the least negative on #6142 MoVO<sub>x</sub>.

Table 6.2.3 summarizes the catalytic performance of some selected catalysts reported in the literature. The literature search data serves as a basis for comparison of the catalytic performance for the catalysts reported in the present work.

The first and second column contains information concerning the catalyst composition and preparation method, respectively. Very different preparation methods (including slurry-, hydrothermal-, solid-solid reaction, impregnation- and spray drying) were used. On the other hand, the extent of characterization reported by the literature sources also differs very much.

For instance, the elemental composition reported by Ai refers to preparative composition [4, 5]. In contrast to that, in the more recent studies a thorough characterization of the catalysts (including surface and bulk sensitive analytical methods) is documented.

Very different reaction conditions were used by the different authors. Ai used highly oxidizing feed (O<sub>2</sub>/C<sub>3</sub>H<sub>8</sub>=40), without employing inert gas (balance gas) besides steam [4, 5]. A reducing feed was used by Ueda et al., Baca et al., Gulians et al. [7, 8, 10], while Celaya Sanfiz et al. worked with stoichiometric feed [12]. As it is shown in Table 6.2.3, in the present work both reducing and stoichiometric feed were used.

Table 6.2.3 summarizes the catalytic performance of some selected catalysts reported in the literature. The literature search data serves as a basis for comparison of the catalytic performance for the catalysts reported in the present work.

**Table 6.2.3.** Comparison of the performance of selected catalysts. Composition as determined by (a) stoichiometry, (b) ICP, (c) EDX, (d) LEIS-surface. Preparation method: slurry (Sl.), hydrothermal (Ht.), Solid-solid (Ss.), Incipient impregnation (Ii.), Spray drying (Sd.). (P) – present work.

Catalyst	Prep. meth.	C <sub>3</sub> H <sub>8</sub> /O <sub>2</sub> /H <sub>2</sub> O/inert (vol%) GHSV/W·F <sup>-1</sup> /τ (h <sup>-1</sup> /g·s·ml <sup>-1</sup> /s)	T (°C)	X <sub>C<sub>3</sub>H<sub>8</sub></sub> (%)	S <sub>AA</sub> (%)	Y <sub>AA</sub> (%)	E <sub>a,C<sub>3</sub>H<sub>8</sub></sub> (kJ·mol <sup>-1</sup> )	Ref.
VPO <sup>a</sup>	Sl.	1,9/76/22,1/0 -/-/9	380	28,1	n.a.	n.a.	126±8	4
VPO+H <sub>3</sub> PMo <sub>12</sub> O <sub>40</sub> <sup>a</sup>			380	34,8	n.a.	n.a.	113±9	
VPO+ H <sub>3</sub> PW <sub>12</sub> O <sub>40</sub> <sup>a</sup>			370	29,4	n.a.	n.a.	195	
VPO+ SO <sub>3</sub> <sup>a</sup>			380	33,0	n.a.	n.a.	79±11	
VPO+TeO <sub>2</sub> <sup>a</sup>			380	24,6	n.a.	n.a.	109±4	
VPO+Nb <sub>2</sub> O <sub>5</sub> <sup>a</sup>			360	34,2	n.a.	n.a.	74	
VPO+Sb <sub>2</sub> O <sub>3</sub> <sup>a</sup>			380	33,2	n.a.	n.a.	88	
VPO+SiO <sub>2</sub> <sup>a</sup>			385	17,1	n.a.	n.a.	107±7	
VPO+B <sub>2</sub> O <sub>3</sub> <sup>a</sup>			400	23,6	n.a.	n.a.	126	
VP <sub>1,15</sub> Te <sub>0,15</sub> O <sup>a</sup>	Sl.	1,9/76/22,1/0	340	18	46	8	n.a.	5
VP <sub>1,15</sub> Te <sub>0,15</sub> Nb <sub>0,1</sub> O <sup>a</sup>			340	25	32	8	n.a.	
VP <sub>1,15</sub> Te <sub>0,15</sub> Zr <sub>0,1</sub> O <sup>a</sup>			340	42	16	7	n.a.	
MoV <sub>0,34</sub> O <sup>b</sup>	Ht.	8/10/45/37 2400/1,5/-	379	32,7	3,4	1	n.a.	6
MoV <sub>0,44</sub> Te <sub>0,1</sub> O <sup>b</sup>			380	36,2	46,6	17	n.a.	
MoV <sub>0,25</sub> Te <sub>0,11</sub> Nb <sub>0,12</sub> O <sup>b</sup>			380	33,4	62,4	21	n.a.	
MoV <sub>0,23</sub> Te <sub>0,11</sub> Nb <sub>0,14</sub> O <sup>c</sup> (M1)	Ht.	6/10/43/41 2500/-/-	380	29,9	52	16	58 ±0,4	11
MoV <sub>0,3</sub> Te <sub>0,32</sub> Nb <sub>0,07</sub> O <sup>c</sup> (M2)	Ss.		410	0,6	22	0,1	n.a.	
MoV <sub>0,33</sub> Te <sub>0,22</sub> Nb <sub>0,11</sub> O <sup>c</sup>	Sl.		380	34,9	53	19	58±18	
MoV <sub>0,5</sub> Te <sub>0,22</sub> Nb <sub>0,11</sub> O <sup>c</sup>	Sl.		400	25,3	46	12	64,8	
Mo <sub>0,97</sub> V <sub>0,95</sub> O <sub>5</sub> <sup>c</sup>	Ht.	6,5/10/45/38,5 3300/-/-	410	26,4	0	0	26±1	
MoV <sub>0,19</sub> O <sup>d</sup>	Ht. MoVO Ii. MO <sub>x</sub>	6,3/9,4/47,3/37 -/1,25/-	400	4,7	4	0,2	168±18	10
MoV <sub>0,68</sub> O <sup>d</sup>			400	11,4	4	0,5	68±6	
MoV <sub>0,36</sub> Te <sub>0,07</sub> O <sup>d</sup>			400	11,1	8	0,9	48	
MoV <sub>0,3</sub> Nb <sub>0,13</sub> O <sup>d</sup>			400	13,6	20	2,7	72±12	
MoV <sub>0,2</sub> Sb <sub>0,07</sub> O <sup>d</sup>			400	18,1	19	3,4	67±23	
MoV <sub>0,69</sub> Te <sub>0,04</sub> Nb <sub>0,13</sub> O <sup>d</sup>			400	10,2	29	3,0	108±13	
MoV <sub>0,31</sub> Nb <sub>0,14</sub> Sb <sub>0,02</sub> O <sup>d</sup>			400	18,1	19	3,4	79±18	
MoV <sub>0,26</sub> Te <sub>0,17</sub> Nb <sub>0,29</sub> O	Ht.	3/6/40/51	400	56	79	44	n.a.	12
MoV <sub>0,26</sub> Te <sub>0,17</sub> Nb <sub>0,29</sub> O		-/0,75, 3/-	400	49	73	36	n.a.	
MoV <sub>0,31</sub> O <sup>c</sup>	Ht. MoVO Ii. EO <sub>x</sub>	6/10/45/39 2400/1,5/-	300	27,9	1,7	0,5	59±8	(P)
MoV <sub>0,29</sub> P <sub>0,13</sub> O <sup>c</sup>			320	27,2	8,4	2,3	47±4	
MoV <sub>0,44</sub> P <sub>0,05</sub> O <sup>c</sup>			320	23,3	3,6	0,8	53±11	
MoV <sub>0,3</sub> Te <sub>0,03</sub> O <sup>c</sup>			320	37,1	2,1	0,8	38±8	
MoV <sub>0,26</sub> Te <sub>0,10</sub> Nb <sub>0,22</sub> O <sup>c</sup>	Ht.	3/6/40/51	400	60,7	58,2	35	56±3	
MoV <sub>0,34</sub> O <sup>c</sup>		4500, 24000/-/-	400	23	1,7	0,4	n.a.	
(Mo <sub>0,93</sub> V <sub>0,07</sub> ) <sub>5</sub> O <sub>14</sub> <sup>c</sup>	Sd.		450	2,1	0	0	125±14	

The first and second column contains information concerning the catalyst composition and preparation method, respectively. Very different preparation methods (including slurry-, hydrothermal-, solid-solid reaction, impregnation- and spray drying) were used. On the other hand, the extent of characterization reported by the literature sources also differs very much.

For instance, the elemental composition reported by Ai refers to preparative composition [4, 5]. In contrast to that, in the more recent studies a thorough characterization of the catalysts (including surface and bulk sensitive analytical methods) is documented.

Very different reaction conditions were used by the different authors. Ai used highly oxidizing feed ( $O_2/C_3H_8=40$ ), without employing inert gas (balance gas) besides steam [4, 5]. A reducing feed was used by Ueda et al., Baca et al., Gulians et al. [7, 8, 10], while Celaya Sanfiz et al. worked with stoichiometric feed [12]. As it is shown in Table 6.2.3, in the present work both reducing and stoichiometric feed were used.

The conversion, selectivity and yield were listed at the given temperature. The apparent activation energy of propane consumption was either taken from the publications or calculated based on the reported catalytic data in the cited sources.

Due to the fact that the reaction conditions used by different groups are different, it is difficult or even impossible to compare directly the catalytic data. A general observation is, however, that both niobium and tellurium are indispensable elements for a high performing Mo and V based catalyst.

### **6.3. Propylene oxidation reactivity on different Mo and V based catalysts**

Besides the phase-pure M1  $MoVTaNbO_x$ , other Mo and V based oxides were tested for propylene oxidation. These catalysts were:

- $MoV_{0,3}Te_{0,03}O_x$  (#6683),
- $(Mo_{0,93}V_{0,07})_5O_{14}$  (#1862) and
- $(Mo_{0,68}V_{0,23}W_{0,09})_5O_{14}$  (#1401).

The results of the catalytic tests are summarized in the following.

Propylene oxidation was performed on  $\text{MoV}_{0,3}\text{Te}_{0,03}\text{O}_x$  #6683 using the following feed:  $\text{C}_3\text{H}_6/\text{O}_2/\text{H}_2\text{O}/\text{N}_2=5/7,5/45/38,5$  vol%. The catalyst was very active, at a temperature interval between 180 and 250°C, conversions between 30 and 80% were measured at a space velocity of 2400  $\text{h}^{-1}$  ( $W/F=1,50$  g·s/ml) (Table 6.3.1). Similarly to the experiments performed on  $\text{MoVTeNbO}_x$  #6902 (section 4.2.5), the production of maleic anhydride was also observed.

Compared to  $\text{MoVTeO}_x$  and  $\text{MoVTeNbO}_x$  catalysts, the  $(\text{Mo}_{0,93}\text{V}_{0,07})_5\text{O}_{14}$  was found to be a less active propylene oxidation catalyst. In the 300-420°C temperature interval, 10-50% conversion was observed for a space velocity of 5000  $\text{h}^{-1}$  (Figure 6.3.1).

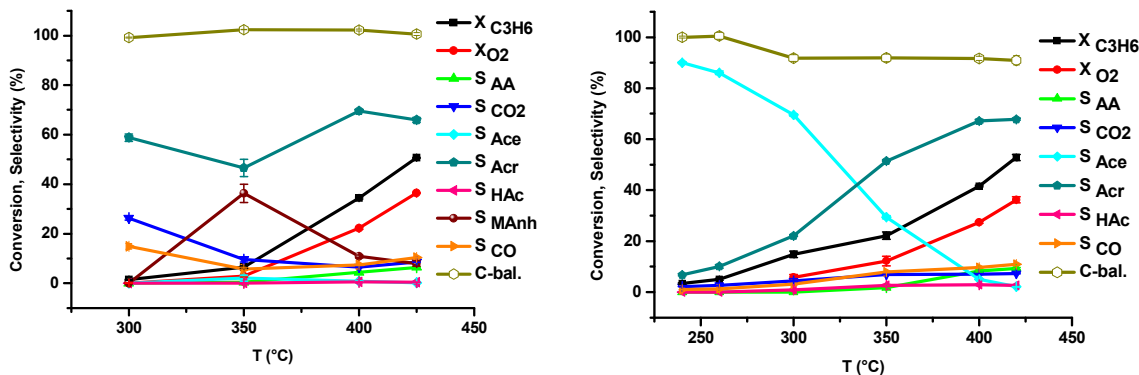
When steam was not introduced in the feed, the main product was found to be acrolein. Interestingly, maleic anhydride was formed in a quite high amount at a reaction temperature of 350°C at the expense of acrolein formation. In this case, the quantitation of maleic anhydride was possible, because in absence of the co-fed steam no hydrolysis occurred. It should be noted, however, that the peak shape of maleic anhydride was highly asymmetric, but quantifiable. Therefore, the carbon balance approached satisfyingly 100%. The acrolein selectivity peaked at ca. 70% at a reaction temperature of 400°C. The acrylic acid selectivity was below 10%, while acetic acid and acetone were produced in traces.

In presence of 40 vol% steam in the feed, the propylene conversion and acrylic acid selectivity was slightly increased. The positive effect of steam on the productivity was in accordance with the observation of steam effect on propane and propylene oxidation over the phase pure M1  $\text{MoVTeNbO}_x$  catalyst (#6902).

Similarly to the experiment carried out on catalyst #6902, acetone was the main product at low temperatures, when steam containing feed was applied. The acetone selectivity dropped according to a sigmoidal curve with increasing temperature.

The acrolein selectivity increased and reached a plateau at 70%, in the temperature interval between 400 and 420°C. The CO and CO<sub>2</sub> production was not influenced very significantly by the presence of steam. On the other hand, the maleic acid was also produced; but its quantification was not possible because of the problems related to hydrolysis. However, because the mass balance was as high as 95%, it can be concluded

that in presence of steam, the maleic acid production was suppressed compared to the experiment carried out in absence of steam.



$C_3H_6/O_2/H_2O/N_2=5/10/0/85$  vol%  
 WHSV=5000 h<sup>-1</sup>, W/F=0,72 gs/ml

$C_3H_6/O_2/H_2O/N_2=5/10/40/45$  vol%  
 WHSV=5000 h<sup>-1</sup>, W/F=0,72 gs/ml

**Figure 6.3.1.** Propylene oxidation over  $(Mo_{0,93}V_{0,07})_5O_{14}$  catalyst (#1862).

The reactivity of  $MoVTeNbO_x$ ,  $MoVTeO_x$  and  $(Mo_{0,93}V_{0,07})_5O_{14}$  in propylene oxidation reaction is summarized in the Table 6.3.1.

The reactivity ranking is the following:  $(Mo_{0,93}V_{0,07})_5O_{14} < (Mo_{0,68}V_{0,23}W_{0,09})_5O_{14} < MoV_{0,3}Te_{0,03}O_x \sim MoVTeNbO_x$ .

As it can be seen, there is a very large difference of about one order of magnitude between the apparent activation energy of propylene activation on  $Mo_5O_{14}$  structures and phase pure M1 Mo and V based oxide catalysts.

The co-fed steam induced a significant decrease of about 50 kJ/mol in the apparent activation energy of propylene over the  $(Mo_{0,93}V_{0,07})_5O_{14}$  catalyst. In presence of steam, the activation energy was similar on  $(Mo_{0,93}V_{0,07})_5O_{14}$  and  $(Mo_{0,68}V_{0,23}W_{0,09})_5O_{14}$  catalysts.

As it can be seen, there is a very large difference of about one order of magnitude between the apparent activation energy of propylene activation on  $Mo_5O_{14}$  structures and phase pure M1 Mo and V based oxide catalysts.

**Table 6.3.1.** Propylene oxidation reactivity on different catalysts.

<b>Catalyst</b>	<b>Feed GHSV</b>	<b>T (°C)</b>	<b>X<sub>C<sub>3</sub>H<sub>6</sub></sub> (%)</b>	<b>S<sub>AA</sub> (%)</b>	<b>Y<sub>AA</sub> (%)</b>	<b>r<sub>C<sub>3</sub>H<sub>6</sub></sub> (μmol/g·s)</b>	<b>E<sub>A</sub> (kJ/mol)</b>
(Mo <sub>0,93</sub> V <sub>0,07</sub> ) <sub>5</sub> O <sub>14</sub> #1862	5/10/0/85 5000	400	34,4±0,3	4,4±0,1	1,5±0,1	0,98	140±3
	5/10/40/45 5000	400	41,6±0,3	8,3±0,4	3,5±0,2	1,18	93±2
(Mo <sub>0,68</sub> V <sub>0,23</sub> W <sub>0,09</sub> ) <sub>5</sub> O <sub>14</sub> #1401	5/10/0/85 5000	400	59,2±0,3	8,3±0,1	4,9±0,1	1,68	92±2
MoV <sub>0,3</sub> Te <sub>0,03</sub> O <sub>x</sub> #6683	5/7,5/45/38,5 2400	220	72,7±0,3	26±3	19±2	0,99	22±2
MoVTeNbO <sub>x</sub> #6902	3/6/40/51 20000	400	94,7±0,2	63±1	60±1	5,83	15±1

The co-fed steam induced a significant decrease of about 50 kJ/mol in the apparent activation energy of propylene over the (Mo<sub>0,93</sub>V<sub>0,07</sub>)<sub>5</sub>O<sub>14</sub> catalyst. In presence of steam, the activation energy was similar on (Mo<sub>0,93</sub>V<sub>0,07</sub>)<sub>5</sub>O<sub>14</sub> and (Mo<sub>0,68</sub>V<sub>0,23</sub>W<sub>0,09</sub>)<sub>5</sub>O<sub>14</sub> catalysts.

Rather low apparent activation energies (22 and 15 kJ/mol) were found for the MoV<sub>0,3</sub>Te<sub>0,03</sub>O<sub>x</sub> and the MoVTeNbO<sub>x</sub> catalysts.

#### **6.4. Exploratory reaction pathway analysis of propane oxidation on phase-pure M1 catalyst**

The kinetic modeling of a complex reaction involves two main steps. The first step is the discrimination between possible networks of reaction pathway.

The second step constitutes the discrimination between rate expressions and fitting the kinetic equations to the experimental data [13-15].

The proposed pathways in the literature state that the oxidative dehydrogenation of propane is the first step. The formed propylene may undergo oxidation to acrolein and then to acrylic acid. Parallel to these steps, in presence of steam, propylene is hydrated to acetone, followed by oxidation to acetic acid [4, 5, 11, 16, 17]. Some proposed pathways

include the oxidation of propane to 1-propanol and 2-propanol in the scheme, in competition with the propane oxidative dehydrogenation step [1, 2, 16, 17]. However, these compounds are seldom reported to be detectable reaction products at high temperature (350-400°C). Additionally, the propylene formation is more favored thermodynamically than the formation of 1-propanol and 2-propanol.

The common feature of all the proposed pathways is that the CO and CO<sub>2</sub> are shown to be produced by total oxidation of acrylic acid and acetic acid. However, the propylene and other undetectable intermediates (acrolein, acetone, etc.) are reactive compounds, which are prone to undergo total combustion reaction pathways. Also in the literature, there is frequently no discrimination between CO and CO<sub>2</sub>, both oxidation products being designated as CO<sub>x</sub>. In the model proposed by Grissted the CO, CO<sub>2</sub> and acetic acid is merged under the term “byproducts” [18-20].

Due to the above described inconsistencies of the proposed models, in this section the identification of reaction pathways and the kinetic modeling based on the reaction pathways is presented.

Among the numerous methods for reaction pathway discrimination described in the literature, the delplot technique was claimed to be one of the most efficient and reliable. This is because its application is not limited to primary products or by reaction orders [15]. This technique is based on the relationships between the conversion (X) and yield (Y), respectively. The mathematical derivation of the formulas corresponding to the  $Y/X^n=f(X)$  n-th order delplots is presented in detail in the cited source [15].

Historically, the plot of product selectivity in function of the conversion is the most widely applied, which is equivalent with a first rank delplot. This plot is a measure of reaction economics, because it directly provides information concerning the maximum productivity. In addition to this, the discrimination of primary products from non-primary products is possible based on this plot. The extrapolation of the curves corresponding to the products towards zero conversion gives an intercept with the selectivity axis. If the intercept is a finite number, the respective product is a primary or first rank product. The products with a zero intercept are non-primary or higher rank products.

To discriminate between secondary, tertiary, etc. rank products, higher rank delplots are used. The second rank delplot represents the yield divided by the square of the

conversion in function of the conversion ( $Y/X^2=f(X)$ ). A diverging curve on this plot is characteristic of a primary product. A finite intercept indicates secondary product, while the curves with zero intercept correspond to product rank higher than two.

On the third rank delplot the  $Y/X^3$  ratio is represented in function of the conversion (X). A diverging curve on the third rank delplot indicates product with a ranking order lower than two. A curve with finite intercept corresponds to a third rank product, while zero intercept indicates a product with higher rank. This method can be continued until all the product ranks are sorted out.

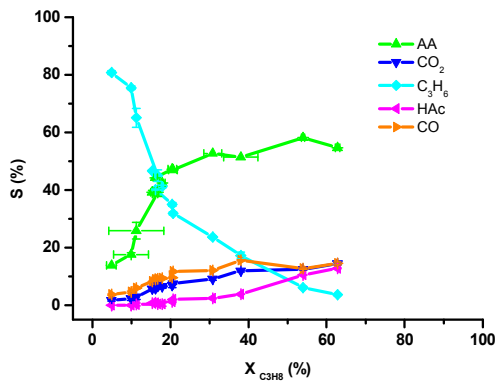
The delplot technique is applied to catalytic data determined for the propane oxidation over the phase pure MoVTaNbO<sub>x</sub> catalyst in order to sort out the reaction product ranks. In the paper published by Bhole et al. the  $Y/X^n$  ratio is plotted in function of the conversion, where n is the rank of the delplot. Because the yield is the product of conversion and selectivity, the  $S/X^{n-1}$  quantity is equivalent with the  $Y/X^n$  quantity. Therefore, here the  $S/X^{n-1}=f(X)$  plots are considered in the following.

Figure 6.4.1 displays the delplots corresponding to the experiment carried out at 400°C using a feed composition of C<sub>3</sub>H<sub>8</sub>/O<sub>2</sub>/H<sub>2</sub>O/N<sub>2</sub>=3/6/40/51 vol%.

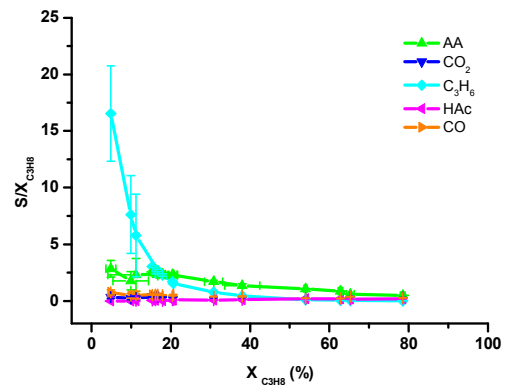
On the first rank delplot the curve corresponding to propylene has a finite intercept which is close to 90%, indicating a first rank product. The acrylic acid and carbon monoxide show an intercept statistically around 3. This may imply that both are second rank products. Carbon dioxide and acetic acid show statistically zero intercept, which indicates that these are higher rank products.

On the second rank delplot the propylene curve is diverging, which supports that this is a primary product. On the other hand, acrylic acid, carbon monoxide, carbon dioxide and acetic acid show finite intercept, indicating that all these are secondary products.

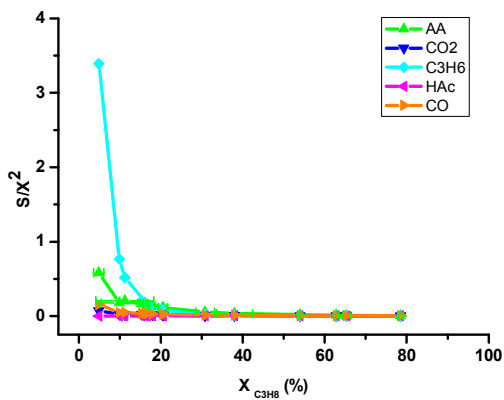
On the third and fourth rank delplots the curves corresponding to propylene and acrylic acid are diverging. Upon magnification it becomes visible that the curves of acetic acid, carbon monoxide and dioxide are diverging as well, indicating that their rank is below three and four. Due to the fact that there are no curves with zero intercept on the third and fourth rank delplots, all product ranks are discriminated by the first and second rank plots.



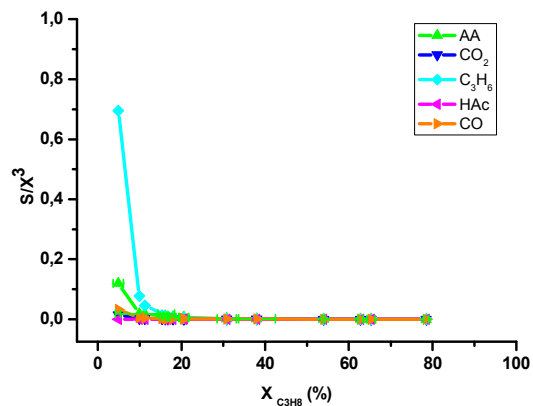
1<sup>st</sup> rank delplot



2<sup>nd</sup> rank delplot



3<sup>rd</sup> rank delplot



4<sup>th</sup> rank delplot

**Figure 6.4.1.** Delplots for propane oxidation using the feed  $C_3H_8/O_2/H_2O/N_2=3/6/40/51$  vol% at  $T=400^\circ C$ . Catalyst ID: #6059

In contrast to the reaction pathways proposed in the literature, the total oxidation products are not formed only in the combustion steps of acrylic acid and acetic acid, because their main rank is two. However, due to the limitation of the delplot technique – that it uses extrapolation of the curves toward zero educt conversion – it is not possible to discriminate whether a product is purely a second rank product or it has a multiple rank of two and three. The third rank delplot diverges in case of a product which has a rank of two and three, suggesting only second rank. Consequently, this method is not applicable to discriminate products with superimposed ranks (Appendix 6.1).

For this reason, the total oxidation products should not be considered to be only second rank products, as the delplots indicate. Due to the fact that acrylic acid as a mainly second rank product is also prone to combustion, the resulting CO and CO<sub>2</sub> are third rank products.

**Table 6.4.1.** Product ranks at different temperatures. For multiple rank products, the main ranks are highlighted by bold letter. P-primary, S-secondary.

T (°C)	Product rank				
	C <sub>3</sub> H <sub>6</sub>	AA	HAc	CO	CO <sub>2</sub>
360	P	P, <b>S</b>	S	P, <b>S</b>	S
380	P	P, <b>S</b>	S	P, <b>S</b>	S
400	P	P, <b>S</b>	S	P, <b>S</b>	S

The product ranks at different temperatures are the same as Table 6.4.1 demonstrates. This indicates that the reaction network is the same in the temperature interval between 360 and 400°C.

The Figure 6.4.2 displays the delplots corresponding to the experiment carried out in absence of steam in the feed, at 400°C.

On the first rank delplot the propylene appears to be a first rank product. However, in contrast to the experiment carried out in presence of steam, the acrylic acid has a statistically zero intercept, indicating a higher rank than one. Both the CO and CO<sub>2</sub> show low finite intercepts, suggesting that they are minor first rank products. The curve corresponding to acetic acid has a zero intercept.

On the second rank delplot the propylene curve is diverging. The curves corresponding to acrylic acid, acetic acid, CO and CO<sub>2</sub> show finite intercepts. Therefore, all these products are second rank products.

The higher rank delplots are diverging, similarly to the experiment carried out in presence of steam.

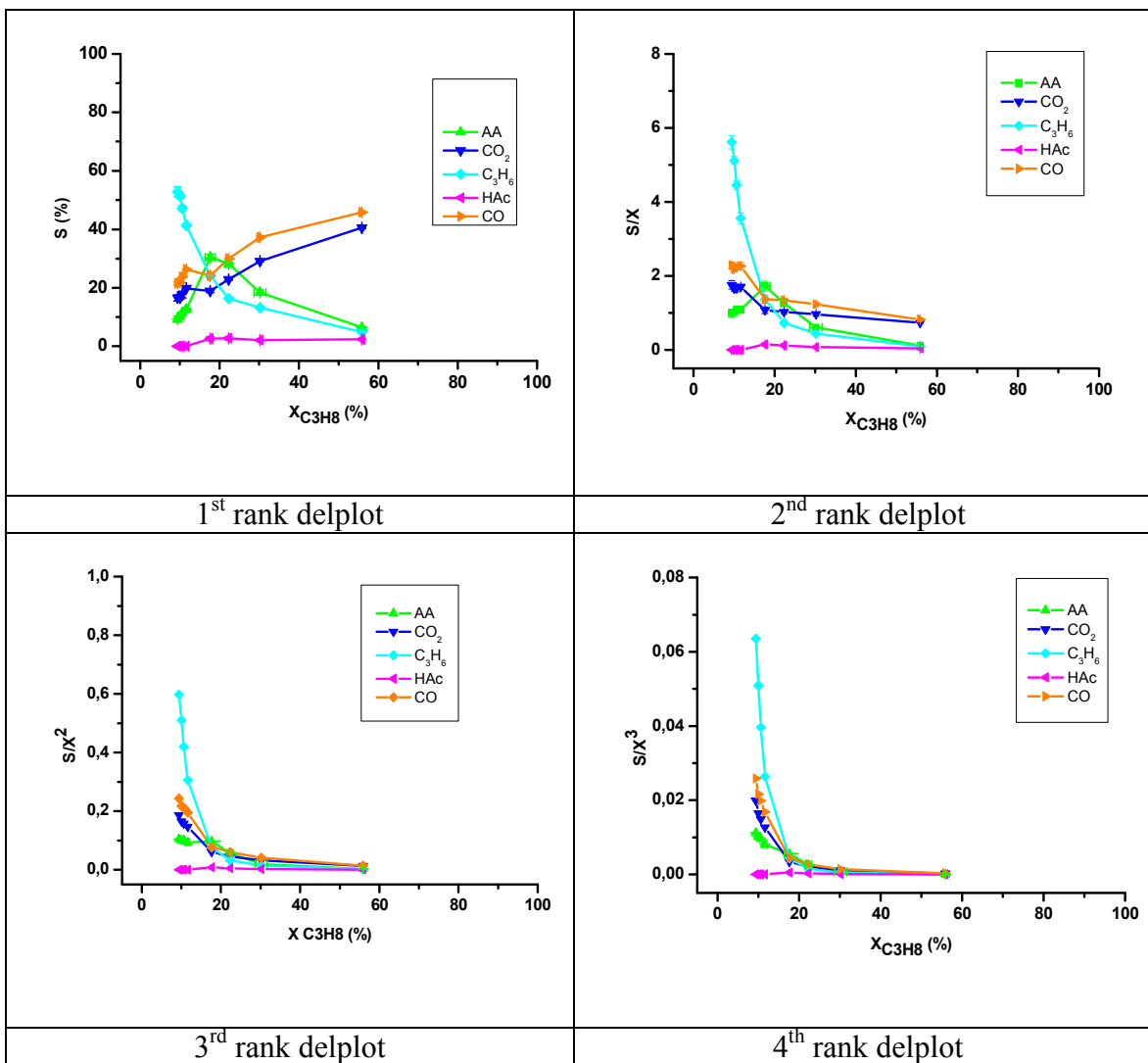


Figure 6.4.2. Delplots for propane oxidation using the feed  $C_3H_8/O_2/H_2O/N_2=3/6/0/91$  vol% at  $T=400^\circ C$ . Catalyst ID: 6059.

The product ranks for the steam content variation experiment are summarized in Table 6.4.2. Between 10 and 40 vol% steam content the ranks are the same, suggesting the same reaction pathway. However, in absence of steam, the acrylic acid is purely a second rank product, while carbon dioxide has a minor primary rank as well. The difference between the product ranks indicates that the reaction pathways are different in presence and in absence of steam.

**Table 6.4.2.** Product ranks at different steam contents. For multiple rank products, the main ranks are highlighted by bold letter. P-primary, S-secondary rank.

H <sub>2</sub> O content (vol%)	Product rank				
	C <sub>3</sub> H <sub>6</sub>	AA	HAc	CO	CO <sub>2</sub>
0	P	S	S	P, S	P, S
10	P	P, S	S	P, S	S
20	P	P, S	S	P, S	S
30	P	P, S	S	P, S	S
40	P	P, S	S	P, S	S

Taking into account the reaction product ranks, the main reaction pathway was found to be propane→propylene→acrylic acid. Due to the fact that acetic acid is a secondary product, it is formed in a parallel step with respect to acrylic acid. Separated CO and CO<sub>2</sub> production pathways were included on the main pathways (Figure 4.2.19 and 4.2.20). As the CO oxidation and water gas shift activity of the catalyst is found to be negligible (see subchapter 4.2.7 and 4.3.3), the inclusion of these steps was omitted in the first approach of kinetic modeling.

Alternative reaction models including the following steps

- coupled production of CO and CO<sub>2</sub> from propylene, acrylic acid and acetic acid,
- coupled production of acetic acid and CO,
- coupled production of acetic acid and CO<sub>2</sub>,
- production of acrylic acid in a single step from propane and in a secondary step from propylene (*cf.* minor first rank component of acrylic acid in presence of steam in the feed)
- simultaneous production of acetic acid from propylene and acrylic acid , followed by combustion to CO,
- simultaneous production of acetic acid from propylene and acrylic acid, followed by slow combustion to CO<sub>2</sub>

were disregarded because the simulated concentration profiles did not match up with the experimental profiles.

The kinetic modeling was performed in Berkeley Madonna software. First order rate equations were set up with respect to each compound. The first order kinetics with respect to propane was experimentally verified (subchapter 4.2.3).

For the integration of the differential equations system corresponding to the reaction models, the fourth order Runge-Kutta method numerical method (RK4) was used. The calculated dimensionless concentration profiles of the products and educt were compared to the experimental dimensionless concentration profiles. The dimensionless concentration of any compound  $i$  was calculated as the ratio between the molar concentration of  $i$  species and the initial molar concentration of propane:

$$y_i = \frac{c_i}{c_{C_3H_8,0}} \quad (\text{Equation 6.4.1})$$

The best correlation of the simulated concentration profiles with the experimental data was found to be in the case of the model shown in Figure 6.4.3. This is highlighted as model 1. This model was found to be applicable for the experiments carried out in the temperature interval between 360 and 400°C and 40 vol% steam content and also for the experiments using 10, 20, 30 and 40 vol% steam in the feed at a reaction temperature of 400°C.

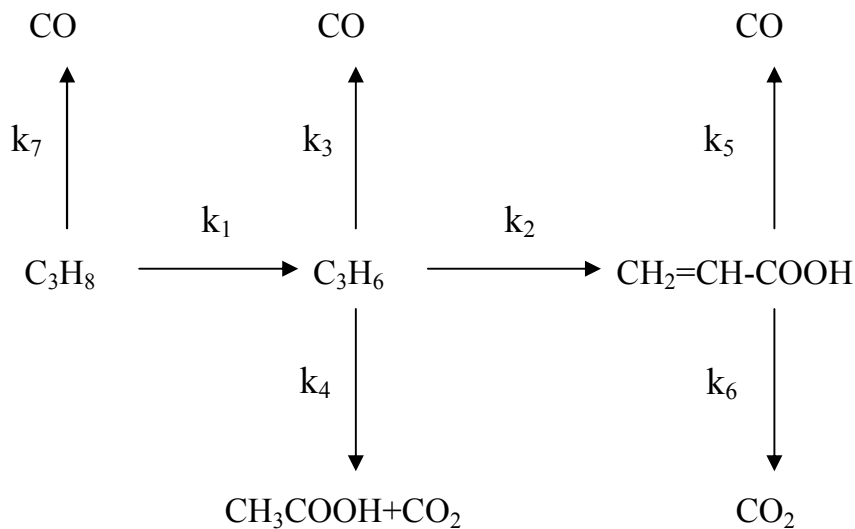


**Figure 6.4.3.** Reaction model 1 for propane oxidation.

The set of differential equations corresponding to model 1 are shown below:

$$-\frac{dy_{C_3H_8}}{dt} = (k_1 + k_8) \cdot y_{C_3H_8} \quad (\text{Equation 6.4.2})$$

$$\frac{dy_{C_3H_6}}{dt} = k_1 \cdot y_{C_3H_8} - (k_2 + k_3 + k_4) \cdot y_{C_3H_6} \quad (\text{Equation 6.4.3})$$

$$\frac{dy_{AA}}{dt} = k_2 \cdot y_{C_3H_6} - (k_5 + k_6) \cdot y_{AA} \quad (\text{Equation 6.4.4})$$

$$\frac{dy_{CO}}{dt} = k_3 \cdot y_{C_3H_6} + k_5 \cdot y_{AA} + k_7 \cdot y_{C_3H_8} \quad (\text{Equation 6.4.5})$$

$$\frac{dy_{CO_2}}{dt} = k_4 \cdot y_{C_3H_6} + k_6 \cdot y_{AA} \quad (\text{Equation 6.4.6})$$

On the other hand, for the experiment carried out in dry feed, delplot technique indicated that CO<sub>2</sub> is also a minor primary product besides propylene and CO. Therefore, in the model valid for the steam free conditions is shown in the Figure 6.4.4.

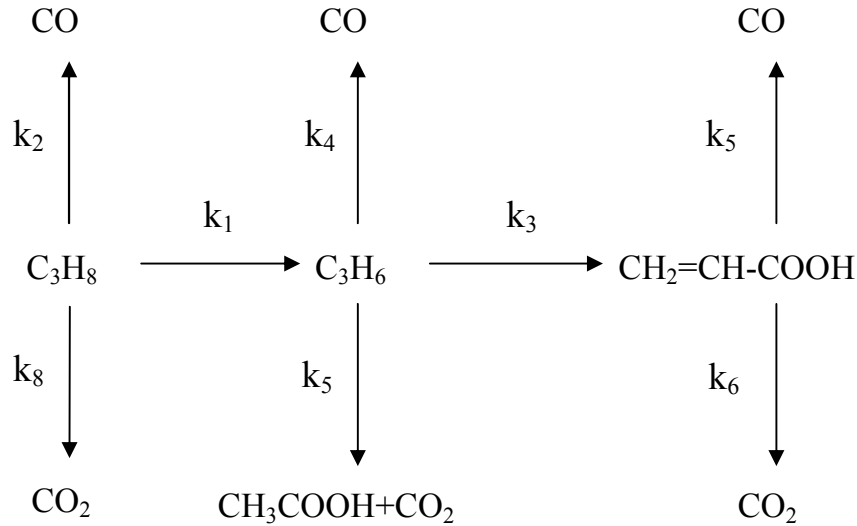


Figure 6.4.4. The reaction model 2.

Including in the reaction model the total oxidation step of propane to carbon dioxide leads to the following set of differential equations:

$$-\frac{dy_{C_3H_8}}{dt} = (k_1 + k_7 + k_8) \cdot y_{C_3H_8} \quad (\text{Equation 6.4.7})$$

$$\frac{dy_{C_3H_6}}{dt} = k_1 \cdot y_{C_3H_8} - (k_2 + k_3 + k_4) \cdot y_{C_3H_6} \quad (\text{Equation 6.4.8})$$

$$\frac{dy_{AA}}{dt} = k_2 \cdot y_{C_3H_6} - (k_5 + k_6) \cdot y_{AA} \quad (\text{Equation 6.4.9})$$

$$\frac{dy_{CO}}{dt} = k_3 \cdot y_{C_3H_6} + k_5 \cdot y_{AA} + k_7 \cdot y_{C_3H_8} \quad (\text{Equation 6.4.10})$$

$$\frac{dy_{CO_2}}{dt} = k_4 \cdot y_{C_3H_6} + k_6 \cdot y_{AA} + k_8 \cdot y_{C_3H_8} \quad (\text{Equation 6.4.11})$$

The implementation in the Berkeley Madonna software of the differential equations corresponding to Model 1 and Model 2 is shown in Appendix 6.2.

## 6.5. Exploratory kinetic modeling on propane oxidation on phase-pure MoVTenbO<sub>x</sub> catalyst

### 6.5.1. The effect of temperature

The kinetic modeling based on reaction model 1 (section 6.4) lead to the rate constants which are summarized in the Table 6.5.1. The model one contains seven reaction steps as follows: propane is oxidatively dehydrogenated to propylene and oxidized in parallel to carbon monoxide. The formed propylene undergoes oxidation to acrylic acid, carbon monoxide and in a coupled step to acetic acid and carbon dioxide. Finally, the acrylic acid undergoes total oxidation as well to carbon monoxide and dioxide.

Propane undergoes mainly oxidative dehydrogenation to propylene. Oxidation of propane to carbon monoxide also takes place, but the rate constant ( $k_7$ ) of this step is very low, in the order of magnitude of  $10^{-6}$  ml/gs. The low rate constant of propane total combustion is in accordance with the low CO selectivity determined at low propane conversion. On the other hand, the low value of the intercept on the first rank delplot also suggests low total oxidation activity towards carbon monoxide.

Propylene is a highly reactive intermediate, as demonstrated by the high values of rate constants of oxidation to acrylic acid ( $k_2$ ), acetic acid and total oxidation products ( $k_3$  and  $k_4$ ). The ratio between the propylene consumption rate constants ( $k_2+k_3+k_4$ ) and the

propylene formation rate constant is 19,8, 21,0 and 17,8, respectively at 360, 380 and 400°C. These are in good accordance with the values reported in the literature.

López-Nieto et al. reported a value of ca. 24 on a predominantly M1 phase containing  $\text{MoV}_{0,24}\text{Te}_{0,24}\text{Nb}_{0,13}\text{O}_x$  catalyst [21].

Naraschewski et al. reported a value of 25 for  $\text{MoVTeNbO}_x$  catalysts with ten different elemental- and phase compositions. However the fitting was made in case of one of the catalyst, the value for each catalyst was not quantified [22].

Gristede reported a propane consumption rate constant of 0,84 gs/ml, and a global consumption rate of propylene of 20,4 gs/ml on a  $\text{MoV}_{0,33}\text{Te}_{0,25}\text{Nb}_{0,17}\text{O}_x$  catalyst at 400°C. The ratio of propylene consumption and formation rate constant is therefore  $20,4/0,84=24,3$  [18-20].

Acrylic acid is also prone to further oxidation mainly to carbon dioxide ( $k_6$ ) and in very minor proportions to carbon monoxide ( $k_5$ ).

It is remarkable, that the highest rate constant in the reaction model corresponds to the selective oxidation step of propylene to acrylic acid.

**Table 6.5.1.** The rate constants corresponding to the steps of the reaction model 1.

T (°C)	$k_1$ (ml/gs)	$k_2$ (ml/gs)	$k_3$ (ml/gs)	$k_4$ (ml/gs)	$k_5$ (ml/gs)	$k_6$ (ml/gs)	$k_7$ (ml/gs)
360	0,519	7,443	2,401	0,451	$5,01 \cdot 10^{-4}$	0,684	$5,97 \cdot 10^{-7}$
380	0,650	8,806	4,211	0,642	$8,17 \cdot 10^{-4}$	0,912	$1,20 \cdot 10^{-6}$
400	0,871	9,244	5,195	1,093	$1,62 \cdot 10^{-3}$	1,089	$2,16 \cdot 10^{-6}$

The activation parameters determined from the above data based on the Arrhenius-plot are shown in Table 4.2.2.

**Table 6.5.2.** The activation energy and preexponential factor of the individual reaction steps.

Reaction step	1	2	3	4	5	6	7
$E_a$ (kJ/mol)	46±4	19±6	69±17	78±10	104±12	41±5	114±4
$\ln A$	8.0±0.8	5.7±1.1	13.9±3.1	14.0±1.9	12.1±2.2	7.5±0.9	7.3±0.7

The activation energy of propane to propylene transformation is in good agreement with the value of  $53 \pm 8$  kJ/mol (section 4.2.4) determined from the temperature dependence of propane conversion.

### 6.5.2. The effect of steam

Reaction kinetic modeling was performed using model 1 for the concentration profiles determined using steam containing feed. Due to the fact that in absence of steam carbon dioxide was also a primary product, an additional total oxidation pathway involving propane was taken into account (model 2). The reaction steps of the models are: propane→propylene→acrylic acid as main pathway, to which  $k_1$  and  $k_2$  rate constants are associated. The unselective pathway involving propane is oxidation to CO (in steam containing feed, characterized by the rate constant  $k_7$ ) and CO<sub>2</sub> (in dry feed, characterized by rate constant  $k_8$ ). One of the unselective pathways starting from propylene intermediate gives carbon monoxide ( $k_3$ ), while the other yields acetic acid and carbon dioxide ( $k_4$ ). The two unselective pathways involving acrylic acid are the total oxidation to CO ( $k_5$ ) and CO<sub>2</sub> ( $k_6$ ). The reaction models are described in more detail in subchapter 4.2.9.

**Table 6.5.3.** The rate constants of the individual steps as determined based on model 1 and model 2.

<b>H<sub>2</sub>O content (vol%)</b>	<b>0</b>	<b>10</b>	<b>20</b>	<b>30</b>	<b>40</b>
$k_1$ (ml/g)	0.431	0.650	0.711	0.821	0.870
$k_2$ (ml/g)	7.772	7.195	8.395	9.394	9.244
$k_3$ (ml/g)	0.736	3.896	4.595	4.395	5.194
$k_4$ (ml/g)	0.675	1.490	1.283	1.589	1.093
$k_5$ (ml/g)	0.668	0.0074	0.00144	0.0076	0.00162
$k_6$ (ml/g)	0.538	0.935	1.037	0.962	1.089
$k_7$ (ml/g)	0.0241	$8.49 \cdot 10^{-6}$	$3.34 \cdot 10^{-6}$	$2.88 \cdot 10^{-6}$	$3.16 \cdot 10^{-6}$
$k_8$ (ml/g)	0.0057	-	-	-	-

The rate constants obtained from the kinetic modeling using reaction model 1 for the steam containing feed and reaction model 2 for the steam free feed are compiled in Table 6.5.3.

In accordance with the catalytic data shown on Figure 4.2.5., the propane consumption rate constant ( $k_1$ ) increases when steam is added to the feed, and it levels off above the concentration of 20 vol%. Addition of steam increases also the rate constant of propylene selective oxidation to acrylic acid ( $k_2$ ). The same trends were reported by Grissted [18, 19].

In presence of steam the rate constants of acetic acid and total oxidation product formation from propylene intermediate are also increased dramatically ( $k_3$  and  $k_4$ ).

The increasing steam content may promote the propylene hydration to isopropanol [23, 26]. Further oxidation of isopropanol gives acetone, and finally acetic acid and total oxidation products. However, neither the isopropanol, nor acetone was detected in the reaction mixture, suggesting that these products are further oxidized rapidly, without desorption.

In the presence of steam the oxidation of acrylic acid to carbon dioxide is increased (reaction step 6), however the total oxidation of propane to carbon monoxide- and dioxide is very significantly suppressed (reaction steps 7 and 8).

Some literature source assigns the positive effect of steam on the catalytic performance to the better heat transfer properties of the steam containing feed [27]. Due to the fact that the propane oxidation reaction is a rather exothermic reaction, the real temperature of the active site might be higher than the measured (macroscopic) temperature of the catalytic bed. Zheng et al. [27] 191-194] speculated that the steam containing feed more efficiently removes the reaction heat, preventing overheating of the active sites, and therefore, total combustion is prevented. However, according to the calculation of Grissted, the maximum temperature increase above the setpoint temperature due to reaction heat is 2°C [19].

The heat capacity and heat conductivity of the feed indeed decreases linearly with the decreasing steam content (Appendix 6.3). Nevertheless, the propane conversion and acrylic acid selectivity is not influenced significantly in the 20-40 vol% steam content

interval, while both catalytic properties are decreasing below 20 vol% steam concentration. If in absence of steam the reaction heat would not be removed efficiently and the catalyst surface would be overheated, the propane conversion would not drop (Figure 4.2.3), but it would increase below 20 vol% steam content (Appendix 6.3). Therefore, it can be excluded that the only effect of steam is that to improve the thermal properties of the feed with respect to heat transfer.

### References Chapter 6

1. M. M. Lin, *Appl. Catal. A*, 207 (2001) 1-16
2. E. K. Novakova, J. C. Vedrine, Propane selective oxidation to propene and oxygenates on metal oxides, in *Metal Oxides - Chemistry and applications*, J.G.L. Fierro (Ed.), 2006, CRC Press, pp. 414-461
3. A. Trunschke, Propane selective oxidation to acrylic acid, in *Nanostructured Catalysts: Selective oxidation reactions*, Ch. Hess, R. Schlögl (Eds.), RCS, Cambridge, in press.
4. M. Ai, *Catal. Today*, 13 (1992) 679-684
5. M. Ai, *J. Catal.*, 101 (1986) 389-395
6. T. Katou, D. Vitry, W. Ueda, *Catal. Today*, 91-92 (2004) 237-240
7. W. Ueda, D. Vitry, T. Katou, *Catal. Today*, 96 (2004) 235-240
8. D. Vitry, Y. Morikawa, J. L. Dubois, W. Ueda, *Appl. Catal. A.*, 251 (2003) 411-424
9. R. K. Grasselli, *Top. Catal.*, 15 (2001) 5
10. V. V. Guliants, R. B. Bhandari, B. Swaminathan, V. K. Vasudevan, H. H. Brongersma, A. Knoester, A. M. Gaffney, S. Han, *J. Phys. Chem. B*, 109 (2005) 24046-24055
11. M. Baca, A. Pigamo, J. L. Dubois, J. M. M. Millet, *Top. Catal.*, 23 (2003) 39-46
12. A. Celaya Sanfiz, T. W. Hansen, D. Teschner, P. Schnörch, F. Girgsdies, A. Trunschke, R. Schlögl, M. H. Looi, S. B. A. Hamid, *J. Phys. Chem. C*, 114 (2010) 1912-1921
13. J. R. Kittrell, *Adv. in Chem. Eng.*, 8 (1970) 97-183
14. P. G. Ashmore, A. Jones, *Reaction Kinetics*, RSC Specialist Periodical Reports, 1 (1975) 291-308
15. N. A. Bhore, M. T. Klein, K. B. Bishoff, *Ind. Eng. Chem. Res.*, 29 (1990), 313-316
16. M. Lin, T. B. Desai, F. W. Kaiser, P. D. Klugherz, *Catal. Today*, 61 (2000) 223-229
17. R. Fushimi, S. O. Shekhtman, A. Gaffney, S. Han, G. Yablonsky, J. T. Gleaves, *Ind. Eng. Chem. Res.* 44 (2005) 6310-6319
18. E. Balcells, F. Borgmeier, I. Grisstede, H-G. Lintz, *Catal. Lett.* 87 (2003) 195,
19. I. Grisstede, Die Partielle Oxidation von Propan zu Acrylsäure, Bestimmung der Reaktionskinetik und in-situ charakterisierung des Katalysators unter

- Betriebsbedingungen, Dissertation, Universität Karlsruhe, 2004,  
Universitätsverlag Karlsruhe, ISBN 3-937300-17-1
20. E. Balcells, F. Borgmeier, I. Gristede, H.-G. Lintz, F. Rosowski, *Appl. Catal. A: General*, 266 (2004) 211
  21. J. M. López-Nieto, B. Solsona, P. Concepción, F. Ivars, A. Dejoz, M. I. Vázquez, *Catal. Today*, 157 (2010) 291-296
  22. F. N. Naraschewski, C. P. Kumar, A. Jentys, J. A. Lercher, *Appl. Catal. A: General*, 391, 1-2 (2011) 63-69
  23. Y. Moro-oka, *Appl. Catal. A: General*, 181 (1999) 323-329
  24. L. Luo, PhD thesis, California Institute of Technology, Pasadena, California, 2001
  25. J. C. Védrine, E. K. Novakova, E. G. Derouane, *Catal. Today*, 81 (2003) 247-262; H.-G. Lintz, S. P. Müller, *Applied Catal. A: General*, 357 (2009) 178-183
  27. W. Zheng, Zh. Yu, P. Zhang, Y. Zhang, H. Fu, X. Zhang, Q. Sun, X. Hu, J. *Natural Gas Chemistry*, 17 (2008) 191-194

## General Conclusions and Outlook

The present work was centered on the systematic kinetic study of the selective oxidation of propane to acrylic acid, using a well defined mixed oxide catalyst.

A well characterized phase-pure M1 MoVTeNbO<sub>x</sub> catalyst was used for the studies, which was synthesized reproducibly on the multi-gram scale.

The objectives were to

- Study the bulk structural stability of the catalyst under the reaction conditions whereby the kinetic experiments are carried out
- Study the effect of the reaction variables (temperature, steam content, redox potential) on the catalytic performance and the kinetics of the propane selective oxidation reaction
- Study the catalytic oxidation propylene, acrolein and carbon monoxide under identical conditions corresponding to the propane oxidation, in order to determine the relative reactivity, and product distributions
- Study the effect of stage-wise addition of oxidizing gases (oxygen, nitrous oxide) in order to verify whether the multi-tubular reactor arrangement is suitable to increase the catalytic performance compared to the conventional single-tube fixed bed reactor
- Study the addition of propylene, carbon monoxide and carbon dioxide, in order to gain more information about the reaction pathways and identify whether these compounds adsorb competitively on the active sites of the catalyst with propane or other intermediates
- Study the effect of post synthesis treatment employing different solutions (neutral, acidic, basic, complexing, oxidizing and reducing) on the bulk structure, surface/bulk composition and catalytic performance of the phase-pure M1 MoVTeNbO<sub>x</sub> catalyst

The knowledge of the stability is an absolute criterion for the proper catalytic, kinetic and structure-relationship studies and mechanistic understanding of the reaction. The structural stability was addressed in a long term in-situ XRD experiment. The feed

composition was varied in such a way that the conditions covered all the relevant ones for catalytic and kinetic experiments (i.e. steam containing and steam free mixture, net oxidizing, stoichiometric and net reducing). The phase purity of the used catalyst is not affected under any of the conditions. The Rietveld refinement revealed that the lattice constants are not affected by the reaction conditions ranging from net oxidizing to net reducing feed, irrespective of the steam content. When the catalyst was exposed to strongly reducing conditions (3 vol% propane in nitrogen) for long time (24 hours), the lattice constants changed, but no new phase could be detected. The STEM analysis of the sample after in-situ reaction showed pitting-like holes on the particles. The voids and their sizes were statistically distributed, which suggests that the recrystallization which occurred upon exposing the catalyst to extreme reducing conditions was controlled by diffusion, as no reaction front could be observed. The EDX analysis performed complementary to the STEM imaging revealed tellurium and oxygen depletion. The results show that the catalyst bulk structure is stable and homogeneous under reaction conditions unless it is exposed to extremely strong reducing conditions for long time. Therefore, the reactivity is determined by the surface properties. The exceptional bulk structural stability permitted the kinetic study of the reaction variables.

The effect of reaction variables was studied in a conventional fixed bed reactor. The detectable products were propylene, acrylic acid, acetic acid, CO and CO<sub>2</sub>. The temperature was varied between 360 and 400°C in 20°C steps. The highest acrylic acid productivity was observed at 400°C. The steam content was varied between 40 and 0 vol% in 10 vol% steps. A decrease of the propane conversion and acrylic acid selectivity was observed below 20 vol% steam content. Stable operation (i.e. no deactivation) was observed in steam free feed. Upon reintroducing the steam in the feed, the same catalytic performance was attained as before exposing the catalyst to dry feed. This shows that the change of the catalytic performance with the steam content is fully reversible.

The redox potential variation covered reducing, stoichiometric and oxidizing conditions (up to 5-fold oxygen excess). Under oxidizing conditions, the same conversion and selectivity was observed as in stoichiometric feed, while under reducing condition the conversion and selectivity to acrylic acid was slightly lower. Cycling experiments

showed reversibility of the catalytic performance upon exposing the catalyst to net reducing conditions. However, the steady state was restored slower (ca. 8 hours time on stream) compared to the steam content variation experiment, whereby the steady state operation was achieved within minutes.

The catalytic oxidation of other substrates (propylene, acrolein and CO) was performed in order to gain more insight into reactivity of these intermediates and the reaction pathways they might be involved in.

The propylene was found to be ca. 7 times more reactive than propane at 400°C and it produced mainly acrylic acid. It was notable that acetone was also produced in significant amounts, while this compound was not detected at all under propane oxidation conditions, even though propylene is a reaction intermediate.

The acrolein was found to be 94 times more reactive compared to propane, at 400°C. The reaction products were acrylic acid (with a yield up to 89%), acetic acid, and carbon oxides.

The CO oxidation performed under stoichiometric and oxidizing conditions in dry and steam-containing feed revealed a very low activity, the highest conversion being below 1% at a space velocity of 3000h<sup>-1</sup> at 400°C. Additionally, the water gas shift activity was found to be even lower compared to the CO oxidation activity. The CO oxidation and water gas shift activity was 80 to 100 times lower compared to the propane oxidation activity. These results suggested that under propane oxidation conditions (400°C, GHSV between 4500 and 66000 h<sup>-1</sup>) the formed CO<sub>2</sub> is not formed via CO oxidation or water gas shift reaction. Given this fact, the formation of CO and CO<sub>2</sub> during the propane oxidation reaction occurs in two different pathways that are independent on each other, which may suggest the existence of two different active sites whereby combustion pathways occur. Based on this finding, the reaction networks proposed in the literature, according to which the total oxidation products are merged together as CO<sub>x</sub>=CO+CO<sub>2</sub>, may be improved. Furthermore, the CO oxidation activity may be used as a proxy for the abundance of the electrophilic oxygen species on the surface. The low CO oxidation activity suggested low abundance of electrophilic oxygen, which activates electron rich centers (such as C=C bond) of the molecule and lead to unselective pathways in nucleophilic oxidation reactions such as propane oxidation to acrylic acid.

The stage-wise addition of oxygen lead to an improvement of the acrylic acid yield by 5%, when compared to the catalytic data obtained in the conventional single-tube reactor. Upon dosing O<sub>2</sub> in the first reactor tube and N<sub>2</sub>O in the second reactor tube of the two-stage setup it was observed that N<sub>2</sub>O is not consumed at all, even if the conditions were chosen in such a way that the oxygen was consumed completely. This suggests that the phase-pure M1 MoVTenbO<sub>x</sub> is not reoxidized by N<sub>2</sub>O.

Upon addition of propylene in the second reactor tube revealed a slight competition of propane and propylene on the active sites or for the available oxygen active species, all the added propylene was oxidized to acrylic acid, acetic acid, CO and CO<sub>2</sub>. It is notable that in contrast to the propylene oxidation experiments, no acetone formation was observed.

Neither the CO, nor the CO<sub>2</sub> influenced the product distribution of propane oxidation reaction. This suggested that none of these gases were competitively adsorbed on the active sites with the educt or intermediates. The added CO was not oxidized to CO<sub>2</sub>, which confirmed the negligible activity observed for the separate CO oxidation experiments.

In a series of experiments carried out separately from the above described ones, the phase-pure M1 MoVTenbO<sub>x</sub> was subjected to treatment with solutions of different nature (neutral, acidic, basic, complexing, oxidizing and reducing) at room temperature. The bulk structure was not affected by any of these treatments as probed by the XRD measurement. The bulk composition varied only marginally, as probed by EDX, while the morphology and the surface composition changed more significantly upon the chemical treatment. The samples treated by neutral, acidic, basic, complexing and reducing solutions exhibited similar catalytic properties in propane and propylene oxidation with the original untreated sample. However, the treatment by an oxidizing solution led to a dramatic decrease in the activity and the selectivity to acrylic acid in the propane oxidation reaction.

The findings of the above summarized experiments on the well defined, structurally exceptionally stable catalyst suggest that the catalyst surface responds dynamically to the changes in the chemical potential of the feed mixture under real reaction conditions. The dynamics is reflected in the changes of the reactivity. This study may contribute to the better understanding of the kinetics and the mechanism of the propane selective oxidation reaction.

## Appendices

### Appendix 5.1. Reaction networks of propane oxidation over the modified catalysts

To find out the reaction pathways on modified catalysts, the delplot technique was applied as it was described in the section 6.4.

The delplots corresponding to the catalytic measurements with H<sub>2</sub>O-, NaBrO<sub>3</sub> and N<sub>2</sub>H<sub>4</sub>-treated samples are presented below.

The H<sub>2</sub>O-treated sample behaves similarly to the parent sample. As it is shown on the Figure A.5.1.1, the first rank delplot gives a fairly high intercept for propylene and acrylic acid (35 and 65%, respectively), indicating that these are primary products. Since the extrapolation is made over a large interval of conversion, the rank of acrylic acid is uncertain.

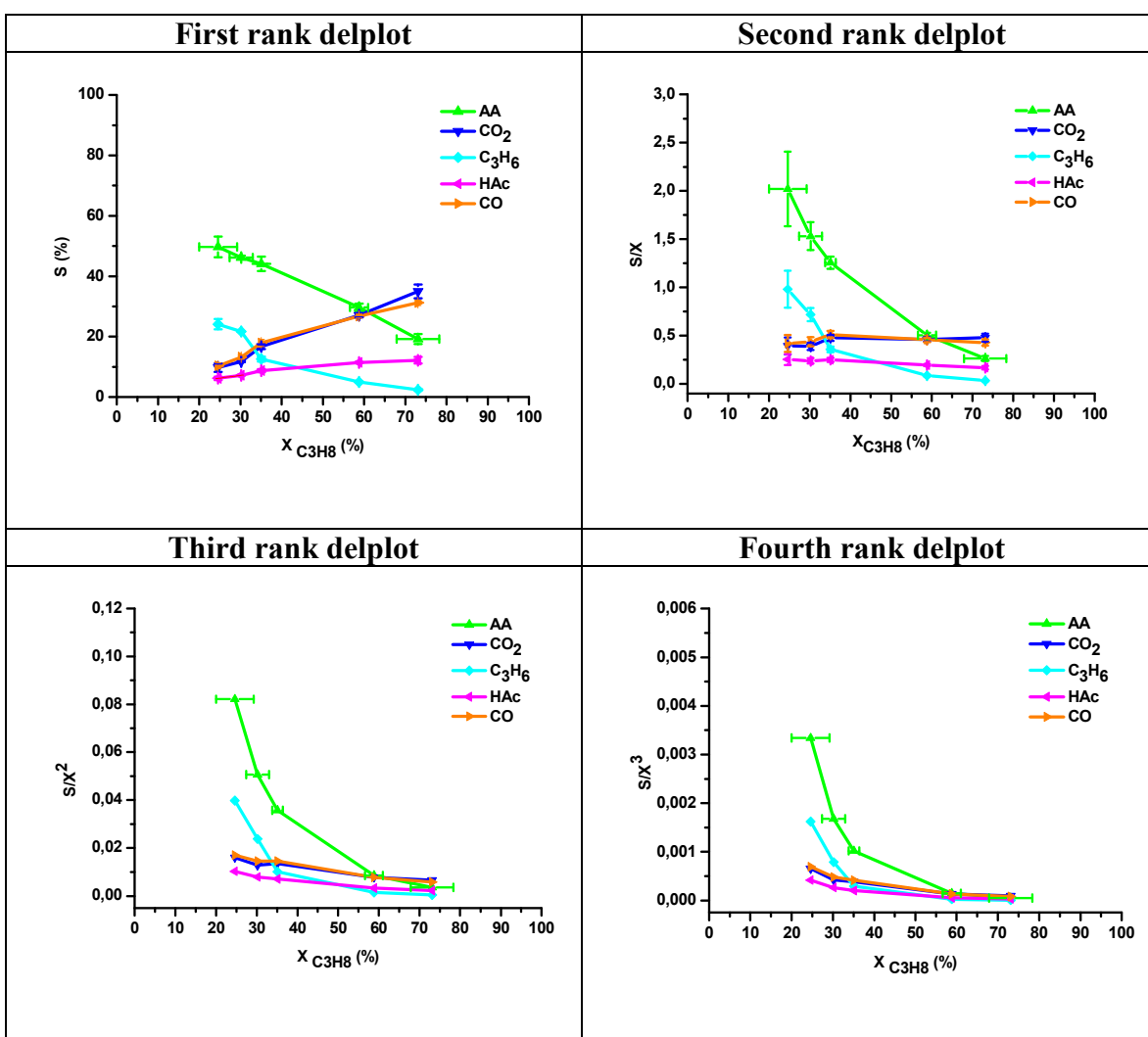


**Figure A.5.1.1.** The delplots corresponding to the propane oxidation using the H<sub>2</sub>O modified sample (#7797). Feed composition: C<sub>3</sub>H<sub>8</sub>/O<sub>2</sub>/H<sub>2</sub>O/N<sub>2</sub>=3/6/40/51 vol%, T=400°C.

Extrapolation over the differential operation is suggested. Usually the conversion-selectivity curve corresponding to acrylic acid goes through a maximum. The increasing

segment of such a curve lies in the low conversion interval. The intercepts corresponding to other products (CO, CO<sub>2</sub> and acetic acid) are low, statistically close to zero on the first rank delplot, suggesting that these are not primary products.

On the second rank delplot the curves of propylene and acrylic acid are diverging, which indicate that the rank of these are primary products. The divergent curves on the third and fourth rank delplots indicate that all the product ranks are less than three and four. The total oxidation products and acetic acid have a finite intercept, suggesting that these are secondary products.

The bromate treated sample (#7800) was less active than the other samples at any space velocity. The lowest conversions were in the differential operation mode. On the first rank delplot finite intercepts were observed for propylene, acrylic acid, CO and CO<sub>2</sub>, indicating that all of these are first rank products. On the second rank delplot the propylene and acrylic acid curves are diverging strongly (Figure A.5.1.2.).

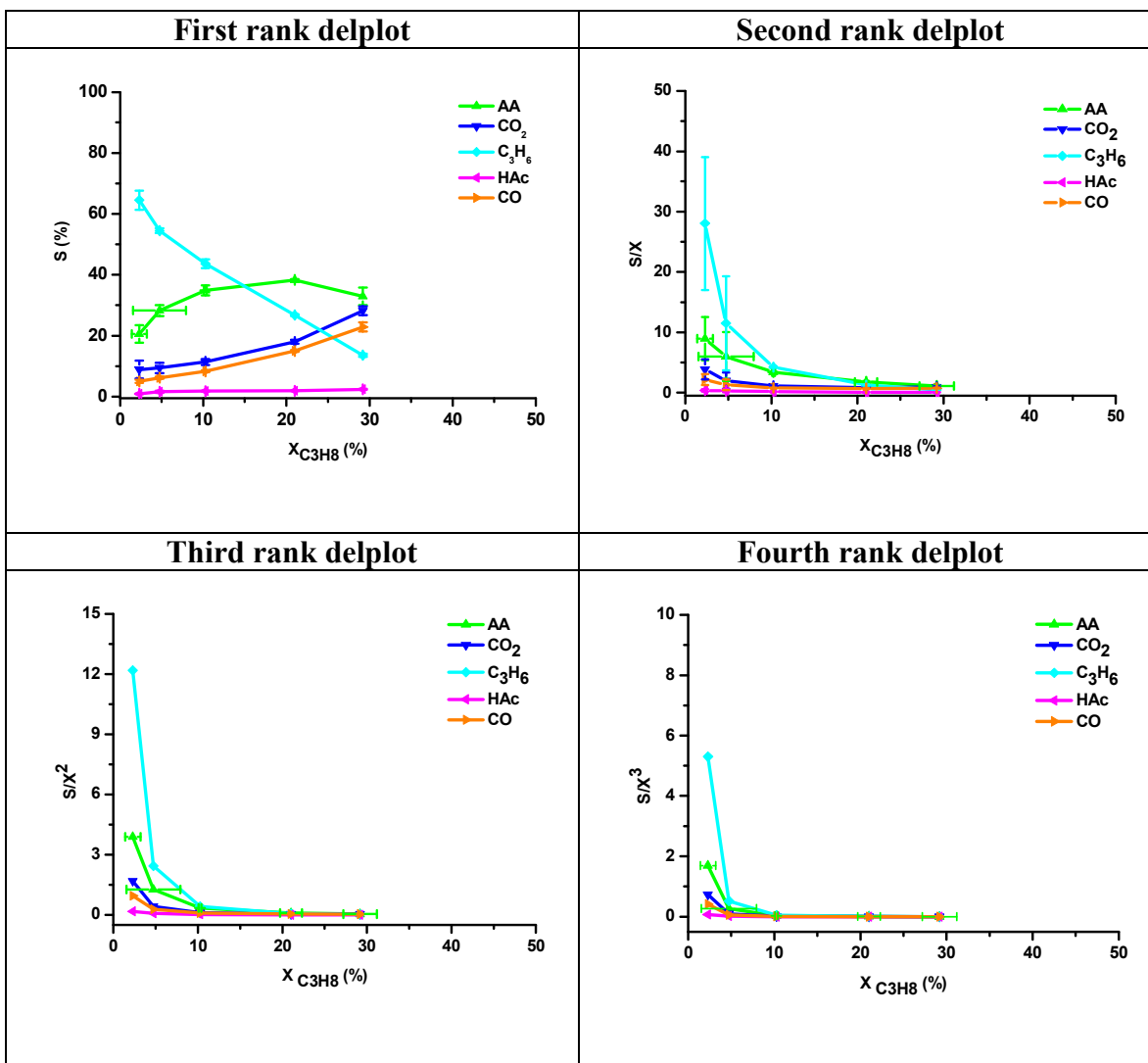


**Figure A.5.1.2.** The delplots corresponding to the propane oxidation using the NaBrO<sub>3</sub> modified sample (#7800). Feed composition: C<sub>3</sub>H<sub>8</sub>/O<sub>2</sub>/H<sub>2</sub>O/N<sub>2</sub>=3/6/40/51 vol%, T=400°C.

The slight divergence of CO and CO<sub>2</sub> indicate that these products are mainly first rank products, but a small second rank component can not be excluded. The acetic acid is a second rank product.

Similarly to the previous cases, the higher rank delplots lead to diverging curves for all the products.

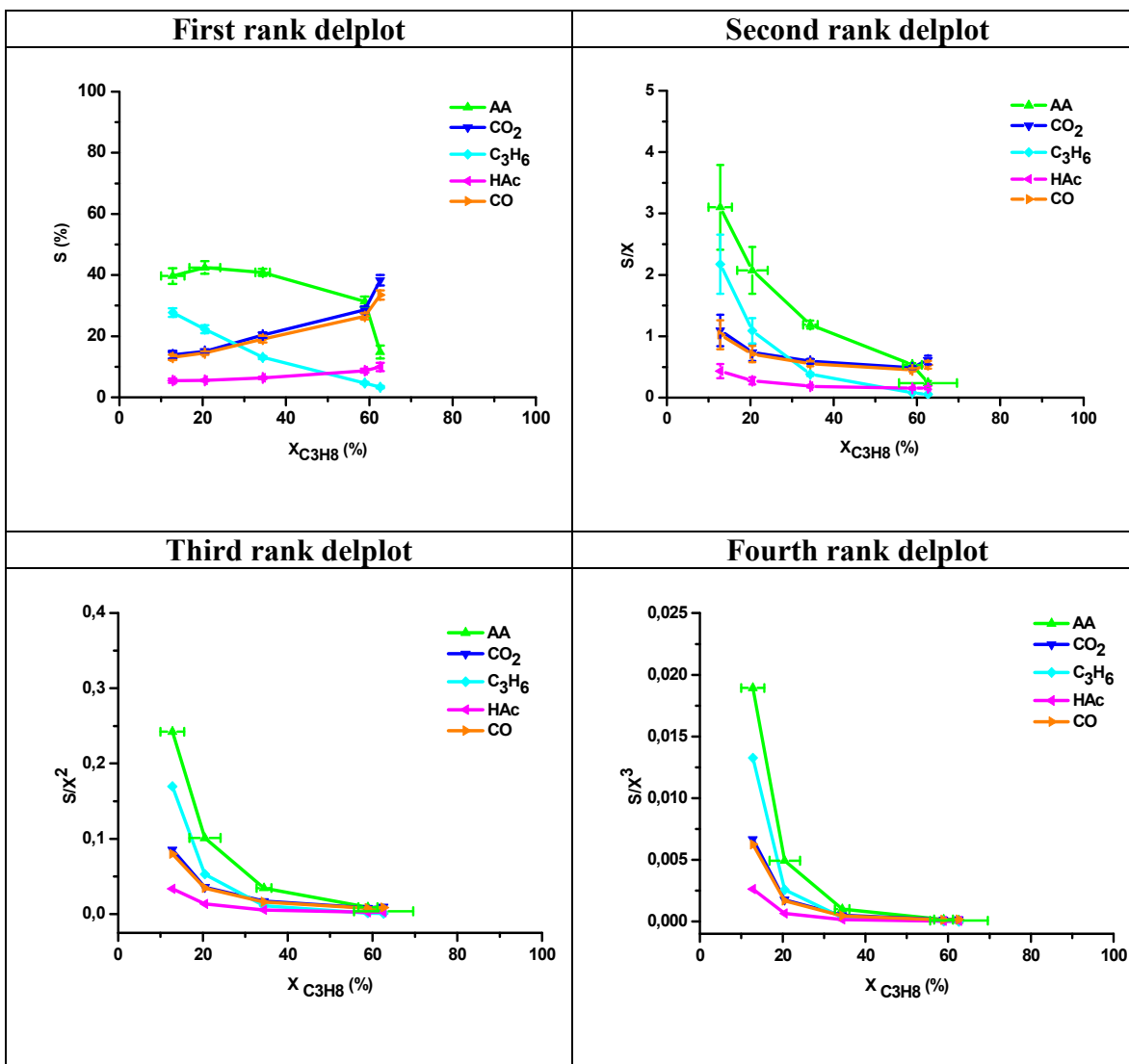


**Figure A.5.1.3.** The delplots corresponding to the propane oxidation using the hydrazine modified sample (#8113). Feed composition: C<sub>3</sub>H<sub>8</sub>/O<sub>2</sub>/H<sub>2</sub>O/N<sub>2</sub>=3/6/40/51 vol%, T=400°C.

Differences were noted also in the catalytic properties of the hydrazine treated sample (#8113) compared to the parent and other modified catalysts. The activity differences were significant only at low conversions, close to the differential operation mode. Nevertheless the product distribution also differs from all the other catalysts. In case of the parent sample and all the other modified the selectivity of CO and CO<sub>2</sub> was higher than one, except the measurement at the lowest space velocity of 3000 h<sup>-1</sup>, whereby

almost complete oxygen conversion (95%) was attained. Compared to these catalysts, on the hydrazine treated sample the ratio between the CO and CO<sub>2</sub> selectivity is inverted at any conversion.

On the first rank delplot corresponding to catalyst #8113 every compound had a nonzero positive intercept, indicating that all are first rank products (Figure A.5.1.3). The strongly diverging curves on the second, third and fourth rank delplot confirmed that every product is mainly a primary product.

The product ranks corresponding to every catalyst mentioned in this chapter are summarized in Table A.5.1.1. It can be observed that propylene is a primary product on all the catalysts. Acrylic acid showed a primary and secondary component in case of the parent sample and the tetramethylethylenediamine treated sample, while for the rest of the samples it was a primary product. A mixed rank for CO and CO<sub>2</sub> was found, except for the water treated sample (#7797) where these were only secondary products, while on the hydrazine treated sample (#8113) only primary products. The acetic acid was mainly a secondary product, except for the #7797 where a primary rank could not be excluded and for #8113, where first rank was observed.

**Table A.5.1.1. Product ranks on the different catalysts. P-primary, S-secondary.**

Catalyst	#6902	#7797	#7798	#7799	#7800	#8113
C <sub>3</sub> H <sub>6</sub> rank	P	P	P	P	P	P
AA rank	P, S	P	P	P, S	P	P
CO rank	P, S	S	P, S	P, S	P, S	P
CO <sub>2</sub> rank	P, S	S	S	P, S	P, S	P
HAc rank	S	P, S	S	S	S	P

Certainly, the CO and CO<sub>2</sub> are multiple rank products, and according to the rationale described in the section 4.2.7 and Appendix 5.2, the tertiary rank can not be excluded. However, in Table A.5.1.1 only those ranks were listed which resulted from the delplots.

Upon summarizing the results of catalytic experiments on propane oxidation over the modified samples, the most striking differences were noted.

The bromate treated sample (#7800) shows the

- lowest activity and selectivity in propane oxidation
- highest apparent activation energy
- mainly primary rank toward acrylic acid.

The hydrazine treated sample (#8113) is unique among the studied catalysts with respect to the followings:

- the ratio of CO/CO<sub>2</sub> selectivity was below one for all the conditions
- all products were found to be mainly primary products.

## Appendix 6.1. Modeling the delplots for a reaction pathway that contains multiple rank product

The applicability of the delplot technique introduced by Bhore et al. was demonstrated on a reaction pathway consisting of one intermediate and two end products. This technique is easily applicable for discernment of product ranks for a network of serial and parallel steps such as isomerisation reactions. However, in the case of oxidation reactions such as propane oxidation, the educt, the intermediate (propylene, acrolein) and the product (acrylic acid) may undergo total oxidation pathways as well, leading to CO and CO<sub>2</sub> (cf. section 6.4 and Appendix 5.1). In most of the proposed networks in the literature, the total oxidation products appear only as end products from oxidation of acrylic acid and acetic acid, respectively. If this would be true, the CO and CO<sub>2</sub> rank would be quaternary. As it was demonstrated by the delplots (subchapter 4.2.9), the curves corresponding to CO and CO<sub>2</sub> on the third and fourth rank delplot are diverging, which indicate that the rank of products are less than three and four. It was found that these products are mainly secondary products, and sometimes they appear also as minor products, depending on the reaction conditions and the catalyst.

To tackle the above noted apparent inconsistency, the delplot technique was applied to a reaction network that contains products with superposed or multiple ranks (primary, secondary and tertiary).

The simplest model for such a network consists of two parallel steps involving the reactant A (Figure A.6.1.1). In one of the steps A is converted to intermediate B, which undergoes a transformation to C. In parallel to this sequence, A is transformed directly to the C species.

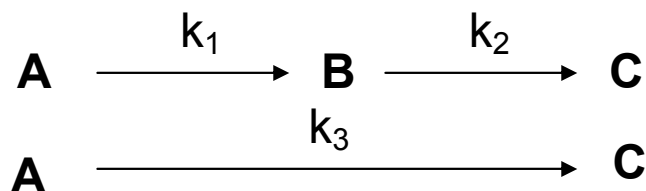


Figure A.6.1.1. Reaction network containing a superposed primary and secondary rank end product.

Therefore, the C species is secondary product in the upper pathway and a primary product in the lower pathway.

This simple model resembles the oxidative dehydrogenation reactions; with the simplification that only one total oxidation product is taken into account (CO or CO<sub>2</sub>). The simplification was made only for the purpose of easier mathematical handling of the kinetic model. The differential equations corresponding to this model are the following:

$$-\frac{dy_A}{dt} = (k_1 + k_3)y_A \quad (\text{Equation A.6.1.1})$$

$$\frac{dy_B}{dt} = k_1y_A - k_2y_B \quad (\text{Equation A.6.1.2})$$

$$\frac{dy_C}{dt} = k_2y_B + k_3y_A \quad (\text{Equation A.6.1.3})$$

This set of differential equations is analytically solvable, but because of the fact that the integrated rate equations are rather complicated, they are not shown here. Moreover, the analytical equation for the calculation of the intercept is even more complicated, the limit of the function can be obtained only by applying the l'Hospital's rule.

Therefore, the set of differential equations was solved numerically in the Berkeley Madonna software, using time steps of 0.02 s.

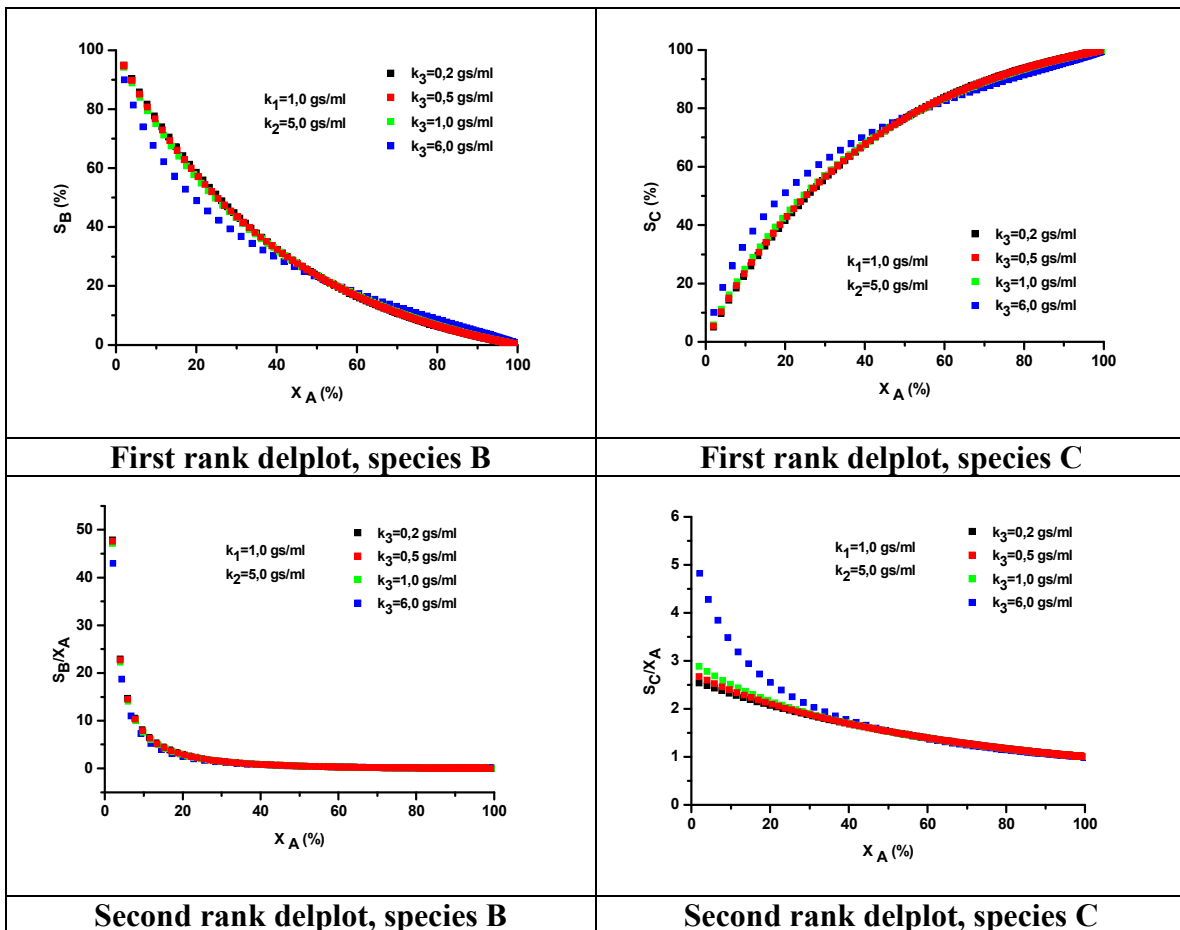


Figure A.6.1.2 The delplot for B and C species corresponding to the reaction pathway depicted on Figure A.6.1.1.

The  $k_1$  rate constant was fixed to 1.0 gs/ml, while  $k_2$  to 5.0 gs/ml. Four different values were tried for  $k_3$ , as follows: 0.2; 0.5; 1.0 and 6.0, respectively. The conversion and selectivities were calculated from the concentrations obtained from the numerical

solution of the differential equations. Then, the first and second rank delplots were constructed for the B and C species (Figure A.6.1.2).

The finite intercept on the first rank delplot corresponding to B species indicated first rank product. On the other hand, the first rank delplot corresponding to C shows an intercept close to zero at low values of  $k_3$  (0.2 and 0.5), while in the case of higher  $k_3$  values the intercept is above zero (around 2). This suggests that at higher  $k_3$  the C species is clearly a first rank product.

The divergent curves corresponding to the B species on the second rank delplot indicated that B is a primary product. However, the curves corresponding to the C species are diverging in the second rank delplot. A slight divergence can be observed for low  $k_3$  values (0.2 and 0.5) while the divergence at high rate constants (1.0 and 6.0) is very pronounced. Therefore, based on exclusively the delplots, one would erroneously conclude that the B and C species are primary products.

A more complicated reaction network is depicted on Figure A.6.1.3. This consists of two parallel pathways involving the reactant A, producing the B and D species. The B intermediate species is also involved in two parallel steps. In one of them, it is transformed to C, while the other represents transformation to the D product. Finally, the C is transformed to D product. Therefore, according to the scheme, B is a primary product; C is a secondary product, while the D is a primary, secondary and a tertiary product as well. This resembles to a simplified network for the oxidation of propane to acrylic acid. The B stands for propylene; the C is acrylic acid, while D represents one of the total oxidation products (CO or CO<sub>2</sub>). The simplification consists of neglecting the pathway leading to acetic acid and considering of only one total oxidation product.

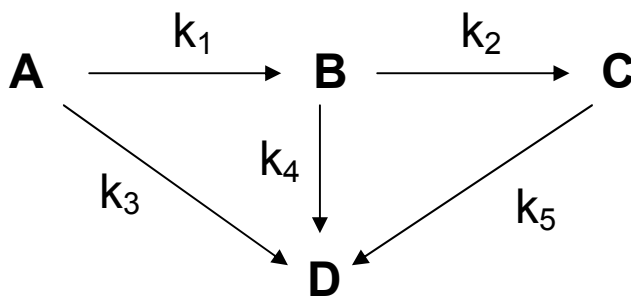


**Figure A.6.1.3.** Reaction network containing a superposed primary, secondary and tertiary end product.

The differential equations corresponding to this reaction network is shown below. This set of differential equations was solved using the Berkeley Madonna software. Since the case of simultaneous formation of a primary and secondary product with different rate constant of the second rank product formation was discussed on the Figure A.6.1.2, in the present case the rate constant of the tertiary product formation ( $k_5$ ) was varied between 0.05 and 3.00 gs/ml, while all the other rate constants were kept constant ( $k_1=1.00$  gs/ml,  $k_2=5.00$  gs/ml,  $k_3=0.05$  gs/ml,  $k_4=0.05$  gs/ml).

$$-\frac{dy_A}{dt} = (k_1 + k_3)y_A \quad (\text{Equation A.6.1.4})$$

$$\frac{dy_B}{dt} = k_2y_A - (k_2 + k_4)y_B \quad (\text{Equation A.6.1.5})$$

$$\frac{dy_C}{dt} = k_2y_B - k_5y_C \quad (\text{Equation A.6.1.6})$$

$$\frac{dy_D}{dt} = k_3y_A + k_4y_B + k_5y_C \quad (\text{Equation A.6.1.7})$$

Because the B was only a primary product, the delplots corresponding to this species are not shown. Only the delplots corresponding to the C and D products are analyzed in the following.

The first rank delplot corresponding to C and D exhibits a low, but nonzero intercept (2 and 4, respectively). This suggests that both are primary products. The D is indeed a primary product on the reaction scheme; however the C is a secondary product. The inconsistency in the rank of C determined from the delplot is due to systematic error introduced by extrapolation.

On the other hand, the second rank delplot corresponding to C confirms that this species is a secondary product, independently on the value of the  $k_5$  rate constant. The third rank delplot showed that indeed, the C has a lower rank than three.

The highly divergent curves corresponding D species on the second rank delplot suggests that this is only a primary product, in contrast to the reaction scheme. Finally, the third rank delplot for the D species are strongly diverging, indicating lower ranks than three. However, according to the reaction scheme, D is a tertiary product as we ll.

As demonstrated by the above two simulated cases, when a reaction network contains a product that is formed in two or more steps (multiple rank product), the delplot technique is not always suitable to find out the ranks. Usually the lowest rank can be identified, but the higher ranks are not identifiable due to diverging curves (these ranks being “masked” by the lowest rank). The curvature strongly depends on the rate constants of the individual reaction steps.

Therefore, in real applications, a great care should be taken when discriminating the pathways leading to potentially multiple rank products such as CO and CO<sub>2</sub> in oxidation catalysis. For the identification of the pathways the “chemical knowledge” arising from reactivity studies involving the reaction intermediates should also be taken into account besides the mathematics of the delplot technique.

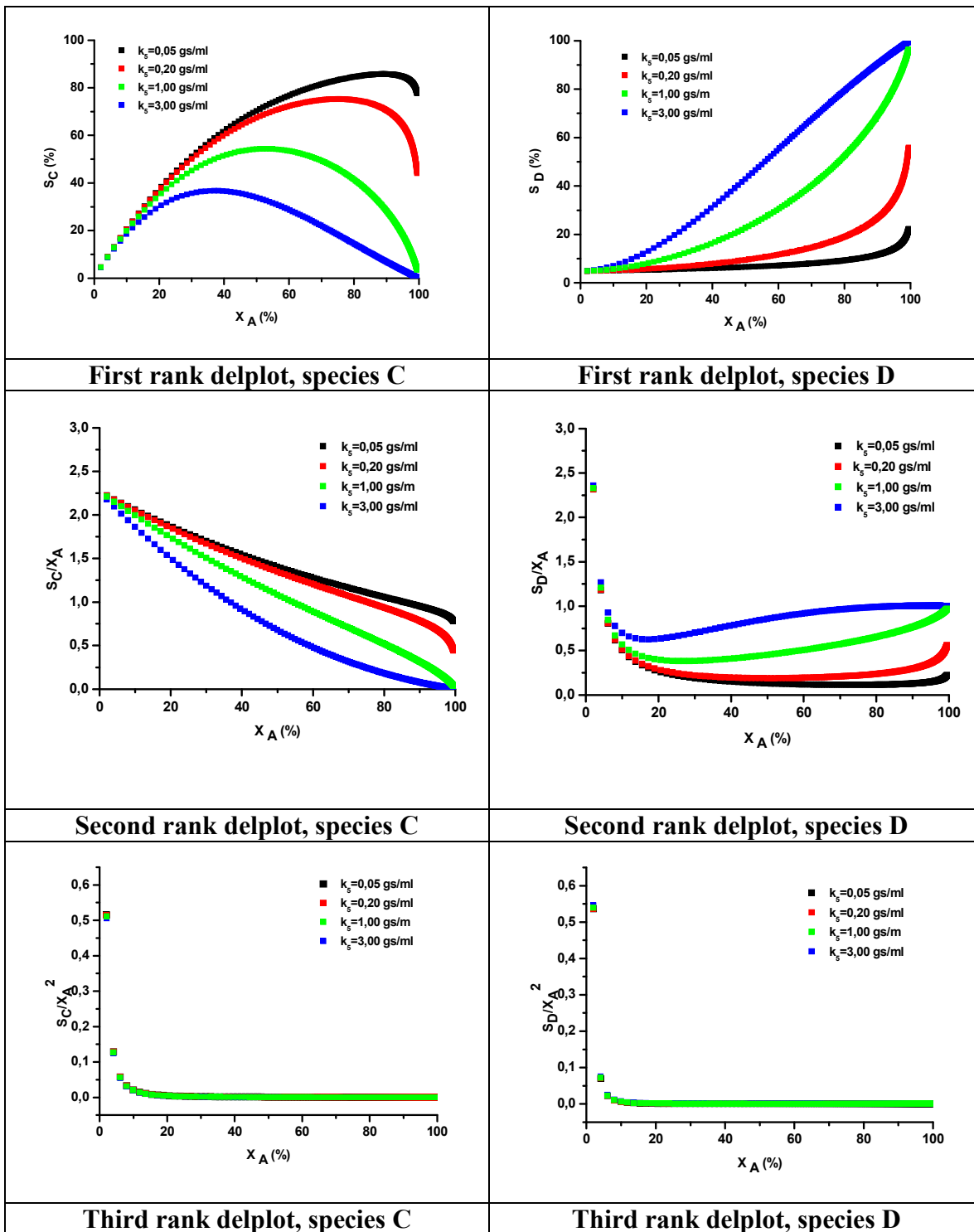


Figure A.6.1.4. The delplots for C and D species corresponding to the parallel-consecutive reaction network depicted on Figure A.6.1.3.

## Appendix 6.2. The kinetic models implemented in the Berkeley Madonna software

Program for implementing Model 1 in Berkeley Madonna

```
Rxn1a1=k1*yC3H8
k1=1.2
rxn1a2=k2*yC3H6
k2=12
rxn1a3=k3*yC3H6
k3=1
rxn1a4=k4*yC3H6
k4=1
rxn1a5=k5*yAA
k5=1
rxn1a6=k6*yAA
k6=1
rxn1a7=k7*yC3H8
k7=1
INIT yC3H8=1
INIT yC3H6=0
INIT yAA=0
INIT yHAc=0
INIT yCO=0
INIT yCO2=0
d/dt(yC3H8)=-rxn1a1-rxn1a7
d/dt(yC3H6)=rxn1a1-(rxn1a2+rxn1a3+rxn1a4)
d/dt(yAA)=rxn1a2-(rxn1a5+rxn1a6)
d/dt(yHAc)=rxn1a4
d/dt(yCO)=rxn1a3+rxn1a5+rxn1a7
d/dt(yCO2)=rxn1a4+rxn1a6
METHOD RK4
STARTTIME = 0
STOPTIME=2
DT = 0.02
```

Program for implementing Model 2 in Berkeley Madonna

```
rxn2a1=k1*yC3H8
k1=1.2
rxn2a2=k2*yC3H6
k2=12
rxn2a3=k3*yC3H6
k3=1
rxn2a4=k4*yC3H6
k4=1
rxn2a5=k5*yAA
k5=1
rxn2a6=k6*yAA
k6=1
rxn2a7=k7*yC3H8
k7=1
rxn2a8=k8*yC3H8
k8=1
INIT yC3H8=1
INIT yC3H6=0
```

```

INIT yAA=0
INIT yHAc=0
INIT yCO=0
INIT yCO2=0
d/dt(yC3H8)=-rxn2a1-rxn2a7-rxn2a8
d/dt(yC3H6)=rxn2a1-(rxn2a2+rxn2a3+rxn2a4)
d/dt(yAA)=rxn2a2-(rxn2a5+rxn2a6)
d/dt(yHAc)=rxn2a4
d/dt(yCO)=rxn2a3+rxn2a5+rxn2a7
d/dt(yCO2)=rxn2a4+rxn2a6+rxn2a8
METHOD RK4
STARTTIME = 0
STOPTIME=2
DT = 0.02

```

### Appendix 6.3. The physical properties of the gas mixtures with different steam contents.

The selected physical properties (such as density, heat capacity, heat conductivity and kinematic viscosity) of mixtures containing C<sub>3</sub>H<sub>8</sub>, H<sub>2</sub>O, O<sub>2</sub> and N<sub>2</sub> are shown in the Table A.6.3.1. The mixtures correspond to the feed compositions used for the steam content variation presented in section 4.2.2. The physical properties were calculated at a temperature of 400°C, using the Fluidat<sup>®</sup> on the Net on-line calculator ([www.fluidat.com](http://www.fluidat.com)) provided by Bronkhorst.

For the estimation of the eventual hot-spot formation on the catalyst surface, all the above mentioned physical properties are needed. Semi-quantitatively the data may be interpreted as follows: if in absence of steam hot-spot formation would occur, the propane conversion would increase and the selectivity would decrease. Since in absence of steam the conversion decreases (Figure A. 6.3.1), the hot-spot formation is not likely to occur. Therefore, isothermal operation mode may be assumed.

**Table A.6.3.1.** Physical properties of different feed mixtures. Mixture 1: C<sub>3</sub>H<sub>8</sub>/O<sub>2</sub>/H<sub>2</sub>O/N<sub>2</sub>=3/6/40/51 vol%, Mixture 2: C<sub>3</sub>H<sub>8</sub>/O<sub>2</sub>/H<sub>2</sub>O/N<sub>2</sub>=3/6/30/61 vol%, Mixture 3: C<sub>3</sub>H<sub>8</sub>/O<sub>2</sub>/H<sub>2</sub>O/N<sub>2</sub>=3/6/20/71 vol%, Mixture 4: C<sub>3</sub>H<sub>8</sub>/O<sub>2</sub>/H<sub>2</sub>O/N<sub>2</sub>=3/6/10/81 vol%, Mixture 5: C<sub>3</sub>H<sub>8</sub>/O<sub>2</sub>/H<sub>2</sub>O/N<sub>2</sub>=3/6/0/91 vol%

Property	Mixture 1	Mixture 2	Mixture 3	Mixture 4	Mixture 5
Density (kg/m <sup>3</sup> )	0.44	0.46	0.48	0.49	0.51
Heat capacity (kJ/kg·K)	1482	1399	1322	1250	1184
Heat conductivity·10 <sup>2</sup> (W/m·K)	6.34	6.10	5.82	5.51	5.27
Kinematic viscosity·10 <sup>5</sup> (m <sup>2</sup> /s)	6.54	6.40	6.24	6.09	6.04

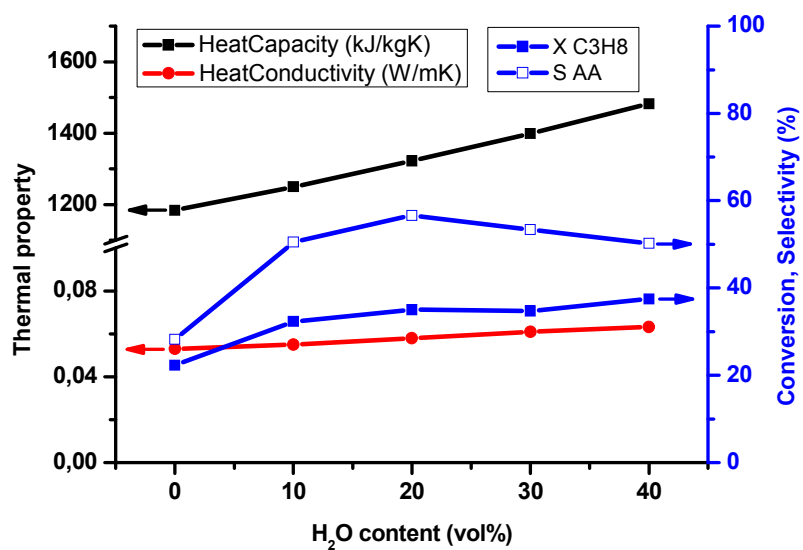


Figure A. 6.3.1. Plot of thermal properties of the feed mixture and the catalytic properties in function of the steam content.

### **Acknowledgements for permission to reprint published materials**

1. Robert K. Grasselli, J. D. Burrington, D. J. Buttrey, P. DeSanto, C. G. Lungmair, A. F. Volpe Jr., T. Weignand, Multifunctionality of Active Centers in (Amm)oxidation Catalysts: From Bi–Mo–O<sub>x</sub> to Mo–V–Nb–(Te, Sb)–O<sub>x</sub>, *Topics in Catalysis*, 23 (2003) 5, with permission from Springer.
2. M.M. Bettahar, G. Costentin, L. Savary, J.C. Lavalley, On the partial oxidation of propane and propylene on mixed metal oxide catalysts, *Applied Catalysis A: General*, 145 (1996) 1-48, with permission from Elsevier.
3. Gang Fu, X. Xu, X. Lu, H. Wan, Mechanisms of Initial Propane Activation on Molybdenum Oxides: A Density Functional Theory Study, *Journal of Physical Chemistry B*, 109, 2005, 6416-6421, with permission from the American Chemical Society.
4. Manhua Lin, Tejal B. Desai, Frederick W. Kaiser, Peter D. Klugherz, Reaction pathways in the selective oxidation of propane over a mixed metal oxide catalyst, *Catalysis Today*, 61 (2000) 223-229, with permission from Elsevier.
5. R. Fushimi, S. O. Shekhtman, A. Gaffney, S. Han, G. S. Yablonsky, J. T. Gleaves, *Industrial & Engineering Chemistry Research*, 44 (2005), 6310-6319, with permission from the American Chemical Society.
6. P. Botella, J. M. López Nieto, B. Solsona, A. Mifsud, F. Márquez, The Preparation, Characterization, and Catalytic Behavior of MoVTenbO Catalysts Prepared by Hydrothermal Synthesis, *Journal of Catalysis*, 209 (2002), 445-455, with permission from Elsevier.
7. C. Hamel, Á. Tóta, F. Klose, E. Tsotsas, A. Seidel-Morgenstern, Analysis of single and multi-stage membrane reactors for the oxidation of short-chain alkanes—Simulation study and pilot scale experiments, *Chemical Engineering Research and Design*, 86 (2008) 753-764, with permission from Elsevier.

## List of abbreviations

AA – acrylic acid

Ace – acetone

Acr – acrolein

AHM – ammonium heptamolybdate

at% - atomic percentage

BESSY – Berliner Elektronenspeicherring-Gesellschaft für Synchrotronstrahlung

BET – Brunauer, Emmett, Teller method

C-bal. – carbon balance

CSTR – continuous-flow stirred tank reactor

DFT – density functional theory

$d_{p,max}$  – the maximum particle diameter of the sieve fraction

$d_{p,min}$  – the minimum particle diameter of the sieve fraction

$d_r$  – the inner diameter of the reactor tube

$E_a$ ,  $E_{a,app}$  – apparent activation energy

EDX – energy dispersive X-ray analysis

ESR – electron spin resonance

FBR – fixed bed reactor

FTIR – Fourier transform infrared spectroscopy

GC-MS – gas chromatograph coupled to mass spectrometer

GHSV – gas hourly space velocity

HAc – acetic acid

HPC – heteropoly-compounds

k – rate constant

LEIS – low energy ion scattering

MAh – malonic anhydride

MFC – mass flow controller

MMO – multi-metal oxide

MSD – mass spectrometric detector

ODH – oxidative dehydrogenation

P – primary product  
PFR – plug-flow reactor  
PI – pressure indicator  
r – reaction rate  
R1, R2 – reactor tubes of the two-stage reactor  
S – secondary product  
SEM – scanning electron microscopy  
 $S_i$  – selectivity to the product appearing in the index  
STEM – scanning transmission electronmicroscopy  
STR – single-tube reactor  
TCD – temperature conductivity detector  
TIC – temperature indicator and controller  
TMEDA – tetramethylethylenediamine  
TSR – two-stage reactor  
UV-Vis – ultraviolet-visible spectroscopy  
VPO – vanadium-phosphorous oxides  
W/F – weight per flow, contact time  
WGS – water gas shift reaction  
WHSV – weight hourly space velocity  
XAS – X-ray absorption spectroscopy  
 $X_i$  – conversion of the species in the index  
XPS – X-ray photoelectron spectroscopy  
XRD – X-ray diffraction  
 $Y_i$  – yield of the species in the index  
 $y_i$  – dimensionless concentration  
 $\Delta H$  – enthalpy change  
 $\Delta H^\#$  – activation enthalpy  
 $\Delta S$  – entropy change  
 $\Delta S^\#$  – activation entropy

## List of figures

### Chapter 1. Introduction and motivation

<b>Figure 1.2.1.</b> Propylene oxidation and ammoxidation mechanism over bismuth molybdate catalysts as proposed by Grasselli et al. [9].....	4
<b>Figure 1.2.2.</b> Mechanism of propylene oxidation by consecutive acid-base and redox steps as proposed by Bettahar et al. [12].....	5
<b>Figure 1.2.3.</b> Some examples of the possible transitional states of hydrogen atom abstraction according to [18]. The numbers on the figures correspond to the calculated bond lengths.....	11
<b>Figure 1.2.4.</b> Reaction network of propane oxidation according to Bettahar et al. [12].....	14
<b>Figure 1.2.5.</b> The relative oxidative stability of several intermediates at different temperatures [22].....	15
<b>Figure 1.2.6.</b> Oxidation pathways of propane according to [22].....	16
<b>Figure 1.2.7.</b> Effect of CO <sub>2</sub> on the acrylic acid yield [30].....	20
<b>Figure 1.2.8.</b> Reaction steps and nature of active and selective sites in the oxidation of propane to acrylic acid on MoVTeNbO <sub>x</sub> catalysts [35].....	21
<b>Figure 1.2.9.</b> The flow rate (left) and concentration distribution of oxygen (right) in the catalytic membrane reactor without reaction taking place. The blue and green curves correspond to different reactor geometries (aspect ratios). The profile corresponding to fixed bed reactor (FBR) is indicated by orange line [61].....	34
<b>Figure 1.2.10.</b> (a) Selectivity of propylene vs. propane conversion, (b) selectivity of propylene vs. temperature. Conditions: $x_{C_3H_8}^{in}=1\%$ , $O_2/C_3H_8=1$ and WHSV=100 and 400 kgs/m <sup>3</sup> [61].....	35

### Chapter 2. Experimental methods

<b>Fig. 2.2.1.</b> The experimental setup denominated as PropOx-1.....	47
<b>Figure 2.2.2.</b> The temperature profile of the reactor tube. Zero centimeter corresponds to the bottom of the heating cartridge. The delimitation of the isothermal zone is marked by blue lines.....	49
<b>Figure 2.2.3.</b> The gas tubing connection of the two stage reactor.....	53
<b>Figure 2.2.4.</b> The dilution ratio in the second reactor (red dots) and the overall space velocity (black squares) change upon oxygen addition in the two-stage reactor system.....	54
<b>Figure 2.2.5.</b> Detection at the MSD. 1: acetic acid, 2: acrylic acid.....	56
<b>Figure 2.2.6.</b> Detection at the TCD. 1: carbon- dioxide, 2: water, 3: propylene, 4: propane, 5: oxygen, 6: nitrogen, 7: carbon-monoxide, *: valve switching.....	56
<b>Figure 2.2.7.</b> Calibration graphs.....	58
<b>Figure 2.3.1.</b> The TEM image of the catalyst #6059.....	62
<b>Figure 2.3.2.</b> The XRD pattern of #6059, #6902 and #8947.....	63

### Chapter 3. Structural stability of the M1 MoVTeNbO<sub>x</sub> catalyst under propane oxidation conditions

<b>Figure 3.3.1.</b> The XRD patterns recorded under different reaction conditions.....	70
<b>Figure 3.3.2.</b> The lattice constants determined for every condition.....	71
<b>Figure 3.3.3.</b> The normalized average intensity corresponding to acrylic acid during the in-situ XRD experiment monitored by on-line MS (black squares). The concentration of acrylic acid determined in the PropOx-1 fixed bed reactor (blue dots).....	72
<b>Figure 3.4.1.</b> STEM images of the catalyst before and after the in-situ XRD experiment.....	73
<b>Figure 3.4.2.</b> The elemental mapping of the catalyst before reaction.....	74
<b>Figure 3.4.3.</b> The elemental mapping of the catalyst after reaction.....	74

### Chapter 4. Kinetic studies of propane oxidation to acrylic acid on a phase-pure MoVTeNbO<sub>x</sub> catalyst

<b>Figure 4.2.1.</b> The evolution of concentrations with the residence time at different temperatures. Squares – experimental data, dashed curves – fitted kinetic curves based on reaction model 1 (for modeling see section 6.4.). Feed composition: C <sub>3</sub> H <sub>8</sub> /O <sub>2</sub> /H <sub>2</sub> O/N <sub>2</sub> =3/6/40/51 vol%, Catalyst ID=6059.....	80
---	----

<b>Figure 4.2.2.</b> The stability of catalytic performance in steam-free feed.....	82
<b>Figure 4.2.3.</b> The effect of steam on the acrylic acid productivity at GHSV=4500, 9000 and 18000 h <sup>-1</sup> ....	83
<b>Figure 4.2.4.</b> The effect of temperature on the catalytic performance at 0, 10 and 40 vol% steam content. Catalyst #6059.....	84
<b>Figure 4.2.5.</b> The effect of steam on the concentration profiles.....	86
<b>Figure 4.2.6.</b> The effect of the propane concentration on the catalytic performance. C <sub>3</sub> H <sub>8</sub> /O <sub>2</sub> /H <sub>2</sub> O/N <sub>2</sub> =x/6/40/(54-x) vol%, T=400°C. GHSV= 34280 h <sup>-1</sup> , W/F=0.11 gs/ml. Catalyst: #6059....	88
<b>Figure 4.2.7.</b> Determination of the reaction order with respect to propane.....	90
<b>Figure 4.2.8.</b> The effect of the oxygen concentration on catalytic performance. C <sub>3</sub> H <sub>8</sub> /O <sub>2</sub> /H <sub>2</sub> O/N <sub>2</sub> =3/y/40/(57-y) vol%, T=400°C. GHSV= 4500 h <sup>-1</sup> , W/F=0.904 gs/ml, catalyst: #6059.....	91
<b>Figure 4.2.9.</b> Determination of the reaction order with respect to oxygen. Cat: #6059.....	92
<b>Figure 4.2.10.</b> Propylene oxidation with #6902. Feed composition: C <sub>3</sub> H <sub>6</sub> /O <sub>2</sub> /H <sub>2</sub> O/N <sub>2</sub> =3/6/40/51 vol%. Top: GHSV=5000 h <sup>-1</sup> , bottom: GHSV=20000 h <sup>-1</sup> . Catalyst: #6902.....	94
<b>Figure 4.2.11.</b> The effect of H <sub>2</sub> O on propylene oxidation. Feed composition: C <sub>3</sub> H <sub>6</sub> /O <sub>2</sub> /H <sub>2</sub> O/N <sub>2</sub> =3/6/z/(91-z) vol%, GHSV=80000 h <sup>-1</sup> , T=400°C. Catalyst: 6902.....	97
<b>Figure 4.2.12.</b> The effect of temperature on acrolein oxidation. Catalyst #6059.....	99
<b>Figure 4.2.13.</b> CO oxidation at different temperatures, space velocities in stoichiometric and oxidizing feed. Catalyst: #8947.....	102
<b>Figure 4.2.14.</b> Space velocity variation for CO oxidation and water gas shift reaction.....	103
<b>Figure 4.2.15.</b> Comparison of the propane, propylene, acrolein (top), propane, CO oxidation and water gas shift activity (bottom) of the catalyst. ....	105
<b>Figure 4.3.1.</b> The dilution ratios (black squares), overall space velocities (black dots) and the oxygen concentrations (empty and full blue triangles) in function of the flow rate of the added oxygen.....	108
<b>Figure 4.3.2.</b> The effect of oxygen addition in the two-stage reactor.....	109
<b>Figure 4.3.3.</b> Comparison of the catalytic performance in the single-tube reactor (STR) and two-stage reactor (TSR).....	110
<b>Figure 4.3.4.</b> Addition of N <sub>2</sub> O in the two-stage reactor. Conditions noted with stars: *- 4,0 vol% O <sub>2</sub> introduced in R1 reactor and 4,0 vol% N <sub>2</sub> O in R2 reactor ; **- 6 vol% O <sub>2</sub> introduced in R1 reactor and 0,0 vol% N <sub>2</sub> O in R2 reactor.....	112
<b>Figure 4.3.5.</b> Reactivation of the catalyst after exposing to reducing conditions.....	113
<b>Figure 4.3.6.</b> The effect of C <sub>3</sub> H <sub>6</sub> addition of in the two-stage reactor.....	115
<b>Figure 4.3.7.</b> The effect of CO addition in the two-stage reactor.....	116
<b>Figure 4.3.8.</b> The effect of CO <sub>2</sub> addition in the two-stage reactor.....	118

## Chapter 5. Post synthesis treatment of the phase-pure M1 MoVTenbO<sub>x</sub> catalyst

<b>Figure 5.2.1.</b> The UV-Vis spectra of the filtrate solutions.....	126
<b>Figure 5.3.1</b> The SEM picture of the catalysts. #6902 (parent sample), #7797 (water treated sample), #7798 (H <sub>3</sub> PO <sub>4</sub> treated sample), #7799 (TMEDA treated sample), #7800 (NaBrO <sub>3</sub> treated sample), #8113 (N <sub>2</sub> H <sub>4</sub> treated sample).....	129
<b>Figure 5.3.2.</b> The elemental composition of the original and the modified catalysts as probed by EDX...130	
<b>5.3.3.</b> NEXAFS spectra of the bromate treated sample( #7800), the parent sample (#6902), the difference spectrum and the V <sup>5+</sup> reference spectrum.....	131
<b>Figure 5.3.4.</b> Normalized surface concentrations. Correlation of Te content and Te/V ratio with the normalized selectivity to acrylic acid (bar-graph).....	133
<b>Figure 5.3.5.</b> Adsorption of propane (educt of the catalytic reaction) at 313 K on fresh (dots) and used M1 (triangle) activated at 423 K under vacuum.....	134
<b>Figure 5.3.6.</b> Adsorption of propylene at 313 K on fresh (dots) and used M1 (triangle) activated at 423 K under vacuum.....	136
<b>Figure 5.3.7.</b> Adsorption of propane at 313 K after propylene adsorption on fresh (open dots) M1 activated at 423 K under vacuum. For comparison, the propane adsorption isotherm and differential heat profile if propane firstly adsorbed on the fresh M1 (dots).....	138
<b>Figure 5.3.8.</b> Microcalorimetry on the bromate-treated phase-pure M1 catalyst (#7800) before and after catalytic experiment.....	139
<b>Figure 5.4.1.</b> The activity of the catalysts.....	141
<b>Figure 5.4.2.</b> The selectivity and yield of the catalysts.....	143

<b>Figure 5.4.3.</b> The apparent activation energy of propane activation over the catalysts.....	143
<b>Figure 5.4.4.</b> The linear representation of the rate law with respect to propane and oxygen. #6902 – original, #7797 – H <sub>2</sub> O modified, #7798 – H <sub>3</sub> PO <sub>4</sub> modified, #7799 – TMEDA modified, #7800 – NaBrO <sub>3</sub> modified, #8113 – N <sub>2</sub> H <sub>4</sub> modified sample.....	145
<b>Figure 5.4.5.</b> Plot of the experimental with calculated $y_{C_3H_6}$ data for catalyst #6902.....	147
<b>Figure 5.4.6.</b> The activity of the catalysts in propane oxidation reaction. #6902 – original, #7797 – H <sub>2</sub> O modified, #7798 – H <sub>3</sub> PO <sub>4</sub> modified, #7799 – TMEDA modified, #7800 – NaBrO <sub>3</sub> modified, #8113 – N <sub>2</sub> H <sub>4</sub> modified sample.....	149
<b>Figure 5.4.7.</b> The selectivity and yield of the catalysts in propane oxidation reaction. #6902 – original, #7797 – H <sub>2</sub> O modified, #7798 – H <sub>3</sub> PO <sub>4</sub> modified, #7799 – TMEDA modified, #7800 – NaBrO <sub>3</sub> modified, #8113 – N <sub>2</sub> H <sub>4</sub> modified sample.....	149
<b>Figure 5.4.8.</b> The CO oxidation activity at different temperatures and GHSV=3000 h <sup>-1</sup> (left). The kinetic curves of CO <sub>2</sub> formation at 400°C (right). Conditions: CO/O <sub>2</sub> /H <sub>2</sub> O/N <sub>2</sub> =3/6/0/91 vol%. Catalysts: #8947 – as prepared M1 MoVTenNbO <sub>x</sub> , #7800 – NaBrO <sub>3</sub> treated #6902, #8113 – N <sub>2</sub> H <sub>4</sub> treated #6902.....	150
<b>Figure 5.4.9.</b> Kinetic curves for CO <sub>2</sub> formation for the CO oxidation in presence of steam and for the water gas shift reactions. Catalysts: #6902 – as prepared M1 MoVTenNbO <sub>x</sub> , #7800 – NaBrO <sub>3</sub> treated sample, #8113 – N <sub>2</sub> H <sub>4</sub> treated sample.....	152

## Chapter 6. Exploratory experiments

<b>Figure 6.2.1.</b> Catalytic performance of different phase-pure Mo and V based oxides.....	162
<b>Figure 6.2.2.</b> The activation parameters of the propane and oxygen conversion on the MoV(Te)(P)(Nb)O <sub>x</sub> catalysts.....	163
<b>Figure 6.3.1.</b> Propylene oxidation over (Mo <sub>0.93</sub> V <sub>0.07</sub> ) <sub>5</sub> O <sub>14</sub> catalyst (#1862).....	168
<b>Figure 6.4.1.</b> Delplots for propane oxidation using the feed C <sub>3</sub> H <sub>8</sub> /O <sub>2</sub> /H <sub>2</sub> O/N <sub>2</sub> =3/6/40/51 vol% at T=400°C. Catalyst ID: #6059.....	172
<b>Figure 6.4.2.</b> Delplots for propane oxidation using the feed C <sub>3</sub> H <sub>8</sub> /O <sub>2</sub> /H <sub>2</sub> O/N <sub>2</sub> =3/6/0/91 vol% at T=400°C. Catalyst ID: 6059.....	174
<b>Figure 6.4.3.</b> Reaction model 1 for propane oxidation.....	176
<b>Figure 6.4.4.</b> The reaction model 2.....	177

## Appendices

### Appendix 5.1. Reaction networks of propane oxidation over the modified catalysts

<b>Figure A.5.1.1.</b> The delplots corresponding to the propane oxidation using the H <sub>2</sub> O modified sample (#7797). Feed composition: C <sub>3</sub> H <sub>8</sub> /O <sub>2</sub> /H <sub>2</sub> O/N <sub>2</sub> =3/6/40/51 vol%, T=400°C.....	189
<b>Figure A.5.1.2.</b> The delplots corresponding to the propane oxidation using the NaBrO <sub>3</sub> modified sample (#7800). Feed composition: C <sub>3</sub> H <sub>8</sub> /O <sub>2</sub> /H <sub>2</sub> O/N <sub>2</sub> =3/6/40/51 vol%, T=400°C.....	190
<b>Figure A.5.1.3.</b> The delplots corresponding to the propane oxidation using the hydrazine modified sample (#8113). Feed composition: C <sub>3</sub> H <sub>8</sub> /O <sub>2</sub> /H <sub>2</sub> O/N <sub>2</sub> =3/6/40/51 vol%, T=400°.....	191

### Appendix 6.1. Modeling the delplots for a reaction pathway that contains multiple rank product

<b>Figure A.6.1.1.</b> Reaction network containing a superposed primary and secondary rank end product.....	193
<b>Figure A.6.1.2.</b> The delplot for B and C species corresponding to the reaction pathway depicted on Figure A.6.1.1.....	194
<b>Figure A.6.1.3.</b> Reaction network containing a superposed primary, secondary and tertiary end product.....	195
<b>Figure A.6.1.4.</b> The delplots for C and D species corresponding to the parallel-consecutive reaction network depicted on Figure A.6.1.3.....	197
<b>Figure A. 6.3.1.</b> Plot of thermal properties of the feed mixture and the catalytic properties in function of the steam content.....	200

## List of tables

### Chapter 1. Introduction and motivation

<b>Table 1.2.1.</b> The characteristics of catalysts studied in [14 ].....	8
<b>Table 1.2.2.</b> The calculated thermodynamic quantities of the supposed hydrogen atom abstraction pathways, in comparison with the experimentally determined values [18].....	12
<b>Table 1.2.3.</b> Optimized catalytic performance of VPO, HPC and MMO catalyst systems for oxidation of propane to acrylic acid, as summarized based on references [2] and [4].....	13
<b>Table 1.2.4.</b> Catalytic effect of the individual phases of the mixture in the propane partial oxidation [2].....	21
<b>Table 1.2.5.</b> Activation energy of propane partial oxidation on different surface-promoted catalysts [36].....	23

### Chapter 2. Experimental methods

<b>Table 2.2.1.</b> The $\Psi$ , $\Phi$ and $\eta$ dimensionless numbers corresponding to propane oxidation reaction.....	52
<b>Table 2.2.2.</b> The resolution for the peak-pairs which elute close to each other.....	57
<b>Table 2.2.3.</b> Vapor pressures of acetic- and acrylic acid at around room temperature [11].....	58
<b>Table 2.3.1.</b> The properties of the phase-pure M1 catalysts #6059, #6902 and #8947.....	62

### Chapter 4. Kinetic studies of propane oxidation to acrylic acid on a phase-pure MoVTenbO<sub>x</sub> catalyst

<b>Table 4.2.1.</b> The activation parameters of propane consumption at different steam contents.....	85
<b>Table 4.2.2.</b> The activation parameters of acrolein oxidation on #6059 catalyst.....	100
<b>Table 4.2.3.</b> The activation parameters of CO oxidation in dry feed.....	102

### Chapter 5. Post synthesis treatment of the phase-pure M1 MoVTenbO<sub>x</sub> catalyst

<b>Table 5.3.1.</b> The BET surface area of the samples.....	127
<b>Table 5.3.2.</b> The lattice parameters of the catalysts before and after catalytic oxidation of propane and propylene.....	128
<b>Table 5.3.3.</b> The binding energies corresponding to every catalyst.....	132
<b>Table 5.3.4.</b> Adsorption and desorption heats corresponding to different coverages.....	135
<b>Table 5.3.5.</b> The adsorption order, monolayer coverage and adsorption constant of propane adsorption for the #6059 and bromate treated sample (#7800).....	140
<b>Table 5.4.1.</b> The catalytic performance of the hydrazine treated catalyst (#8113) compared before and after the complete oxygen conversion experiment.....	142
<b>Table 5.4.2.</b> The apparent rate constants of propane and oxygen consumption.....	145
<b>Table 5.4.3.</b> The rate constants of propane and propylene consumption.....	147
<b>Table 5.4.4.</b> Activation energy of CO oxidation. Feed composition: CO/O <sub>2</sub> /H <sub>2</sub> O/N <sub>2</sub> =3/6/0/91 vol%, #8947 – as prepared M1 MoVTenbO <sub>x</sub> , #7800 – NaBrO <sub>3</sub> treated #6902, #8113 – N <sub>2</sub> H <sub>4</sub> treated #6902.....	151
<b>Table 5.4.5.</b> The CO conversion at GHSV=3000 h <sup>-1</sup> and 400°C.....	152
<b>Table 5.4.6.</b> Rate constants of CO <sub>2</sub> formation at 400°C.....	153

### Chapter 6. Exploratory experiments

<b>Table 6.2.1.</b> The used catalysts and reaction conditions. Catalyst preparation methods: SD – spray drying, HT – hydrothermal.....	159
<b>Table 6.2.2.</b> Comparison of the catalytic performance of MoVTenbO <sub>x</sub> (#6059) and MoVO <sub>x</sub> (#8103) samples at 400°C, feed composition: C <sub>3</sub> H <sub>8</sub> /O <sub>2</sub> /H <sub>2</sub> O/N <sub>2</sub> =3/6/40/51 vol%.....	160
<b>Table 6.2.3.</b> Comparison of the performance of selected catalysts. Composition as determined by (a) stoichiometry, (b) ICP, (c) EDX, (d) LEIS-surface. Preparation method: slurry (Sl.), hydrothermal (Ht.), Solid-solid (Ss.), Incipient impregnation (Ii.), Spray drying (Sd.). (P) – present work.....	165
<b>Table 6.3.1.</b> Propylene oxidation reactivity on different catalysts.....	169
<b>Table 6.4.1.</b> Product ranks at different temperatures. For multiple rank products, the main ranks are highlighted by bold letter. P-primary, S-secondary.....	173

<b>Table 6.4.2.</b> Product ranks at different steam contents. For multiple rank products, the main ranks are highlighted by bold letter. P-primary, S-secondary rank.....	175
<b>Table 6.5.1.</b> The rate constants corresponding to the steps of the reaction model 1.....	179
<b>Table 6.5.2.</b> The activation energy and preexponential factor of the individual reaction steps.....	179
<b>Table 6.5.3.</b> The rate constants of the individual steps as determined based on model 1 and model 2.....	180

## Appendices

### Appendix 5.1. Reaction networks of propane oxidation over the modified catalysts

<b>Table A.5.1.1.</b> Product ranks on the different catalysts. P-primary, S-secondary.....	192
---	-----

### Appendix 6.3. The physical properties of the gas mixtures with different steam contents.

<b>Table A.6.3.1.</b> Physical properties of different feed mixtures. Mixture 1: C <sub>3</sub> H <sub>8</sub> /O <sub>2</sub> /H <sub>2</sub> O/N <sub>2</sub> =3/6/40/51 vol%, Mixture 2: C <sub>3</sub> H <sub>8</sub> /O <sub>2</sub> /H <sub>2</sub> O/N <sub>2</sub> =3/6/30/61 vol%, Mixture 3: C <sub>3</sub> H <sub>8</sub> /O <sub>2</sub> /H <sub>2</sub> O/N <sub>2</sub> =3/6/20/71 vol%, Mixture 4: C <sub>3</sub> H <sub>8</sub> /O <sub>2</sub> /H <sub>2</sub> O/N <sub>2</sub> =3/6/10/81 vol%, Mixture 5: C <sub>3</sub> H <sub>8</sub> /O <sub>2</sub> /H <sub>2</sub> O/N <sub>2</sub> =3/6/0/91 vol%.....	199
---	-----